WELD EFFECTIVE SECTION MODULI FOR CHS MOMENT T-CONNECTIONS

by

ZHIYUAN YANG

Submitted in partial fulfilment of the requirements for
the degree of Master of Applied Science

at

Dalhousie University
Halifax, Nova Scotia
December 2021

TABLE OF CONTENTS

LIST OF TABLES

LIST OF FIGURES

WELD EFFECTIVE SECTION MODULI FOR CHS MOMENT T-CONNECTIONS

Zhiyuan Yang
MASc
Department of Civil and Resource Engineering
Dalhousie University
2021

ABSTRACT

An experimental program was developed to test various unreinforced circular hollow section (CHS)-to-CHS 90° T-connections subject to branch in-plane bending moment with the objective of determining the effective section moduli of the welded joints. Twelve specimens were designed to be weld-critical (i.e., to fail by weld rupture), and tested by applying a single quasi-static point load, laterally, to the top of each branch. An equation for the weld effective section modulus for CHS-to-CHS moment T-connections is developed, and various design formulae are assessed through first-order reliability analysis. The scope of this research covers fillet and partial-joint-penetration groove welded connections with $0.31 \leq$ branch-to-chord width ratio (β) ≤ 0.91 and $31 \leq$ chord slenderness (D/t) ≤ 46, to illustrate the influence of these key parameters (as well as weld type) on flexural strength. Recommendations are made for weld design using the "effective length approach" in conjunction with AISC 360 and CSA S16.

ACKNOWLEDGEMENTS

First, I would like to thank my supervisor, Dr. Kyle Tousignant, for offering me the opportunity to study under his guidance. His support has been indispensable. I would also like to thank the laboratory technicians in the Department of Civil and Resource Engineering at Dalhousie University: Mr. Jordan Maerz, Mr. Jesse Kean and Mr. Dean Grijm. They have been a tremendous help in preparing and carrying out the tests conducted as part of this research. Thanks, as well, to the friends and classmates who have helped me throughout this journey. Further thanks are extended to Atlas Tube, for donating the circular hollow section (CHS) material used in this research, and to Cherubini Metal Works, for fabrication of the test specimens. Finally, I would like to thanks to my family, who has supported and encouraged me throughout my education.

ABBREVIATIONS AND SYMBOLS

AISC	=	American Institute of Steel Construction
AWS	=	American Welding Society
CSA	=	Canadian Standards Association
CIDECT	=	International Committee for the Development and Study of Tubular Construction
CISC	=	Canadian Institute of Steel Construction
CEN	=	European Committee for Standardization
CHS	=	circular hollow section
COV	=	coefficient of variation
DIF	=	directional increase factor
HSS	=	hollow structural section
LRFD	=	load and resistance factor design
RHS	=	rectangular hollow section
TC	=	tensile coupon
A_g	=	gross area of member
A_m	=	area of fusion face between weld and base metal
A_w	=	effective throat area of weld (= $t_w l_w$)
A_{we}	=	effective area of weld (same as A_w)
B_b	=	overall width of the RHS branch
B_{bi}	=	overall width of the overlapping RHS branch
B_{bj}	=	overall width of the overlapped RHS branch
B_e	=	effective width of RHS branch member or plate
B_{ej}	=	effective width of RHS overlapping branch member
B_{ej}	=	effective width of RHS overlapped branch member
D	=	overall diameter of CHS chord
D_b	=	overall diameter of CHS branch
E	=	Young's modulus
E_{ave}	=	average Young's modulus
F_c	=	available stress in the main member
F_{EXX}	=	electrode ultimate strength in AISC 360
F_{nw}	=	nominal strength of the weld metal per unit area
F_u	=	ultimate stress of the HSS
$F_{w,Ed}$	=	design value of the weld force per unit length using in EN 1993-1-8
F_{nw}	=	design weld resistance per unit length using in EN 1993-1-8
F_y	=	yield stress; yield stress of HSS chord

F_{yb}	=	yield stress of HSS branch
F_{yw}	=	yield stress of weld metal
H	=	overall height of the RHS chord
H_b	=	overall height of the RHS branch
H_{bi}	=	overall depth of the overlapping RHS branch
H_{bj}	=	overall depth of the overlapped RHS branch
I	=	moment of inertia of the HSS
I_{ip}	=	moment of inertia of the HSS for in-plane bending
I_{op}	=	moment of inertia of the HSS for out-of-plane bending
$M_{n\text{-}ip}$	=	nominal flexural strength for in-plane bending
$M_{n\text{-}op}$	=	nominal flexural strength for out-of-plane bending
M_{ip}	=	factored flexural strength for in-plane bending
M_{op}	=	factored flexural strength for out-of-plane bending
M_{ro}	=	required flexural strength in chord at a joint, on the side of joint with lower compression stress
M_u	=	required flexural strength using LRFD load combinations
M_w	=	strength reduction factor in CSA S16-14 to allow for the variation in deformation capacity of weld elements with different orientations
O_v	=	overlapping connection coefficient (l_{ov}/l_p)
P	=	applied force
P_n	=	nominal axial strength
P_{ro}	=	required axial strength in chord at a joint, on the side of joint with lower compression stress
P_u	=	required axial strength in chord using LRFD load combinations
Q_f	=	chord-stress interaction parameter
R_n	=	nominal resistance
S	=	elastic section modulus of HSS
S_{ip}	=	effective elastic section modulus of weld for in-plane bending
S_{op}	=	effective elastic section modulus of weld for out-of-plane bending
U	=	utilization ratio
V_D	=	coefficient of variation of live load effect
V_G	=	coefficient of variation of geometry
V_L	=	coefficient of variation of dead load effect
V_M	=	coefficient of variation of material
V_P	=	coefficient of variation of profession
V_R	=	coefficient of variation of resistance
V_S	=	coefficient of variation of load
V_r	=	factored shear resistance of a member or component
X_u	=	electrode ultimate strength in CSA S16 (= F_{EXX})
Z	=	plastic section modulus of the HSS
a	=	effective weld throat using in EN 1993-1-8 (= t_w)
e	=	eccentricity in a truss connection; loading eccentricity in a fillet weld
f_u	=	nominal ultimate tensile strength of the weaker part joined in EN 1993-1-8

$f_{vw,d}$	=	design shear strength of the weld in EN 1993-1-8
g	=	gap between PJP weld surface and branch base metal, after grinding
i	=	subscript/term used to identify the overlapping branch member; subscript/term used to identify weld elements
l	=	length of chord
l_b	=	weld leg size contact with branch
l_c	=	weld leg size contact with chord
l_e	=	weld effective length
l_{ov}	=	overlap length measured along the connecting face of the chord beneath the two branches
l_p	=	projected length of the overlapping branch on the chord
l_{pb}	=	projected weld leg size on the branch on the vertical
l_{pc}	=	projected weld leg size on the chord on the horizontal
l_w	=	total weld length
t	=	wall thickness of HSS chord member
t_b	=	wall thickness of HSS branch member
t_w	=	weld effective throat dimension
α	=	chord length parameter (= $2l/D$ for CHS)
α_D	=	load factor of dead load
α_L	=	load factor of live load
β	=	ratio of overall branch width to chord width for RHS; ratio of overall branch diameter to chord diameter for CHS; theoretical angle between the plane of the effective throat and the fusion face corresponding to l_v
β_w	=	correlation factor for fillet welds in EN 1993-1-8
γ	=	half diameter-to-thickness ratio of the chord (= $D/2t$)
γ_{M2}	=	partial safety factor of 1.25 for the resistance of weld in EN1993-1-8
γ_{M5}	=	partial safety factor of 1.0 for the resistance of connection in hollow section lattice girder in EN 1993-1-8
δ_d	=	bias coefficient for discretization
δ_G	=	bias coefficient for the geometry
δ_M	=	bias coefficient for the material factor
δ_P	=	bias coefficient for the professional factor
δ_R	=	bias coefficient for the resistance
ε	=	engineering strain
ε_{avg}	=	average engineering strain
ε_f	=	failure strain
$\varepsilon_{f,ave}$	=	average failure strain
ε_u	=	ultimate engineering strain
ε_y	=	yield strain
$\varepsilon_{y,ave}$	=	average yield strain
θ	=	angle of loading measured from the weld longitudinal axis, for fillet weld strength calculations (in degrees); branch inclination angle
θ_l	=	angle of loading (in degrees) for the weld element under consideration

θ_i	=	included angle between the overlapping branch and chord
θ_j	=	included angle between the overlapped branch and chord
ρ_R	=	bias coefficient for the resistance
$\sigma_{\perp}$	=	normal stress perpendicular to the plane of the throat
$\sigma_{/\!/}$	=	normal stress parallel to the axis of the weld
τ	=	branch-to-chord thickness ratio
$\tau_{\perp}$	=	shear stress (in the plane of the throat) perpendicular to the axis of the weld
$\tau_{/\!/}$	=	shear stress (in the plane of the throat) parallel to the axis of the weld
ϕ	=	resistance factor (associated with the LRFD or LSD method)
ϕ_w	=	resistance factor for welds
Ψ	=	local dihedral angle (angle between base metal fusion faces)
Ω	=	Safety factor

Chapter 1: INTRODUCTION

1.1. HOLLOW STRUCTURAL SECTIONS

Steel hollow structural sections (HSS) are wildly used in construction around the world. This is owed, in part, to their high strength-to-weight ratios, high radius of gyration-to-area ratios, and – hence – greater stiffness when compared to other steel products. These properties make HSS a cost-effective and efficient option for owners and constructors of many structures, including low-storey buildings, towers, bridges, and offshore platforms.

Since about the 1950s, the behaviour of HSS has been investigated under static loading, fire, for use in composite structures, and fatigue loading. Research results, coming from Canada and internationally, have been widely reported, and many of these have led to updates in national and international codes and guidelines, including the American Institute of Steel Construction's (AISC's) *Specification for Structural Steel Buildings* (AISC 360-16) (2016), Canadian Standard Association's (CSA's) *Design of Steel Structures,* (CSA S16:19) (2019), and Eurocode 3 Part 1-8: Design of joints (CEN 2018).

(a) (b)

Figure 1-1 Typical HSS structures: (a) bridges and (b) offshore platforms (Wardenier et al. 2010)

1.1.1. CONNECTIONS TO HSS

Connections to HSS are typically classified as either "directly welded" or "bolted", which each have unique advantages (for both manufacturing and design). Directly welded connections do not typically require additional materials, like gusset plates, and may hence save on fabrication cost. They are also considered more aesthetically pleasing. Bolted connections, on the other hand, require less skilled labour to make, and can be easily assembled on-site. Bolted connections are often desired for erection purposes. Planar, directly welded HSS connections (the focus of this thesis) can generally be classified as T-, Y-, X-, K- and N-connections, or some combination of these, as shown in Figure 1-2 (Packer & Henderson 1997).

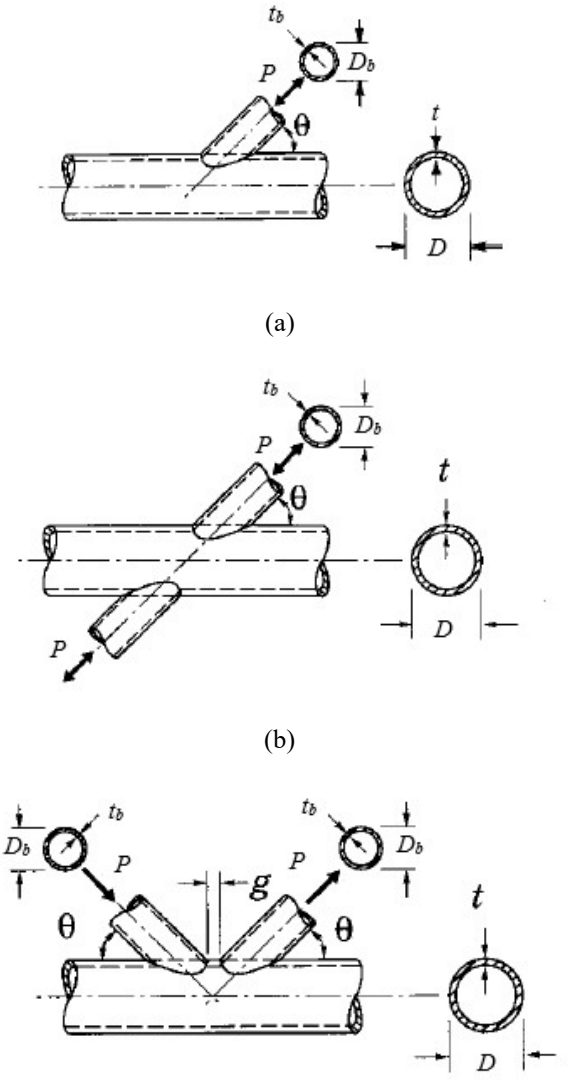

Figure 1-2 Different types of HSS connections: (a) T, Y; (b) cross (X) and (c) K (Packer & Henderson 1997)

As shown in Figure 1-2, the appearance of a connection can briefly help to classify (i.e., hint) at its type (e.g., T-connections look like "T"s, and K-connections look like "K"s); however, the true classification of an HSS connection is based solely on the mechanism of load transfer from each of the branches in the joint. According to AISC 360-16 (2016), HSS connections are classified as follows:

- T- or Y-connections are those in which the punching load in the branch member (normal to the chord) is predominantly equilibrated by beam shear in chord member;
- X-connections are those in which the punching load in the branch member is transmitted through the chord and equilibrated by other branch member(s) on the opposite side; and
- K- or N-connections are those in which the punching load in the branch member is essentially equilibrated by loads in other branch member(s) on the same side of the chord.

Regardless of classification, HSS connections are generally designed for axial load and/or in-plane/out-of-plane bending moment applied to the branch member(s). In other words, the connections capacity is expressed in terms of the brace member force(s). The limit states that must be considered in the design of HSS connections (under branch axial load or bending) include:

1. Plastification of the chord connecting face (termed "chord plastification" herein);
2. chord sidewall failure;
3. punching shear of the chord connecting face [termed "shear yielding (punching)" herein];
4. branch local yielding due to uneven load distribution;
5. shearing of the chord sidewalls;
6. shearing of the branch members, parallel to the chord connecting face;
7. local yielding of the chord;
8. distortional failure of the chord cross section under torsional loading; and
9. weld fracture.

Design resistance expressions for most of these limit states (i.e., limit states 1 to 7) are given in Packer et al. (2009), Wardenier et al. (2010), IIW (2012) and ISO 14346 (2013). Although written in different formats, these design recommendations/expressions are consistent with each other.

In the above-referenced design guides or standards/codes, the relevant limit state checks for different connection types and/or similar connection types with different non-dimensional parmaters are reduced in number. For example, from past research (e.g., Wardenier & Stark 1978; Kurobane et al. 1980; Kurobane 1981), limit state checks for K- and N-connections have been reduced to include only chord plastification (limit state 1), punching shear failure (limit state 3), tension failure or local buckling of the web member (due to uneven load distribution) (limit state 4), overall shear failure of the chord (limit state 5), and local buckling of the chord walls (limit state 2), whereas for T-connections, limit state checks include only chord plastification (limit state

1) and punching shear failure (limit state 3) (Packer & Henderson 1997) (i.e., these two limit states will only ever govern).

Several limit states are illustrated below, in Figure 1-3, for RHS-to-RHS K- and N-connections.

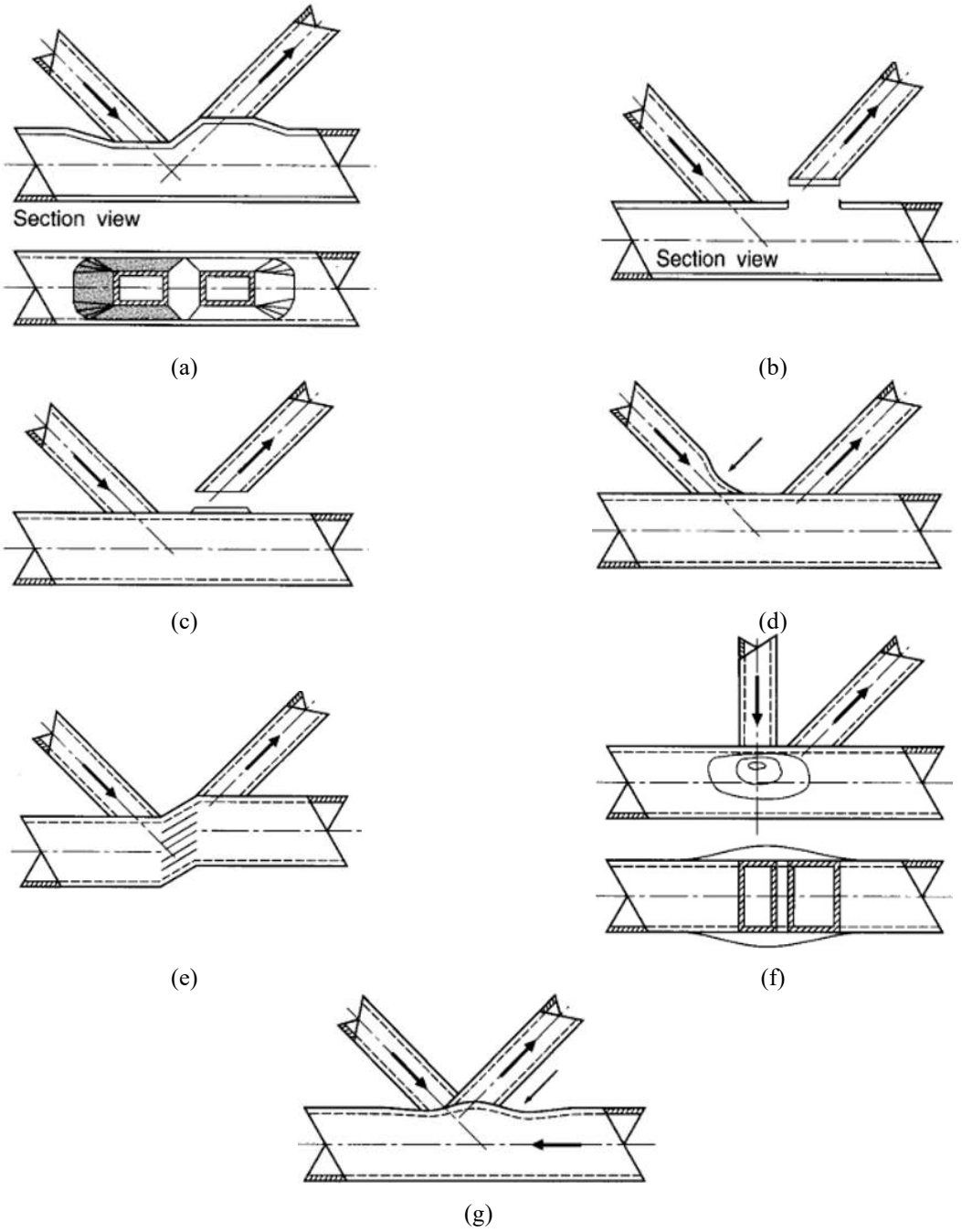

Figure 1-3 Failure modes for RHS-to-RHS K- and N-connections: (a) Plastic failure of chord face; (b) Punching shear failure; (c) Web tension failure; (d) Web local buckling; (e) Overall shear failure; (f) Chord wall local buckling and (g) Chord face local buckling (Packer & Henderson 1997)

1.1.2. WELD DESIGN PHILOSOPHY FOR HOLLOW SECTION CONNECTION

In relation to weld fracture (limit state 9 in Section 1.1.1), various international codes, standards, and design guides (e.g., Wardenier et al. 2008; Packer et al. 2009, 2010; ISO 2013; AISC 2016; CSA 2019) acknowledge two different design/sizing philosophies (for welds between HSS):

1. Method 1: The weld can be sized to develop the yield strength of the connected branch. (Using the yield strength of branch as the design strength of a fillet-welded joint produces an upper bound on the weld size.)
2. Method 2: The weld can be sized to resist the actual force(s) in the connected branch. [This method requires the use of "weld effective properties" (lengths or section moduli) for the weld group – to take into account the nonuniform load transfer that occurs through the weld around an HSS branch perimeter (Frater & Packer 1992a,b; Packer & Cassidy 1995; Packer & Sun 2011; McFadden & Packer 2014; Tousignant & Packer 2015a,b, 2017, 2018, 2019a,b, 2020; Yaghoubshahi et al. 2019)].

Method 1 is generally appropriate when the design force(s) in the branch, or the use of Method 2, are uncertain, or when plastic stress redistribution is required in the connection. Method 2, on the other hand, generally results in smaller weld sizes, which can increase connection efficiency and lower the cost of fabrication. Method 2 is also the basis of weld design rules for HSS connections in AISC 360-16 Chapter K, on which this thesis is primarily focussed.

Currently, AISC 360-16 Chapter K provides weld design rules for connections to RHS (and not CHS) members. Although, to date, a small amount of work has been completed to determine weld effective lengths in axially loaded CHS-to-CHS X-connections, by Tousignant and Packer (2017; 2018; 2019a,b; 2020a,b), and these results have been incorporated into the coming edition of the code, AISC 360-21 (AISC 2021). For all other connection types, including CHS-to-CHS moment T-connections, AISC 360 is noticeably silent.

1.2. RESEARCH PROGRAM OVERVIEW

An experimental program was hence developed at Dalhousie University to test various unreinforced CHS-to-CHS 90-degree T-connections under in-plane bending moment applied to the branch member. The objective of this study was to investigate the resistance of the welds around the branches (ergo, the weld effective section moduli) and the at the ultimate limit state. Twelve test specimens, with enough "chord end distance" (e) to eliminate the "end effects" (see Section 2.2.2), were designed to be weld-critical (i.e., to fail, intentionally, by weld fracture). The effect of key connection parameters known to influence weld strength, including branch-to-chord width ratio ($\beta = D_b/D$) (ranging from 0.31 to 0.91) and chord wall slenderness (D/t) (see Figure 1-2) (of 31, 34, 35, 38 and 46) was studied.

Herein:

- Chapter 2 summarizes various strength criteria for CHS-to-CHS moment T-connections, previous research performed on weld-critical RHS-to-RHS and CHS-to-CHS connections, the historical development of the "weld effective length" design approach/equations, and general methods used for design of fillet and partial-joint-penetration (PJP) groove welds according to various national standards (AISC 360, CSA S16, and EN 1993-1-8) (AISC 2016; CSA 2014, 2019; CEN 2018).
- Chapter 3 presents the details of the current test program.
- Results from the current test program are presented in Chapter 4.
- Chapter 5 provides a first-order reliability method (FORM) analysis of current and recommended design provisions in conjunction with the results from Chapter 4.
- Chapter 6 presents the conclusions and recommendations arising from this research, as well as recommendations for future work.

Chapter 2: BACKGROUND AND LITERATURE REVIEW

This chapter provides an overview of research and design guidance on directly welded CHS-to-CHS moment T-connections. Specific criteria for CHS-to-CHS moment T-connections according to AISC 360-16 are discussed, and previous research on weld effective properties for HSS-to-HSS connections [i.e., full-scale tests and finite element (FE) models] is described. A general overview of weld design according to AISC 360, CSA S16, and EN 1993-1-8 (AISC 2016; CSA 2014, 2019; CEN 2018) is also provided, for use in Chapter 4.

2.1. CHS MOMENT T-CONNECTION BEHAVIOUR, STRENGTH AND FLEXIBILITY

Research on directly welded CHS-to-CHS moment T-connections has shown that their behaviour, in terms of flexural strength and rigidity, is primarily affected by the branch-to-chord width ratio (β) and the chord wall slenderness (D/t) (Packer & Henderson 1997). Connections generally approach "rigid" (as opposed to "pinned") when the β ratio is large (approaching 1.0) and D/t is small but, otherwise, in the absence of stiffening, CHS-to-CHS moment T-connections are classified as "semi-rigid" (and "partial strength"), since they tend to be flexible and unable to develop the capacity of the connected branch member in flexure. In contrast, a "full-strength" connection is one that can resist a moment greater than the flexural capacity of the branch. These seldom exist with HSS connections.

Failure modes for CHS-to-CHS moment T-connections are similar to those for RHS-to-RHS moment T-connections (as well as some of those for RHS-to-RHS K- and N-connections, as described in Figure 1-3). As above, these are influenced by β and D/t, as well as the nonuniform normal stress distribution in the branch, adjacent to the weld. From AISC 360-16 Chapter K (AISC 2016), the limit states considered for CHS-to-CHS moment T-connections (excluding the weld) are:

1. chord plastification (Fig. 2.1a); and
2. shear yielding (punching) (Fig. 2.1b).

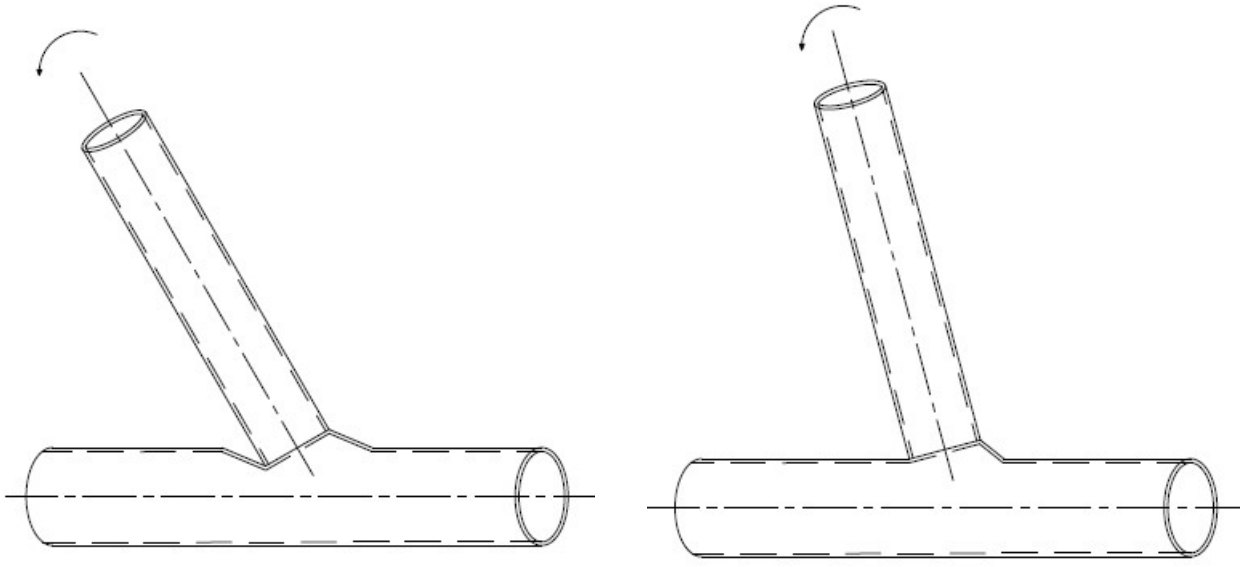

(a) (b)

Figure 2-1 Failure modes for CHS-to-CHS moment T-connections (a) chord face plastification and (b) cracking in the chord (punching shear)

2.2. STRENGTH OF CHS MOMENT T-CONNECTIONS

2.2.1. ACCORDING TO AISC 360-16

CHS-to-CHS moment T-connections are defined by AISC 360-16 (AISC 2016) as: "connections with one branch loaded by bending moment and welded along the perimeter of the branch contact with a continuous chord". As noted in Section 2.1, these connections can be considered "rigid" or "semi-rigid" depending on their non-dimensional parameters (β and D/t) and, hence, their flexibility.

In AISC 360-16 Chapter K, the in-plane flexural strength of CHS-to-CHS moment T-connections is given in Equation K4-1 (for the chord plastification limit state) and Equation K4-2 [for the shear yielding (punching) limit state] (see Figure 2-1). It is important to note, however, that AISC 360-16 includes two basic design methods that are used to consider connection strength (AISC 2016):

1. Allowable Stress Design (ASD): The nominal strength (or M_n, the nominal moment resistance) of the connection is calculated according to Table K4.1 of AISC 360-16 and divided by a safety factor (Ω), which results in an allowable strength that must be greater than or equal to the required strength calculated by using ASD load combinations (specified in the applicable code).
2. Load and Resistance Factor Design (LRFD): M_n of the connection is multiplied by a resistance factor (ϕ) that must be greater than or equal to the required strength calculated by using LRFD load combinations (specified in the applicable code).

The ASD method and LRFD methods are both acceptable for use in the United States; however, the LRFD method is more comparable to the Limit States Design (LSD) method that is currently utilized by the Canadian standard (CSA S16:19). Although only the LRFD method is discussed/used herein, the results of this research are applicable to both methods.

The LRFD resistance of a CHS-to-CHS moment T-connection is taken as the lowest value calculated from AISC 360-16 Table K4-1 (AISC 2016). Table 2-1 (below) shows the equations given therein for the nominal in-plane flexural strength ($M_{n\text{-}ip}$). The factored in-plane flexural strength (M_{ip}) is obtained by multiplying $M_{n\text{-}ip}$ (in the second column) by ϕ (in the third column) (i.e. $M_{ip} = \phi M_{n\text{-}ip}$). In addition, the centerline of the branch and chord member must lie in the same plane for the following AISC 360-16 Chapter K design criteria to apply.

Table 2-1 Strength of CHS-to-CHS moment T-connections according to AISC 360 (2016)

Limit State	$M_{n\text{-}ip}$	ϕ	Equation Number
Chord Plastification	$5.39F_y t^2 \gamma^{0.5} \beta D_b Q_f$	0.9	(2.1)
Shear Yielding (Punching)	$0.6F_y t D_b{}^2 (\frac{1+3\sin\theta}{4\sin^2\theta})$	0.95	(2.2)

where for chord (connecting surface) in compression:

$$Q_f = 1.3 - 0.4\frac{U}{\beta} \tag{2.3}$$

$$U = \left|\frac{P_{ro}}{F_c A_g} + \frac{M_{ro}}{F_c S}\right| \tag{2.4}$$

and for chord (connecting surface) in tension:

$$Q_f = 1.0 \tag{2.5}$$

where F_y = specified minimum yield stress of chord; D_b = outside diameter of round HSS member; t = thickness of wall of chord; γ = chord slenderness ratio (= $D/2t$); β = branch to chord diameter ratio (=D_b/D); θ = angle between branch and chord; Q_f = chord-stress interaction parameter; $P_{ro} = P_u$ (required axial strength in chord using LRFD load combination); $M_{ro} = M_u$ (required flexural strength using LRFD load combination); F_c = available stress in main member; A_g = gross area of member; S = elastic section modulus about the axis of bending; and U = utilization ratio. The geometric dimensions above are shown below, in Figure 2-2, for clarity.

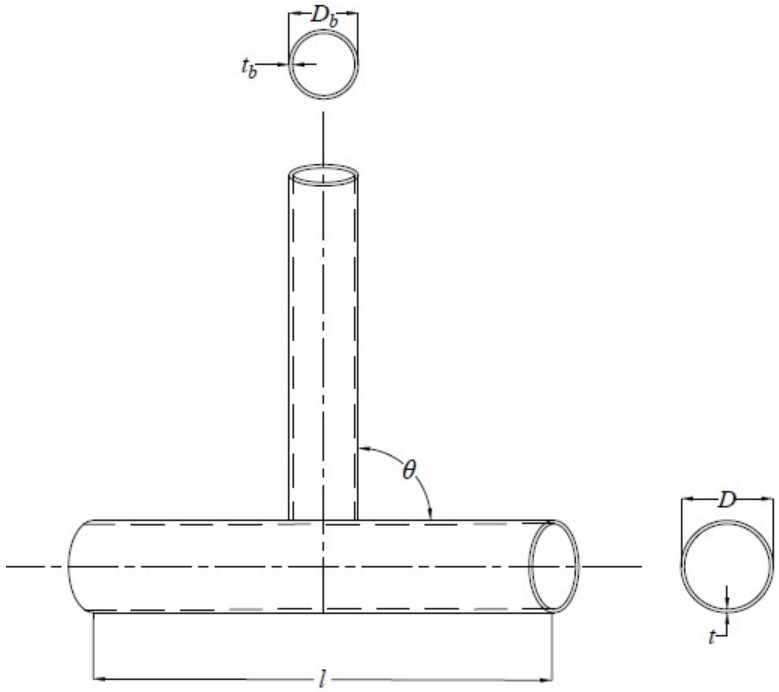

Figure 2-2 Geometric dimensions for CHS-to-CHS connections

Equations like those in Table 2-1 are also included in Canadian HSS design guide (Packer & Henderson 1997), which, despite being nearly 24 years old, is referenced from the Canadian steel code, CSA S16:19 (CSA 2019). For design according to both AISC 360-16 (AISC 2016) and CSA S16:19 (CSA 2019), the flexural strength of the branch member itself – and the weld (between the branch and the chord) – must also be calculated and checked against the factored loading.

2.2.2. Influence of End Effects

In addition to the above, research has shown that the capacity of an HSS connection can be influenced by its location relative to the end(s) of the chord and by the boundary conditions of the chord (Bolt et al. 1992; Choo et al. 2006; van der Vegte & Makino 2006, 2010; Fan & Packer 2017; Tousignant 2019). When the connection is close to the chord end, the strength of connection will no longer coincide with the equations in Table 2-1, due largely to a change in the chord stiffness under transverse loading. From prEN1993-1-8 Clause 9.1.2(10) (CEN 2018), this so-called "end effect" is related to both the distance from toe (end point of compression face) or heel (end point of tension face) of the closest branch to the end of the chord member, and the chord diameter. In prEN1993-1-8 Clause 9.1.2(10) (CEN 2018), the following requirement is specified to mitigate end effects:

"for joints with a chord end not connected to other members, the chord end shall be at a distance of at least $(2\gamma/10)D$ from the heel or toe of the closest brace, with a minimum of $2.5D$…otherwise, the end shall be welded

to a cap plate with a thickness of at least 1.5*t*, at a minimum distance of 0.5*D*(1 – β)…from the brace toe or heel…"

This requirement was transcribed from a minimum α requirement [where α= chord length parameter (= *2l/D*) and *l* = chord length] based on research by van der Vegte and Makino (2006, 2010), and hence implies:

$$\alpha_{\min} = \max(0.8\gamma, 10) \tag{2.6}$$

In relation to this research, previous work by Tousignant (2019), which looked at the effect of chord boundary conditions on welds in CHS-to-CHS X-connections under axially loading, showed that there is a range in which $\alpha < \alpha_{min}$ given by Equation 2.6 [Eq. (4) in Figure 2.3] has a small or negligible influence on weld strength (as shown in Figure 2-3). This is considered in the test specimen design, discussed in Chapter 3, and serves as a limitation of the current "weld effective property" framework (see Section 2.4).

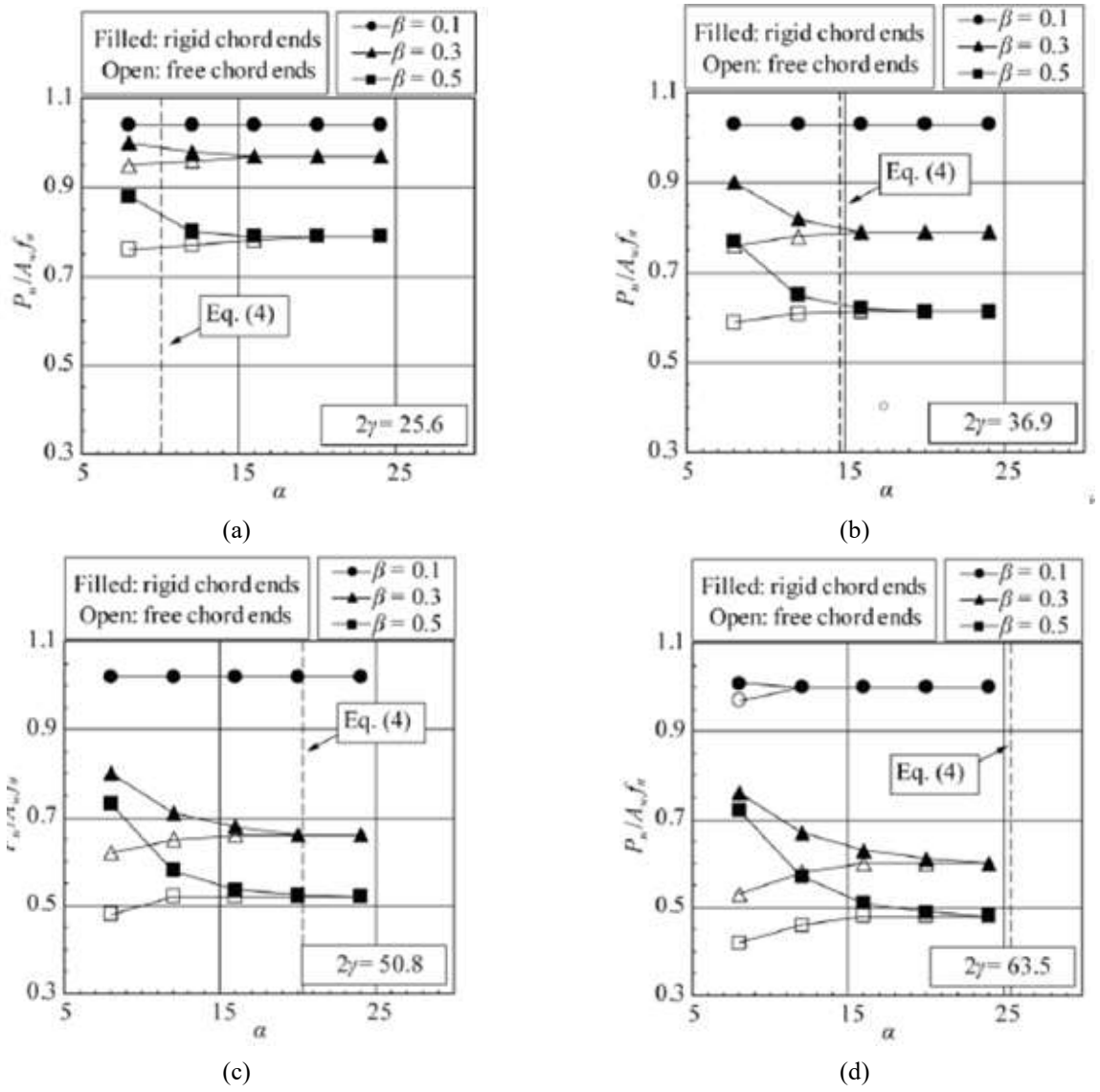

Figure 2-3 α and the magnitude of end effect on axially loaded CHS-to-CHS T-connections (Tousignant 2019)

2.3. DESIGN OF FILLET AND PJP GROOVE WELDS

Design criteria for fillet and PJP welds have been investigated for some time, and much test data now exists/has been produced through experimental research. However, fillet and PJP welds in HSS-to-HSS connections are known to be a unique case, in which non-uniform stress along the perimeter of branches create a "weld effective length" phenomenon – a shear-lag effect, that can lead to premature fracture.

The following section discusses the design of fillet and PJP welds in "simple joints" according to various national and international steel codes, specifications, and guidelines – as well as some previous research that sheds light on the inherent conservatism of these approaches. In Section 4, the background and application of AISC 360-16 Chapters J and K to welds in HSS-to-HSS connections are discussed.

2.3.1. AISC 360-16

The design strength of a fillet, partial joint penetration (PJP) or complete-joint penetration (CJP) welded joint (Equation 2.7, 2.8) is taken as the product of the nominal weld strength (F_{nw}) and the effective area of the weld (A_{we}). According to AISC 360-16 Equations (J2-4) and (J2-5), for fillet welds:

$$R_n = F_{nw} A_{we} = 0.60 F_{EXX} (1.0 + 0.5 \sin^{1.5} \theta) A_{we} \tag{2.7}$$

for PJP welds, Table J2.5 given:

$$R_n = F_{nw} A_{we} = 0.60 F_{EXX} A_{we} \tag{2.8}$$

where the effective area (A_{we}) of a weld is defined as the effective weld length l_e (which discussed in Section 2.4) multiplied by the effective weld throat (t_w) (i.e., the shortest distance from the root to the face of the diagrammatic weld, for fillet welds); R_n = nominal strength; F_{nw} = nominal stress of the weld metal; A_{we} = effective area of weld; F_{EXX} = filler metal classification strength; and θ = angle between the load and the weld longitudinal axis.

For PJP groove welds, the Structural Welding Code, AWS D1.1-15, Clause 3 Figure 3.2 (AWS 2015) states that the effective throat is the shortest distance from the root to the face of a diagrammatic weld (i.e., the same as for fillet welds). This is also stated in CSA W59-19 Clause 4.3.1 and Figure A.1 (CSA 2018).

For fillet welds, the 0.60 factor in Equation 2.7 implies that the failure mode is by shear rupture along the plane of the effective throat; however, for PJP groove welds, it is an arbitrary reduction factor that has been in effect since the early 1960s to compensate for the notch effect of the unfused area of the joint; it does not imply that the failure mode (in tension) is shear rupture. Because lengths were taken to establish a high degree of certainty with respect to the fusion area (see Chapter 3), a more suitable factor of 1.00 is used herein (for PJP welds).

2.3.2. CSA S16-14

Prior to 2019, the factored resistance for direct shear and tension- or compression-induced shear (Vr) in fillet welds was given, by CSA S16-14 (CSA 2014), as:

$$V_r = \phi_w F_{nw} A_w = 0.67 \phi_w X_u (1.0 + 0.5 \sin^{1.5} \theta) M_w A_w \quad (2.9)$$

where ϕ_w = resistance factor of weld; X_u = ultimate strength of weld metal (= F_{EXX}); M_w = strength reduction factor for multi-orientation fillet welds and A_w = effective throat area of a weld.

For PJP and CJP welds, CSA S16-14 (CSA 2014) includes two limit states, which are based on failure of the weld along: (i) the fusion face with the base metal and (ii) the plane of the effective weld throat. For limit state (i) for PJP welds, the ultimate strength of its base metal (branch member, for HSS) is used to calculate the strength of the fusion face, i.e.:

$$V_r = 0.67 \phi_w A_m F_u \quad (2.10)$$

where F_u = specified minimum tensile strength; and A_m = area of fusion face.

For limit state (ii) for PJP welds, the strength of the joint is determined by using the strength of the weld metal, assuming failure occurs along the effective weld throat. For PJP welds subjected to shear:

$$V_r = \phi_w A_w F_{nw} = 0.67 \phi_w A_w X_u \quad (2.11)$$

For PJP welds subjected to tension, the factored resistance (for design) is calculated based on the strength of the base metal. This criterion is not considered suitable for the research herein, however, since failure of the test specimens was always in the weld (see Chapter 3).

2.3.3. CSA S16:19

According to CSA S16:19 (CSA 2019), for fillet welds:

$$V_r = \phi_w F_{nw} A_w = 0.67 \phi_w A_w X_u \quad (2.12)$$

However, CSA S16:19 (CSA 2019) also states: “For cases other than single-sided fillet welds connected to an element in tension, the fillet weld resistance may be multiplied by the following strength-enhancement factor ($1.00 + 0.50 \sin^{1.5}\Theta$). For fillet weld groups concentrically loaded and consisting of weld segments in different orientations, the strength of each weld segment shall be multiplied by the reduction factor, M_w, given as 1.0 for the weld segment with the largest θ and 0.85 for the other weld segments.”

According to this statement, fillet welds in CHS-to-CHS moment T-connections, do not meet the requirement for use of the controversial “strength-enhancement” factor ($1.00 + 0.50 \sin^{1.5}\Theta$). The resistance of fillet welds should hence be taken as the resistance given by Equation 2.12, with appropriate modifications for bending using the weld effective section modulus, as discussed by Tousignant & Packer (2020), and later on in this thesis.

For PJP or CJP welds, CSA S16:19 (CSA 2019) includes the same two limit states noted above for CSA S16-14 (CSA 2014) (Equation 2.10 and 2.11).

2.3.4. prEN1993-1-8:2018

This section compares the two design methods used for determining the resistance of welds according to European standard, prEN-1993-1-8 (CEN 2018): the directional method and the simplified method.

For the directional method, the applied force on the weld is resolved into normal stresses perpendicular to the throat ($\sigma_{\perp}$) and parallel to the longitudinal axis ($\sigma_{\parallel}$), and shear stresses perpendicular to the plane of the throat ($\tau_{\perp}$) and parallel to the axis of the weld ($\tau_{\parallel}$) (CEN 2018). All stresses are assumed to act uniformly along the design throat area. For a load acting on an HSS branch, the resultant normal stresses and shear stresses acting on the effective throat plane are shown in Figure 2-4 (CEN 2018).

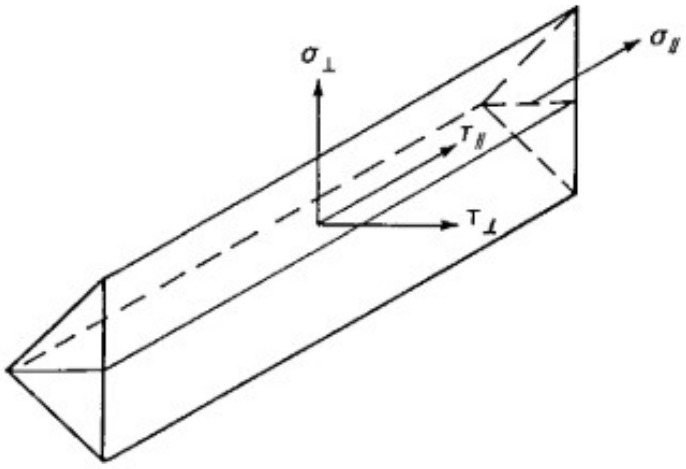

Figure 2-4 Stresses acting on the design throat area of a fillet weld (CEN 2018)

According to prEN 1993-1-8, Equations 2.13 and 2.14 below (Equation 4.1 of EN1993-1-8) give the required design resistance of a fillet weld (CEN 2018):

$$\sqrt{\sigma_{\perp}^2 + 3(\tau_{\perp}^2 + \tau_{\parallel}^2)} \le f_u / (\beta_w \gamma_{M2}) \tag{2.13}$$

$$\sigma_{\perp} \le 0.9 f_u / \gamma_{M2} \tag{2.14}$$

where f_u = nominal tensile strength of the weaker section; β_w = correlation factor for fillet welds which is shown in Table 2-2; γ_{M2} = safety factor for the resistance, taken as 1.25 (CEN 2018).

Table 2-2 Correlation factor for fillet welds according to prEN-1993-1-8 (2018)

Standard and steel grade			Correlation factor
EN 10025 (hot rolled)	EN 10210 (hot finished)	EN 10219 (cold-formed)	
S 235 S 235 W	S 235 H	S 235 H	0.8
S 275 S 275 N/NL S 275 M/ML	S 275 H S 275 NH/NLH	S 275 H S 275 NH/NLH S 275 MH/MLH	0.85
S 355 S 355 N/NL S 355 M/ML S 355 W	S 355 H S 355 NH/NLH	S 355 H S 355 NH/NLH S 355 MH/MLH	0.9
S 420 N/NL S 420 M/ML		S 420 MH/MLH	0.88
S 460 N/NL S 460 M/ML S 460 Q/QL/QL1	S 460 NH/NLH	S 460 NH/NLH S 460 MH/MLH	0.85

The simplified method of EN 1993-1-8 (CEN 2018) is an alternative to the directional method, in which the required weld strength is given as (CEN 2018):

$$F_{w,Ed} \leq F_{w,Rd} \tag{2.15}$$

$$F_{w,Rd} = f_{vw,d}\, a \tag{2.16}$$

$$f_{vw,d} = \frac{f_u / \sqrt{3}}{\beta_w \gamma_{M2}} \tag{2.17}$$

where $F_{w,Ed}$ = design value of the weld force per unit length; $F_{w,Rd}$ = design weld resistance per unit length; $f_{vw,d}$ = design shear strength of the weld.

The simplified method is different from the directional method because, in the former, it is assumed that the direction of the applied force does not affect the weld resistance. According to both methods, welds can be sized by proportioning the weld such that its resistance per unit length ($F_{w,Rd}$) is greater than or equal to the resultant force per unit length that it is required to transmit ($F_{w,Ed}$).

According to prEN 1993-1-8 (CEN 2018), for PJP welds, the weld resistance is calculated the same as for fillet welds, where the effective weld throat area (per unit length) is the same as that given for deep penetration fillet welds (i.e., the minimum distance from the root to the face of the diagrammatic weld).

2.4. Recent Research on the Strength of Fillet and PJP Welds

The weld strength based on CSA, AISC, and prEN 1993-1-8 includes several factors to reduce or increase the weld resistance and/or to convert the tensile strength of an electrode (X_u or F_{EXX}) to shear strength. From Equation 2.7 to 2.12, it can be found that the latter factor (i.e., shear-to-ultimate strength ratio) is 0.6 for AISC

and 0.67 for CSA, and there are some discrepancies with respect to the use of the sinθ factor between these codes.

Research done by Tousignant and Packer (2017), on the other hand, has shown that, for HSS connections, these factors, in fact, change with branch thickness and weld size (Tousignant & Packer 2017). They showed that for CHS-to-CHS connections, under axial load, fillet weld strength is well described by Equation 2.18:

$$V_r = \phi_w F_{nw} A_w = \phi_w \left[0.984 - 0.226 \left(\frac{t_w}{t_b} \right) \right] X_u A_w \tag{2.18}$$

where t_w = effective weld throat thickness; and t_b = branch wall thickness.

Since the parameter F_{nw}, above, is based on the wall thickness and effective weld throat, it winds up being different for all test specimens/connections discussed in Chapter 4.5 of this research. For the equivalent equations in CSA S16 and AISC 360, F_{nw} (the weld failure stress) is effectively constant.

As highlighted, the factor above does not apply to PJP-welded specimens, and in design codes, "F_{nw}" for these connections are riddled by several simplifications, which make them quite conservative. In fact, recent research, by Luo et al. (2020), highlighted the presence of a directional increase factor (DIF) for PJP welds (which are inherently single-sided) that is similar to that used for double-sided fillet welds. The DIF was also found to be a function of loading angle (θ), and the type of connection (T-joint vs. B-joint) (see Figure 2-5, where S_1 = weld size along the branch direction and a = effective weld throat thickness = t_w).

(a) (b)

Figure 2-5 Typical macro etched specimens: (a) PJP-T joint and (b) PJP-B joint (Luo et al. 2020)

Test specimens in the experiments by Luo et al. (2020) had loading angles between 90° and 155.5°, from which the following equation(s) for the weld resistance (for PJP-T joints) can be derived:

$$V_r = \phi_w F_{nw} A_w (\text{DIF}) \tag{2.19}$$

$$\text{DIF} = 1 + 0.629\theta + 0.068\theta^2 \tag{2.20}$$

The weld failure stress (F_{nw}) can be deduced from the above equation(s).

In this research, the joint type for all PJP-welded connections is considered to be "PJP-T" (see Chapter 3), and subject to failure at a loading angle of $\theta = 90°$.

2.5. WELD EFFECTIVE PROPERTIES FOR HSS CONNECTIONS

Weld-critical tests, in which weld fracture was designed to occur, have been used in the study of HSS connections and trusses (Frater & Packer 1992a, b; Packer & Cassidy 1995) over the last 30 years. These have led to the development of a "fit-for-purpose" approach to weld design for HSS connections (IIW 2012; ISO 2013). This approach (Method 2, described in Section 1.1.2) is based on using the actual force in the branch member to proportion the weld, rather than proportioning the weld to develop the branch yield strength. As discussed previously, it requires the use of so-called "weld effective lengths" or "weld effective section moduli" to account for the non-uniform distribution of stress on the weld, to prevent premature rupture.

Weld effective lengths and section moduli have been developed for a number of axially loaded RHS-to-RHS connections, including T-, Y-, X-, gapped and overlapped K-connections, as well as RHS-to-RHS moment T-connection (Frater & Packer 1992a,b; Packer & Cassidy 1995; McFadden & Packer 2014; Tousignant & Packer 2015), with recommendations from this research now forming the basis of HSS weld design criterion in AWS D1.1-15 (AWS 2015) and AISC 360-16 (AISC 2016).

In AISC 360-16 Chapter K5, Method 2 is devoted for RHS-to-RHS connections; a similar design method, for CHS-to-CHS connections, is conspicuous by its absence. While, recommendations for weld effective lengths in axially loaded CHS T-, Y-, and X-connections for AISC 360 (AISC 2016) (Tousignant & Packer 2019a), CSA S16-19 (Tousignant & Packer 2020b), and Eurocode 4 (Tousignant & Packer 2020a) have been recently developed, with the former now include in AISC 360-16 Table K5.2 (2016), a considerable amount of work is still needed in order for Table K5.2 to match Table K5.1 (for RHS) in its coverage. The following section summarizes the "weld effective property" design approach for HSS connections in AISC 360-16, and its historical development.

2.5.1. DESIGN APPROACH ACCORDING TO AISC 360-16

According to AISC 360-16 Section K5, the available strength of branch connections shall be determined considering the nonuniformity of load transfer along the line of weld, due to differences in relative stiffness of HSS walls in HSS-to-HSS connections and between elements in transverse plate-to-HSS connections, as follows:

$$P_n \ or \ R_n = F_{nw} t_w l_e \tag{2.21}$$

$$M_{n-ip} = F_{nw} S_{ip} \tag{2.22}$$

$$M_{n-op} = F_{nw} S_{op} \tag{2.23}$$

where $P_n = R_n$ = nominal resistance of connection; S_{ip} = effective elastic section modulus of welds for in-plane bending; S_{op} = effective elastic section modulus of welds for out-of-plane bending; $M_{n\text{-}ip}$ = nominal flexural strength for in-plane bending; $M_{n\text{-}op}$ = nominal flexural strength for out-of-plane bending.

2.5.2. Historical Development of Weld Effective Property Equations

2.5.2.1. RHS-to-RHS T-, Y- and X-Connections

Packer and Cassidy (1995) tested 16 full-scale, weld-critical connections to develop an equation for the weld effective length in RHS-to-RHS T-, Y-, and X-connections with different branch angles. The equation proposed by Packer and Cassidy (1995), which was later verified and improved by McFadden and Packer (2013), is shown in Equation 2.24 and included in AISC 360 (2016) Table K5.1.

$$l_e = \frac{2H}{\sin\theta} + 2B_e \tag{2.24}$$

$$B_e = \left(\frac{10t}{B}\right)\left(\frac{F_y t}{F_{yb} t_b}\right) B_b \le B_b \tag{2.25}$$

where H = overall height of the rectangular HSS member; B_b = overall width of rectangular HSS branch; B_e = effective width of rectangular HSS branch.

2.5.2.2. RHS-to-RHS Gapped K- and N-Connections

Weld effective lengths for gapped K- and N-connections were developed by Frater and Packer (1992a, b) and included in AISC 360-16 (2016); these equations were subsequently verified by Tousignant and Packer (2020b). The equations cover branch inclination angles of $\theta \le 50°$ and $\theta \ge 60°$, with linear interpolation recommended when $50° < \theta < 60°$.

- For $\theta \leqslant 50°$:

$$l_e = \frac{2(H_b - 1.2t_b)}{\sin\theta} + 2(B_b - 1.2t_b) \tag{2.26}$$

- For $\theta \geqslant 60°$:

$$l_e = \frac{2(H_b - 1.2t_b)}{\sin\theta} + B_b - 1.2t_b \tag{2.27}$$

2.5.2.3. RHS-to-RHS Overlapped K- and N-connections

Weld effective lengths for RHS-to-RHS overlapped K-connections have been shown to relate to the overlap (O_v), and are hence discretized for $25\% \leq O_v < 50\%$, $50\% \leq O_v < 80\%$, and $80\% \leq O_v \leq 100\%$ in AISC 360-16 Equation K5-10, K5-11, and K5-12 (AISC 2016) (shown in Equation 2.28 to 2.30). Experiments done by Tousignant and Packer (Tousignant & Packer 2015) have shown the AISC equations (Equation 2.28 to 2.30) are conservative.

- For $25\% \leqslant O_v < 50\%$:

$$l_e = \frac{2O_v}{50}\left[\left(1 - \frac{O_v}{100}\right)\frac{H_{bi}}{\sin\theta_i} + \frac{O_v}{100}\frac{H_{bi}}{\sin(\theta_i + \theta_j)}\right] + B_{ei} + B_{ej} \tag{2.28}$$

- For $50\% \leqslant O_v < 80\%$:

$$l_e = 2\left[\left(1 - \frac{O_v}{100}\right)\frac{H_{bi}}{\sin\theta_i} + \frac{O_v}{100}\frac{H_{bi}}{\sin(\theta_i + \theta_j)}\right] + B_{ei} + B_{ej} \tag{2.29}$$

- For $80\% \leqslant O_v \leqslant 100\%$:

$$l_e = 2\left[\left(1 - \frac{O_v}{100}\right)\frac{H_{bi}}{\sin\theta_i} + \frac{O_v}{100}\frac{H_{bi}}{\sin(\theta_i + \theta_j)}\right] + B_{bi} + B_{ej} \tag{2.30}$$

where O_v = overlap connection coefficient; H_{bi} = overall height of rectangular HSS branch overlapping member; B_{ei} = effective width of rectangular HSS branch overlapping member; B_{ej} = effective width of rectangular HSS branch overlapped member; B_{bi} = overall width of rectangular HSS branch overlapping member; θ_i = branch to chord incline angle of overlapping member; θ_j = branch to chord incline angle of overlapped member.

2.5.2.4. CHS-to-CHS T-, Y- and X-connections

For CHS-to-CHS connections, Tousignant and Packer (2018) found that the branch slenderness (D/t), branch-to-chord ratio (β) and branch-to-chord thickness ratio (τ) affect the ratio of the effective-to-total weld length (l_e/l_w) (Tousignant & Packer 2018). The branch inclination angle (θ), on the other hand, does not change the effective length significantly; however, it does affect the total weld length.

Using experiments and FE modeling, the effective weld length in CHS-to-CHS T-, Y- and X-connections with $0 \leq \beta \leq 0.50$ and $60° \leq \theta \leq 90°$ was found to be as shown in Equation 2.31 and 2.32 (Tousignant & Packer 2019a). The effective weld length (l_e) implied by Equation 2.31 is illustrated in Figure 2-6.

$$l_e = \frac{4}{\sqrt{2\beta(D/t)}} l_w \leq l_w \tag{2.31}$$

$$l_w = \pi D_b \frac{1+1/\sin\theta}{2} \tag{2.32}$$

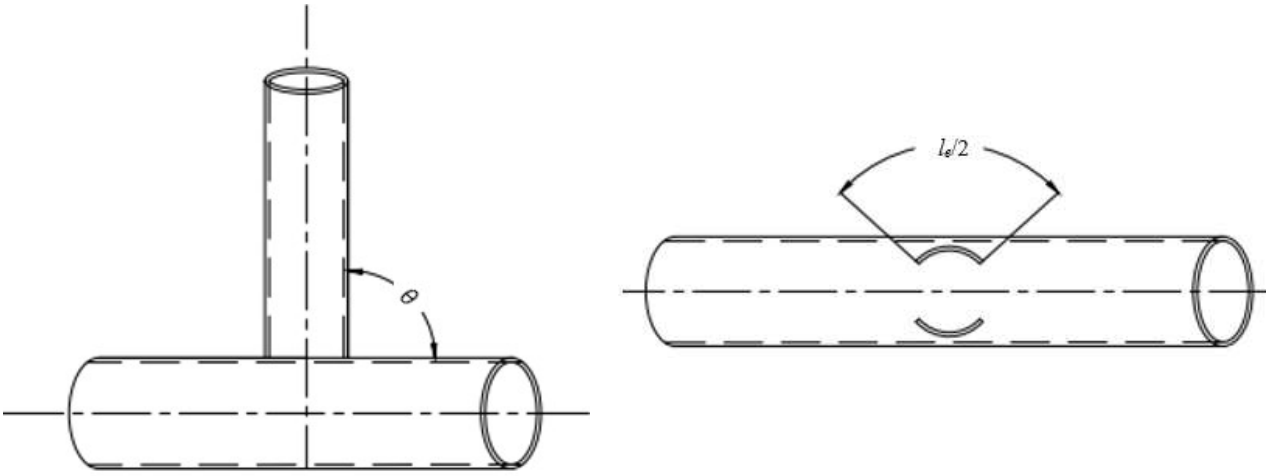

(c) (d)

Figure 2-6 Weld effective length terminology for T-, Y-, and X- (Cross-) connections under branch axial load or bending

2.5.2.5. RHS-to-RHS Moment T-, Y- and X-Connections

In AISC 360-16 (AISC 2016), weld effective section moduli for RHS-to-RHS T-, Y- and X-connections subjected to in-plane and out-of-plane bending are given by Equations K5-6 and K5-7 (Equation 2.33 and 2.34), respectively, i.e.:

$$S_{ip} = \frac{t_w}{3}\left(\frac{H_b}{\sin\theta}\right)^2 + t_w B_e \left(\frac{H_b}{\sin\theta}\right) \tag{2.33}$$

$$S_{op} = t_w \left(\frac{H_b}{\sin\theta}\right) B_b + \frac{t_w}{3} B_b^{\,2} - \frac{(t_w/3)(B_b - B_e)^3}{B_b} \tag{2.34}$$

These equations are derived from the weld effective length equations, presented previously (Equation 2.27), in the manner shown by Equations 2.38 to 2.41:

$$I_{ip} = 2\left[\frac{t_w}{12}\left(\frac{H_b}{\sin\theta}\right)^3 + t_w B_e \left(\frac{H_b}{2\sin\theta}\right)^2\right] \tag{2.38a}$$

$$= \frac{t_w}{6}\left(\frac{H_b}{\sin\theta}\right)^3 + \frac{1}{2} t_w B_e \left(\frac{H_b}{\sin\theta}\right)^2 \tag{2.38b}$$

$$S_{ip} = I_{ip} / \left(\frac{H_b}{2\sin\theta}\right) \tag{2.39}$$

$$I_{op} = 2[\frac{t_w}{12}(B_b)^3 - \frac{t_w}{12}(B_b - B_e)^3 + t_w(\frac{H_b}{\sin\theta})(B_b / 2)^2] \quad (2.40a)$$

$$= \frac{t_w}{6}B_b^3 + \frac{t_w}{6}(B_b - B_e)^3 + \frac{t_w}{2}(\frac{H_b}{\sin\theta})B_b^2 \quad (2.40b)$$

$$S_{op} = I_{op} / (\frac{B_b}{2}) \quad (2.41)$$

where I_{ip} = moment of inertia of the HSS about in-plane bending; I_{op} = moment of inertia of the HSS about out-of-plane bending.

The effective section modulus for welds in CHS-to-CHS connections, for both in-plane and out-of-plane bending (S_{ip} and S_{op}), is derived, as part of this work, in Section 4.2.

2.6. COMMENTS AND SUMMARY

Based on the results from research on HSS connections on effective weld properties and moment connections, it is well-known that:

1. the distribution of normal stress (ergo strain) adjacent to the welded joint in HSS connections is non-uniform, which generally causes the weld to be partially effective.
2. The effective weld length and effective weld section moduli are related to each other; and
3. national or international codes (including AISC 360) do not include weld effective section modulus equations for CHS-to-CHS moment connections.

Moreover, the effective weld properties of RHS-to-RHS connections are defined by Equation K5-5, K5-6, K5-7, K5-8, and K5-9 of AISC 360-16 (AISC 2016) (Equation 2.28 to 2.29, and 2.36 to 2.37, above) have been proven by research.

The effective weld length equation derived for CHS-to-CHS moment T-connections (Equation 2.34), which is now adopted in the next edition of AISC 360, Table K5.2 (AISC 2021; Tousignant & Packer 2019a) has been substantiated by testing and FE analysis. This equation provides the necessary information with which a rational weld effective section modulus equation can be developed; however, at present, no experimental evidence, in the form of weld-critical on CHS-to-CHS moment T-connections, exists to substantiate it. Chapter 3 discusses an experimental program aimed at developing these necessary results.

Chapter 3: EXPERIMENTAL PROGRAM

3.1. SCOPE

An experimental program was developed at the Dalhousie University to test various CHS-to-CHS moment T-connection under branch in-plane bending. Twelve test specimens, with enough end distance to eliminate the "end effects" (see Section 2.2.2), were designed with variations in branch-to-chord width ratio (β) (varying from 0.31 to 0.91) and chord wall slenderness (D/t) (31, 34, 35, 38 and 46) to be weld-critical.

Since welds were expected to undergo non-uniform loading, normal strain in the branch, adjacent to the weld, was measured by using strain gauges which oriented longitudinally along with the branch member at uniform spacing increments around the branch perimeter. To induce the bending moment in the connection, a 500-kN capacity MTS actuator mounted to a steel support frame was used to apply a lateral point load to the top of each branch member. Tensile coupon tests and geometric measurements on/of both the CHS (base metal) and weld metal were also done to determine the exact properties of the specimens.

3.2. DESIGN PROCEDURE OF WELD-CRITICAL CONNECTIONS

Twelve test specimens were designed using cold-formed ASTM A500 Grade C CHS (ASTM 2018) (with a nominal yield strength of F_y = 317 MPa) to be weld critical. Their geometric properties and key parameters that influence the weld or connection under in-plane bending moment, β and D/t, were selected based on experimental needs and available material from the supplier, Atlas Tube. Nominal wall thicknesses of 9.5 mm (0.375 in) and 13 mm (0.5 in) was selected for chords, while a nominal wall thickness of 9.5 mm (0.375 in) was selected for all branches. The outside diameters of chords and branches were selected as 127 mm (5 in), 273 mm (10.75 in), 324 mm (12.75 in), 356 mm (14 in) and 406 mm (16 in), to produce a reasonable spread in β and D/t while reducing the total number of sections required. The nominal dimensions and key parameters (i.e. β and D/t) of each individual test specimen are shown in Table 3-1, and the general configurations for the welds (which included fillet and PJP welds) are shown in Figure 3-1.

Table 3-1 Test specimen details and key parameters

Experimental Designation	Branch Designation (HSS)		Chord Designation (HSS)		β	D/t	α	τ
	Metric	Imperial	Metric	Imperial				
T273-127-1P	127 x 9.5	5 x 0.375	273 x 9.5	10.75 x 0.375	0.47	16	12.38	1.0
T273-127-1	127 x 9.5	5 x 0.375	273 x 9.5	10.75 x 0.375	0.47	16	12.38	1.0
T324-127-1	127 x 9.5	5 x 0.375	324 x 9.5	12.75 x 0.375	0.39	19	13.96	1.0
T356-127-1	127 x 9.5	5 x 0.375	356 x 9.5	14 x 0.375	0.36	21	15.28	1.0
T356-273-1P	273 x 9.5	10.75 x 0.375	356 x 9.5	14 x 0.375	0.77	21	15.28	1.0
T356-324-1P	324 x 9.5	12.75 x 0.375	356 x 9.5	14 x 0.375	0.91	21	15.28	1.0
T406-127-1	127 x 9.5	5 x 0.375	406 x 9.5	16 x 0.375	0.31	24	18.31	1.0
T406-273-1P	273 x 9.5	10.75 x 0.375	406 x 9.5	16 x 0.375	0.67	24	18.31	1.0
T406-324-1P	324 x 9.5	12.75 x 0.375	406 x 9.5	16 x 0.375	0.80	24	18.31	1.0
T406-127-0.7	127 x 9.5	5 x 0.375	406 x 13	16 x 0.5	0.31	18	13.79	0.7
T406-273-0.7P	273 x 9.5	10.75 x 0.375	406 x 13	16 x 0.5	0.67	18	13.79	0.7
T406-324-0.7P	324 x 9.5	12.75 x 0.375	406 x 13	16 x 0.5	0.80	18	13.79	0.7

Note: Test specimens with $\beta \leq 0.47$ are fillet welded at the connection while test specimens with $0.47 \leq \beta$ are partial joint penetration (PJP) welds and their general configurations show in Figure 3-1 (a) and (b) respectively.

(a) (b)

Figure 3-1 CHS-to-CHS moment T-connection weld configurations: (a) fillet weld and (b) PJP weld

It is important to note that the local dihedral angle (Ψ), which is shown in Figure 3-2, can impede the use of welds with full root penetration when it is less than 30° or exceeds 120° (AWS 2020). Both AWS D1.1 and CSA W59 state a limitation on this range of 60° to 120° (CSA 2018; AWS 2020). Since all branches in this research are perpendicular to the chord, the lower bound of the range is not a concern; the maximum local dihedral angle, on the other hand, occurs at the saddle point of the connections (as shown in Figure 3-2, again).

Research by Luvites and Post has shown that the branch-to-chord diameter ratio β must not exceed 0.5 for 90° CHS-to-CHS T-connections if fillet welds are to be used with $\Psi < 120°$ (Luvties & Posts 1988). Hence, this is the approach adopted in this research (i.e., all fillet welded connections have $\beta < 0.5$). For PJP welds, local dihedral angle Ψ is less important, since the chord can be bevelled to enable good penetration.

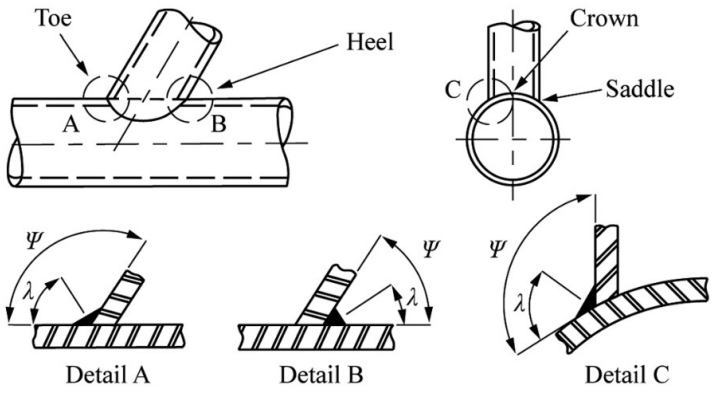

Figure 3-2 Local dihedral angle in CHS-to-CHS connections (Tousignant & Packer 2020a)

Once the branches and chords were "matched up", the specimens were designed to be weld-critical by, first, calculating the member resistance and the connection resistance (using the equations in Table 2-1) and, hence, the corresponding flexural strength for each branch (AISC 2016). For this phase of the project (i.e. design of the test specimens), all results from above calculations were taken as the nominal resistance(s) based on the LRFD method of AISC 360-16 (i.e., with resistance factor, ϕ = 1). The calculated strengths and governing limit states (not including weld rupture) for each specimen are shown in Table 3-2. Sample calculations using the AISC equations with exact CHS dimensions and material properties are provided in Appendix A.

Table 3-2 LRFD flexural resistance for CHS-to-CHS moment T-connections based on nominal properties

Experimental Designation	Chord Plastification: Equation 2.1		Punching Shear: Equation 2.2		Branch Flexure: $M_{n\text{-}ip}=F_{yb}S$		Governing Limit State (omitting weld fracture)
	kN-m	kip-ft	kN-m	kip-ft	kN-m	kip-ft	
T273-127-1P	29.64	21.86	**26.32**	**19.41**	38.36	28.29	Punching Shear
T273-127-1	29.64	21.86	**26.32**	**19.41**	38.36	28.29	Punching Shear
T324-127-1	27.21	20.07	**26.32**	**19.41**	38.36	28.29	Punching Shear
T356-127-1	**25.97**	**19.16**	26.32	19.41	38.36	28.29	Chord Plastification
T356-273-1P	**120.10**	**88.58**	121.71	89.77	190.52	140.52	Chord Plastification
T356-324-1P	**168.93**	**124.60**	171.21	126.28	270.40	199.44	Chord Plastification
T406-127-1	**24.29**	**17.92**	26.32	19.41	38.36	28.29	Chord Plastification
T406-273-1P	**112.34**	**82.86**	121.71	89.77	190.52	140.52	Chord Plastification
T406-324-1P	**158.02**	**116.55**	171.21	126.28	270.40	199.44	Chord Plastification
T406-127-0.7	37.35	27.55	**35.06**	**25.86**	38.36	28.29	Punching Shear
T406-273-0.7P	172.73	127.40	**162.14**	**119.59**	190.52	140.52	Punching Shear
T406-324-0.7P	242.97	179.20	**228.08**	**168.22**	270.40	199.44	Punching Shear

Based on the preceding calculations, a lower bound approach was used to design the welds to ensure that weld rupture preceded connection failure – i.e., so that the predicted flexural strength of the weld was less than or equal to the nominal flexural strength for the governing limit state calculated in Table 3-2. The resulting weld sizes are shown in Table 3-3, under the column heading Ground Weld Throat Size. The rupture moments on the right have been calculated for these weld sizes by comparing the strength of welds with the connection strength which includes Equations 2.1 and 2.2.

Although the above-noted weld sizes (in Table 3-3) were deemed necessary to ensure that those test specimens would fail by weld rupture, the weld size for fabrication was determined by using the minimum weld sizes for both fillet welds and PJP groove welds specified in ANSI/AWS D1-1 *Structural Welding Code* (2020) (AWS 2020) and CSA W59 *Welded Steel Construction* (2018) (CSA 2018) to satisfy minimum requirements of the weld size. Matching electrodes, with a strength of 490 MPa (71 ksi) were used for both the above calculations and for fabrication. These weld sizes are summarized in Table 3-3, under the column heading Specified Weld Leg Size. Since the minimum weld sizes according to AWS D1.1 (AWS 2020) and CSA W59 (CSA 2010) were larger than the maximum weld sizes needed to ensure the connection was weld-critical, it was accepted that welds for all test specimens would be "ground down" after fabrication to ensure weld rupture governed the moment resistance. The weld rupture moment calculated in Table 3-3 is an upper-bound estimate made by using the nominal strength of weld metal (490 MPa) times the elastic section modulus, as shown in Equation 3.1. These rupture moment predictions are updated with measured material properties in Chapter 4.

$$M_{ip} / \phi_w = S_{ip} F_{nw} = \frac{\pi[(D_b + t_w)^4 - D_b^4]}{32(D_b + t_w)} F_{nw} \tag{3.1}$$

Table 3-3 Maximum flexural strength of the weld section based on nominal properties

Experimental Designation	Specified Weld Leg Size		Desire Weld Throat Size		Weld Rupture Moment	
	mm	in	mm	in	kN-m	kip-ft
T273-127-1P	6.00	0.24	4.00	0.16	17.19	12.68
0T273-127-1	6.00	0.24	4.00	0.16	25.79	19.02
T324-127-1	6.00	0.24	4.00	0.16	25.79	19.02
T356-127-1	6.00	0.24	4.00	0.16	25.79	19.02
T356-273-1P	6.00	0.24	4.00	0.16	78.08	57.59
T356-324-1P	6.00	0.24	4.00	0.16	109.57	80.81
T406-127-1	6.00	0.24	4.00	0.16	25.79	19.02
T406-273-1P	6.00	0.24	4.00	0.16	78.08	57.59
T406-324-1P	6.00	0.24	4.00	0.16	109.57	80.81
T406-127-0.7	6.00	0.24	4.00	0.16	25.79	19.02
T406-273-0.7P	6.00	0.24	4.00	0.16	78.08	57.59
T406-324-0.7P	6.00	0.24	4.00	0.16	109.57	80.81

As discussed previously, the welds in the connections did not have a constant local dihedral angle (see Figure 3-2), making their geometries exceptionally complex. Hence, a computer-numerically controlled (CNC) cutting/profiling machine was used, in conjunction with several "trial specimens" (Figure 3-3), for both fillet welds and PJP welds, to ensure that no large gap existed between the branch and the chord before welding was performed.

(a) (b)

Figure 3-3 Welding of trial specimens: (a) before welding (b) after welding

A 14 mm (0.052 inch) diameter AWS A5.20 E71T solid wire electrode with a shielding gas of 100% carbon dioxide was used to weld all trial/test specimens. Due to the complex geometry of the joint, the welding position varied from flat to vertical. While the trial welds appeared to be good quality from a basic visual inspection, the trail specimens were subsequently cut into pieces along and normal to the chord axis to observe the weld cross-sections. These "macro-etch examinations" are shown in Figure 3-4.

(a) (b)

Figure 3-4 Cross-section of the welded trial specimens (a) fillet weld and (b) PJP weld

As shown in Figure 3-4, the trial fillet and PJP welds both had slightly convex faces, and sound penetration is observed (to the root of the weld). No visible discontinuities can be seen in either weld.

Based on these results, it was concluded that the fit-up and welding procedure(s) were both of acceptable quality.

3.3. TEST SPECIMEN FABRICATION PROCESS

The chord and branch members were next cut to the lengths specified in the fabrication drawings (see Appendix B) (using the CNC cutting machine, shown in Figure 3-5). Chord members were cut, once, perpendicular to the member axis, while the branch members were required to have a curved/saddle-shaped end preparation to allow tight fit-up. The cutting angle, i.e., the angle between the nozzle and the branch was limited by the machine but did not affect the cutting of fillet-welded branches, which were profiled to saddle perfectly onto the chord [see Figure 3-5 (b)]. The PJP-welded branches, on the other hand, were bevelled with a specified edge preparation (see Appendix B), whereby the branch surface was cut back to produce a groove with a known depth, as shown in Figure 3-5 (c). Because the specified bevel angle (60 degrees) was not possible using the CNC machine, it was decided to cut a 30-degree outside bevel and then grind it to 60-degrees by using a handheld grinder. It was confirmed that the cutting and grinding of the branch bevel remained within the tolerances given in CSA W59-18 table 5.5 (CSA 2018), which are shown in Table 3-4. Moreover, this grinding did not affect the groove depth.

Table 3-4 CSA W59-18 workmanship tolerance for groove welds

	Root not gouged	Root gouged
Root face of joint	±2mm (1/16”)	Not limited
Root opening without steel backing	±2mm (1/16”)	+2mm (1/16”) -3mm (1/8”)
Root opening with steel backing	+6mm (1/4”) -2mm (1/16”)	Not applicable
Groove angle of joint	+10° -5°	+10° -5°

(a)

(b)

(c)

Figure 3-5 Specimen fabrication: (a) CNC cutting machine; (b) fillet weld preparation, and (c) PJP weld preparation

The branches of each test specimen were then tack-welded to the chord (Figure 3-6 (a)); and the connections were placed on a set of supports. Next, the welder immobilized the connections and welded the joint (Figure 3-6 (b)). Both sides of the specimens were welded in the same positions (flat and horizontal), by turning the chord 180°.

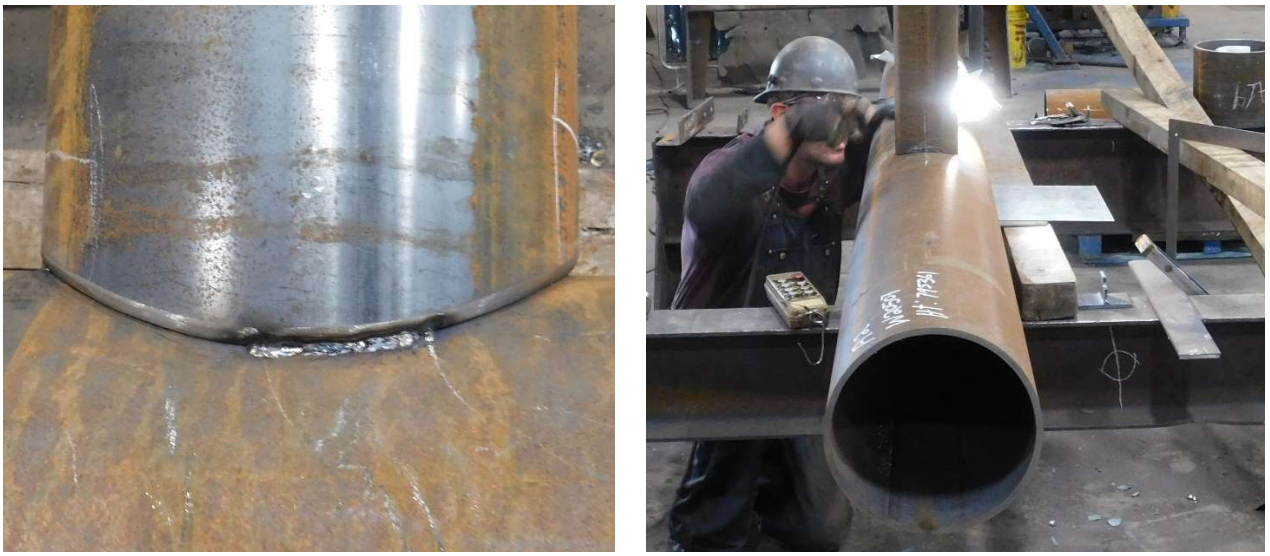

(a) (b)

Figure 3-6 Specimen welding: (a) tack weld; and (b) welding

The welded joints were executed by a qualified welder at Cherubini Metal Works in Dartmouth, Nova Scotia. The GMAW process was used in conjunction with the welding equipment shown in Figure 3-7 (Lincoln Electric LN-25 and a Miller Power source).

(a) (b)

Figure 3-7 Welding tool: (a) power source and (b) welding machine

A 14mm (0.052”) diameter AWS A5.20 E71T solid wire electrode with a nominal specified tensile strength of 595 MPa (86ksi) and a shielding gas of 100% carbon dioxide supplied was used to weld the test specimens. Welding process parameters were recorded and are provided in Table 3-5. These parameters were the same for all test specimens. To satisfy the qualification requirements of the ANSI/AWS D1.1 (2020) for prequalified welded joints, numerous trial specimens (discussed previously) were created and cut before welding the actual test specimens.

Table 3-5 Average welding process parameters for all specimens

Specified Weld Leg Size (mm)	Voltage (V)	Wire Feed Speed (ipm)
6	26	345

Once completed, the welded joints were visually inspected to check for discontinuities, in accordance with Clause 6 of ANSI/AWS D1.1 (2020) (AWS 2020). Figure 3-8 shows the completed weld joints, which all satisfied the visual inspection criteria.

(a) (b)

Figure 3-8 Final welded CHS-to-CHS T-connections: (a) fillet welds and (b) PJP welds

3.4. MATERIAL PROPERTY TESTS

Material property (i.e., tensile coupon) tests were conducted on the CHS material and as-laid weld metal. All material used for these tests came from the CHS stock and weld (ASTM E8/E8M-21 2021) (i.e., from the same heat as the material used in the test program). The materials were tested to determine yield stress (F_y), yield strain (ε_y), ultimate tensile strength (F_u), ultimate strain (ε_u) and Young’s Modulus (E).

3.4.1. TENSION TESTS: BASE METAL

Three TCs for each size of CHS used in the experimental program were created (15 in total), whereby all coupons were saw-cut from the base metal: one from the opposite side of the weld seam, and two others adjacent to it, as shown in Figure 3-9 (a) and Appendix D. For the CHS, TCs were cut from the middle of a 1-m long offcut in accordance with ASTM E8/E8M-21 (ASTM 2021). The dimensions of the TCs were measured and recorded in Appendix D. Stress-strain plots for all CHS TCs are provided in Appendix D, and a sample is shown below in Figure 3-9 (b). Table 3-6 summarizes the material properties of the CHS base metal.

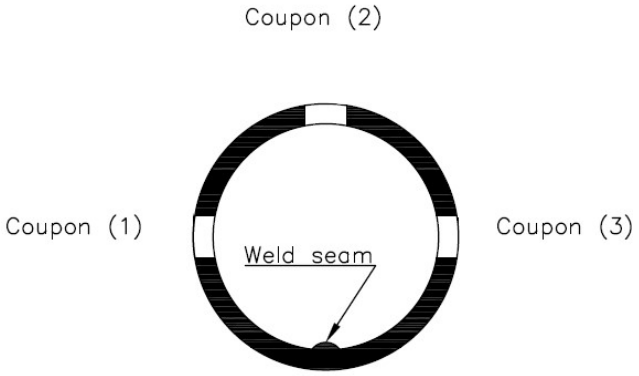

(a)

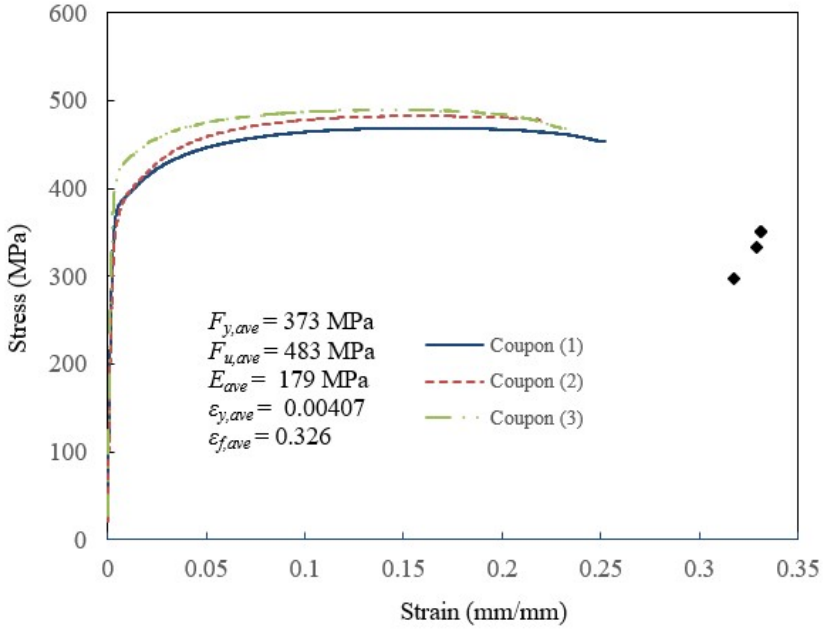

(b)

Figure 3-9 Tensile coupons tests (a) location cutting from CHS samples and (b) sample plot of tests

Table 3-6 CHS base metal property summary

CHS Designation	Elastic Modulus (MPa)	Strength (MPa)		Strain ($\mu\varepsilon$)	
		yield	ultimate	yield	ultimate
HSS 127 x 9.5	170	417	480	0.00458	0.343
HSS 273 x 9.5	198	352	477	0.00205	0.348
HSS 324 x 9.5	196	382	494	0.00426	0.322
HSS 356 x 9.5	196	398	466	0.00405	0.368
HSS 406 x 9.5	179	373	483	0.00407	0.326
HSS 406 x 13	211	312	450	0.00350	0.387

3.4.2. TENSION TESTS: WELD METAL

Three all-weld-metal tensile coupons were created in accordance with Clause 4 ANSI/AWS D1.1 (2015) by welding steel test plates with a nominal yield strength of 540 MPa (78 kpi) to the dimensions shown in Figure 3-10. The welded test plates were created using the same electrode spool, equipment, and fabrication processes as those used for the welded joints tested in the experimental program. The following welding process parameters, which are the same as the average values presented in Table 3-5, were used:

- Arc voltage = 26V.
- Wire feed speed = 345ipm.

The all-weld-metal TCs were cut from the welded test plates at the Dalhousie University Structural Testing Facility and fabricated to the dimensions shown in the fabrication drawings (Appendix D). Those dimensions were measured using the caliper shown in Figure 3-11 in Chapter 3.5.2, and then recorded on the TC test data sheets in Appendix E. Based on the TC tests, the ultimate strength (F_u) of the weld metal was found to be 592 MPa.

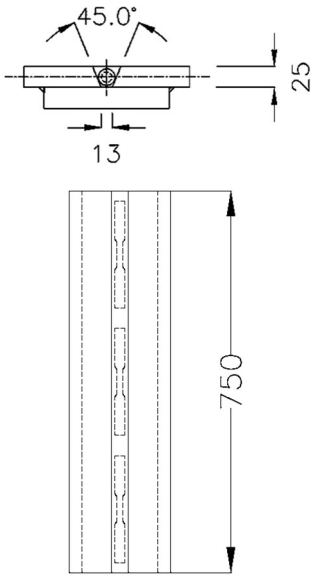

Figure 3-10 Tensile coupon cutting from CHS samples unit: mm

Table 3-7 Maximum flexural strength of the weld section based on nominal properties

Experimental Designation	Specified Weld Leg Size		Ground Weld Throat Size		Weld Rupture Moment	
	mm	in	mm	in	kN-m	kip-ft
T273-127-1P	6.00	0.24	3.00	0.12	23.17	17.09
T273-127-1	6.00	0.24	3.00	0.12	23.17	17.09
T324-127-1	6.00	0.24	3.00	0.12	23.17	17.09
T356-127-1	6.00	0.24	3.00	0.12	23.17	17.09
T356-273-1P	6.00	0.24	3.00	0.12	105.73	77.99
T356-324-1P	6.00	0.24	3.00	0.12	148.46	109.50
T406-127-1	6.00	0.24	3.00	0.12	23.17	17.09
T406-273-1P	6.00	0.24	3.00	0.12	105.73	77.99
T406-324-1P	6.00	0.24	3.00	0.12	148.46	109.50
T406-127-0.7	6.00	0.24	3.00	0.12	23.17	17.09
T406-273-0.7P	6.00	0.24	3.00	0.12	105.73	77.99
T406-324-0.7P	6.00	0.24	3.00	0.12	148.46	109.50

3.5. GEOMETRICAL MEASUREMENTS

3.5.1. CHS CROSS-SECTIONAL DIMENSIONS

The actual geometric properties of CHS (given in Appendix D, and Table 3-8) were next measured and checked with the permissible tolerances and then, subsequently, used to re-calculate the actual predicted connection, branch and weld flexural strengths. The thickness of each CHS wall was re-measured using a

150mm (6in) caliper (accurate to 0.01mm), shown in Figure 3-11 (a) the details of the measurement are present in Table 3-8.

The geometric properties of each CHS were measured by a caliper shown in Figure 3-11 (a) and a regular measuring tape measure the thickness and the diameter of the cross-section respectively. The average values of the measurements are shown in Table 3-8 including the average diameter and thickness.

(a)

(b)

Figure 3-11 Measurement tool of (a) Caliper and (b) weld measuring gauge

Table 3-8 Average measured cross-sectional dimension of CHS

CHS Designation	Average Thickness		Average Diameter	
	mm	in	mm	in
HSS 127 x 9.5	8.85	0.35	127.6	5.0
HSS 273 x 9.5	8.86	0.35	274.4	10.8
HSS 324 x 9.5	9.31	0.37	325.0	12.8
HSS 356 x 9.5	9.32	0.37	355.9	14.0
HSS 406 x 9.5	8.90	0.35	407.4	16.0
HSS 406 x 13	11.82	0.47	407.4	16.0

3.5.2. Weld Cross Sectional Dimensions External Measurement

Before testing, grinding work was done to reduce the weld sizes to close to those specified in Table 3-7, to ensure weld-critical behaviour. Before any grinding occurred, measurement locations for the effective weld throat were demarcated at 12 locations along the branch perimeter (30 deg arc-angle increments), as shown in Figure 3-12, to allow for the calculation of the local dihedral angle (which relates the weld legs to the weld throat, for fillet welds) at each point of interest.

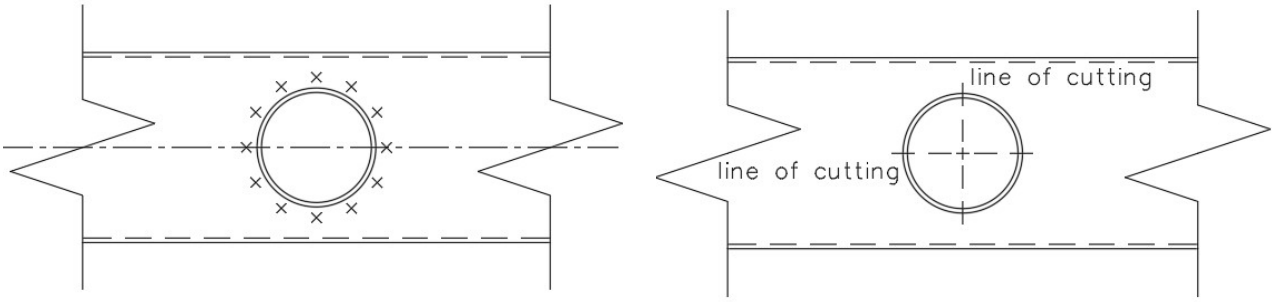

(a) (b)

Figure 3-12 Location of (a) weld size measurement and (b) cutting after tests

3.5.2.1. Fillet Welds

To determine the throat dimensions of the fillet welds, after grinding, measurement was done at the locations shown in Figure 3-12(a) to obtain the "projected leg size" on both chord face and branch face. Due to the non-90° local dihedral angles, these measurements were taken as shown in Figure 3-13. By using the local dihedral (ψ), calculated at each location, the "true" leg size along the chord and branch could then be determined. For this, Equations 3.2 (a) and (b) were used. In addition, the measurement can not be done along the plane of weld cross-section since it is perpendicular to the longitudinal direction of the welds which needs further calculation to get the exact "leg size".

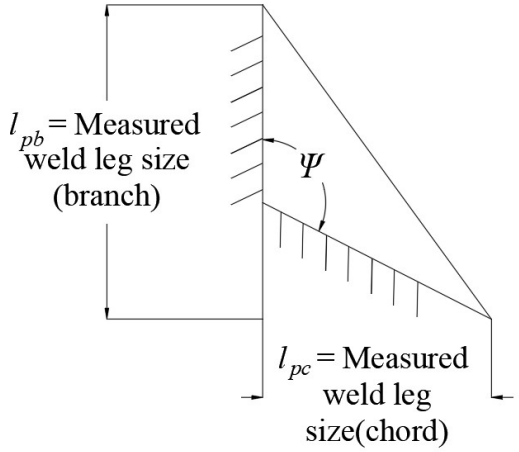

Figure 3-13 Measured weld size

$$l_c = \frac{l_{pc}}{\cos(\psi - 90^\circ)} \tag{3.2a}$$

$$l_b = l_{pb} - \frac{l_{pc}}{\cos(\psi - 90^\circ)} \tag{3.2b}$$

where all measured "weld leg sizes" are the dimension of weld along the planes include the branch axis (called measurement plane here); l_{pc} = measured leg size on chord (in the measurement plane)= projection of chord weld leg size (in the measurement plane) to horizontal; l_c = weld leg size along chord (in the measurement plane); l_{pb} = measured leg size on branch (in the measurement plane)= weld leg size along branch (in the measurement plane) plus projection of chord weld leg size to branch direction (in the measurement plane); l_b = branch leg size (in the measurement plane).

In addition to the above, it is important to note that the measured leg sizes are associated with a vertical plane (along the axis of the branch), meaning that the plane of the weld "leg" measurement is often different from the plane of weld throat (since the weld throat is in a plane perpendicular to the weld axis).

To obtain the true weld leg and throat measurements (i.e. the weld cross-sectional dimensions), a model was developed using the computer-aided design (CAD) program Solidworks. The procedure used in Solidworks to obtain the effective weld throat is as follows, where the results are summarized in Table 3-9.

- The measured weld legs (on the vertical plane) are drawn first, at the 12 measurement locations, to establish the weld.
- These planes are "lofted" together to create a three-dimensional profile.
- The plane of the local dihedral angle (i.e., a plane perpendicular to the weld direction) is then drawn through each section, and the weld is "cut" along this plane.
- In the above orientation, the weld legs (along the branch and chord) are measured.
- The effective weld throat (distance from root normal to the surface) is then measured, or it can be calculated from the measured weld leg dimensions and the local dihedral angle.

Table 3-9 Summary of effective weld throat and calculated section modulus based on weld fully effective

Experimental designation	Effective weld throat (mm) by external measurement	Fully effective section modulus (10^3 mm^3)
T273-127-1P	2.98	31.15
T273-127-1	2.71	35.48
T324-127-1	2.86	37.39
T356-127-1	2.77	36.22
T356-273-1P	3.01	155.58
T356-324-1P	3.83	191.77
T406-127-1	2.72	35.59
T406-273-1P	2.98	157.20
T406-324-1P	3.03	254.57
T406-127-0.7	2.65	34.56
T406-273-0.7P	3.00	156.27
T406-324-0.7P	3.02	255.23

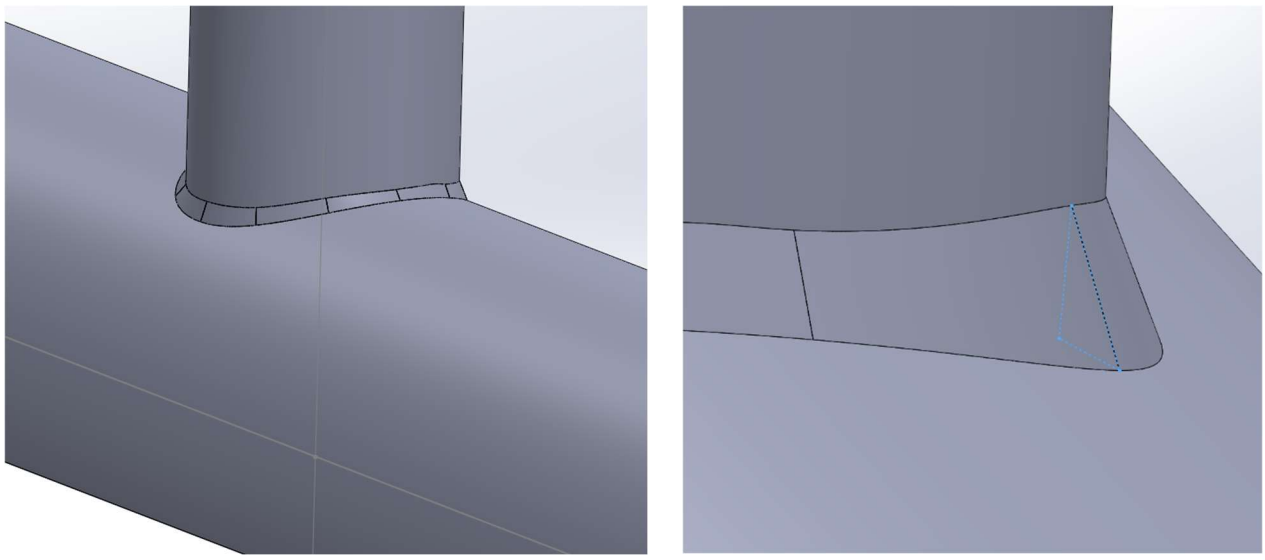

(a) (b)

Figure 3-14 Solidworks model of (a) overview and (b) weld legs

3.5.2.2. PJP Welds

The measurement of PJP welded specimens was decidedly easier since the effective weld throat is always measured perpendicular to the branch direction according to AWS-D1.1-15 and CSA W59-18 (ASTM 2015) (CSA 2018). All dimensions of PJP weld throats are shown in Appendix A (external measurement) and Appendix E (exact measurement).

After testing, all connections (fillet and PJP) were cut normal to the weld axis along and perpendicular to the chord and branch to compare the above-noted external measurements to those obtained from macro-etch examinations. The latter are discussed in Chapter 4.1.2 and summarized in Appendix E.

3.6. TEST SETUP AND INSTRUMENTATION

Since no experiments of this same type had been performed before at Dalhousie, the entire test setup assembly had to be designed. The test setup included: a support frame for the actuator, which could create a pure in-plane bending moment acting on the connection, and simple supports (pin-and-roller) for the chord ends. The measurement of non-uniform normal strain around the branch, adjacent to the weld, and connection deformation were also important components. The overall test set up is shown in Figure 3-15.

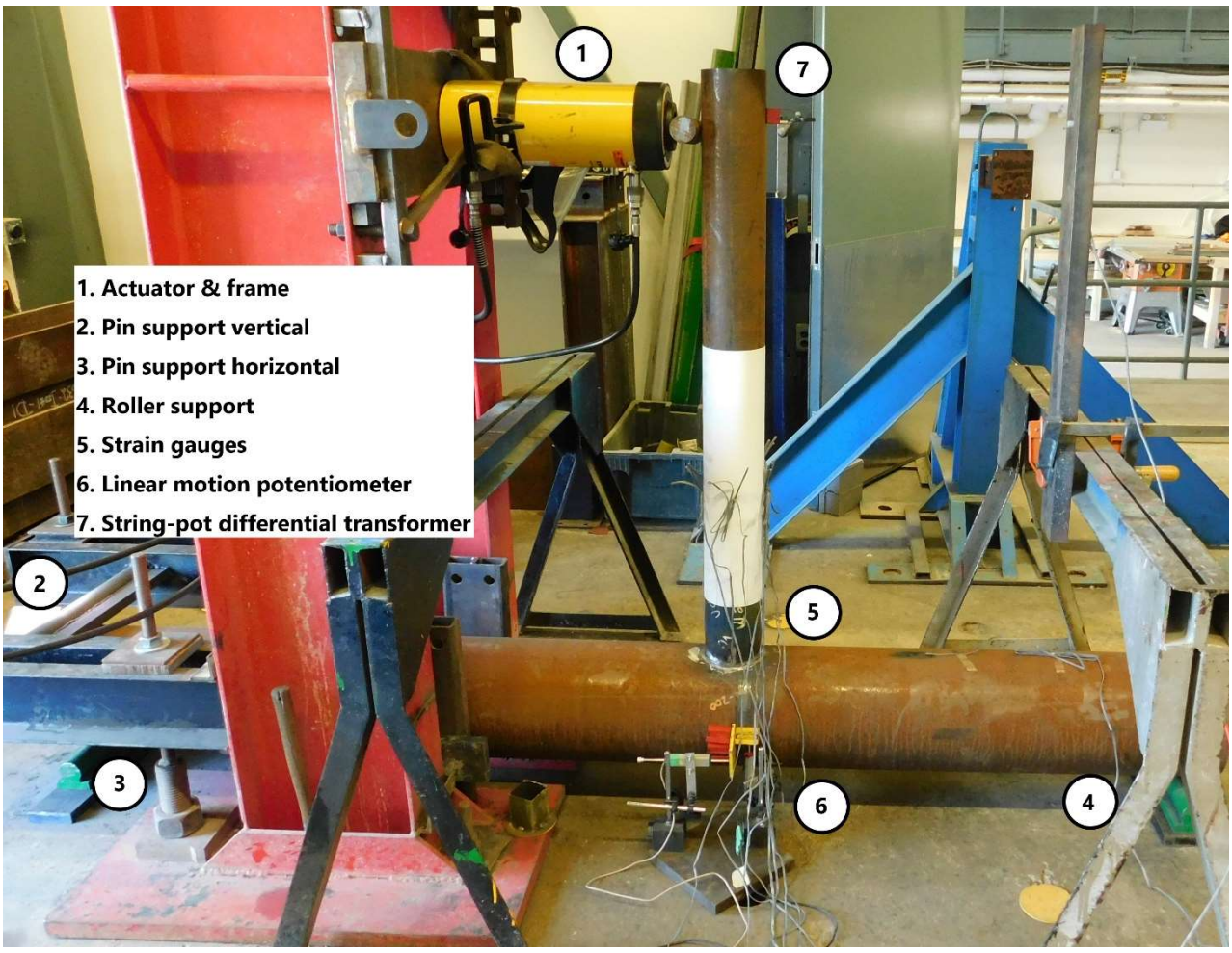

Figure 3-15 General test set up assembly for full-scale experiment

3.6.1. Support Frame and Actuator

The frame had two vertical columns spaced at 435mm. Post-tensioned anchor rods prevented the steel support frame from horizontal movement under the reaction load of the actuator. A displacement-controlled portable MTS actuator with a capacity of 500 kN and a stroke of 500-mm was calibrated before the test, and operated by a trained technician. The actuator was secured to the frame using four bolts and a plate, as shown in Figure 3-16. No additional lateral support was provided. Out-of-plane buckling or bending was not a concern.

During testing, the point load device (ram) that transferred the load from the actuator to the branch caused some deformation of the branch adjacent to it; however, this did not affect the experiment, since it did not affect the load transferred to the connection, and branch deflection (at the top of the branch) was measured on the opposite side. Nonetheless, for large diameter chords, a stiffer was welded inside of the branch in order to prevent overall member failure by local buckling.

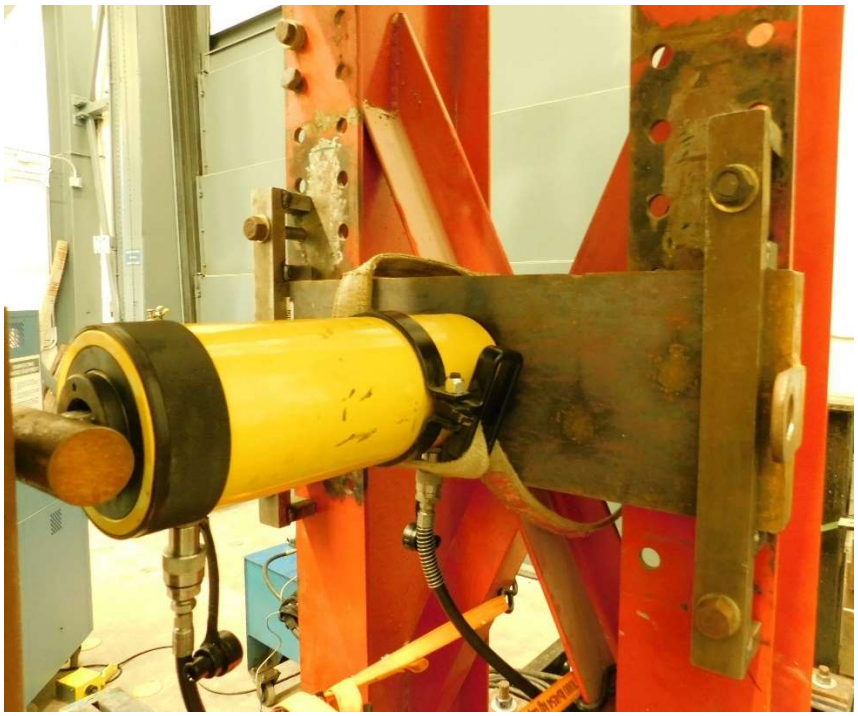

Figure 3-16 Frame and actuator

3.6.2. Supports and Point Load Device

The test specimen chords were simply supported by a pin (on the end near the frame) and a roller (on the other end). Both pin and roller supports were made using rigid steel plates placed on the ground. The roller support provided only a vertical upward reaction, as shown in Figure 3-17. The pin support provided a vertical downward and horizontal reaction, as shown in Figure 3-17(b). The assembly for the pin included four 875 mm

(34.5 inch) MC 150×10.4 channels, drilled and welded, with a 680 mm (2.23 ft) long 63.5 mm (2.5 inch) diameter steel rod. This pin support was reused and adjusted for each different sized chord. As can be seen Figure 3-17(b), it restricted in both horizontal and vertical direction, but it still allowed rotation.

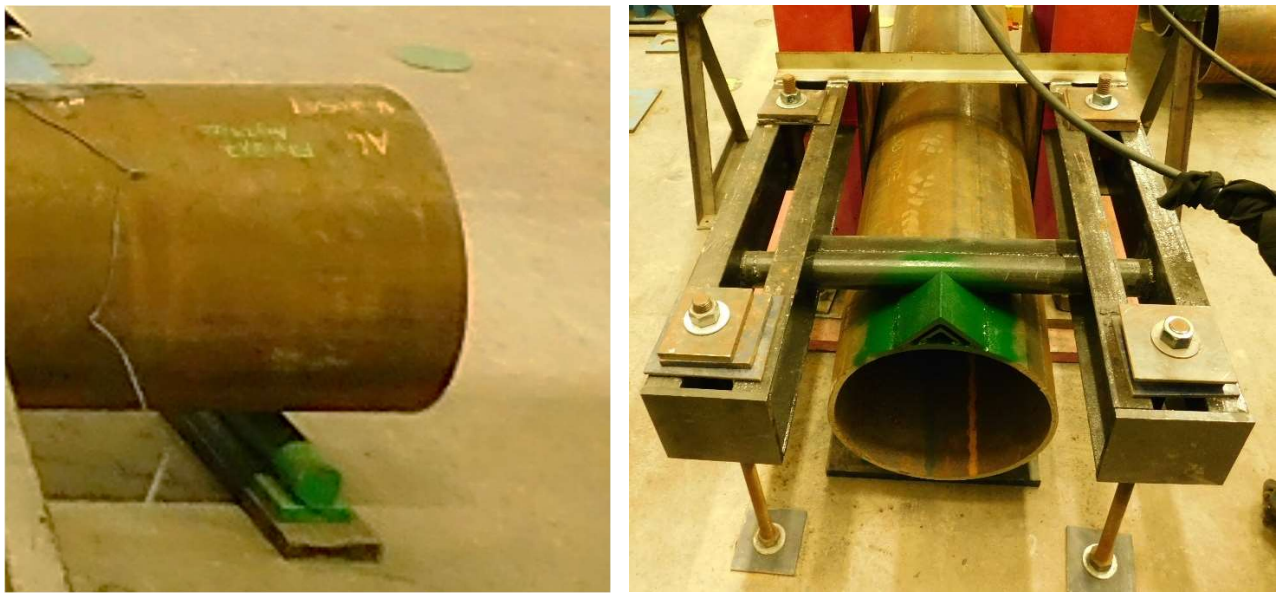

(a) (b)

Figure 3-17 Supports for experiments: (a) roller and (b) pin

3.6.3. Strain Gauges and Linear Potentiometers

Since the normal strain around the branch near the weld was expected to be non-uniform, strain gauges were used, oriented along the longitudinal axis of the branch, to measure this variation. A total of seven strain gauges were evenly distributed from the toe (end point of compression face) to the heel (end point of tension face) with one on the saddle (theoretical neutral axis) on the opposite other side to determine if any significant out-of-plane effects occurred throughout the experiments. The stain gauges were placed approximately 15 mm (0.6 in) above the toe of the weld(s), for both fillet welds and PJP welds, to avoid the high strain region that exists close to the weld toe due to the notch effect (Cassidy 1993). A set of typical strain gauges adjacent to the weld are shown in Figure 3-18(a). Figure 3-18(b) shows a schematic overview of the strain-gauge locations, orientations and spacing used for all experiments. The strain gauges used were “Tokyo Measuring Instrument Lab, type F Series Goblet”.

(a)

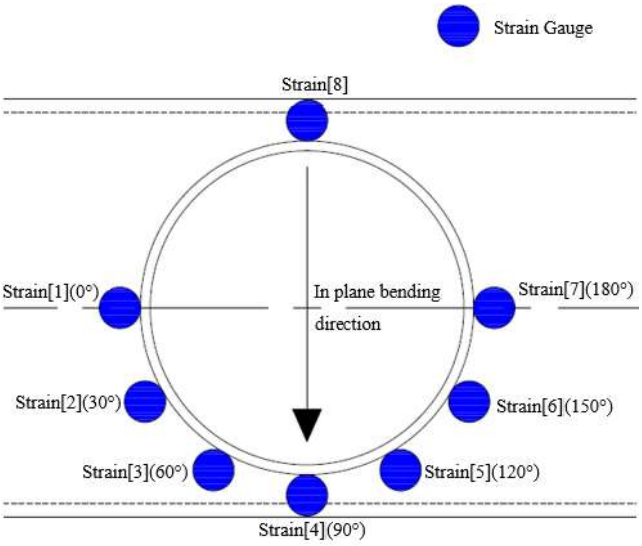

(b)

Figure 3-18 Strain gauges adjacent to the weld (a) picture and (b) details

3.7. TESTING PROCEDURE

During each test, the actuator pushed until the specimen broke, due to weld fracture. Strain adjacent to the weld, and deflection of the connection and top of branch, and at the connection node point, were recorded. Once the experiment was finished, the specimen was cut by a technician in order to obtain the weld size at the crown and saddle points, to verify the externally measured weld dimensions. The specimens were tested in the following order:

1. T406-324-1;
2. T406-324-0.7;

3. T406-273-0.7;
4. T406-273-1;
5. T406-127-1;
6. T406-127-0.7;
7. T356-324-1;
8. T356-273-1;
9. T356-127-1;
10. T324-127-1;
11. T273-127-1; and, finally,
12. T273-127-1P.

During the test of specimen T406-324-0.7, there was an unforeseen issue with branch local buckling, which interrupt the test. As noted previously, it was after this point that a stiffener was added to the inside of the branch, adjacent to the load, before resuming the test. This stiffening method was adopted for remaining tests that were deemed susceptible to the same failure mode.

Chapter 4: RESULTS

The failure mode(s), strain in the branch(es) adjacent to welds, and deflection of branch/rotation, as well as chord deformation, for each test, are summarized in this Chapter. Where applicable, strengths and deformations have been calculated by using actual measured geometric and material properties, as discussed in Chapter 3 (for materials) and Chapter 4. These properties are summarized in Appendix E.

4.1. ACTUAL GEOMETRY OF CHS AND WELDS

4.1.1. GEOMETRIC PROPERTIES OF THE AS-LAID WELDS

The geometric properties of the as-laid welds were measured after the experiment to obtain the effective weld size. All test specimens were cut into 4 pieces, along the plane of the local dihedral angle at the crown and saddle points, before measurement. the location of cutting was shown in Figure 3-12(b). A Cannon scanner, shown in Figure 4-1 (a), was then used to scan the cross-section of the weld, after cutting. The weld size was then found by using AutoCAD, as shown in Appendix E.

Where the scanned cross-sections of the welds did not show a clear boundary between the weld and the base metal, a 5% nital etchant, shown in Figure 4-1 (b), was applied on the cross-section.

Moreover, since, after cutting, each cross-section includes 2 faces, the weld size at each location was determined by taking the average of measurements on these 2 faces. The resulting measurements were then compared with the external measurements discussed in Chapter 3.4.2.

The effective weld throat from the macro-etch measurements was determined in 3 ways:

1. Minimum-distance measurement (MDM): by measuring the minimum distance from the root to the surface;
2. Fracture-length measurement (FLM): by measuring the length of the weld along the fracture plane; and
3. Leg-size measurement (LSM): by measuring the leg sizes, and then calculating the weld throat form geometry.

(a) (b)

Figure 4-1 Weld measurement tool (a) scanner and (b) nital etchant

Images of the scanned welds cross-sections are shown in Figure 4-2 and Appendix E where:

1. the yellow line shows the boundary between the weld and base metal;
2. the solid blue line shows the weld size determined from macro-etch leg measurements (LSM);
3. the dashed blue line shows the weld size determined from external leg measurements; and
4. the red line shows the minimum distance from the root to weld surface (MDM).

The so-called “exact measurements” from macro-etching, are compared to the external measurements in Table 4-1.

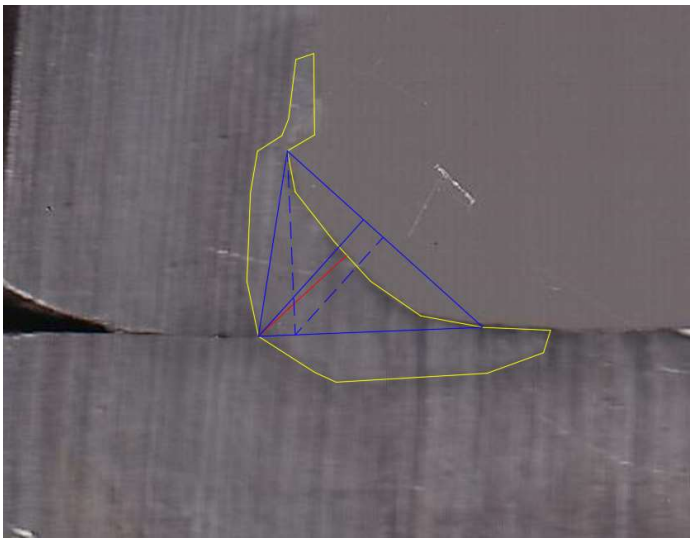

Figure 4-2 Sample weld cross-section

Table 4-1 External and actual effective weld throat

Test Designation	External Measurement (mm)	Exact Measurement (mm)		
		MDM	FLM	LSM
T273-127-1P	2.98	4.58	4.67	NA
T273-127-1	2.71	2.61	2.81	3.31
T324-127-1	2.86	2.96	2.97	3.44
T356-127-1	2.77	2.32	2.33	3.33
T356-273-1P	3.01	5.57	NA	NA
T356-324-1P	3.83	5.06	5.12	NA
T406-127-1	2.72	2.81	2.90	3.34
T406-273-1P	2.98	4.42	4.42	NA
T406-324-1P	3.29	4.11	4.15	NA
T406-127-0.7	2.65	2.24	2.51	2.91
T406-273-0.7P	2.88	4.95	4.95	NA
T406-324-0.7P	3.29	5.36	5.35	NA

Note: NA means there are no available data, or the measurement type does not apply for the connection.

When comparing the effective weld throat dimensions obtained from different measurement techniques, the external measurements are much different than the "exact measurements", for both fillet and PJP welds. This is primarily due to penetration, as shown in Appendix E, which cannot be measured externally. Moreover, the MDM and FLM measurements are similar. Because these measurements are believed to be the most accurate, and the ones used by designers – if they are known – **the MDM measurement will be adopted herein, for the remainder of the analysis**.

4.2. MOMENT-ROTATION PLOTS AND NONUNIFORM STRAIN DISTRIBUTIONS

In all 12 full-scale tests on CHS-to-CHS moment T-connections, the actual flexural strength of the welded joint and overall branch defection/rotation was measured. It should be noted that the strength of test T273-127-1 (154.12 kNm) was found to be much higher than expected (e.g., T273-127-1P had a similar weld size and CHS properties, and a strength of 39.77 kNm). The former result is hence considered spurious.

In the following section, the deflection of the top of the branch (at the actuator) relative to the connection work point was determined using LPs, and the moment was calculated from multiplying the load applied by the actuator by the distance between the loading point and the top of the chord. In addition, the branch indentation (into the chord, on the compression side) is calculated, and represented as a percentage of the chord diameter. These results have been summarized in Appendix G.

All test specimens failed by weld fracture, as planned, which initiated near the heel of the connection (where the maximum tensile stress is located), as shown in Figure 4-5 to 4-27. In all cases, the weld failed suddenly along a bumpy plane, which is believed to be due, in part, to the changing weld throat caused by griding and varying degrees of penetration. An instantaneous loud noise, caused by the energy release at weld fracture, marked the completion of each test, at which time the load reading from the actuator also dropped, suddenly, and the weld fractured. Figure 4-3, below, shows the deformation of chord surface (as a % of the chord diameter), where the vertical line at 3% is the widely accepted "chord-plastination limit" (AISC 360 2016). From Figure 4-3, three (of the 12) tests exceed the 3% deformation limit; however, in all cases, the load continued to increase until weld fracture. All connections can hence be deemed "weld-critical". The following sections summarize the results of individual tests.

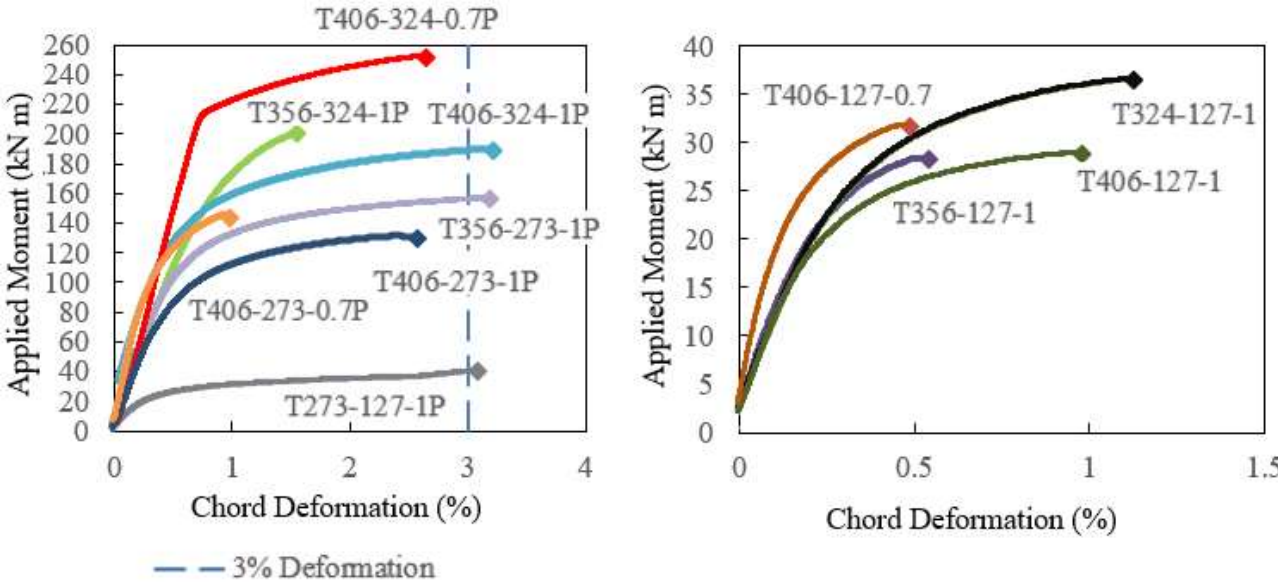

(a) (b)

Figure 4-3 Moment-chord deformation relationship: (a) PJP weld and (b) fillet weld

4.2.1. T273-127-1P

For test T273-127-1P, the branch deflection (at the loading point), at the ultimate moment, was 168.99 mm, and the chord face deformation was calculated to be 3.08% of the chord diameter, vertically, at the crown. The ultimate moment resistance of the weld in specimen T273-127-1P was 39.77 kNm (34.89 kN of applied load with a 1.14 m level arm). Figure 4-4 shows the failure mode of the specimen, by weld fracture.

(a)

(b)

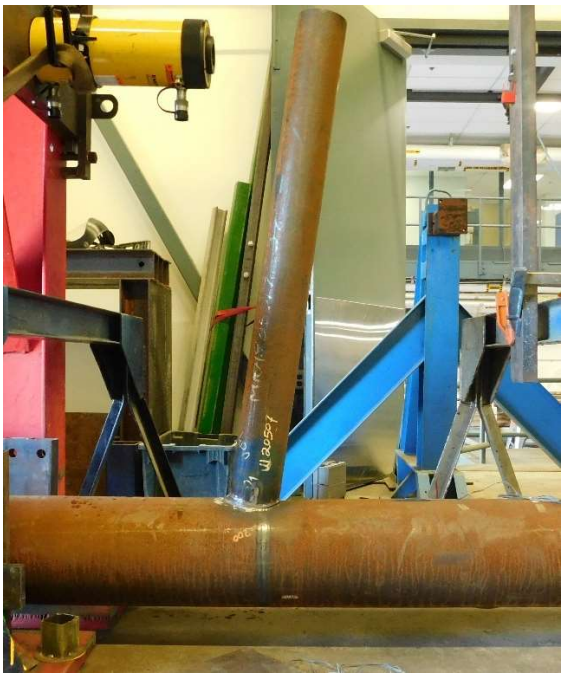

(c)

Figure 4-4 Failure of T273-127-1P (a) weld fracture, (b) chord deformation and (c) branch deformation

Figure 4-5(a) shows that the overall moment-deflection response of the connection is linear-elastic near the start of the test then gradually decreases in stiffness until the end of the test. The distribution of normal stain around the branch under different applied moment are shown in Figure 4-5(b) where the subtended angle (x-axis) is the branch arc length measured from the toe (end point of compression face). The stain distribution is nearly symmetric when the applied moment is low, while the stain becomes highly unsymmetric with large moment, which may be caused by ovalization of the chord.

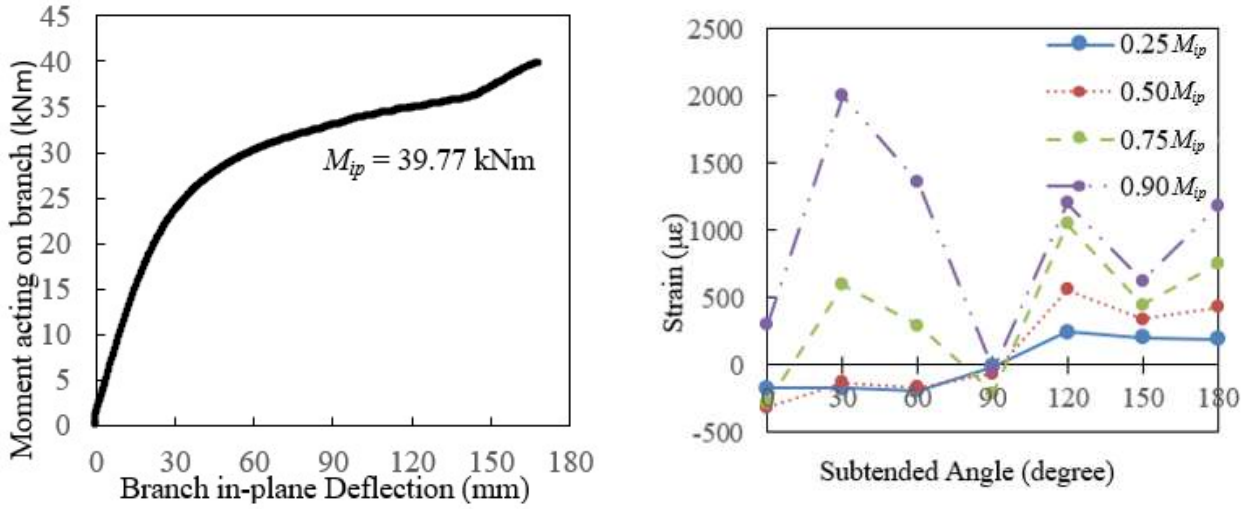

(a) (b)

Figure 4-5 T273-127-1P (a) moment-deflection and (b) normal strain distribution

4.2.2. T273-127-1

From the test readings, the ultimate moment resistance of T273-127-1 was found to be 154.12 kNm (134.15 kN load with a 1.14 m level arm). Figure 4-6 shows the failure mode of the specimen – again – by weld fracture.

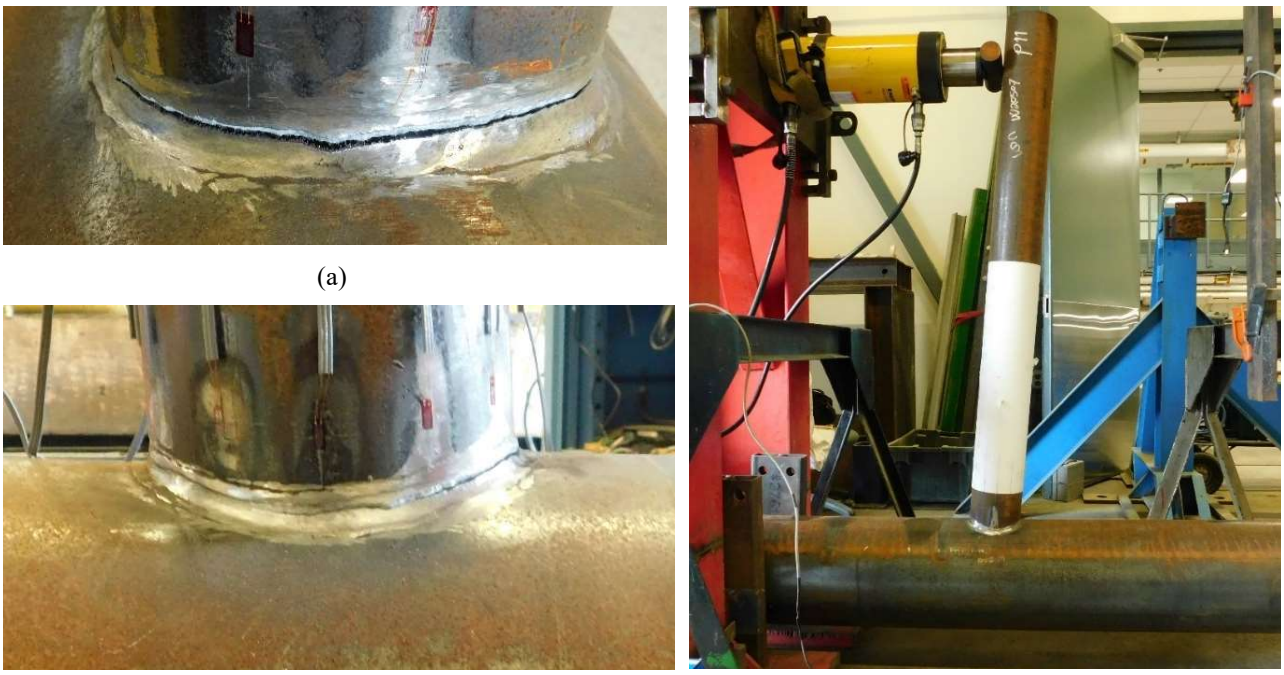

(a)

(b) (c)

Figure 4-6 Failure of T273-127-1 (a) weld fracture, (b) chord deformation and (c) branch deformation

The moment-deflection relationship is shown in Figure 4-7 (a), where the connection starts with a linear-elastic behavior near the start of the test then gradually decreased in stiffness until the end of the test. The distribution of normal stain around the branch under different applied moment are shown in Figure 4-7 (b), where the stain distribution is nearly symmetric when the apply moment is low while the stain becomes slightly unsymmetric with high moment which may have again been caused by ovalization of the chord.

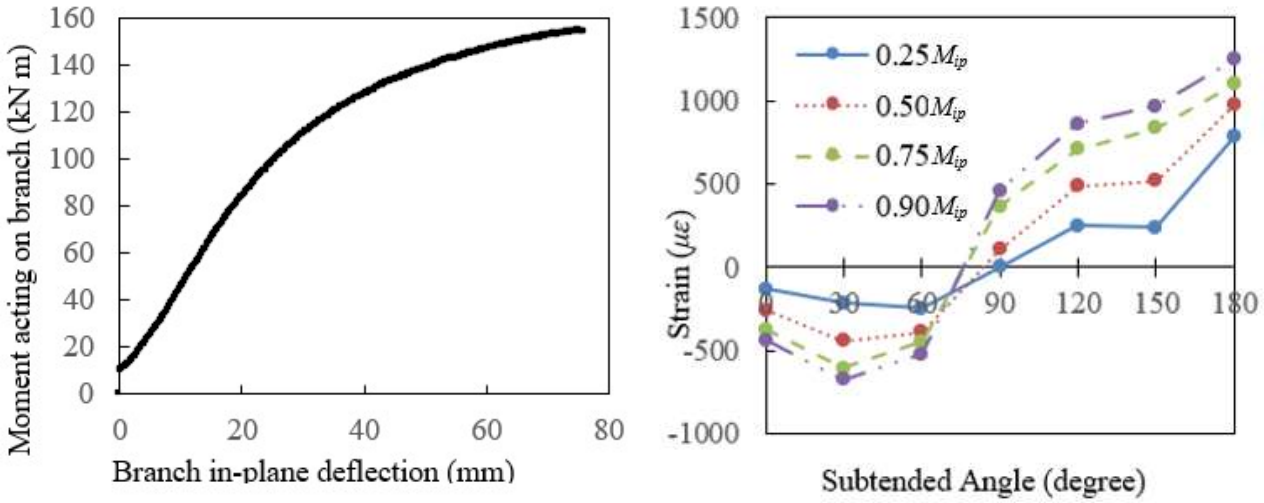

(a) (b)

Figure 4-7 T273-127-1 (a) moment-deflection and (b) normal strain distribution

4.2.3. T324-127-1

For test T324-127-1, the branch deflection (at the loading point), at the ultimate moment, was 76.04 mm and the branch face deformation was calculated to be 1.13 % of the chord diameter, vertically, at the crown of the weld. The ultimate moment resistance of the weld in specimen T324-127-1 was 36.47 kNm (34.08 kN load with 1.07 m level arm). Figure 4-8 shows the failure of the specimen by weld fracture.

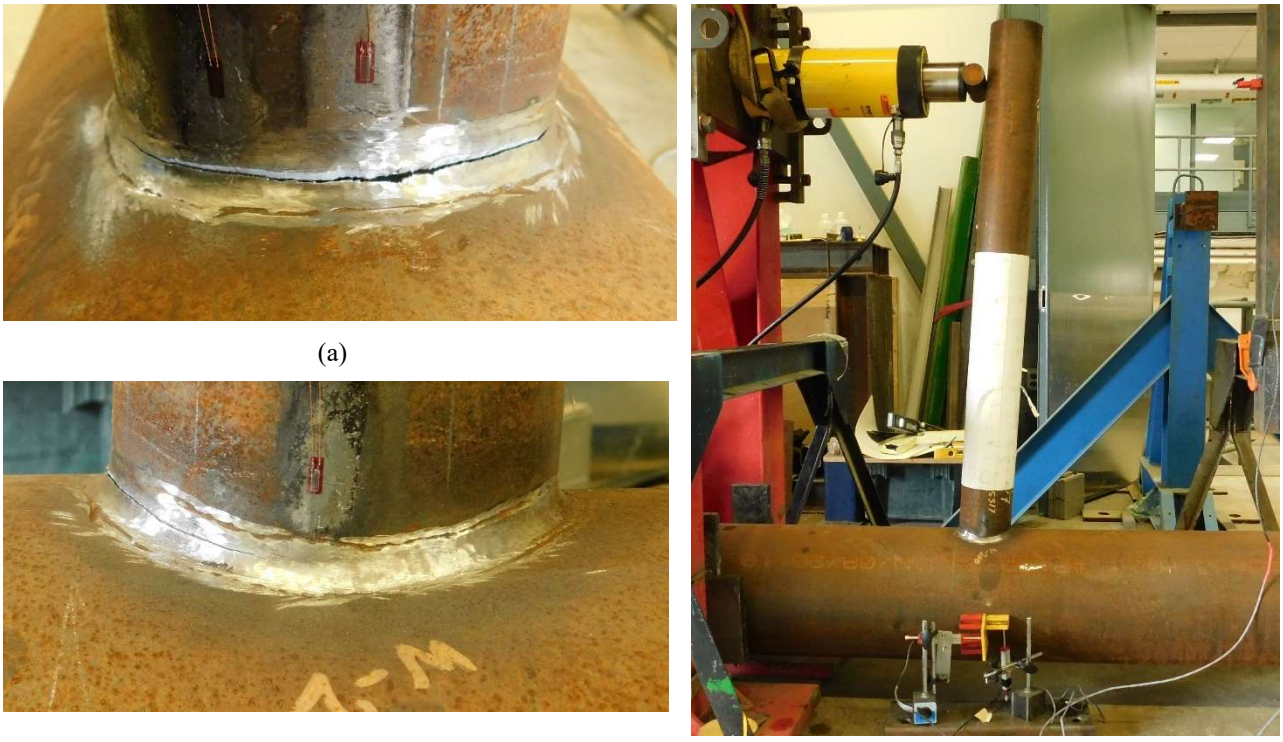

(a)

(b) (c)

Figure 4-8 Failure of T324-127-1 (a) weld fracture, (b) chord deformation and (c) branch deformation

The moment deflection relationship is shown in Figure 4-9 (a) and the distributions of normal stain around the branch under different applied moment are shown in Figure 4-9 (b).

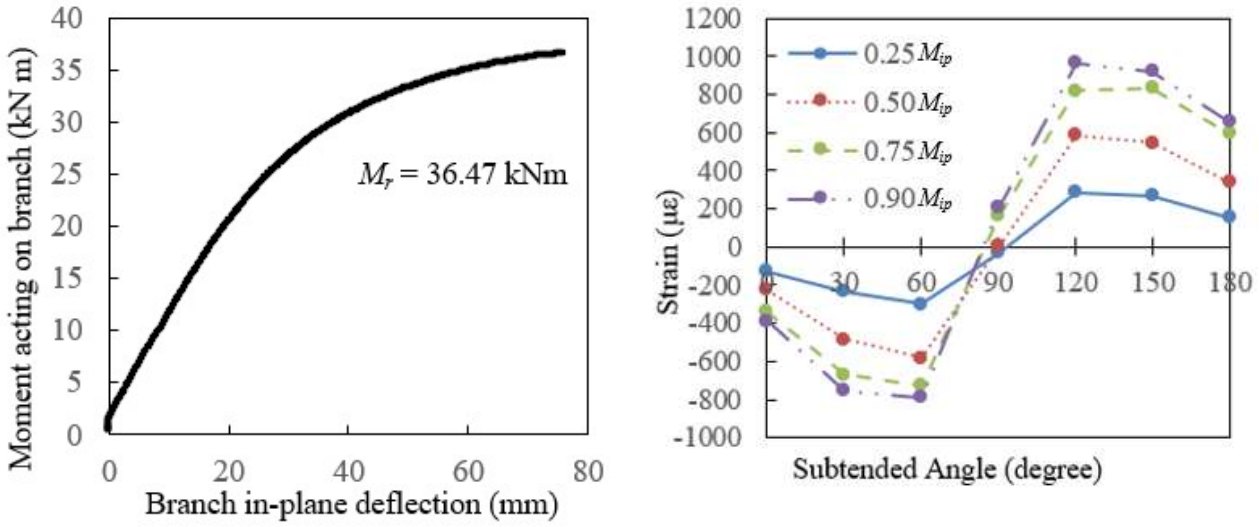

(a) (b)

Figure 4-9 T324-127-1 (a) moment-deflection and (b) normal strain distribution

4.2.4. T356-127-1

For test T356-127-1, the branch deflection (at the loading point), at the ultimate moment, was 42.14 mm and the chord face deformation was calculated to be 0.54 % of the chord diameter, vertically, at the crown of the weld. The ultimate moment resistance of the weld was 28.33 kNm (27.28 kN load with 1.04 m level arm). Figure 4-10 shows the failure of the specimen by weld fracture.

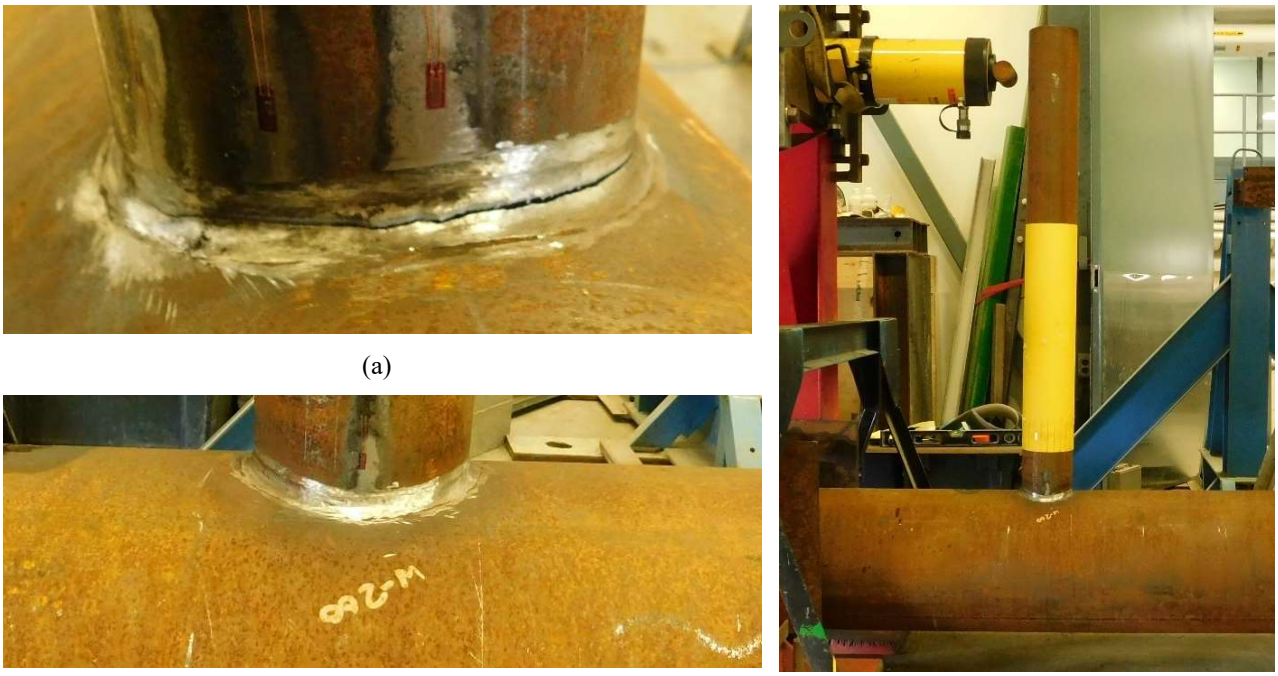

(a) (b) (c)

Figure 4-10 Failure of T356-127-1 (a) weld fracture, (b) chord deformation and (c) branch deformation

The moment-deflection relationship is shown in Figure 4-11 (a), and the distributions of normal stain around the branch under different applied moments are shown in Figure 4-11 (b). The stain distribution is nearly symmetric when the applied moment is low, while the stain becomes slightly unsymmetric with high moment, which is similar to the other test result.

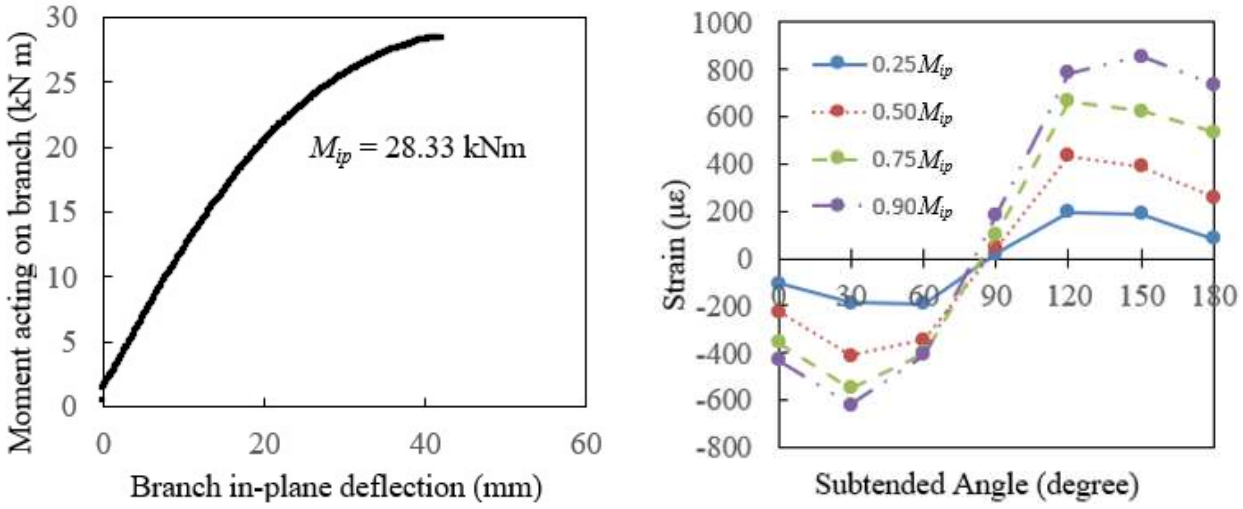

(a) (b)

Figure 4-11 T356-127-1 (a) moment-deflection and (b) normal strain distribution

4.2.5. T356-273-1P

For the test T356-273-1P, the branch deflection (at the loading point), at the ultimate moment, was 91.76 mm and the chord face deformation was calculated to be 3.19 % of the chord diameter, vertically, at the crown of the weld. After the moment calculation from the load reading, the ultimate moment resistance of the weld was 155.88 kNm (148.46 kN load with 1.05 level arm). Figure 4-12 shows the failure of the specimen by weld fracture.

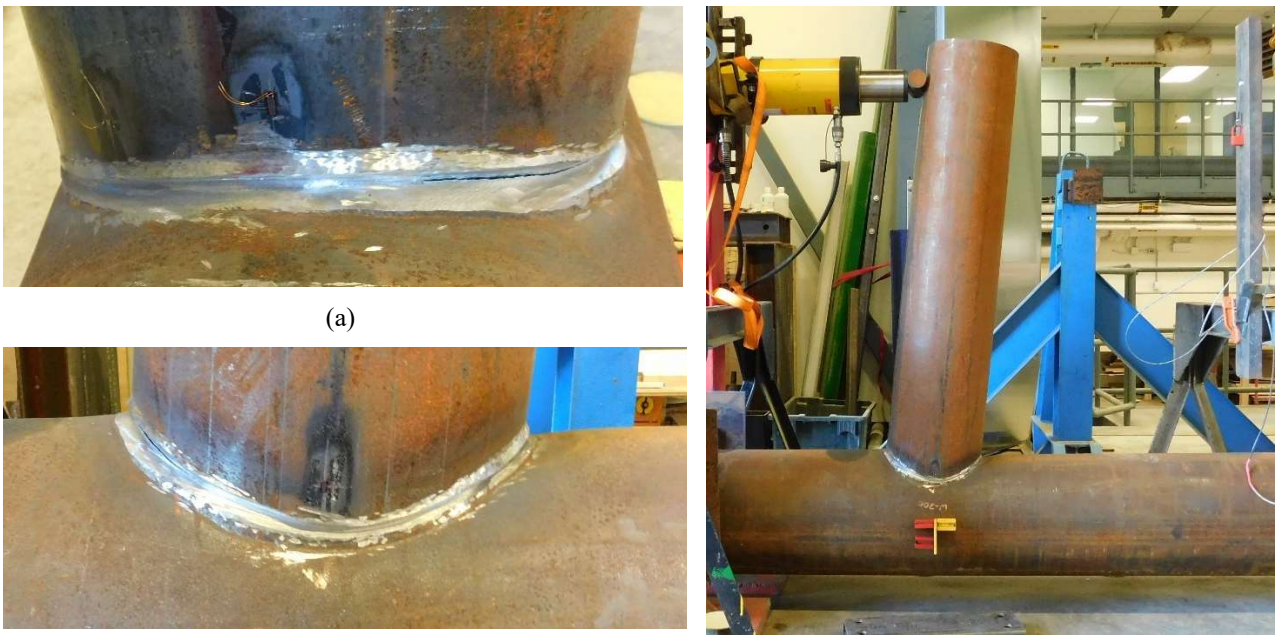

(a)

(b) (c)

Figure 4-12 Failure of T356-273-1P (a) weld fracture, (b) chord deformation and (c) branch deformation

The moment-deflection relationship is shown in Figure 4-13 (a). The distribution of normal stain around the branch under different applied moment are shown in Figure 4-13 (b).

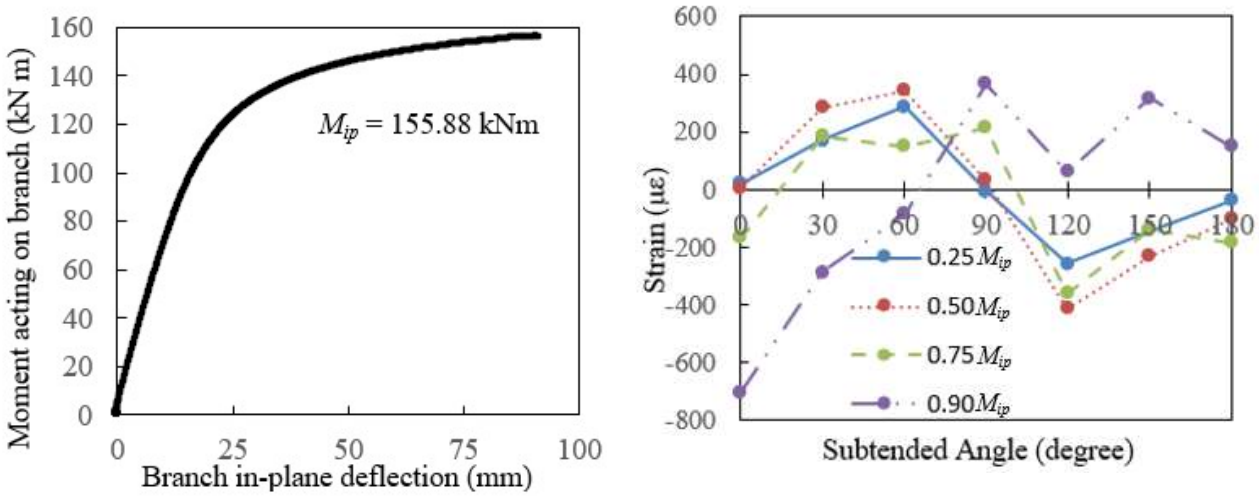

(a) (b)

Figure 4-13 T356-273-1P (a) moment-deflection and (b) normal strain distribution

4.2.6. T356-324-1P

For test T356-327-1P, the branch deflection (at the loading point), at the ultimate moment, was 38.69 mm and the chord face deformation was calculated to be 1.55 % of the chord diameter, vertically, at the crown of the weld. The ultimate moment resistance of the weld was 199.83 kNm (192.15 kN load with 1.04 m level arm). Figure 4-14 shows the failure of the specimen by weld fracture.

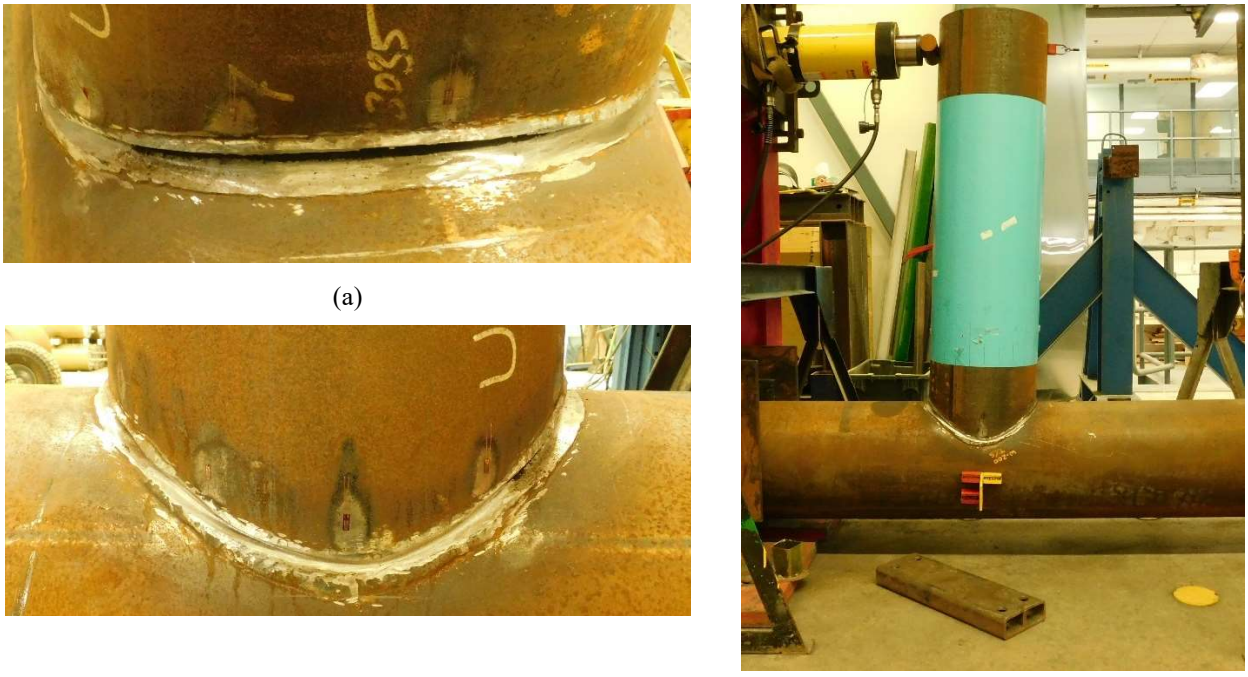

(a) (b) (c)

Figure 4-14 Failure of T356-324-1P (a) weld fracture, (b) chord deformation and (c) branch deformation

The moment-deflection relationship is shown in Figure 4-15 (a). The distribution of normal stain around the branch under different applied moment are shown in Figure 4-15 (b), where the subtended angle is the branch arc angle measured from the toe (end point of compression face). As with all other tests, the stain distribution is nearly symmetric when the applied moment is low, and becomes unsymmetric under higher applied moments.

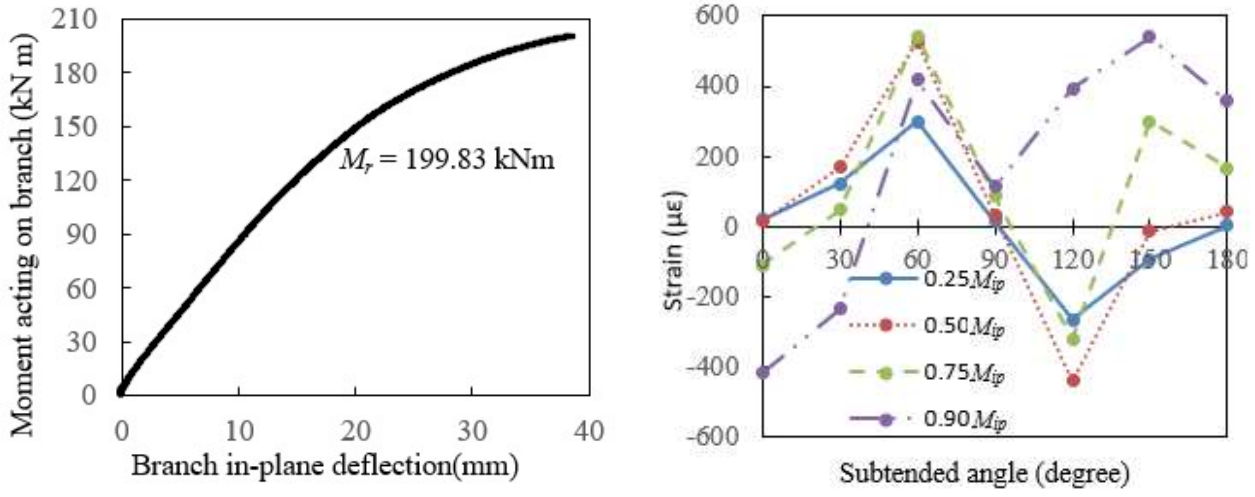

(a) (b)

Figure 4-15 T356-324-1P (a) moment-deflection and (b) normal strain distribution

4.2.7. T406-127-1

For the test T406-127-1, the branch deflection (at the loading point), at the ultimate moment, was 74.175 mm, and the chord face deformation was calculated to be 0.98 % of the chord diameter, vertically, at the crown of the weld. The ultimate moment resistance of the weld was 28.77 kNm (28.32 kN load with 1.02 m level arm). Figure 4-16 shows the failure of the specimen by weld fracture.

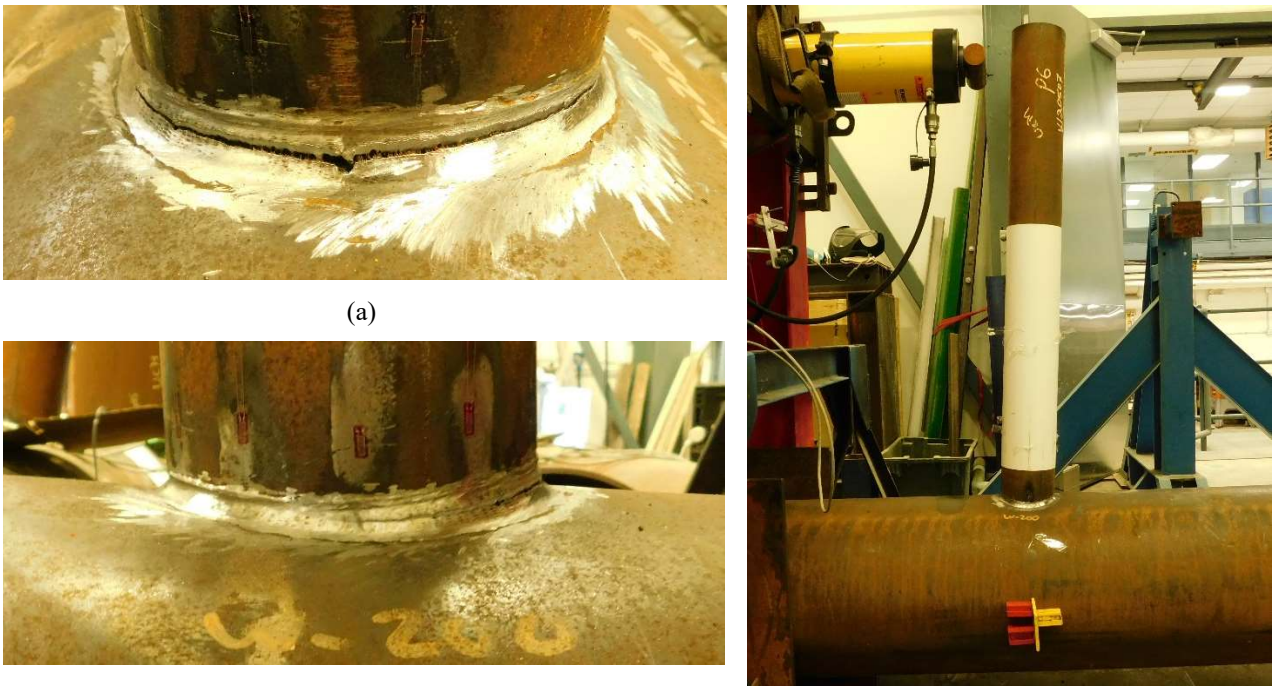

(a) (b) (c)

Figure 4-16 Failure of T406-127-1 (a) weld fracture, (b) chord deformation and (c) branch deformation

The moment-deflection relationship is shown in Figure 4-17 (a) where the weld starts with a linear-elastic behavior near the start of the test then gradually decreased in stiffness until the end of the test. The distribution of normal stain around the branch under different applied moment are shown in Figure 4-17 (b) where the subtended angle means the branch arc angle measured from the toe (end point of compression face). The stain distribution is nearly symmetric when the applied moment is low, while the stain becomes unsymmetric under higher applied moments.

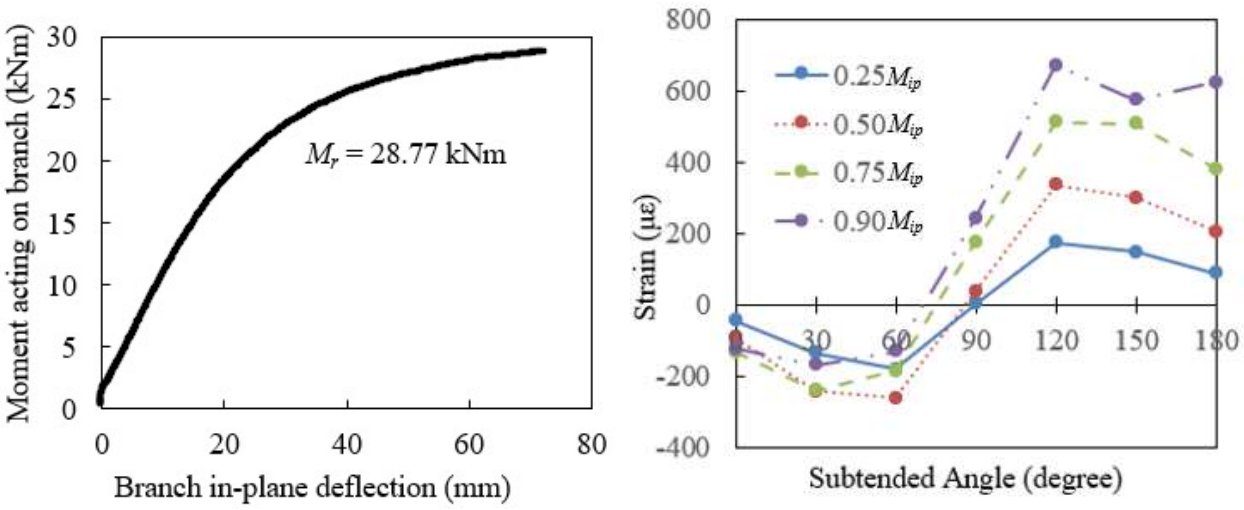

(a) (b)

Figure 4-17 T406-127-1 (a) moment-deflection and (b) normal strain distribution

4.2.8. T406-273-1P

For test T406-273-1P, the branch deflection (at the loading point), at the ultimate moment, was 81.61 mm, and the chord face deformation was calculated to be 2.57 % % of the chord diameter, vertically, at the crown of the weld. After the moment calculation from the load reading, the ultimate moment resistance of the weld in specimen T406-273-1P was 129.97 kNm (127.42 kN load with 1.02 m level arm). Figure 4-18 shows the failure of the specimen by weld fracture.

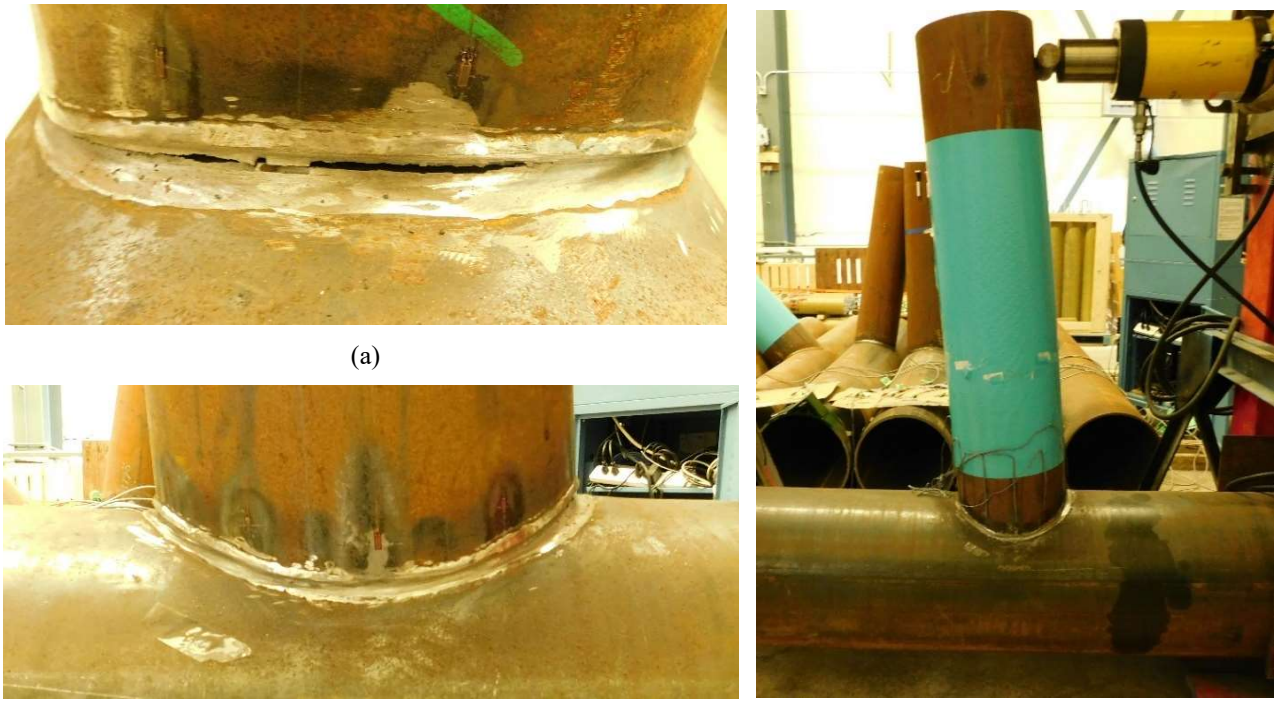

(a) (b) (c)

Figure 4-18 Failure of T406-273-1P (a) weld fracture, (b) chord deformation and (c) branch deformation

The moment-deflection relationship is shown in Figure 4-19 (a), where the weld starts with a linear-elastic behavior near the start of the test then gradually decreased in stiffness until the end of the test. The distribution of normal stain around the branch under different applied moment are shown in Figure 4-19 (b).

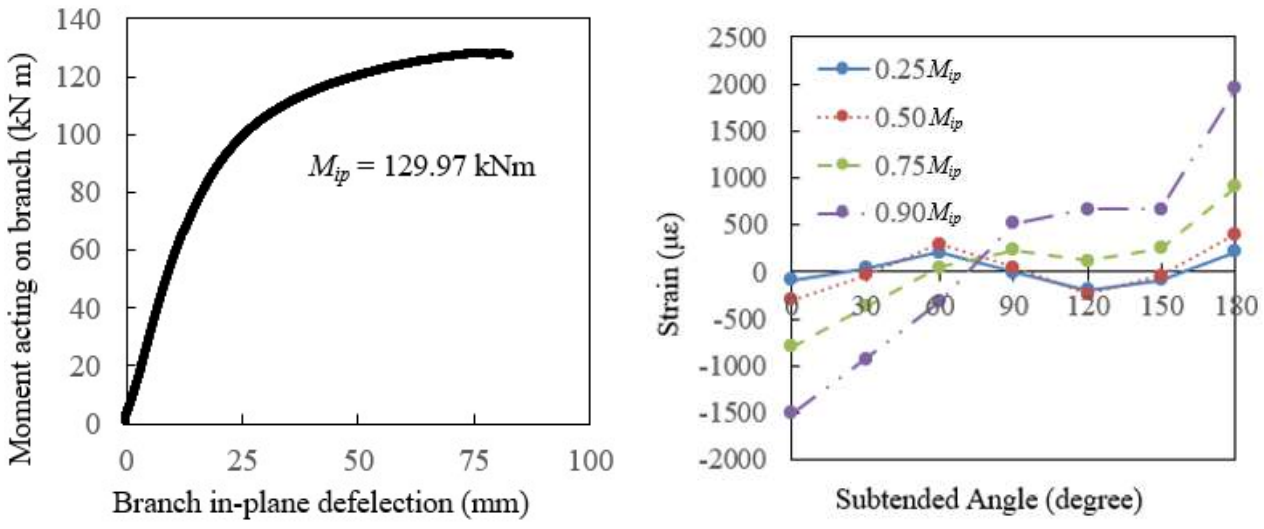

(a) (b)

Figure 4-19 T406-273-1P (a) moment-deflection and (b) normal strain distribution

4.2.9. T406-324-1P

For the test T406-324-1P, the branch deflection (at the loading point), at the ultimate moment, was 84.47 mm, and the chord face deformation was calculated to be 3.21 % of the chord diameter, vertically, at the crown of the weld. The ultimate moment resistance of the weld was 188.97 kNm (187.10 kN load with 1.01 m level arm). Figure 4-20 shows the failure of the specimen by weld fracture.

(a)

(b)

(c)

Figure 4-20 Failure of T406-324-1 (a) weld fracture, (b) chord deformation and (c) branch deformation

The moment-deflection relationship is shown in Figure 4-21 (a), where the weld starts with a linear-elastic behavior near the start of the test then gradually decreased in stiffness until the end of the test. During testing, it was observed that the frame “slid”, which resulted in a “jump” in the overall deformation measurement that can be seen near the beginning of the figure. The distribution of normal stain around the branch under different applied moment are shown in Figure 4-21 (b).

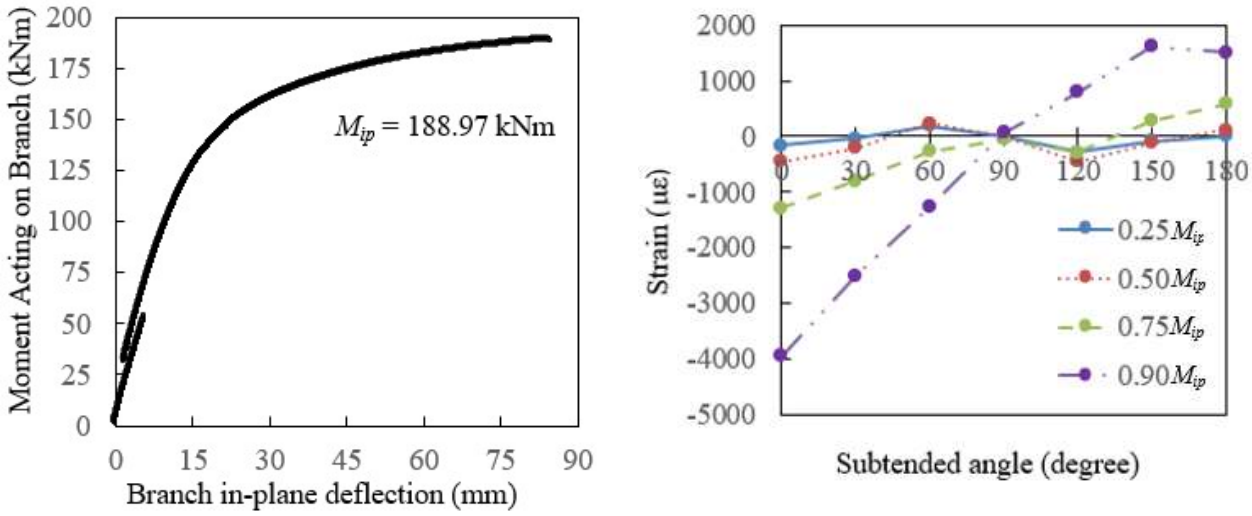

(a) (b)

Figure 4-21 T406-324-1P (a) moment-deflection and (b) normal strain distribution

4.2.10. T406-127-0.7

For test T406-127-0.7, the branch deflection (at the loading point), at the ultimate moment, was 43.33 mm, and the chord face deformation was calculated to be 0.49 % of the chord diameter, vertically, at the crown of the weld. After the moment calculation from the load reading, the ultimate moment resistance of the weld in specimen T406-127-0.7 was 31.59 kNm (30.97 kN load with 1.02 m level arm). Figure 4-22 shows the failure of the specimen by weld fracture.

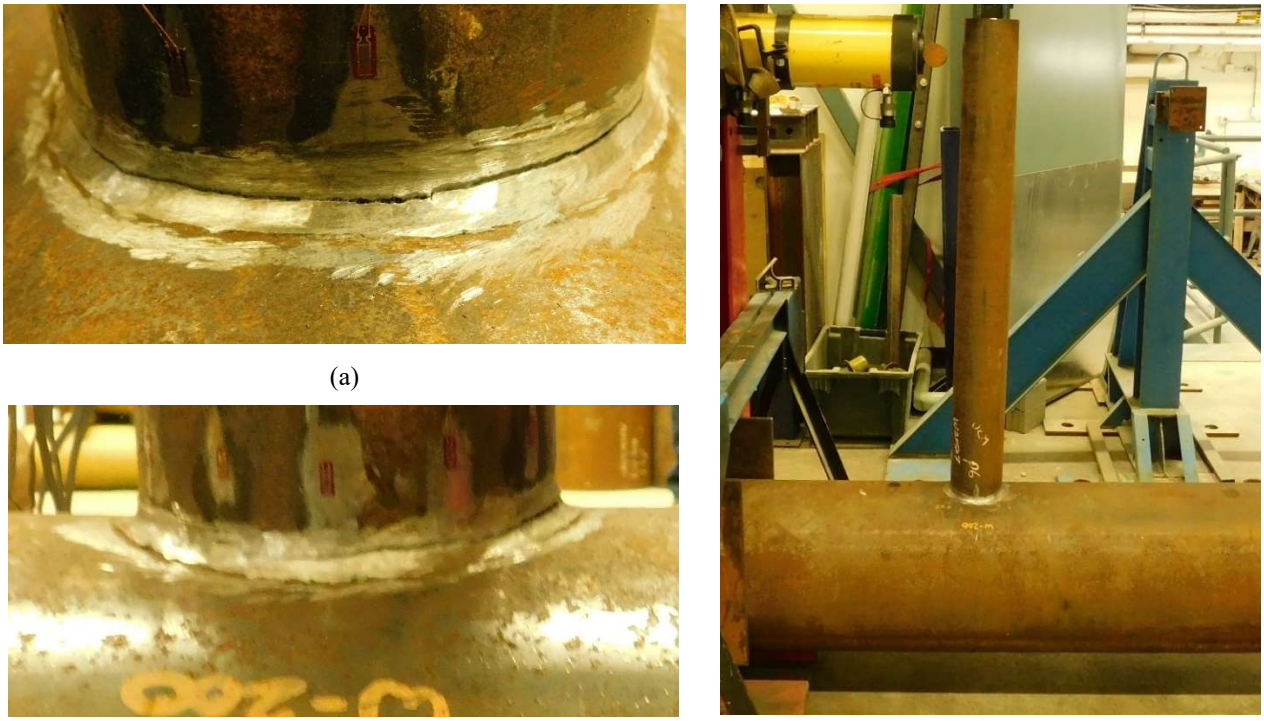

(a) (b) (c)

Figure 4-22 Failure of T406-127-0.7 (a) weld fracture, (b) chord deformation and (c) branch deformation

The moment deflection relationship is shown in Figure 4-23 (a) where the weld starts with a linear-elastic behavior near the start of the test then gradually decreased in stiffness until the end of the test. The distribution of normal stain around the branch under different applied moments are shown in Figure 4-23 (b).

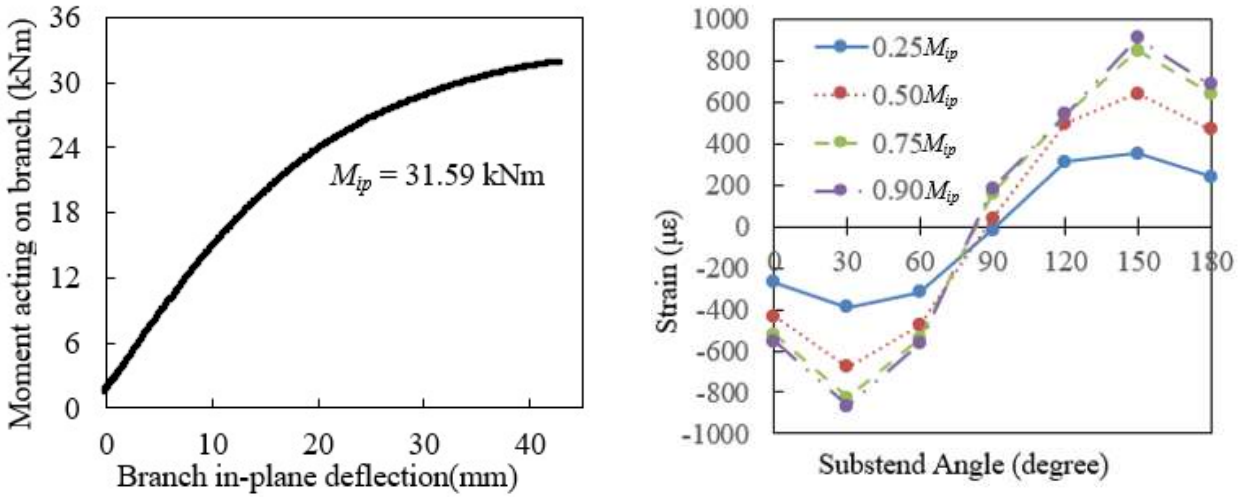

(a) (b)

Figure 4-23 T406-127-0.7 (a) moment-deflection and (b) normal strain distribution

4.2.11. T406-273-0.7P

For test T406-273-0.7P, the branch deflection (at the loading point), at the ultimate moment, was 33.61 mm, and the chord face deformation was calculated to be 0.99 % of the chord diameter, vertically, at the crown of the weld. The ultimate moment resistance of the weld was 144.97 kNm (143.54 kN load with 1.01 m level arm). Figure 4-24 shows the failure of the specimen by weld fracture.

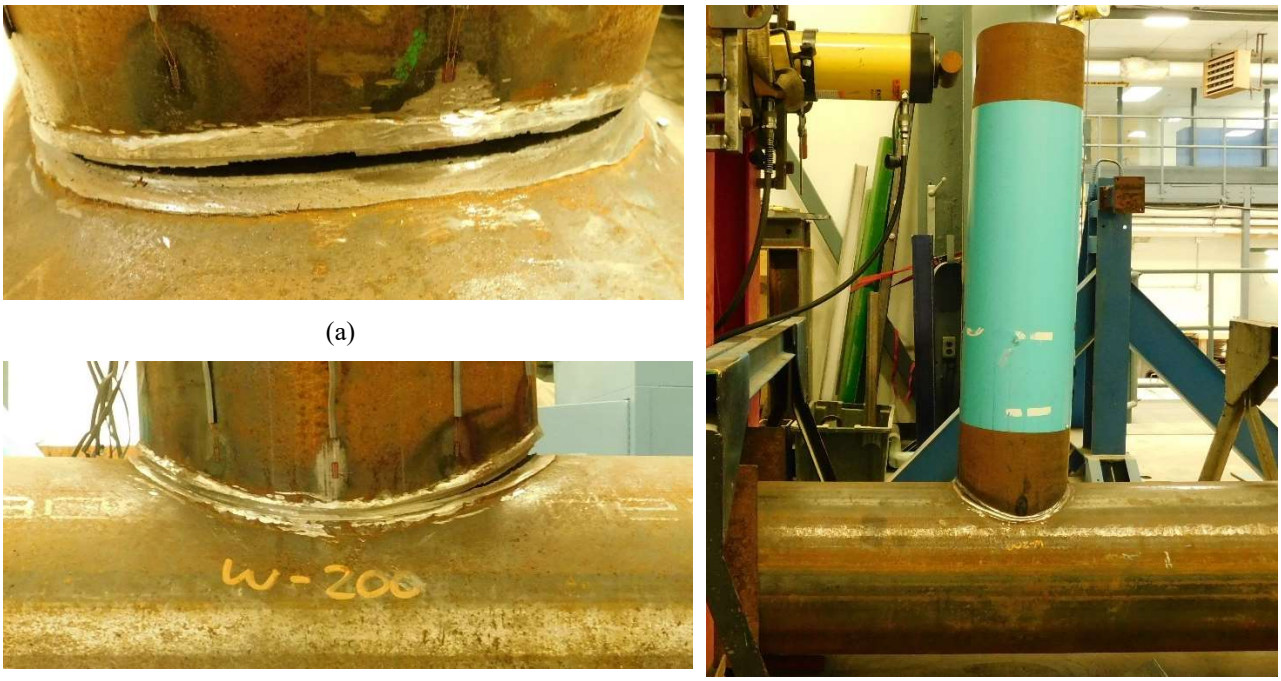

(a) (b) (c)

Figure 4-24 Failure of T406-273-0.7P (a) weld fracture, (b) chord deformation and (c) branch deformation

The moment-deflection relationship is shown in Figure 4-25 (a) and the distribution of normal stain around the branch under different applied moment are shown in Figure 4-25 (b).

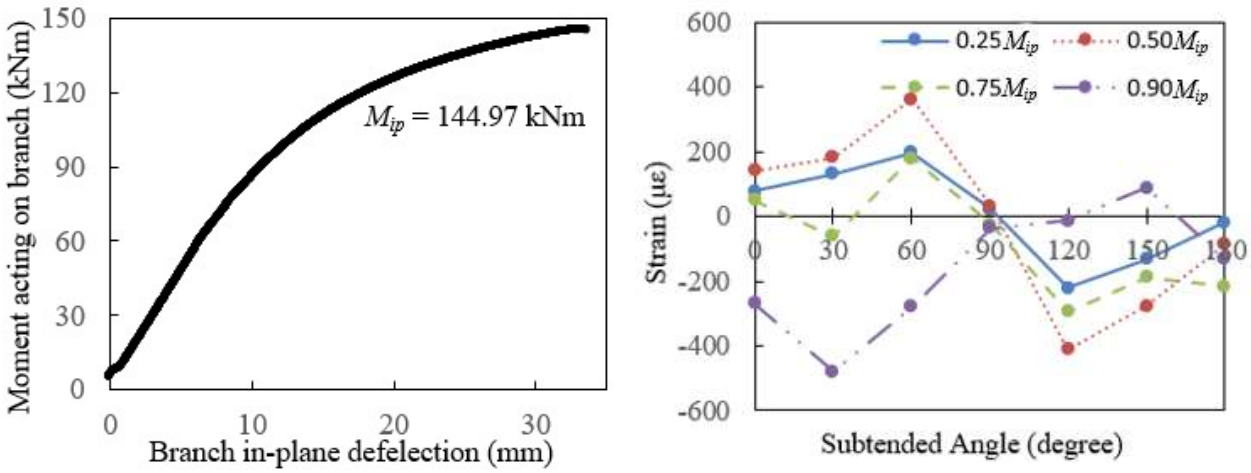

(a) (b)

Figure 4-25 T406-273-0.7P (a) moment-deflection and (b) normal strain distribution

4.2.12. T406-324-0.7P

For test T406-324-0.7P, the branch deflection (at the loading point), at the ultimate moment was 71.08 mm, and the chord face deformation was calculated to be 2.64 % of the chord diameter, vertically, at the crown of the weld. The ultimate moment resistance of the weld in specimen T406-324-0.7P was 251.60 kNm (249.11 kN load with 1.01 m level arm). Figure 4-26 shows the failure of the specimen by weld fracture.

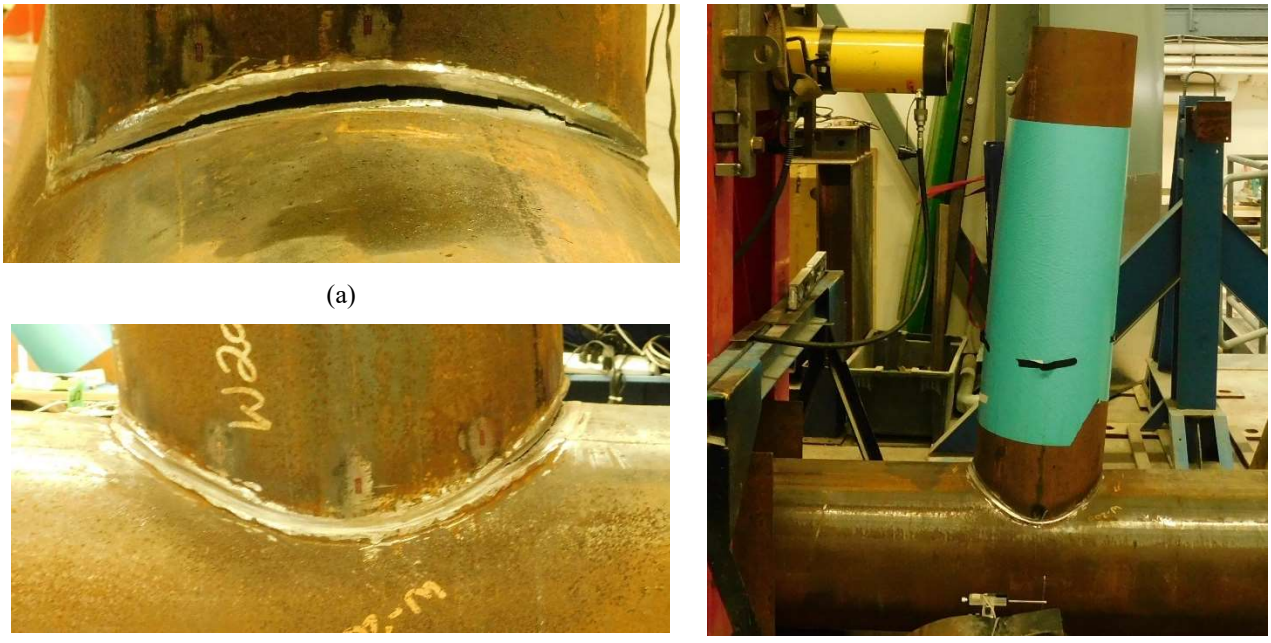

(a) (b) (c)

Figure 4-26 Failure of T406-324-0.7P (a) weld fracture, (b) chord deformation and (c) branch deformation

The moment-deflection relationship is shown in Figure 4-27 (a). The distribution of normal stain around the branch under different applied moments are shown in Figure 4-27 (b).

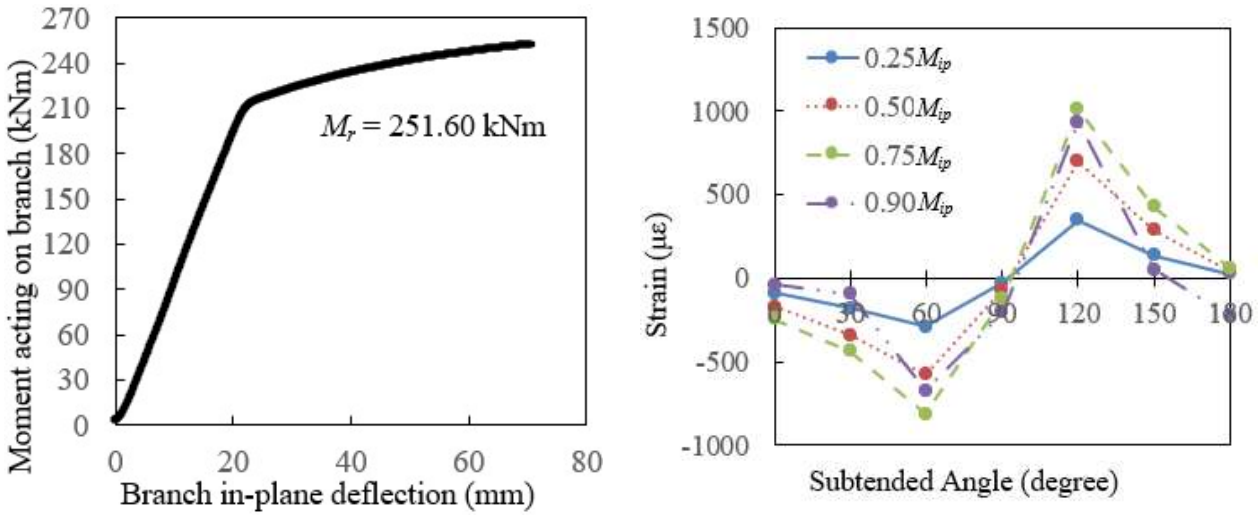

(a) (b)

Figure 4-27 T406-324-0.7P (a) moment-deflection and (b) normal strain distribution

4.3. DEVELOPMENT OF AN EQUATION FOR THE WELD EFFECTIVE SECTION MODULUS

In Section 2.4.1, the weld effective section modulus for in-plane bending for RHS-to-RHS moment T-connections was shown in Equation 2.31 - 2.34. This was based on the weld effective length, for the same connection(s), given in Equation 4.1 and 4.2. If the weld in a CHS-to-CHS+ moment T-connection is assumed to be in a single, flat plane, then a weld effective section modulus for in-plane bending for CHS-to-CHS moment T-connections can be found in a similar manner, based on Equation 4.2. A summary of the procedure is shown below; the full derivation is shown in Appendix A.

$$I_{ip} = \frac{1}{4}[(\frac{D_b}{2} + t_w)^4 - (\frac{D_b}{2})^4](\frac{l_e}{D_b} - \sin\frac{l_e}{D_b}) \text{ for fillet welds} \quad (4.1a)$$

$$I_{ip} = \frac{1}{4}[(\frac{D_b}{2} - g)^4 - (\frac{D_b}{2} - g - t_w)^4](\frac{l_e}{D_b} - \sin\frac{l_e}{D_b}) \text{ for PJP welds} \quad (4.1b)$$

$$S_{ip} = I_{ip} / (\frac{D_b}{2}\sin\frac{l_e}{2D_b}) \quad (4.2)$$

where l_e is given in Equation 2.34; g = gap between PJP weld surface and branch base metal (see Appendix A.2). Hence, for the calculation of flexural strength using the above equations:

$$M_{ip} = \phi S_{ip} F_{nw} \quad (4.3)$$

Equations 4.1 – 4.3 have been determined based on the principle of elastic deformation (and, hence, reflect the effective elastic section modulus). An equation for the effective plastic section modulus (Z_{ip}) of the welds can also be determined, as shown below. The full derivation is shown in Appendix A.

$$Z_{ip} = \frac{1}{2} l_e D_b t_w \sin(\frac{l_e}{4D_b}) \tag{4.4}$$

Hence, for the calculation of flexural strength using the above equation:

$$M_{ip} = \phi Z_{ip} F_{nw} \tag{4.5}$$

The following assumptions have been made in Equation. (4.4) for application to both fillet welds and PJP welds (details shown in Appendix A):

1. The inside diameter of the weld is assumed to be equal to the outside diameter of the branch for PJP welded specimens, since the thickness removed from the CHS wall to create the PJP weld detail is small compared to D_b.
2. The t_w^2 term is ignored during calculation since the weld throat size is very small compared to D_b.

Herein, the weld effective section moduli (and corresponding predicted flexural strengths) are determined in the following ways, for comparison to test results:

1. Using the effective elastic section modulus (S_{ip}) (Equation 4.1 to 4.3) with l_e calculated by using Equation 2.34 – termed the "effective elastic section modulus" (EESM) method.
2. Using an effective elastic section modulus (S_{ip}) (Equation 4.1 to 4.3) with $l_e = l_w$ (Equation 2.35) – termed the "fully effective elastic section modulus" (FEESM) method.
3. Using an effective plastic section modulus (Z_{ip}) (Equation 4.4 and 4.5) with l_e calculated by using Equation 2.34 – termed the "effective plastic section modulus" (EPSM) method.
4. Using an effective plastic section modulus (Z_{ip}) (Equation 4.4 and 4.5) with $l_e = l_w$ (Equation 2.35) - termed the "fully effective plastic section modulus" (FEPSM) method.

Additionally, the following critical weld stress(es) at failure are considered:

For fillet welds, designed in accordance with AISC 360-16 (AISC 2016):

$$F_{nw} = 0.60 F_{EXX} (1.00 + 0.5 \sin^2 \theta) \tag{4.6}$$

For PJP welds, designed in accordance with AISC 360-16 (AISC 2016):

$$F_{nw} = 0.60 F_{EXX} \tag{4.7}$$

For fillet welds, designed in accordance with CSA S16:19 (CSA 2019):

$$F_{nw} = 0.67 F_{EXX} (1.00 + 0.5 \sin^2 \theta) \tag{4.8}$$

For PJP welds, designed in accordance with CSA S16:19 (CSA 2019):

$$F_{nw} = 0.67 F_{EXX} \tag{4.9}$$

For fillet welds, using a rational analysis, with F_{nw} from Tousignant and Packer (2017):

$$F_{nw} = (0.984 - 0.226\frac{t_w}{t_b})F_{EXX} \tag{4.10}$$

For PJP welds, using a rational analysis, with F_{nw} from Luo et al. (2020):

$$F_{nw} = 0.60 F_{EXX}(1 + 0.629\theta + 0.068\theta^2) \text{ for AISC} \tag{4.11a}$$

$$F_{nw} = 0.67 F_{EXX}(1 + 0.629\theta + 0.068\theta^2) \text{ for CSA} \tag{4.11b}$$

4.4. ULTIMATE RESISTANCE AND PREDICTION

4.4.1. AISC 360-16

Herein, the predicted flexural strength of weld is calculated based on Equations 4.1 to 4.7, using ϕ = 1.0 and measured weld properties (F_{EXX} = 592 MPa and weld throats according to MDM). The results, as well as the mean values and COVs for each method, are shown in Table 4-2. Figures 4-28 to 4-31 show correlation plots of the actual vs. predicted weld strength according to the above-noted methods. The mean values and COVs in Figs. 4-28 to 4-31 correspond to the actual-to-predicted nominal strength ratios listed in Table 4-2.

Table 4-2 Predicted and actual strength of each test specimen according to AISC standard

Test Designation	Actual Strength (kNm)	Predictions Associate with (kNm)							
		EESM	A/P	EPSM	A/P	FEESM	A/P	FEPSM	A/P
T273-127-1P	39.77	9.07	4.41	17.21	2.32	25.44	2.36	33.63	1.78
T273-127-1	154.12	10.54	NA	14.55	NA	18.14	NA	23.55	NA
T324-127-1	36.47	12.65	2.88	17.29	2.11	20.62	1.77	26.84	1.36
T356-127-1	28.33	9.81	2.89	13.60	2.08	16.14	1.76	20.91	1.36
T356-273-1P	155.88	28.78	5.44	48.74	3.21	158.12	1.49	205.54	1.14
T356-324-1P	199.83	37.38	5.37	62.68	3.21	204.19	1.48	264.15	1.14
T406-127-1	28.74	11.47	2.51	15.76	1.82	19.59	1.47	25.47	1.13
T406-273-1P	129.97	23.57	5.54	39.36	3.32	127.08	1.54	164.49	1.19
T406-324-1P	188.97	27.79	6.83	45.53	4.17	169.27	1.68	218.31	1.30
T406-127-0.7	31.59	15.13	2.09	20.52	1.54	19.59	1.61	25.47	1.24
T406-273-0.7P	144.97	34.65	4.20	58.02	2.51	141.51	1.54	183.52	1.19
T406-324-0.7P	251.60	47.26	5.35	78.08	3.24	217.88	1.74	282.10	1.34
Mean			4.22		2.63		1.67		1.28
COV			0.375		0.312		0.159		0.152

Note: NA means the data is not applicable for analysis.

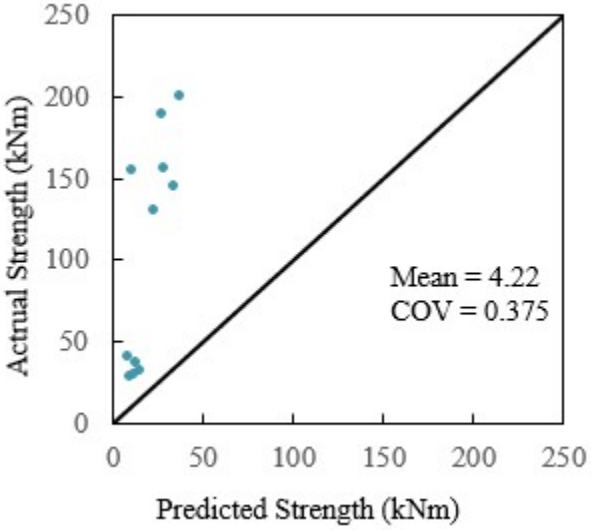

Figure 4-28 Correlation plot of actual strength and prediction using EESM

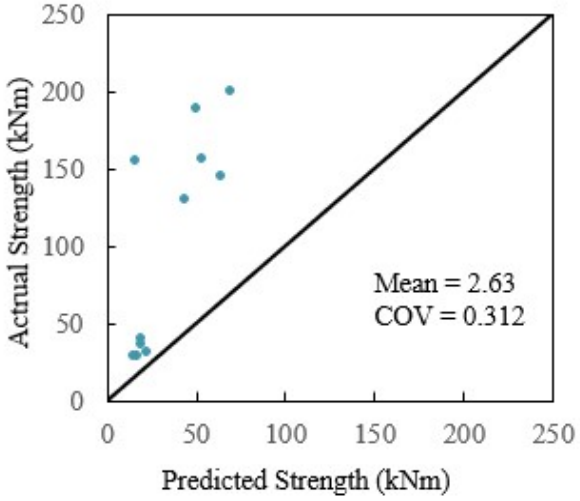

Figure 4-29 Correlation plot of actual strength and prediction using EPSM

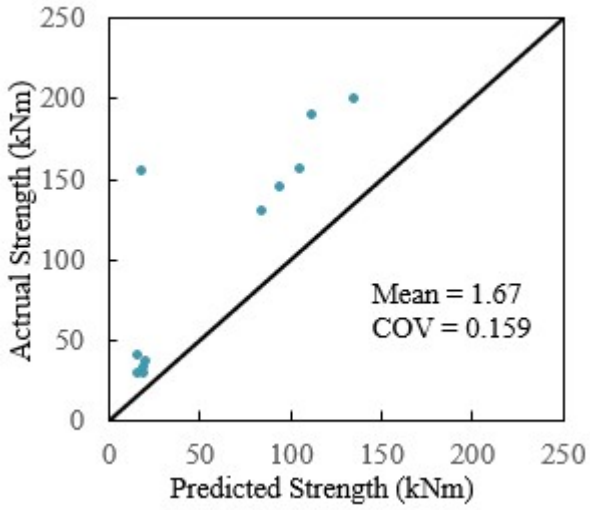

Figure 4-30 Correlation plot of actual strength and prediction using FEESM

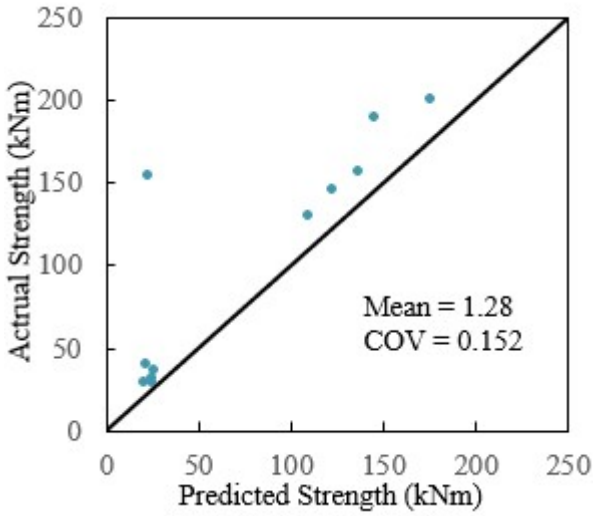

Figure 4-31 Correlation plot of actual strength and prediction using FEPSM

From the table and plots above, the strength calculated by using the effective weld length is conservative, for both elastic and plastic section moduli (EESM and EPSM, respectively). The predicted strength increases, but is still generally conservative, when the total weld length is used, with both elastic and plastic analysis (FEESM and FEPSM, respectively).

4.4.2. CSA S16-19

Herein, the predicted flexural strength of weld is calculated based on Equations 4.1 to 4.5, 4.8 and 4.9 using $\phi = 1.0$ and measured weld properties ($X_u = 592$ MPa and weld throats according to MDM). The results, as well

as the means and COVs for each method, are shown in Table 4-3. Figures 4-32 to 4-35 show correlation plots of actual vs. predicted weld strength according to each method. The mean values and COVs in Figs. 4-32 to 4-35 correspond to the actual-to-predicted nominal strength ratios listed in Table 4-3.

Table 4-3 Predicted and actual strength of each test specimen according to CSA standard

Test Designation	Actual Strength (kNm)	Predictions Associate with (kNm)							
		EESM	A/P	EPSM	A/P	FEESM	A/P	FEPSM	A/P
T273-127-1P	39.77	10.08	3.95	19.12	2.07	18.85	2.11	24.91	1.60
T273-127-1	154.12	11.77	NA	16.25	NA	20.26	NA	26.30	NA
T324-127-1	36.47	14.13	2.58	19.31	1.89	23.03	1.58	29.98	1.22
T356-127-1	28.33	10.95	2.58	15.19	1.87	18.02	1.57	23.35	1.21
T356-273-1P	155.88	31.97	4.87	54.15	2.88	117.13	1.33	152.25	1.02
T356-324-1P	199.83	41.53	4.81	69.65	2.87	151.25	1.32	195.66	1.02
T406-127-1	28.74	12.81	2.24	17.60	1.63	21.88	1.31	28.44	1.01
T406-273-1P	129.97	26.19	4.96	43.73	2.97	94.13	1.38	121.84	1.07
T406-324-1P	188.97	30.88	6.12	50.59	3.74	125.38	1.51	161.71	1.17
T406-127-0.7	31.59	16.90	1.87	22.92	1.38	21.88	1.44	28.44	1.11
T406-273-0.7P	144.97	38.50	3.77	64.46	2.25	104.82	1.38	135.94	1.07
T406-324-0.7P	251.60	52.51	4.79	86.76	2.90	161.40	1.56	208.96	1.20
Mean			3.78		2.35		1.49		1.15
COV			0.375		0.312		0.159		0.152

Note: NA means the data is not applicable for analysis.

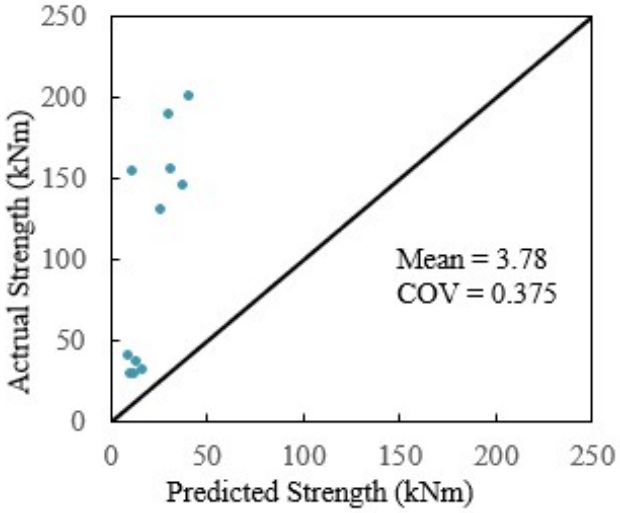

Figure 4-32 Correlation plot of actual strength and prediction using EESM

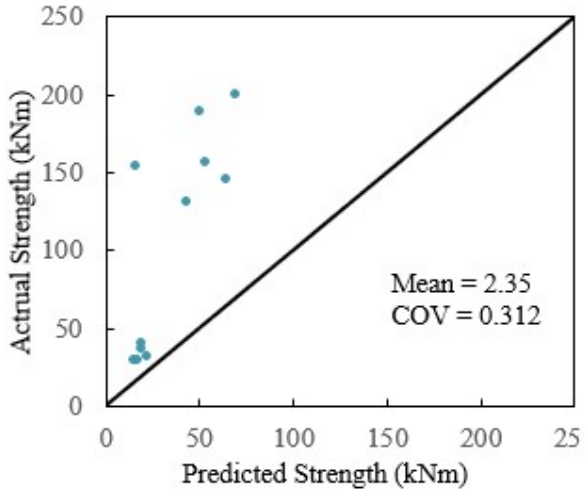

Figure 4-33 Correlation plot of actual strength and prediction using EPSM

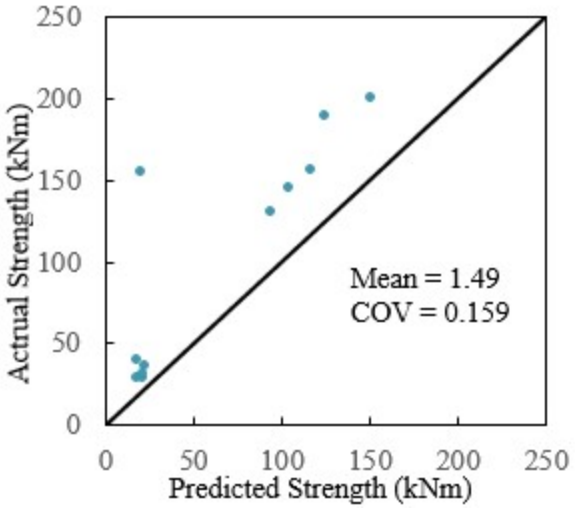

Figure 4-34 Correlation plot of actual strength and prediction using FEESM

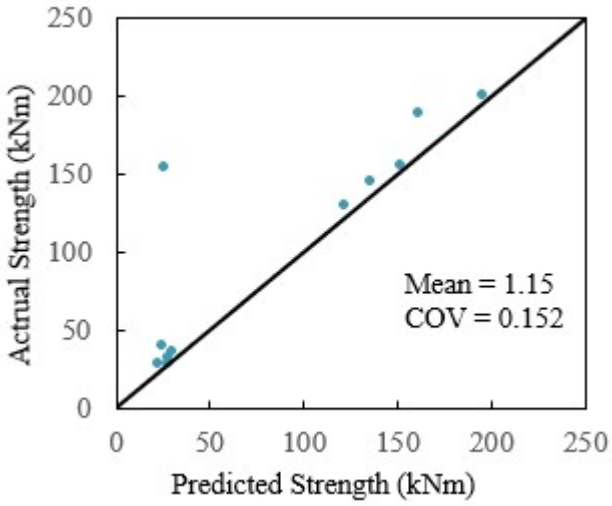

Figure 4-35 Correlation plot of actual strength and prediction using FEPSM

4.4.3. RATIONAL ANALYSIS

In Section 2.4, it was shown that the strength of PJP welds in codes is generally conservative, i.e., based on rational and FE analyses, a directional strength-increase factor (DIF) was shown to apply to the welds, based on the loading angle (Luo et al. 2020). This DIF is not embodied in codes. Moreover, Tousignant & Packer (2017) showed that the strength of a fillet weld to an HSS branch is a function of the thickness, diameter, and weld size.

Herein, the recommendations from these two studies are applied (see Equations 4.10 and 4.11), taking the angle between the applied load and the weld axis, $\theta = 90°$, where necessary.

Table 4-4 shows the actual and predicted strength of each test specimen, and Figure 4-36 to 4-39 shown the correlation plots for each method assessed. From the comparisons, it can be seen that the predicted strengths using effective properties (EESM and EPSM) approaches the actual strengths of the weld. In the following Chapter, all of the calculation approaches studied herein will be evaluated by using a first-order reliability method (FORM) analysis technique to calculate reliability indices (β) for comparison to targets specified in North American standards.

Table 4-4 Predicted and actual strength of each test specimen include both fillet weld parameter and PJP DIF

Test Designation	Actual Strength (kNm)	Predictions Associate with (kNm)							
		AISC Standard				CSA Standard			
		EESM	A/P	EPSM	A/P	EESM	A/P	EPSM	A/P
T273-127-1P	39.77	19.46	2.04	37.10	1.08	21.73	1.83	41.23	0.96
T273-127-1	154.12	10.80	NA	14.91	NA	10.80	NA	14.91	NA
T324-127-1	36.47	12.83	2.84	17.54	2.08	12.83	2.84	17.54	2.08
T356-127-1	28.33	10.13	2.80	14.05	2.02	10.13	2.80	14.05	2.02
T356-273-1P	155.88	61.74	2.52	104.54	1.49	68.94	2.80	116.74	1.34
T356-324-1P	199.83	80.19	2.49	134.46	1.48	89.54	2.26	150.15	1.33
T406-127-1	28.74	11.68	2.46	16.05	1.79	11.68	2.23	16.05	1.79
T406-273-1P	129.97	50.56	2.57	84.44	1.54	56.45	2.46	94.28	1.38
T406-324-1P	188.97	59.61	3.17	98.66	1.93	66.56	2.30	109.05	1.73
T406-127-0.7	31.59	15.42	2.05	20.91	1.51	15.42	2.83	20.91	1.51
T406-273-0.7P	144.97	74.33	1.95	124.45	1.16	83.00	2.05	138.97	1.04
T406-324-0.7P	251.60	101.28	2.48	167.50	1.50	113.21	1.75	187.04	1.35
Mean			2.49		1.61		2.34		1.52
COV			0.157		0.212		0.171		0.251

Note: NA means the data is not applicable for analysis.

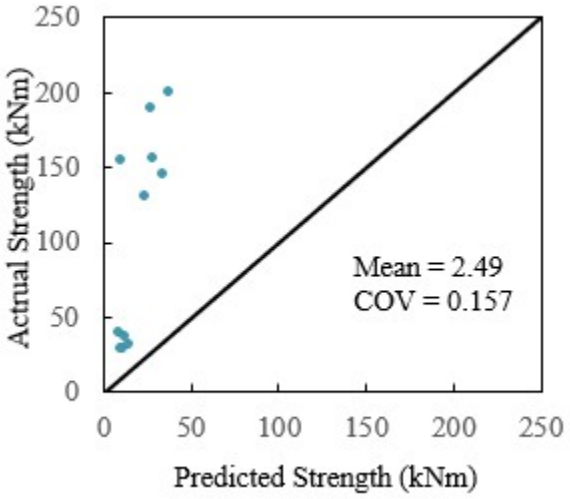

Figure 4-36 Correlation plot of actual strength and prediction using EESM (AISC)

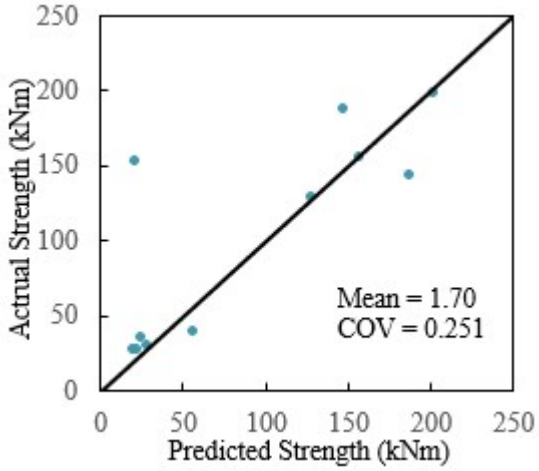

Figure 4-37 Correlation plot of actual strength and prediction using EPSM (AISC)

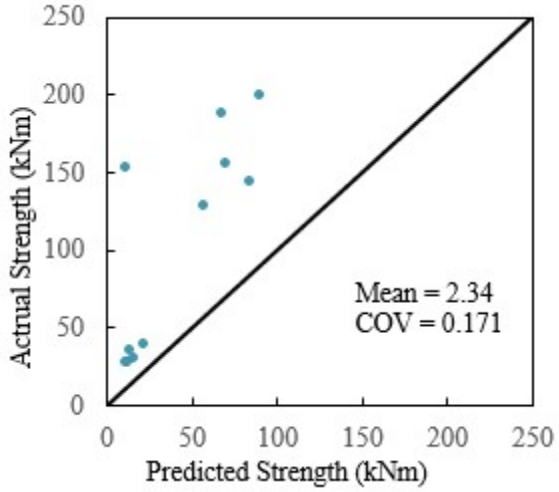

Figure 4-38 Correlation plot of actual strength and prediction using EESM (CSA)

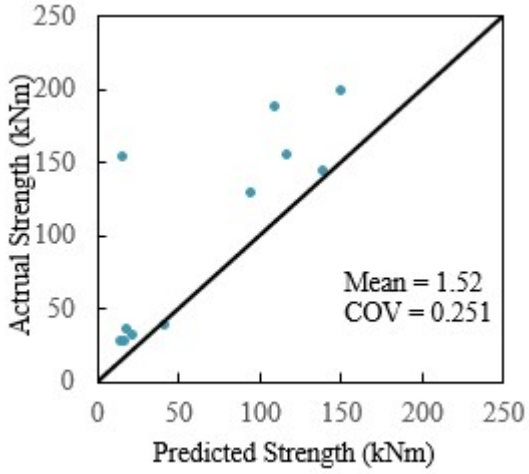

Figure 4-39 Correlation plot of actual strength and prediction using EPSM (CSA)

Chapter 5: EVALUATION OF THE RECOMMENDED EQUATION

The relationship between the reliability index (β) and the resistance factors (ϕ) spelled out in North American codes can be summarized using Equation 5.1, which has been widely used in previous research (Kennedy & Lesik 1990; MacPhedran & Grondin 2011; CSA 2019b). The target reliability index (β) for non-ductile failures, such as welds, in both AISC and CSA is 4.0, with resistance factors for welds (ϕ) of 0.75 and 0.67, respectively.

$$\phi = \delta_R \frac{\alpha_D + \alpha_L (L/D)}{\delta_D + \delta_L (L/D)} \exp[-\beta \sqrt{V_R^2 + V_S^2}] \tag{5.1}$$

where δ_R = bias coefficient of resistance; δ_D = bias coefficient of dead load; δ_L = bias coefficient of live load; α_D = load factor of dead load; α_L = load factor of live load; L/D = live to dead load ratio; β = reliability index; V_R = coefficient of variation of resistance; and V_S = coefficient of variation of load.

The calculation of the reliability index requires the value of the bias coefficients and the coefficients of variation (COV) for both the resistance and load effects. Since the resistance varies with both material and geometric properties, as well as the inherent "accuracy" of design equations, the bias coefficient and COV of the resistance are often computed by using Equations 5.2 and 5.3 (CSA S6:19 Clause 14.15.2.3) which include geometry (denoted as G), material (denoted as M), and professional (denoted as P), factors, i.e.:

$$\delta_R = \delta_G \delta_M \delta_P \tag{5.2}$$

$$V_R = \sqrt{V_G^2 + V_M^2 + V_P^2} \tag{5.3}$$

where δ_G = bias coefficient of geometry; δ_M = bias coefficient of material; δ_P = bias coefficient of profession; V_G = coefficient of variation (geometry); V_M = coefficient of variation (material); V_P = coefficient of variation (profession).

The values of these parameters can be obtained from experimental result or previous research. The professional factor, for example, is obtained by the comparison of predicted and actual (nominal) strengths (as done in the previous section). In this study, the remainder of the variables are taken from the literature.

The COV of load the load effects (V_S) is related to the dead and live load by Equation 5.3 (CSA 2019):

$$V_S = \frac{\sqrt{(\delta_D V_D)^2 + (\delta_L V_L (L/D))^2}}{\delta_D + \delta_L (L/D)} \tag{5.4}$$

where V_L = COV of the dead load effect and V_D = COV of the live load effect.

Herein, the load parameters (δ_D, V_D, δ_L, and V_L) are obtained from previous research by MacPhedran and Grondin (2011). The values of δ_D = 0.90, V_D = 0.10 δ_L = 1.05 and V_L = 0.27 are hence used. The geometric parameters are obtained from research done by Callele et al. (2009) on fillet welds, i.e., δ_G = 1.03 and V_G = 0.10 (Callele et al. 2009).

The material parameters (δ_M and V_M) are obtained from Lesik and Kennedy (1990), as summarized in Table 5-1. The factor of δ_M and V_M are equal to 1.123 and 0.077, respectively.

Table 5-1 Measured-to-nominal ratios of ultimate tensile strength of weld metal (Lesik & Kennedy 1990)

Source	Sample size n	Nominal tensile strength X_u	Mean tensile strength σ_u	Measured nominal (σ_u / X_u)	Standard deviation	Coefficient of variation
Miazga & Kennedy (1986)	3	480 MPa	537.7 MPa	1.120	0.0158	0.0141
Gagnon & Kennedy (1987)	10	480 MPa	579.9 MPa	1.208	0.0482	0.0355
Swannell & Skewes (1979b)	2	410 MPa	538.8 MPa	1.314	0.0262	0.0199
Fisher et al. (1978)	127	60 ksi	66.0 ksi	1.100	0.0427	0.0388
	138	70 ksi	74.9 ksi	1.070	0.0381	0.0356
	136	80 ksi	87.9 ksi	1.099	0.0543	0.0494
	16	90 ksi	100.2 ksi	1.113	0.0480	0.0431
	72	110 ksi	116.9 ksi	1.063	0.0426	0.0400
	128	70 ksi	85.4 ksi	1.220	0.0681	0.0559
	40	70 ksi	86.8 ksi	1.240	0.1411	0.1138
Total	672			1.123	0.087	0.077

5.1.1. AISC 360-16

As mentioned in the previous section, in AISC 360-16, the resistance factor for weld metal is $\phi = 0.75$ for fillet welds and $\phi = 0.80$ for PJP welds, and the target reliability index is 4.0. The load factors used in ASCE-7 are: $\alpha_D = 1.4$ and $\alpha_L = 0$ (for the dead-load only case), and $\alpha_D = 1.2$ and $\alpha_L = 1.6$ (for the dead plus live load case). The factored load from both load cases are set to be equaled to calculate the critical live-to-dead load ratio. For AISC 360/ASCE-7, the latter load case governs when $L/D > 0.125$.

Based on the bias coefficients and COVs obtained from the experiments in Chapter 4, and previous research, β is calculated two ways: using $\phi = 0.75$ for all tests (Figure 5-1), and using $\phi = 0.80$ for all tests (Figure 5-2). The former approach is conservative for PJP welds.

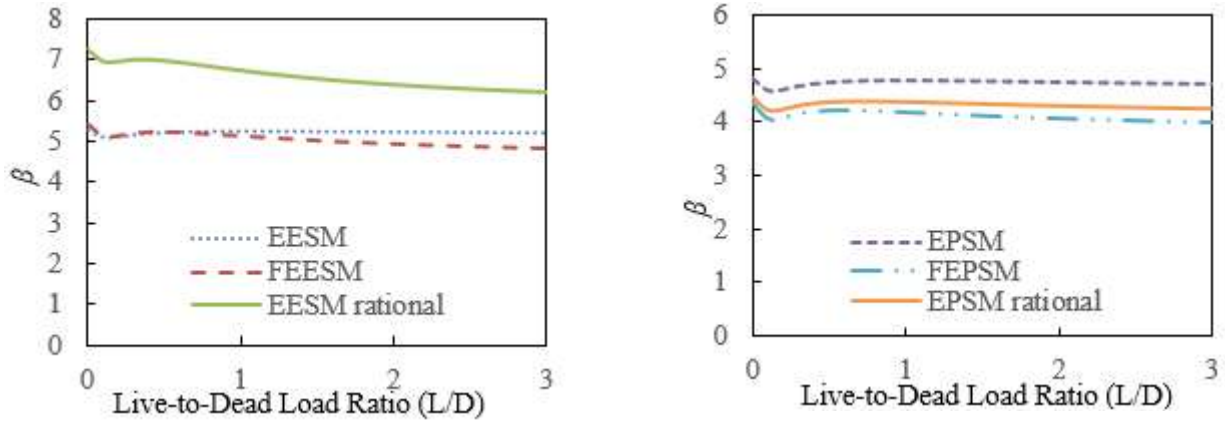

(a) (b)

Figure 5-1 Reliability index for AISC based on: (a) elastic and (b) plastic section modulus with $\phi = 0.75$

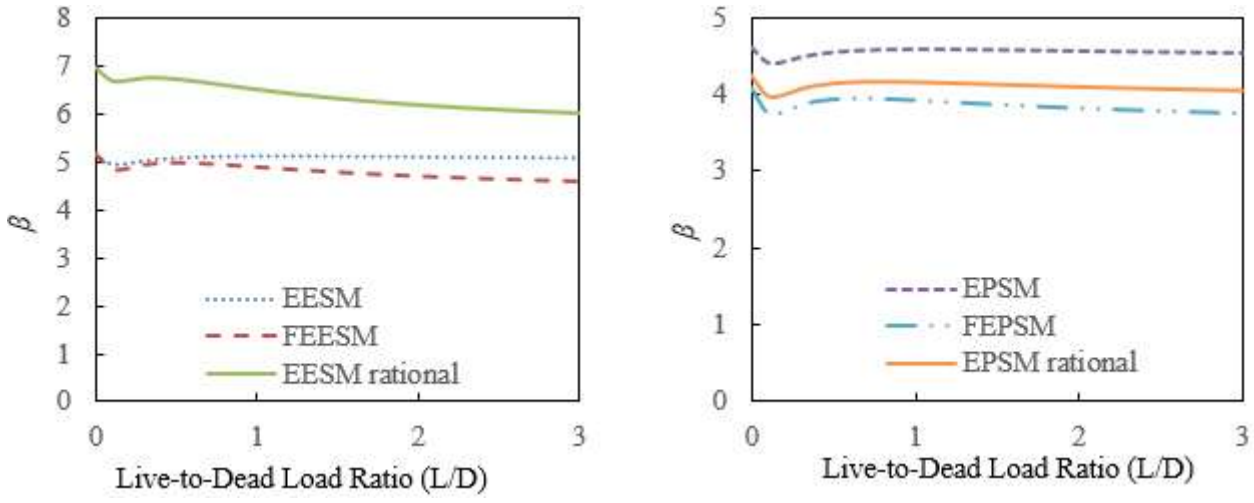

(a) (b)

Figure 5-2 Reliability index for AISC based on: (a) elastic and (b) plastic section modulus with $\phi = 0.80$

5.1.2. CSA S16-19

In CSA S16-19, the resistance factor for weld metal is $\phi = 0.67$ for both fillet and PJP welds, and the target reliability index is 4.0. The load factors used in the NBC are: $\alpha_D = 1.4$ and $\alpha_L = 0$ (for the dead-load only case), and $\alpha_D = 1.25$ and $\alpha_L = 1.5$ (for the dead plus live load case). The factored load from both load cases are set to be equaled to calculate the critical live-to-dead load ratio. For CSA S16:19/NBC, the latter load case governs when $L/D > 0.10$.

Based on the bias coefficients and COVs obtained from the experiments in Chapter 4, β is calculated using $\phi = 0.67$ for all tests, over a range of $0 \leq L/D \leq 3$ (Figure 5-3).

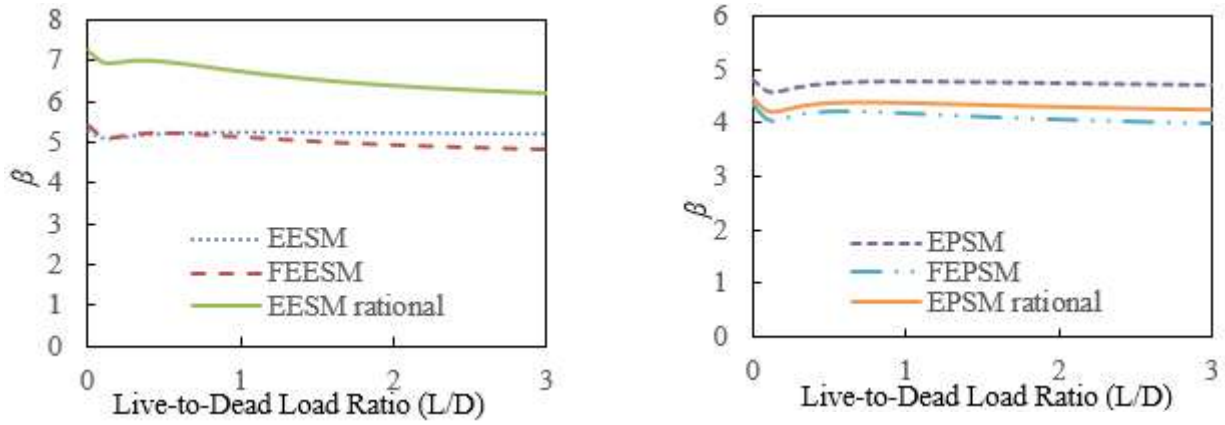

(a) (b)

Figure 5-3 Reliability index for CSA based on: (a) elastic and (b) plastic section modulus

5.1.3. Summary of Reliability Analysis

The results of the reliability analysis are summarized in Table 5-2. As can be seen, all of the calculation methods based on using the elastic section modulus (EESM, FESM, EESM rational) satisfy the reliability requirements of both AISC and CSA (i.e., $\beta \geq 4.0$). When the plastic section modulus is used, some methods show a lower "minimum" reliability index, and hence may not be suitable for design. In addition, the strain distributions in Section 4.2 showed that the weld did not reach its fully plastic deformation. Use of the plastic section modulus is not recommended herein for the design of welds in CHS-to-CHS moment T-connection.

Table 5-2 Reliability index summary

Standard	Data type	Calculation method					
		EESM	FEESM	EESM (rational)	EPSM	FEPSM	EPSM (rational)
AISC $\phi = 0.75$	Max	5.29	5.44	7.26	4.81	4.38	4.49
	Min	5.11	4.83	6.22	4.60	3.98	4.22
AISC $\phi = 0.80$	Max	5.14	5.16	6.98	4.63	4.09	4.25
	Min	4.95	4.61	6.00	4.42	3.76	3.97
CSA $\phi = 0.67$	Max	5.30	5.45	7.16	4.82	4.39	4.20
	Min	5.12	4.69	6.08	4.61	3.85	3.95

Chapter 6: CONCLUSION AND RECOMMENDATIONS

From 12 tests conducted on fillet and PJP-groove welds in CHS-to-CHS moment T-connections, and comparisons of the actual strength to predicted strength based on several different calculation methods, the following can be concluded:

- Strain gauge data adjacent to the weld shows that welds in CHS-to-CHS moment T-connections are only partially effective; i.e, the maximum strain/stress does not occur at the crown point, in tension and compression.
- Strain gauge data adjacent to the weld also shows that welds in CHS-to-CHS moment T-connections do not develop a fully plastic stress/strain distribution through the branch cross-section.
- Despite this, the ratio of actual-to-predicted strength from tests using an "effective elastic section modulus" (EESM) and "fully effective elastic section modulus" (FEESM) approach range from 3.65-4.22 (for AISC and CSA) and 1.49-1.70 (for AISC and CSA), respectively.
- Interestingly, the ratio of actual-to-predicted strength using a "fully effective plastic section modulus" (FEESM) approach is close to unity (1.15-1.30, for AISC and CSA, respectively).

Based on a FORM analysis of the 12 tests, it is recommended to use the EESM approach as a "lower bound" to calculate the strength of welds in CHS-to-CHS moment T-connections subjected to in-plane bending. A more accurate (yet, safe) prediction can be obtained by using the FEESM approach.

The EPSM and FEPSM approaches are not recommended, since strain gauge data indicates that the welds are not capable of full plastic stress redistribution.

REFERENCES

American Institute of Steel Construction (AISC) 2010. ANSI/AISC 360-10. Specification for structural steel buildings. Chicago, IL, USA.

American Institute of Steel Construction (AISC) 2011. Steel construction manual, 14th ed., Chicago, IL, USA.

American Institute of Steel Construction (AISC) 2016. ANSI/AISC 360-16. Specification for structural steel buildings. Chicago, IL, USA.

American Institute of Steel Construction (AISC). 2021. ANSI/AISC 360-21. Specification for structural steel buildings – Public review draft dated February 5th, 2021, Chicago, IL, USA.

ASTM International (ASTM) 2013. ASTM A500-13. Standard specification for cold-formed welded and seamless carbon steel structural tubing in rounds and shapes. West Conshohocken, PA, USA.

ASTM International (ASTM) 2015a. ASTM A1085-15. Standard specification for cold-formed welded steel hollow structural sections (HSS). West Conshohocken, PA, USA.

ASTM International (ASTM) 2015b. ASTM E340-15. Standard test method for macroetching metals and alloys. West Conshohocken, PA, USA.

ASTM International (ASTM) 2017. ASTM A370-17. Standard test methods and definitions for mechanical testing of steel products. West Conshohocken, PA, USA.

ASTM International. (2021). *E8/E8M-21 Standard Test Methods for Tension Testing of Metallic Materials.*

American Welding Society (AWS). 2015. AWS D1.1/D1.1M:2015. Structural welding code – Steel, 23rd ed., Miami, FL, USA.

Bolt, H. M., Seyed-Kebari, H. and Ward, J. K. 1992. The Influence of Chord Length and Boundary Conditions on K-Joint Capacity, in *Proceedings of the 2nd International Offshore and Polar Engineering Conference*, 347-354, International Society of Offshore and Polar Engineers, San Francisco, CA.

Canadian Standards Association (CSA) 2018. CSA W59-18. Welded steel construction (metal arc welding). Toronto, Canada: Canadian Standards Association.

Canadian Standards Association (CSA) 2019. CSA S16-19. Design of steel structures. Toronto, Canada: Canadian Standards Association.

Canadian Standards Association (CSA) 2019b. CSA S6:19. Canadian highway bridge design code. Toronto, Canada: Canadian Standards Association.

Cassidy, C. E. (1993). Effective weld length for HSS T, Y, and X connections. Master of Applied Science Thesis. Toronto, Canada: University of Toronto.

Choo, Y. S., Quian, X. D. and Wardenier, J. 2006. Effects of Boundary Conditions and Chord Stresses on Static Strength of Thick-Walled CHS K-Joints, *J. Constr. Steel Res.* 62, 316-328.

European Committee for Standardization (CEN) 2005. EN 1993-1-8. Design of steel structures – Part 1-8: Design of joints. European Committee for Standardization, Brussels, Belgium.

Fan, Y. and Packer, J. A. 2017. RHS-to-RHS Axially Loaded X-Connections near an Open Chord End. *Can. J. Civ. Eng, CSCE*, 44, 881-892.

Frater, G. S. & Packer, J. A. 1992a. Weldment design for RHS truss connections. I: Applications. *Journal of Structural Engineering, American Society of Civil Engineers* 118(10): 2784-2803.

Frater, G. S. & Packer, J. A. 1992b. Weldment design for RHS truss connections. II: Experimentation. *Journal of Structural Engineering, American Society of Civil Engineers* 118(10): 2804-2820.

Luo, P., Asada, H., Uang, C. & Tanaka, T. 2020. Directionality Effect on Strength of Partial-Joint-Penetration Groove Weld Joints. *Journal of Structural Engineering, American Society of Civil Engineers* 146(4): 4020030.

Luyties W.H. & Post J.W. 1988 Local dihedral angle equations for tubular joints and related applications, Weld. Welding Journal 77 (4): 51–60.

International Institute of Welding (IIW) 2012. IIW Doc. XV-1402-12. Design recommendations for hollow section joints – Predominatly statically loaded, 3rd ed., Paris, France.

International Organization for Standardization (ISO). 2013. ISO 14346:2013 (E). Static design procedure for welded hollow section joints – Recommendations. Geneva, Switzerland.

McFadden, M. R. & Packer, J. A. 2013. Effective weld properties for RHS-to-RHS moment T-connections. Phase 1 Report to the American Institute of Steel Construction. Toronto, Canada: University of Toronto.

McFadden, M. R. & Packer, J. A. 2014. Effective weld properties for hollow structural section T-connections under branch in-plane bending. *Engineering Journal, American Institute of Steel Construction* 51(4): 247-266.

Packer, J. A. & Cassidy, C. E. 1995. Effective weld length for HSS T, Y, and X connections. *Journal of Structural Engineering, American Society of Civil Engineers* 121(10): 1402-1408.

Packer, J. A. & Henderson, J. E. 1997. Hollow structural section connections and trusses – A design guide, 2nd ed., Toronto, Canada: Canadian Institute of Steel Construction.

Packer, J. A., Sherman, D. R., & Lecce, M. (2010). Hollow Structural Section Connections. AISC Steel Design Guide No. 24. Chicago, IL: American Institute of Steel Construction.

Packer, J. A. & Sun, M. 2011. Weld design for rectangular HSS connections. *Engineering Journal, American Institute of Steel Construction* 48(1): 31-48.

Packer, J. A., Wardenier, J., Zhao, X. L., van der Vegte, G. J. & Kurobane, Y. 2009. Design guide for rectangular hollow section (RHS) joints under predominantly static loading, CIDECT Design Guide No. 3, 2nd ed., Geneva, Switzerland: CIDECT

prEN 1993-1-8 (2018) Design of steel structure. Part 1-8: Design of joints. Brussels, Belgium.

Tousignant, K. 2019. Effect of chord length and boundary conditions on welds in CHS X-joints. in *Proceedings of the 17th International Symposium on Tubular Structures (ISTS17)* 63-70.

Tousignant, K. & Packer, J. A. 2015a. Weld effective lengths for rectangular HSS overlapped K-connections. *Engineering Journal, American Institute of Steel Construction* 52 (4): 259-282.

Tousignant, K. & Packer, J. A. 2015b. Investigation of weld effective length rules for RHS overlapped K-connections. In Batista, E., Vellasco, P. & Lima, L. (Eds.), *Tubular Structures XV; Proc. Intern. Symp., Rio de Janeiro 27-29 May 2015.* Rotterdam: Balkema, 357-364.

Tousignant, K. & Packer, J. A. 2017. Fillet weld effective lengths in CHS X-connections. I: Experiments. *Journal of Constructional Steel Research* 138: 420-431.

Tousignant, K. & Packer, J. A. 2017. Numerical investigation of fillet welds in HSS-to-rigid end-plate connection. *Journal of Structural Engineering* 142(12): 4017165.

Tousignant, K., & Packer, J. 2018. Fillet weld effective lengths in CHS X-connections. II: Finite element modelling, parametric study and design. *Journal of Constructional Steel Research* 141, 77-90.

Tousignant, K., & Packer, J. 2019a. Weld effective lengths for round HSS cross-connections under branch axial loading. *Engineering Journal, American Institute of Steel Construction* 56(3): 173-186.

Tousignant, K. and Packer, J.A. 2019b. Fillet welds around circular hollow sections. *Welding in the World, IIW* 63: 421-433

Tousignant, K., & Packer, J. 2020a. Optimized design of fillet welds for CHS joints according to EN 1993‐1‐8. *Steel Construction*, 13(1), 41-51.

Tousignant, K., & Packer, J. 2020b. Weld design for Hollow Structural Section connections: application to Canadian standards. *Canadian Journal of Civil Engineering* Published on the web 16 January 2020, https://doi.org/10.1139/cjce-2019-0608.

Weld Design for Hollow Structural Section Connections: Application to Canadian Standards

van der Vegte, G.J. & Makino, Y. 2006. The ultimate strength of axially loaded CHS uniplanar T-joints subjected to axial chord load. Welding in the World, 50, 104-111.

van der Vegte, G.J. & Makino, Y. 2010. Further research on chord length and boundary conditions of CHS T- and X-joints. *Advanced Steel Construction* 6(3): 879-890.

Wardenier, J. (1982). *Hollow Section Joints.* Delft, The Netherlands: Delft University Press.

Wardenier, J., Kurobane, Y., Packer, J. A., van der Vegte, G. J. & Zhao, X. L. 2008. Design guide for circular hollow section (CHS) joints under predominantly static loading, CIDECT Design Guide No. 1, 2nd ed. Geneva, Switzerland: CIDECT.

Wardenier, J., Packer, J. A., Zhao, X. L. & van der Vegte, G. J. 2010. Hollow sections in structural applications, CIDECT Design Guide No. 1, 2nd ed. Geneva, Switzerland: CIDECT.

Yaghoubshahi, M., Sun, M. and Tousignant, K. 2019. Design of Fillet Welds in RHS-to-RHS Moment T-Connections under Branch in-plane Bending. *J. Const. Steel Res.* 159, 122-133.

Appendix A: SAMPLE CALCULATIONS AND RESISTANCE TABLES

Appendix A provides the supplementary calculations for resistance and section properties of test specimens which include:

Chord plastification, punching shear, branch yielding, derivation and calculation of Sip, Mip,

A.1. CALCULATION OF POSSIBLE FAILURE MODE

A list of sample calculation of possible failure mode of CHS-to-CHS moment connection which include: chord plastification; punching shear and branch yielding. All specimens are calculating exact same as sample calculation except using their own specimen parameter. All properties using in this part is the nominal or design properties of test specimen since all design should be done before sent to the fabricator.

The sample calculation is based on test T406-127-0.7.

Branch properties: HSS 127×9.5

Outside diameter	Nominal thickness	Design thickness
D_b = 127 mm	t_b(nominal) = 9.5mm	t_b (design) = 8.58mm

F_{yb} (MPa)	F_{ub} (MPa)	S_b (10^3 mm^3)	Z_b (10^3 mm^3)
317	427	88.6	121

Chord properties: HSS 406×13

Outside diameter	Nominal thickness	Design thickness
D_b = 406.4 mm	t_b(nominal) = 13mm	t_b (design) = 11.43mm

F_{yb} (MPa)	F_{ub} (MPa)	S_b (10^3 mm^3)	Z_b (10^3 mm^3)
317	427	1360	1780

Limitations of the applicability from AISC S360-10 Table K4.1A:

Name	Symbols	Requirement	Actual	
Slenderiness ratio	$2\gamma = D/t$	≤ 50	36	Satisfy
Branch Slenderness ratio	D_b/t_b	≤ 50 ≤ 0.05 E/F_{yb}	14.8	Satisfy
Branch to chord diameter ratio	$\beta = D_b/D$	$0.2 < \beta < 1$	0.31	Satisfy
Yield strength	F_y & F_{yb}	≤ 360 MPa	317 MPa	Satisfy
Ductility	F_y/F_u & F_{yb}/F_{ub}	≤ 0.8	0.74	Satisfy

Connection strength, AISC S360-10 Table K4.1:

Chord plastification

$M_{ip}\sin\theta = 5.39F_y t^2\gamma^{0.5}\beta D_b Q_f$ where θ = 90°

Q_f = 1 for chord face in tension (settlement design)

$$M_{ip} = 5.39\times317\times8.58^2\times(36/2)^{0.5}\times0.31\times127\times1$$

$M_{ip} = 37.35kNm$ for nominal resistance

Punching shear:

$$M_{ip} = 0.6F_y t D_b^2\left(\frac{1+3\sin\theta}{4\sin^2\theta}\right)$$

$$M_{ip} = 0.6\times317\times11.43\times127^2\times1$$

$M_{ip} = 35.06kNm$ for nominal resistance

Branch flexural strength CSA S6-19 13.5:

Check class:

$\frac{D_b}{t} = \frac{127}{8.58} = 14.86 < \frac{13000}{F_y} = 41$ which is class 1 section:

$M_{ip} = \phi Z F_y$

$M_{ip} = \phi \times 121 \times 317$

$M_{ip} = 38.36 kNm$ for nominal resistance

The branch failed at punching shear and M_{ip} = 35.06 kNm

A.2. DERIVATION OF EFFECTIVE SECTION MODULUS

The elastic effective weld section modulus is calculate based on the effective weld length. Where a piece of ring has a moment of inertia of (CSA 2016):

$$I_{ip} / 2 = \frac{1}{4}(R^4 - r^4)(\frac{\pi\alpha}{180} - \sin\alpha\cos\alpha)$$

For fillet welds:

$$R = D_b / 2 + t_w$$

$$r = D_b / 2$$

For PJP welds:

$$R = D_b / 2 - g$$

$$r = R - t_w$$

where:

$$l_e / 2 = 2\alpha R \text{ which } \alpha = \frac{l_e}{4R} \approx \frac{l_e}{2D_b}$$

$$l_e = \frac{4}{\sqrt{2\beta(D/t)}} l_w \le l_w = \pi D_b \frac{1 + 1/\sin\theta}{2}$$

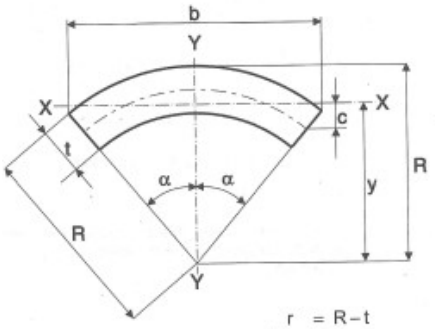

$$r = R - t$$

$$A = \frac{\pi\alpha}{180}(R^2 - r^2)$$

$$b = 2R\sin\alpha$$

$$c = \frac{120\sin\alpha\,(R^3 - r^3)}{\pi\alpha(R^2 - r^2)} - \frac{(R+r)\cos\alpha}{2}$$

$$y = \frac{120\sin\alpha\,(R^3 - r^3)}{\pi\alpha(R^2 - r^2)}$$

$$I_x = \frac{1}{4}(R^4 - r^4)\left(\frac{\pi\alpha}{180} + \sin\alpha\cos\alpha\right) - \frac{80\sin^2\alpha(R^3 - r^3)^2}{\pi\alpha(R^2 - r^2)}$$

$$I_y = \frac{1}{4}(R^4 - r^4)\left(\frac{\pi\alpha}{180} - \sin\alpha\cos\alpha\right)$$

Figure A-1 Geometric property (CSA 2016)

The effective section modulus can be found as:

$$S_{ip} = \frac{I_{ip}}{y}$$

since the difference between D_b and D_b+2t_w (fillet) and D_b – 2t_w - 2g, the distance from neutral axis to the end of effective weld length can be written as:

$$y = \frac{D_b}{2}\sin(\frac{l_e}{2D_b})$$

$$I_{ip} / 2 = \frac{1}{4}[(\frac{D_b}{2} + t_w)^4 - (\frac{D_b}{2})^4](\frac{l_e}{2D_b} - \frac{1}{2}\sin\frac{l_e}{D_b})$$

$$= \frac{1}{4}[(\frac{D_b}{2} + t_w)^4 - (\frac{D_b}{2})^4](\frac{l_e}{D_b} - \sin\frac{l_e}{D_b}) \quad \text{(Fillet, Equation 4.1a)}$$

$$I_{ip} / 2 = \frac{1}{4}[(\frac{D_b}{2} - g)^4 - (\frac{D_b}{2} - g - t_w)^4](\frac{l_e}{2D_b} - \frac{1}{2}\sin\frac{l_e}{D_b})$$

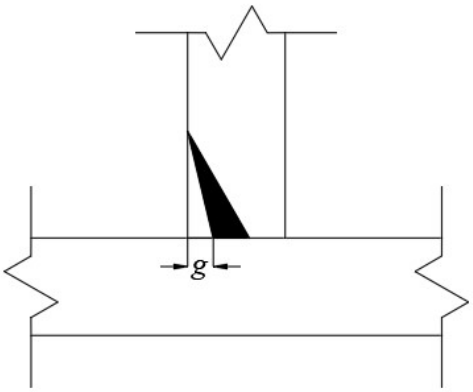

Figure A-2 Classification of g

$$= \frac{1}{4}[(\frac{D_b}{2} - g)^4 - (\frac{D_b}{2} - g - t_w)^4](\frac{l_e}{D_b} - \sin\frac{l_e}{D_b}) \quad \text{(PJP, Equation 4.1b)}$$

The plastic effective weld section modulus is calculate based on the effective weld length:

Assumptions are made to simplify the equation for both fillet welds and PJP welds into a single equation:

1. Inside diameter of the ring (weld metal) is assumed equal to the otter diameter of the branch CHS for PJP welded specimens since the thickness removed from CHS is very small comparing to the outside diameter of CHS.
2. The t_w^2 term is ignored in $t_w D_b + t_w^2$ term since the weld throat size is very small comparing to the weld throat is very small comparing to the branch diameter D_b.

$$Z = A\frac{b}{2}$$

$$A = (R+t_w)^2\frac{\theta}{2} - R^2\frac{\theta}{2} = \frac{(R+t_w)^2 - R^2}{D_b}l_e$$

$$\theta = \frac{l_e}{D_b / 2}$$

$$A = (2t_w R + t_w^2)\frac{l_e}{D_b}$$

Since the inner radius of the weld R is much greater than t_w, the term t_w^2 can be ignored. In addition, the difference between the radius R and the radius of branch CHS $D_b/2$ is g (Figure A-2) plus t_w for PJP weld (0 for fillet). This difference is very small comparing to the radius itself where the radius R can be approximately equal to $D_b/2$ and the area can be simplified as:

$$A = \frac{t_w D l_e}{D_b} = t_w l_e$$

From Figure A-1:

$$\frac{1}{2}b = R\sin(\alpha / 2)$$

$$\alpha = \frac{1}{4}\frac{l_e}{R_b} = \frac{l_e}{2D_b}$$

$$\frac{1}{2}b = \frac{1}{2}D_b\sin(\frac{l_e}{4D_b})$$

$$Z = \frac{1}{2}t_w l_e D_b \sin(\frac{l_e}{4D_b})$$

A.3. EFFECTIVE WELD THROAT FOR PJP WELDS

Since the weld flexural strength require the dimension of the weld, this part is before the prediction of each test specimen:

Measurement of the weld shows the average of effective weld throat directly while PJP weld can not measure the weld throat directly. The measurement of the PJP weld is based on the gap g shown in Appendix A.2 and the effective weld throat is calculated by minus the gap and branch remaining thickness (designed). The following table shows the measured gap and effective weld throat for each specimen.

Table A-1 Deformation table

Test Designation	t_b (mm)	g (mm)	Remaining thickness (mm)	t_w (mm)
T273-127-1P	8.853	2.975	3.0	2.878
T273-127-1	8.853	Fillet	Fillet	2.714
T324-127-1	8.853	Fillet	Fillet	2.857
T356-127-1	8.853	Fillet	Fillet	2.770
T356-273-1P	8.856	3.008	3.0	2.848
T356-324-1P	9.311	3.829	3.0	2.482
T406-127-1	8.853	Fillet	Fillet	2.723
T406-273-1P	8.856	2.979	3.0	2.878
T406-324-0.7P	9.311	3.025	3.0	3.286
T406-127-0.7	8.853	Fillet	Fillet	2.646
T406-273-0.7P	8.856	2.996	3.0	2.860
T406-324-0.7P	9.311	3.017	3.0	3.295

A.4. CALCULATION OF WELD FLEXURAL STRENGTH

From the measurement and calculation of effective weld throat, the weld flexural strength can be calculate based on Equation 4.1 to 4.5 where the sample calculation using T406-127-0.7 while the dimension of weld is using the external measurement and the dimension of CHS is using the exact measurement:

$$I_{ip} = \frac{1}{4}[(\frac{D_b}{2} + t_w)^4 - (\frac{D_b}{2})^4](\frac{l_e}{D_b} - \sin\frac{l_e}{D_b})$$

where: $l_e = \frac{4}{\sqrt{2\beta(D/t)}} l_w \le l_w$

$$l_w = \pi D_b \frac{1+1/\sin\theta}{2} = \pi \times 127.6 \times \frac{1+1/\sin 90}{2} = 400.87mm$$

$$l_e = \frac{4}{\sqrt{2\beta(D/t)}} l_w = \frac{4}{\sqrt{2\times 127.6/407.4\times(407.4/11.82)}} \times 400.87 = 345.05 \le l_w$$

$$I_{ip} = \frac{1}{4}[(\frac{127.6}{2} + 2.646)^4 - (\frac{127.6}{2})^4](\frac{345.05}{127.6} - \sin\frac{345.05}{127.6}) = 1.667\times 10^6 mm^4$$

$$S_{ip} = I_{ip} / (\frac{D_b}{2} \sin \frac{l_e}{2D_b}) = \frac{1.667 \times 10^4}{127.6/2 \times \sin(345.05/2/127.6)} = 26.77 \times 10^3 mm^3$$

$M_{ip} = \phi S_{ip} F_{nw}$ where ϕ = 1 for nominal strength

For CSA fillet weld:

$$F_{nw} = 0.67 F_{EXX} (1.00 + 0.5 \sin \theta) = 592 MPa$$

$$M_{ip} = \phi S_{ip} F_{nw} = 1 \times 26.77 \times 10^3 \times 592 = 15.85 kNm$$

For AISC:

$$F_{nw} = 0.60 F_{EXX} (1.00 + 0.5 \sin \theta) = 530.15 MPa$$

$$M_{ip} = \phi S_{ip} F_{nw} = 1 \times 26.77 \times 10^3 \times 530.15 = 14.19 kNm$$

Calculation based on weld fully effective:

$$S_{ip} = \frac{\pi[(D_b + 2t_w)^2 - D_b^2]}{32(D_b + 2t_w)^2} = \frac{\pi[(127.6 + 2 \times 2.646)^2 - 127.6^2]}{32(127.6 + 2 \times 2.646)^2} = 34.56 \times 10^3 mm^3$$

For CSA fillet weld:

$$M_{ip} = \phi S_{ip} F_{nw} = 1 \times 34.56 \times 10^3 \times 592 = 20.56 kNm$$

For AISC:

$$M_{ip} = \phi S_{ip} F_{nw} = 1 \times 26.77 \times 10^3 \times 530.15 = 18.41 kNm$$

Appendix B: FABRICATION DRAWINGS

Appendix B provides the supplementary drawings for tests specimens and tensile coupons.

B.1. FABRICATION OF CONNECTIONS

Appendix B.1 provides the drawing of fabrications as well as the cross-section of the weld and the local dihedral angle along the branch. Meanwhile, the PJP welded specimens are grinded after cutting to get the desire cutting profile.

Following drawings are list as the order of: T273-127-1P; T273-127-1; T324-127-1; T356-127-1; T356-273-1P; T356-324-1P; T406-127-1; T406-273-1P; T406-324-1P; T406-127-0.7P; T406-273-0.7P; T406-324-0.7P where the branch and chord information are shown in drawings and tittles.

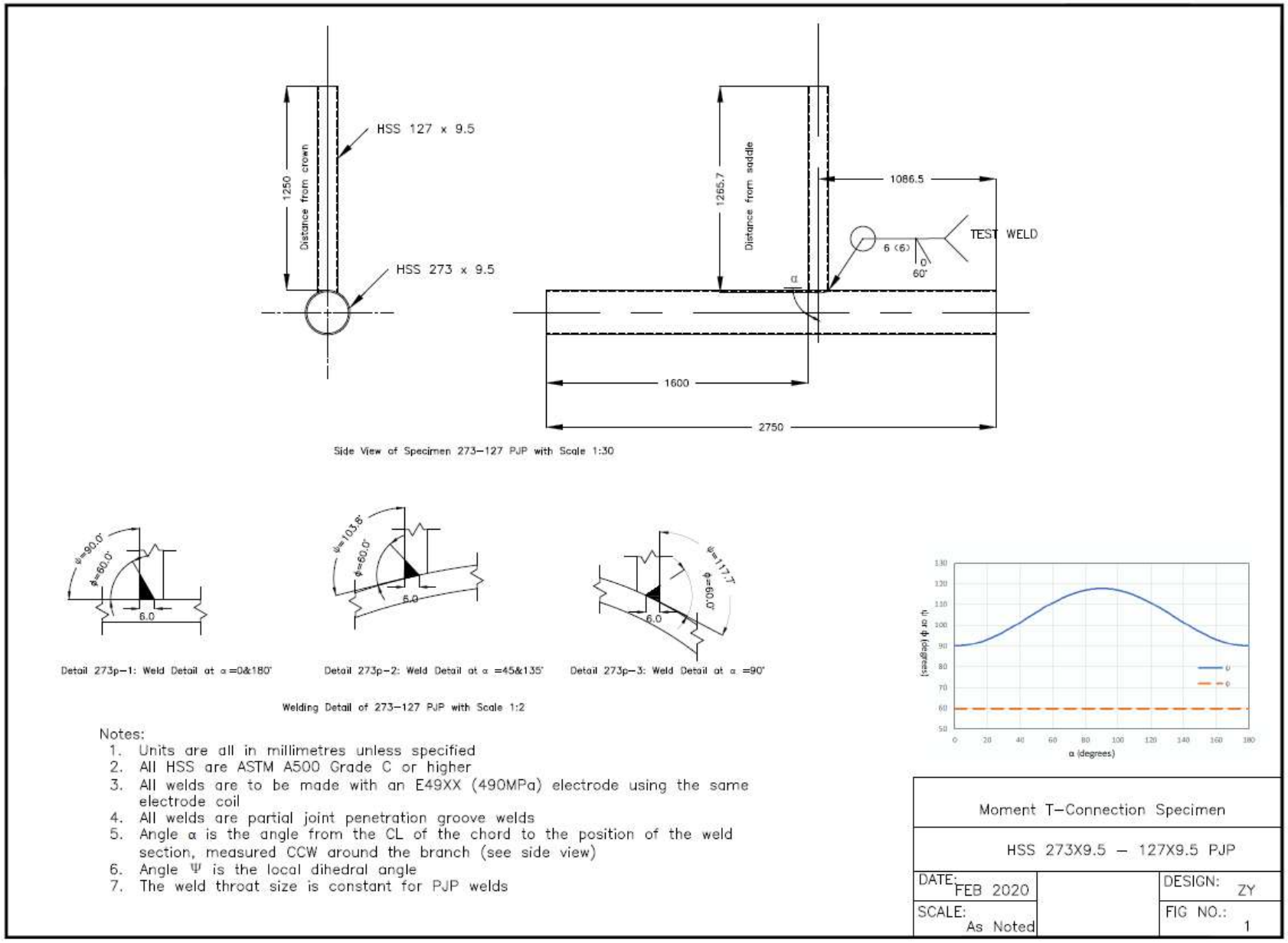

Figure B-1 Fabrication drawing of T273-127-1P

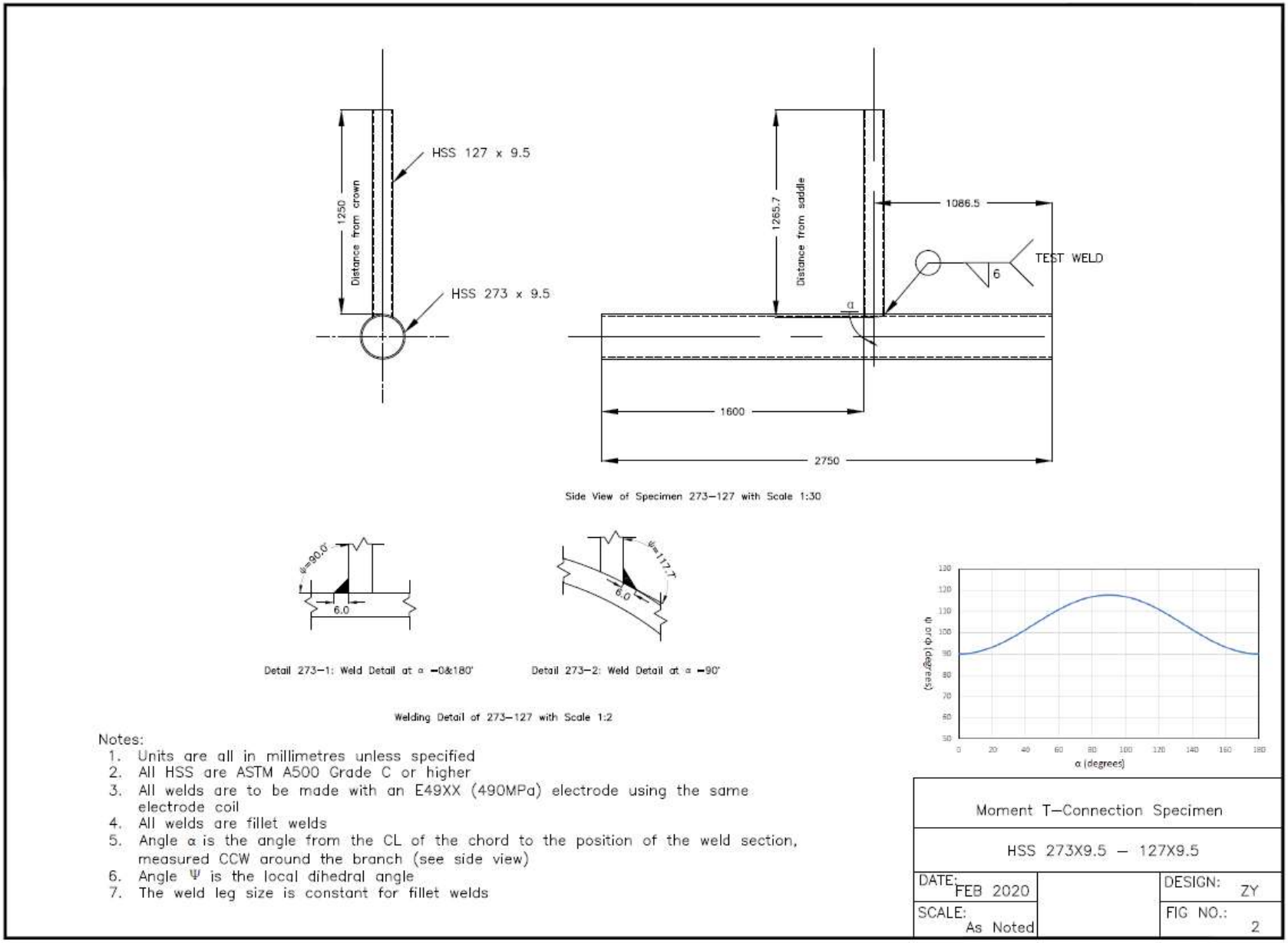

Figure B-2 Fabrication drawing of T273-127-1

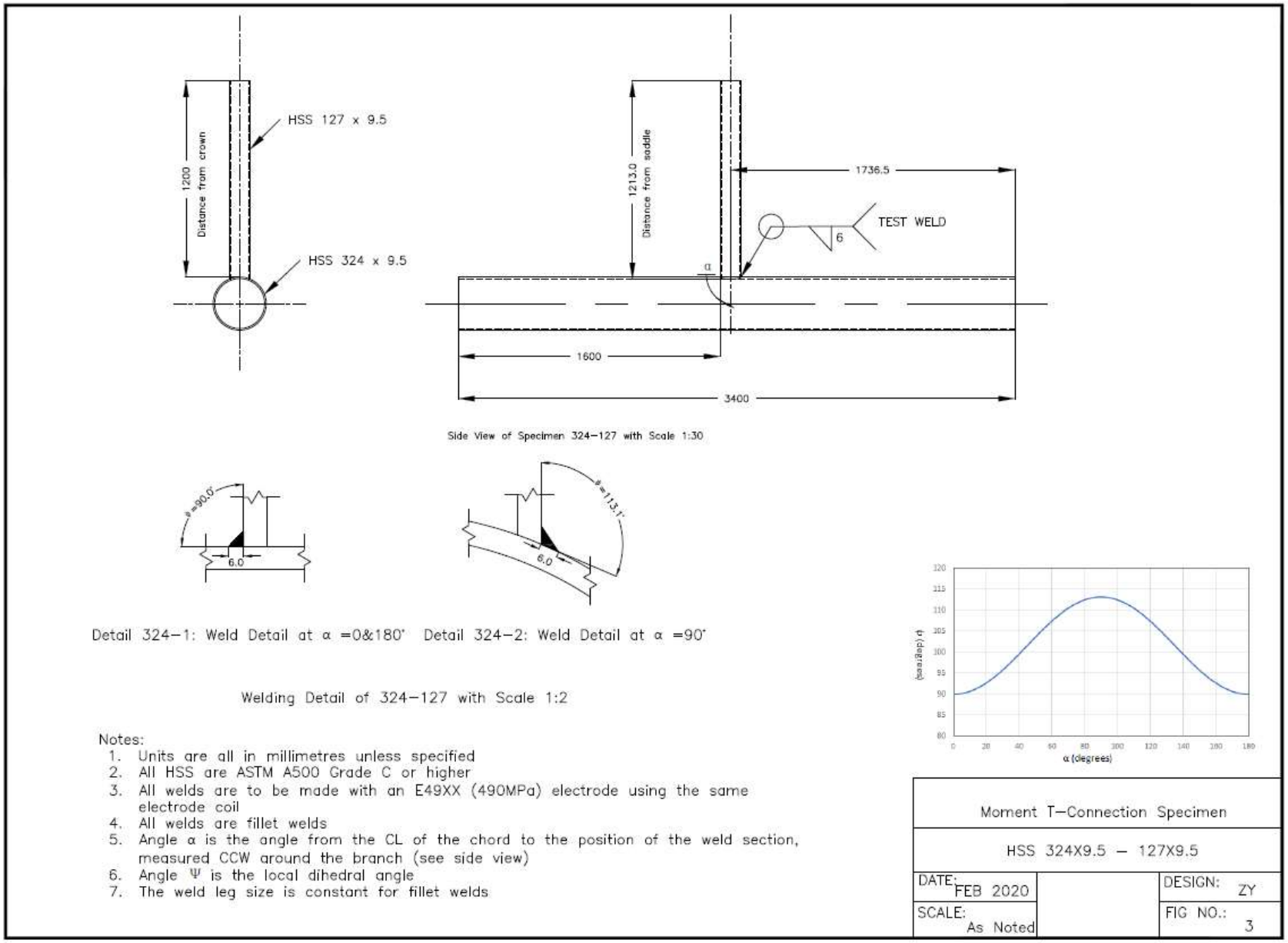

Figure B-3 Fabrication drawing of T324-127-1

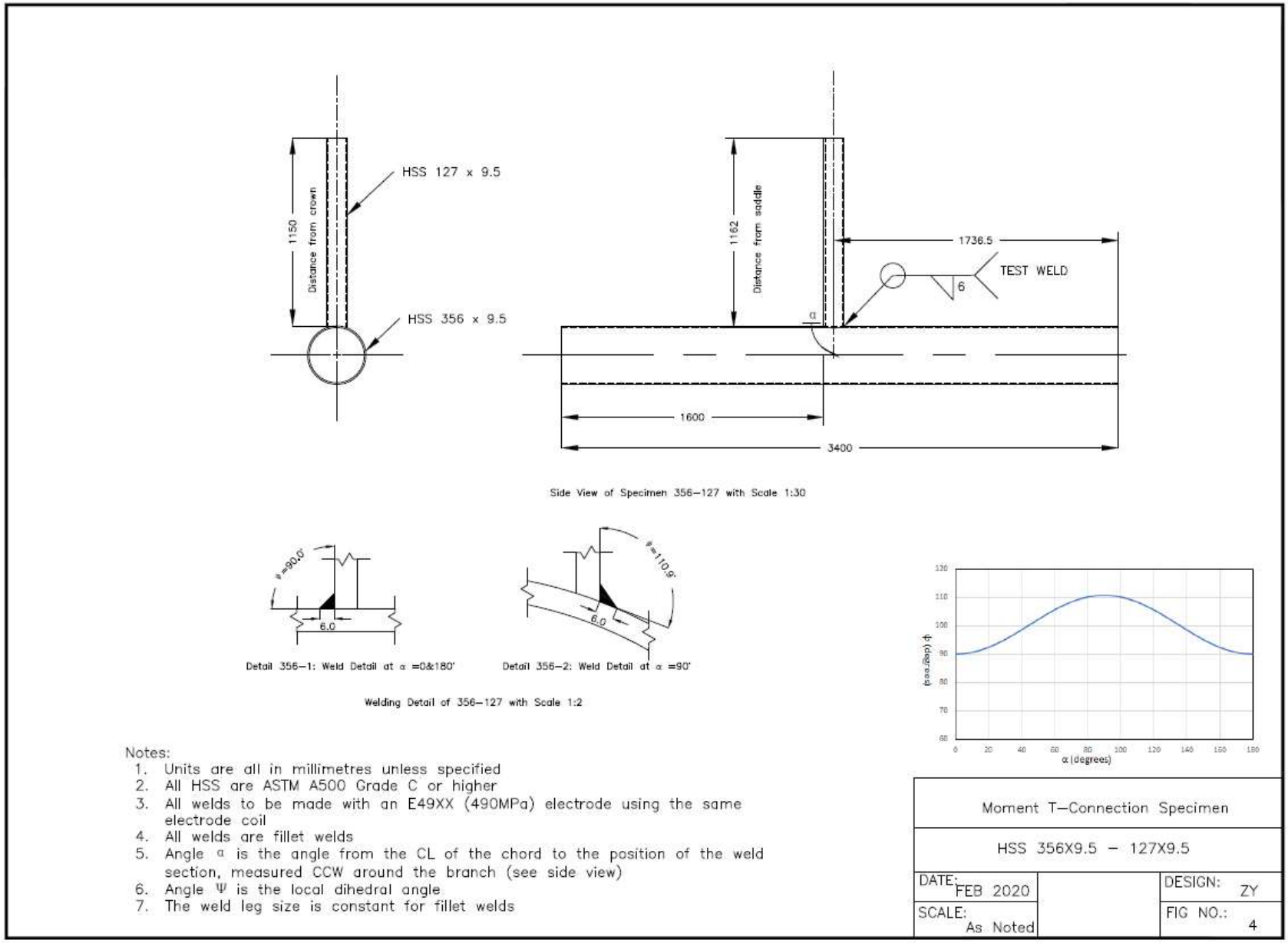

Figure B-4 Fabrication drawing of T356-127-1

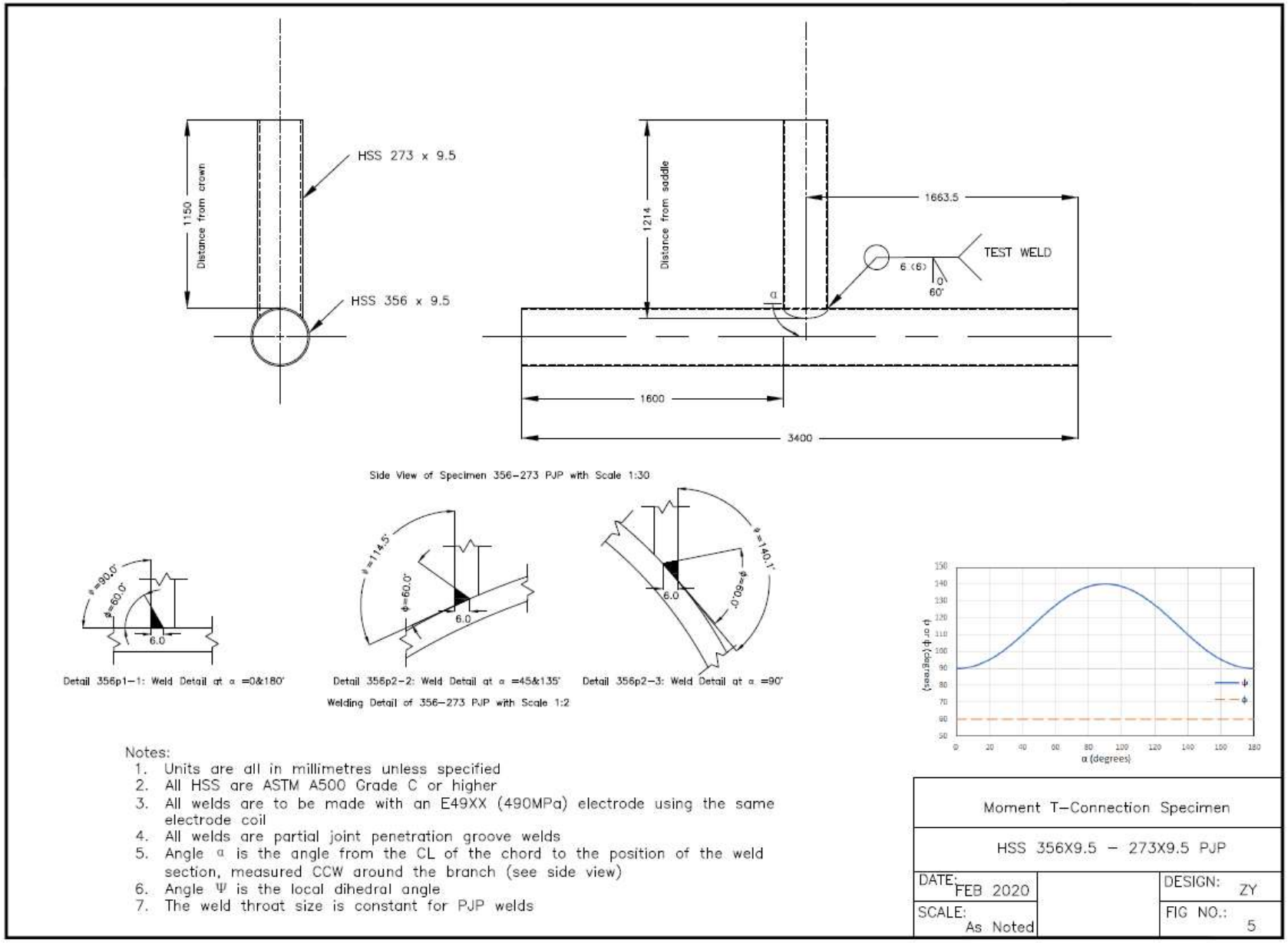

Figure B-5 Fabrication drawing of T356-273-1P

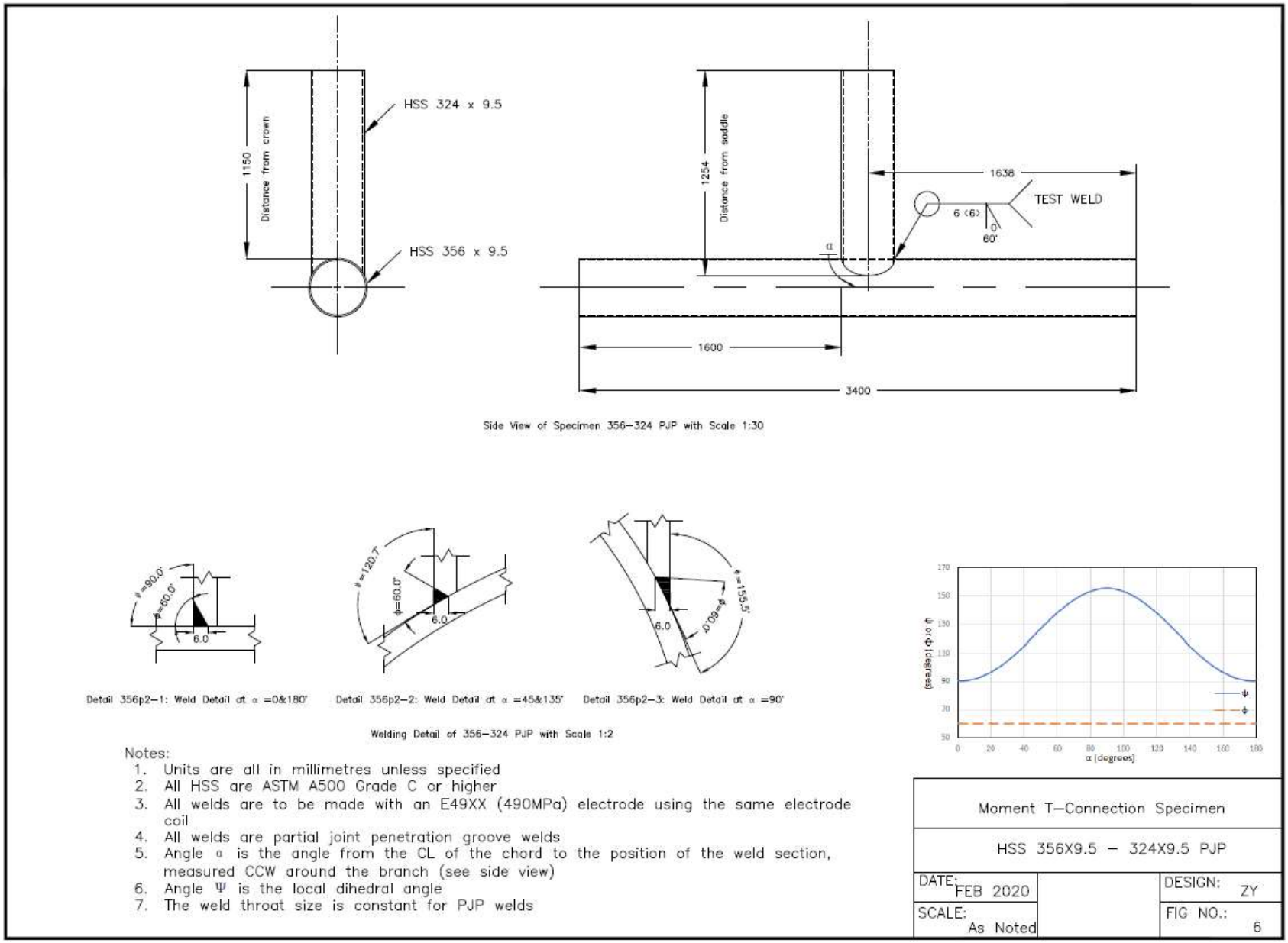

Figure B-6 Fabrication drawing of T356-324-1P

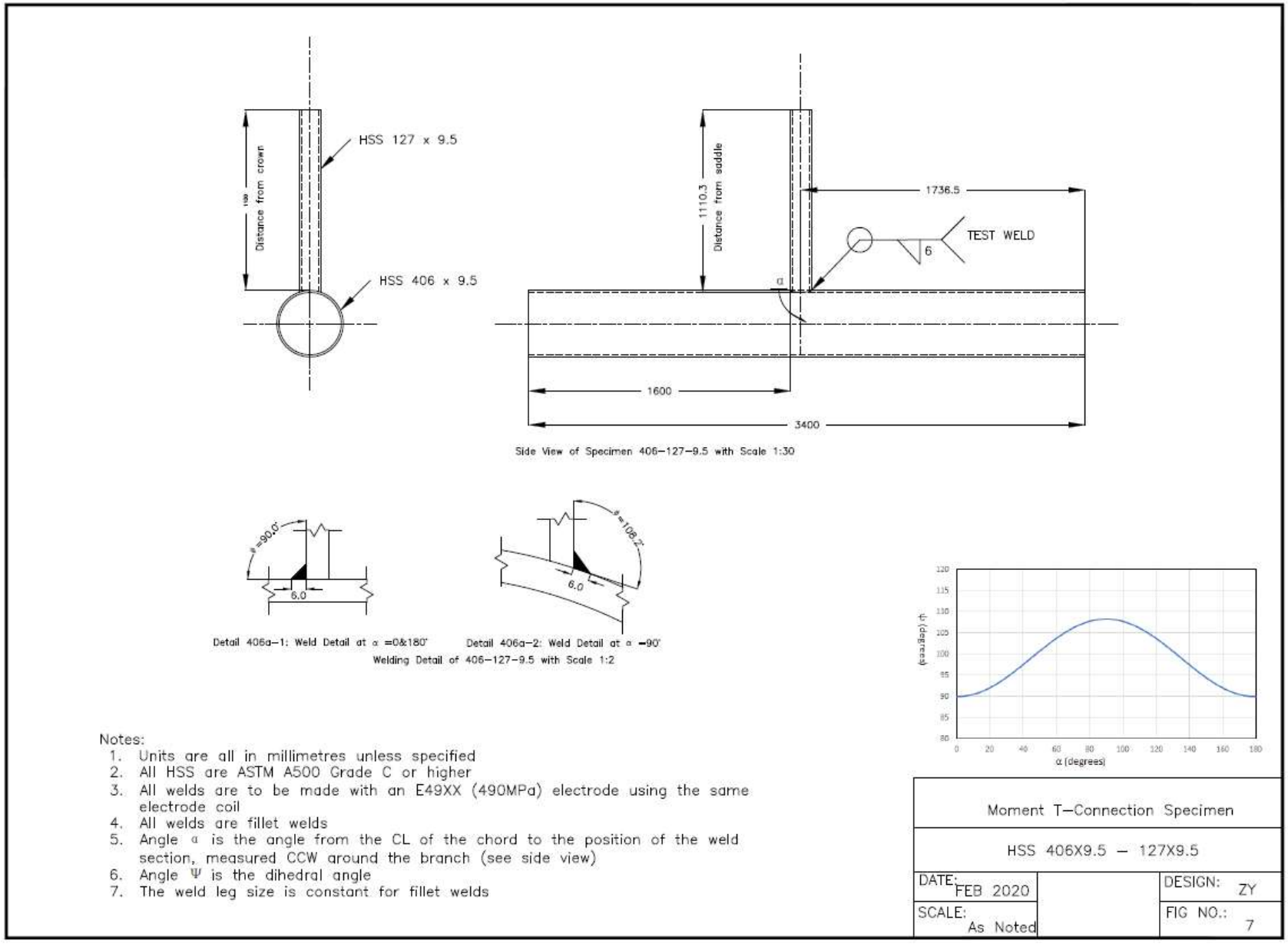

Figure B-7 Fabrication drawing of T406-127-1

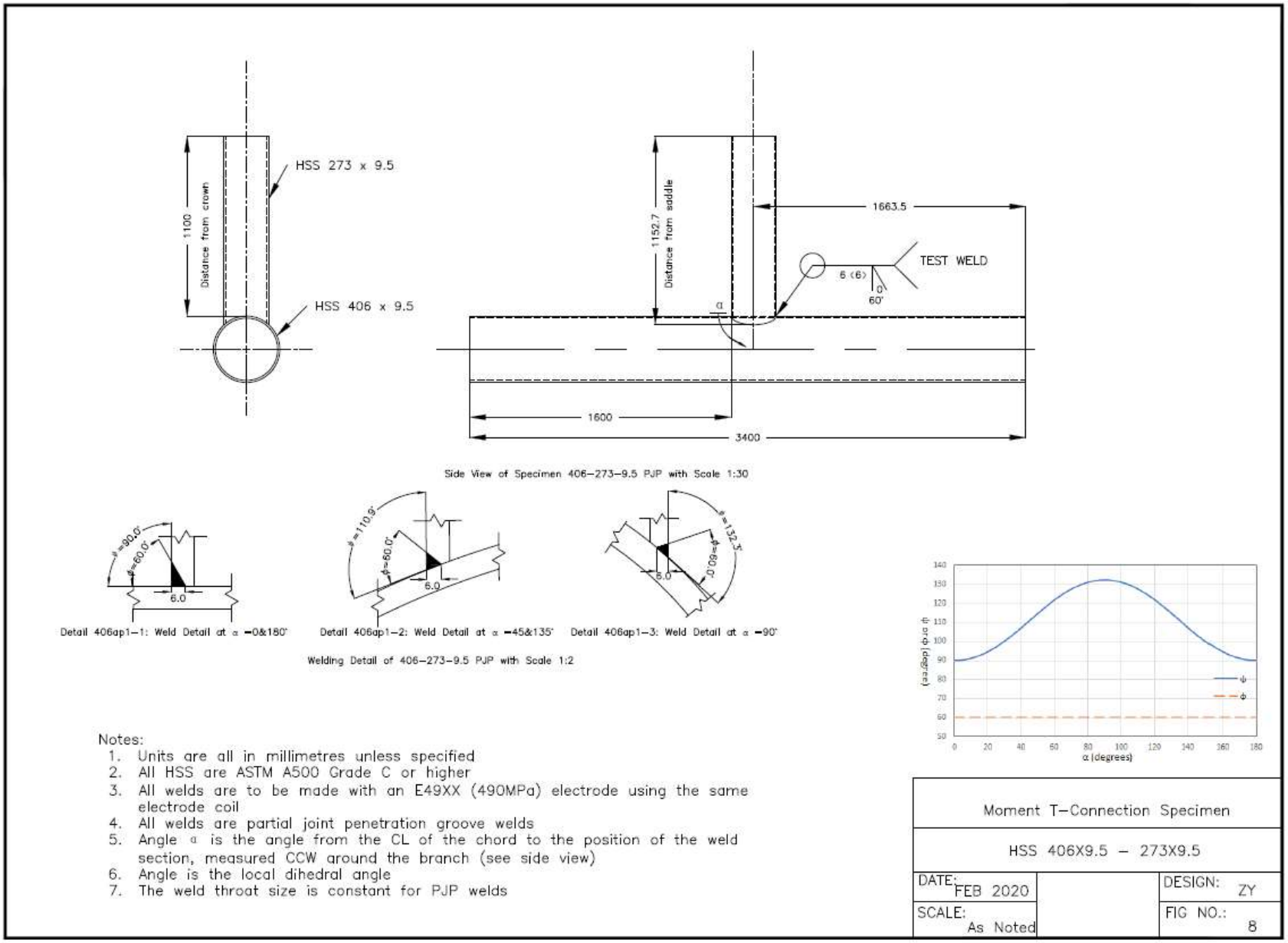

Figure B-8 Fabrication drawing of T406-273-1P

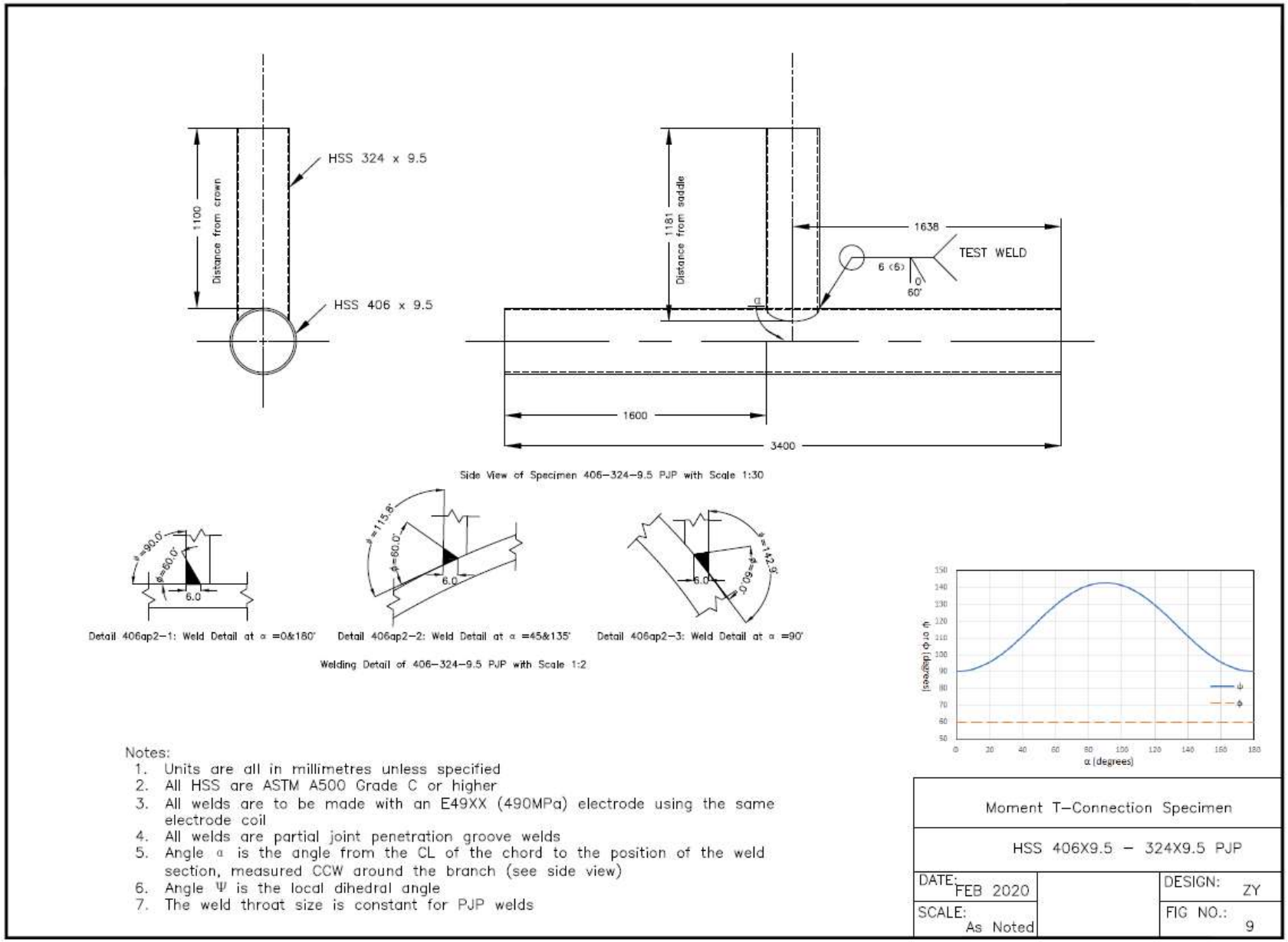

Figure B-9 Fabrication drawing of T406-324-1P

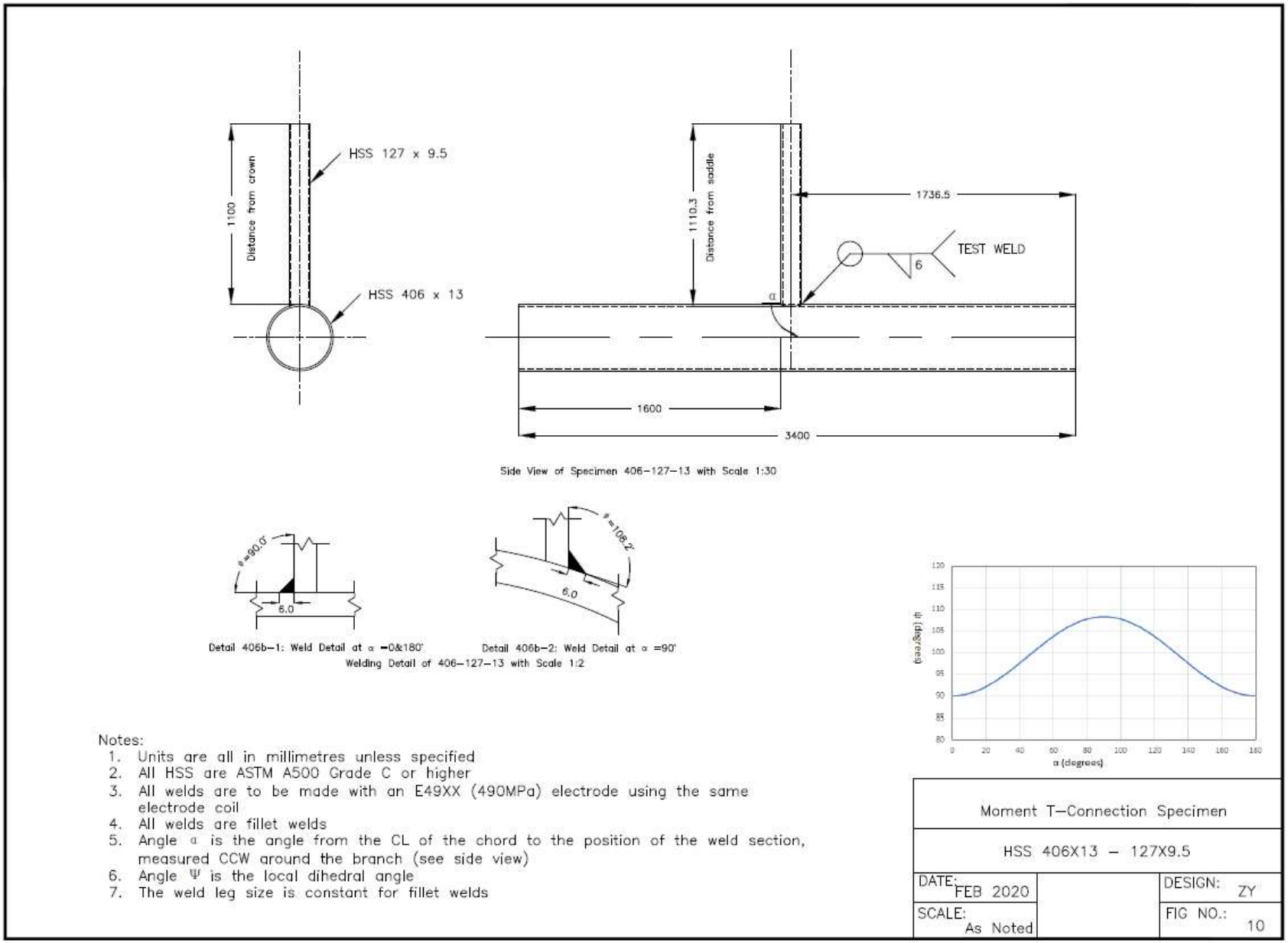

Figure B-10 Fabrication drawing of T406-127-0.7

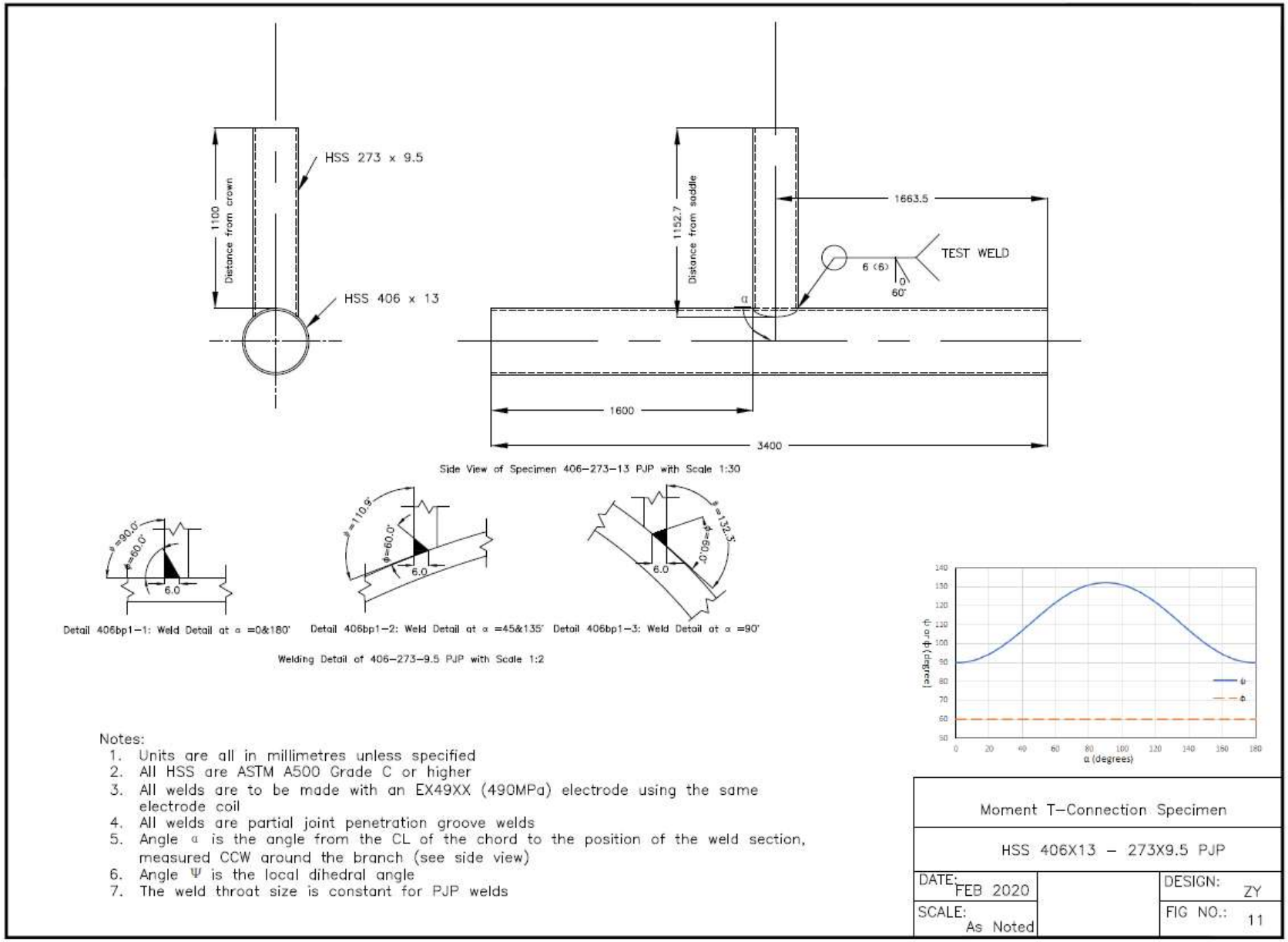

Figure B-11 Fabrication drawing of T406-273-0.7P

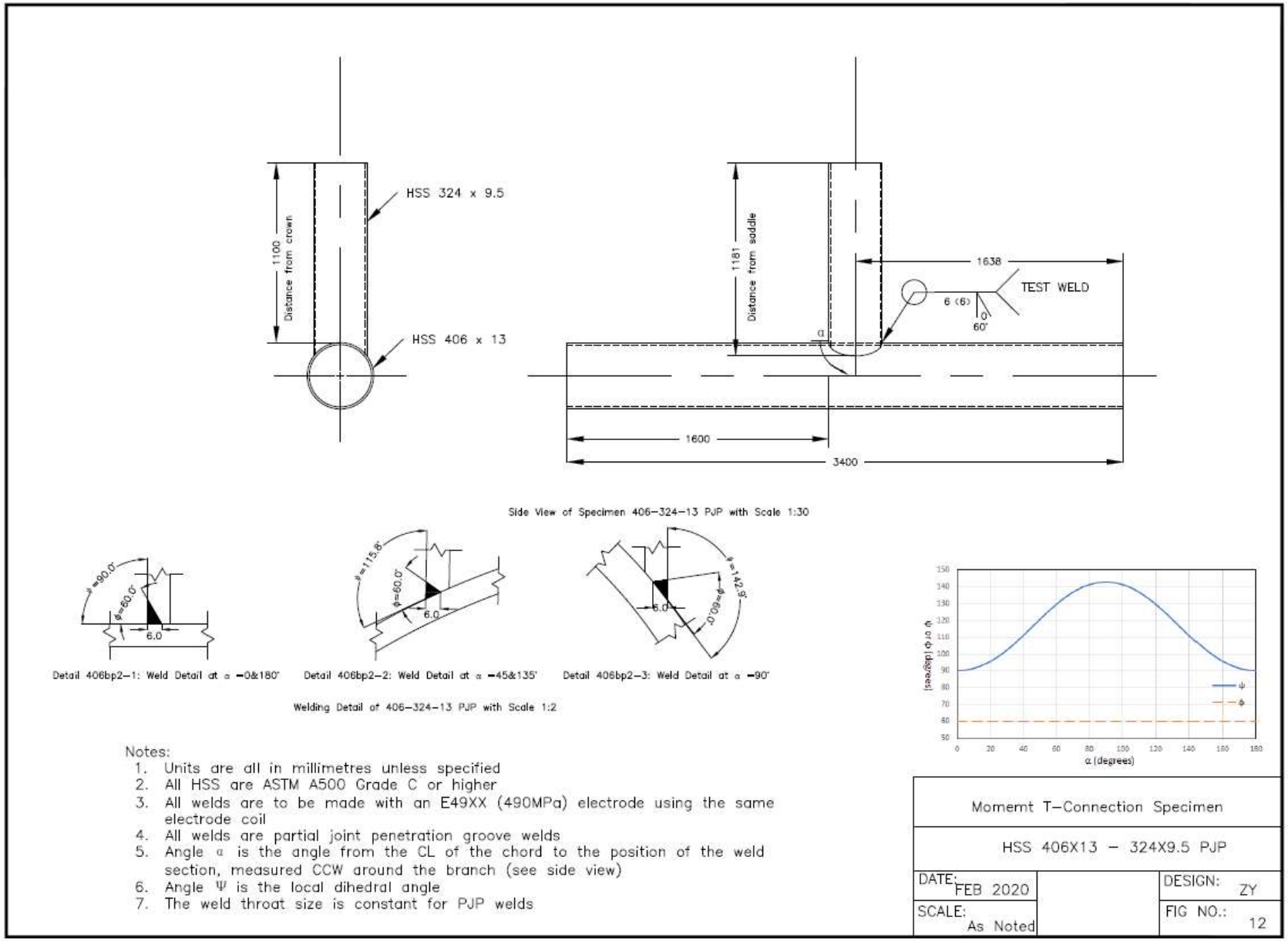

Figure B-12 Fabrication drawing of T406-324-0.7P

B.2. SAMPLE SPECIMENS AND TENSILE COUPONS

In this sub-appendix, sample specimens of fillet weld and PJP weld as well as the tensile coupons for CHS and all-weld metal. Drawings of tensile coupons fabrication are also shown in this appendix.

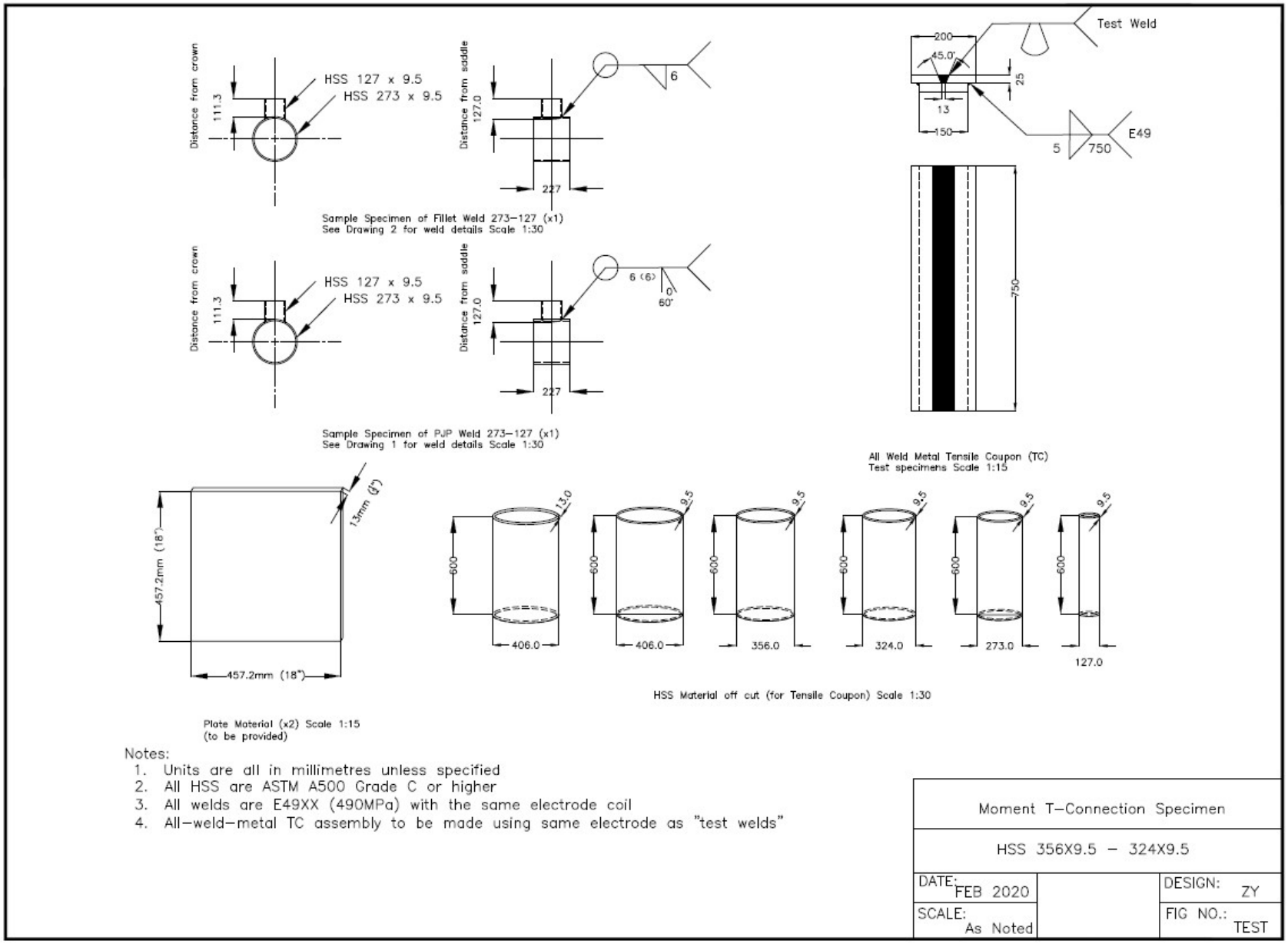

Figure B-13 Sample specimen and TC specimen drawing

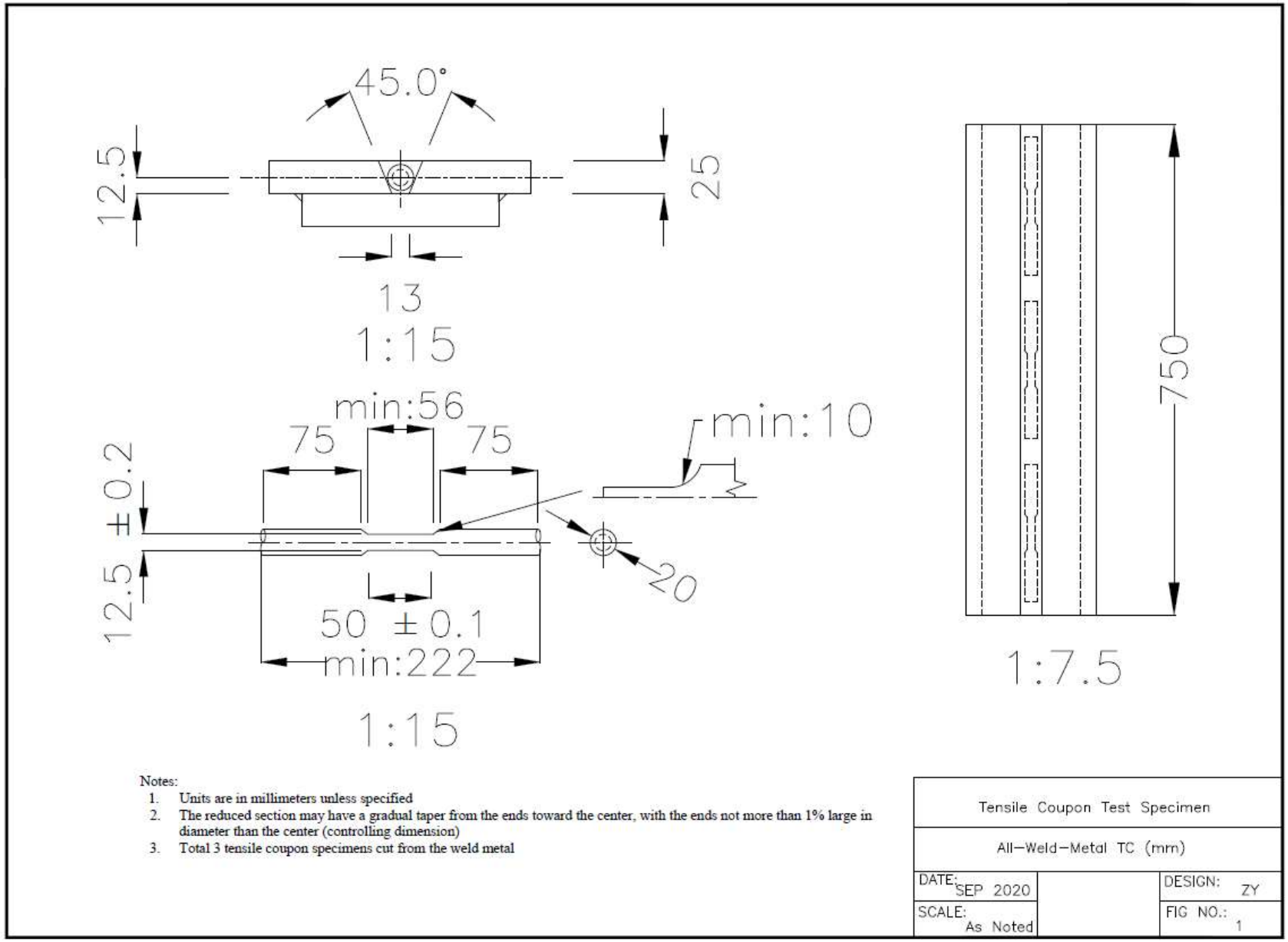

Figure B-14 All-weld metal tensile coupont drawing

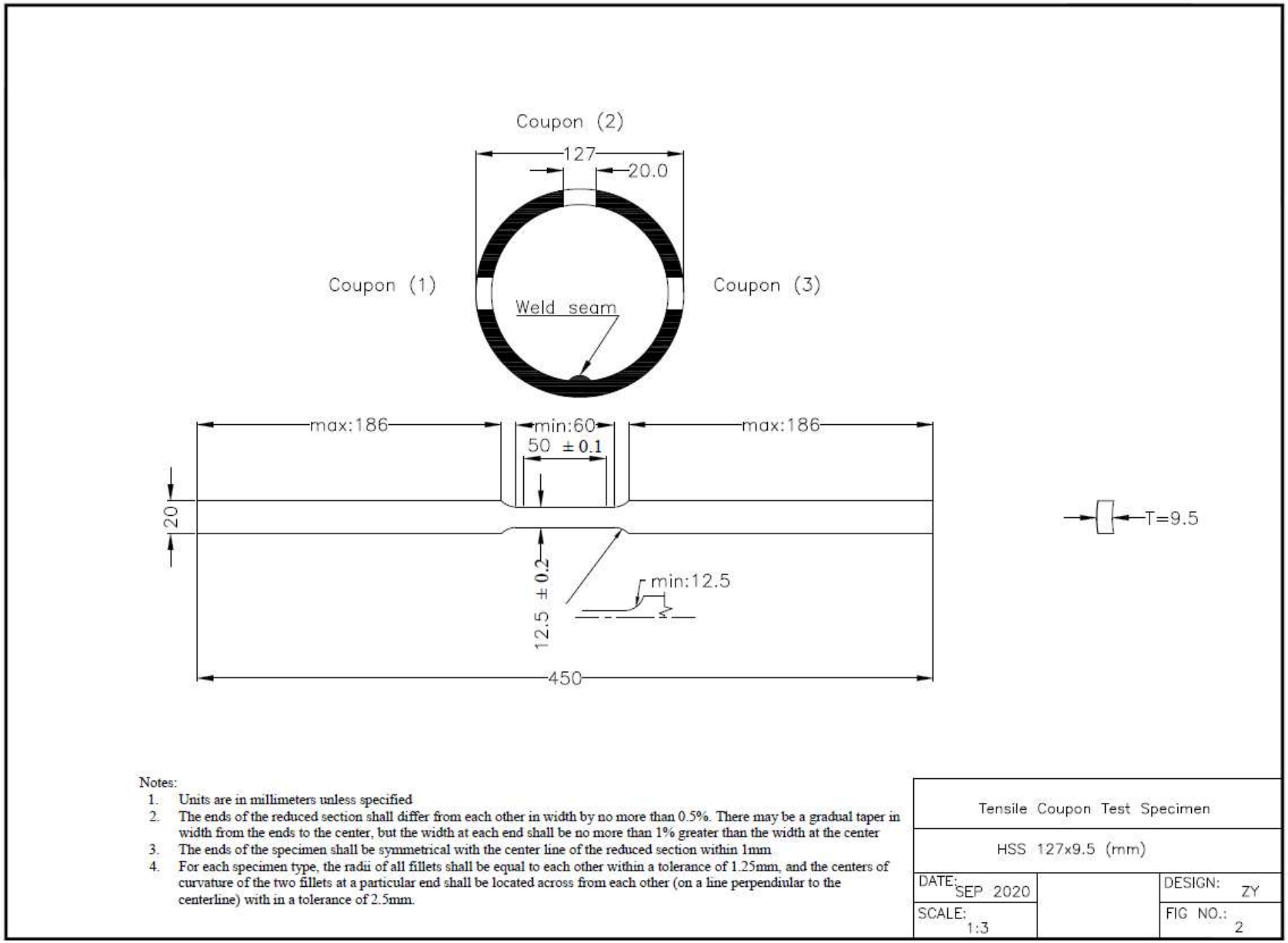

Figure B-15 HSS 127×9.5 tensile coupon drawing

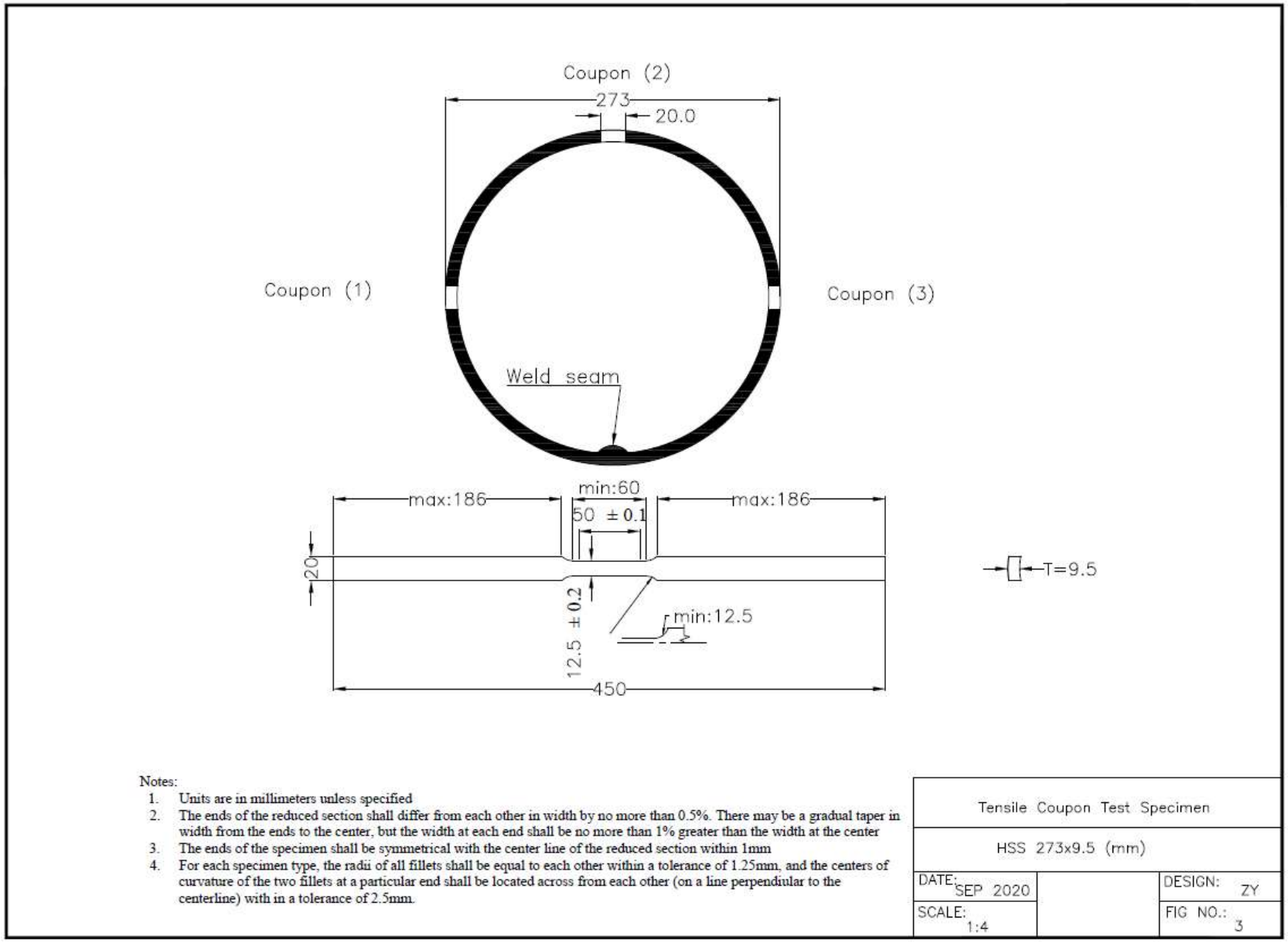

Figure B-16 HSS 273×9.5 tensile coupon drawing

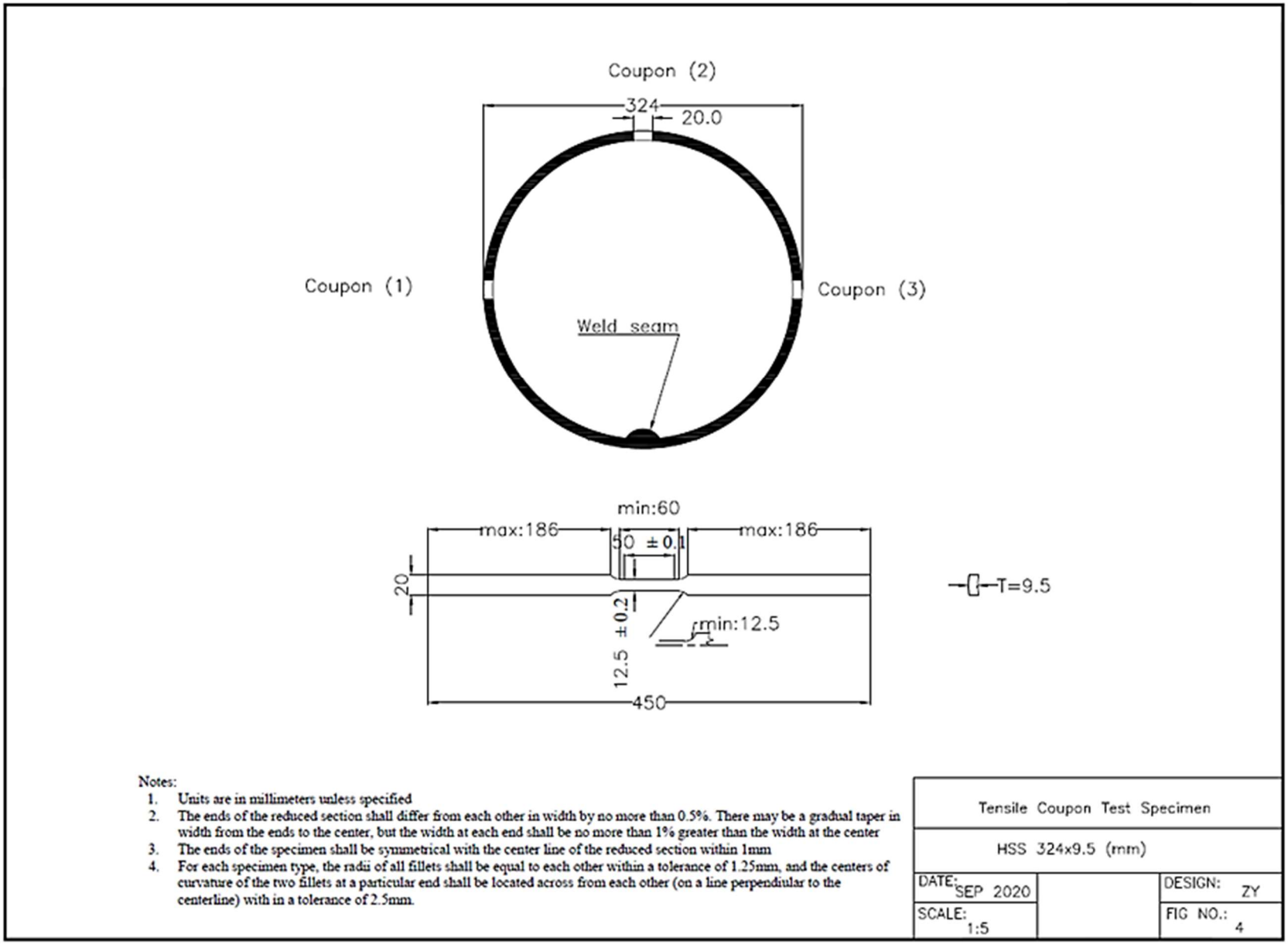

Figure B-17 HSS 324×9.5 tensile coupon drawing

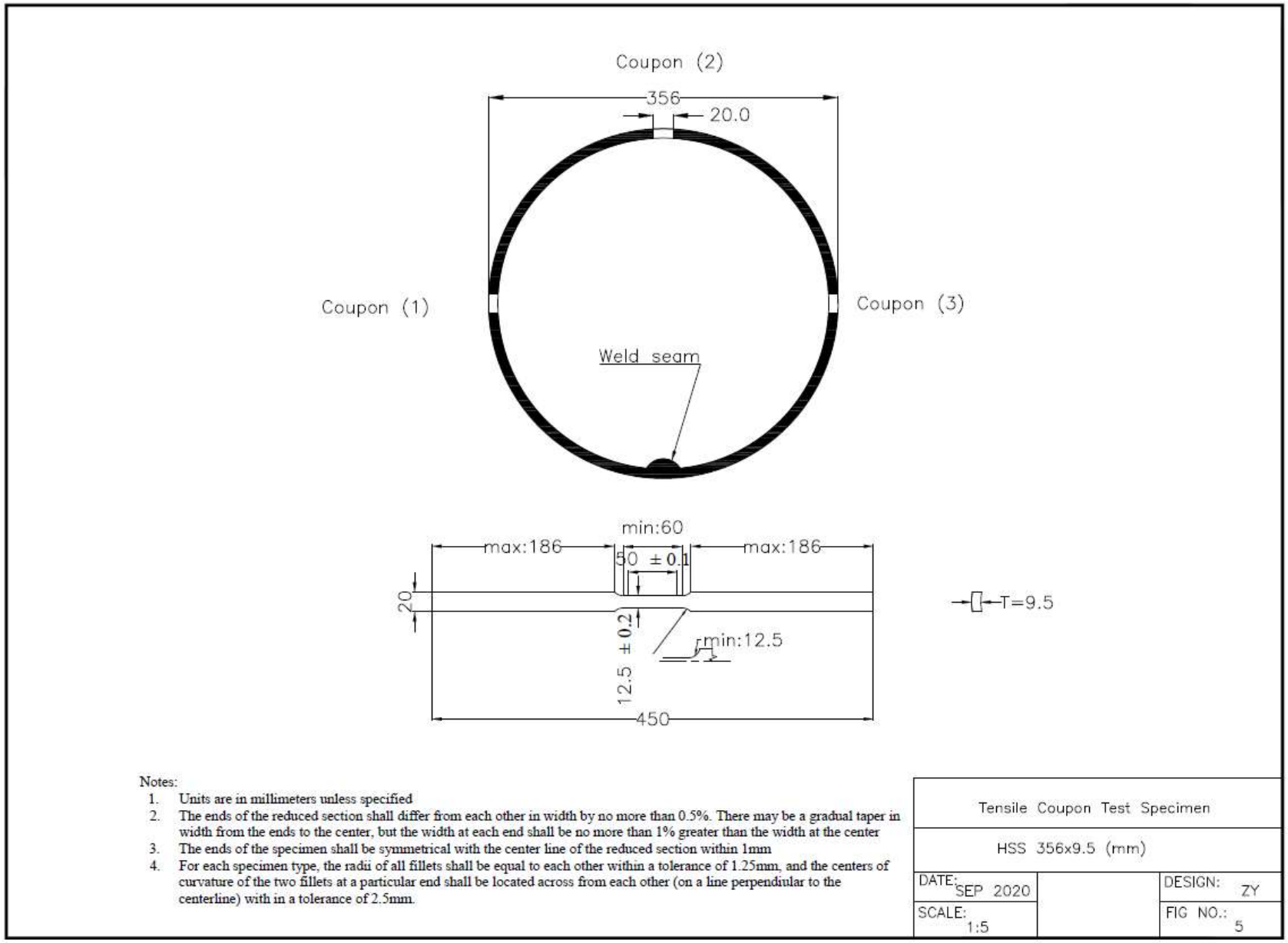

Figure B-18 HSS 356×9.5 tensile coupon drawing

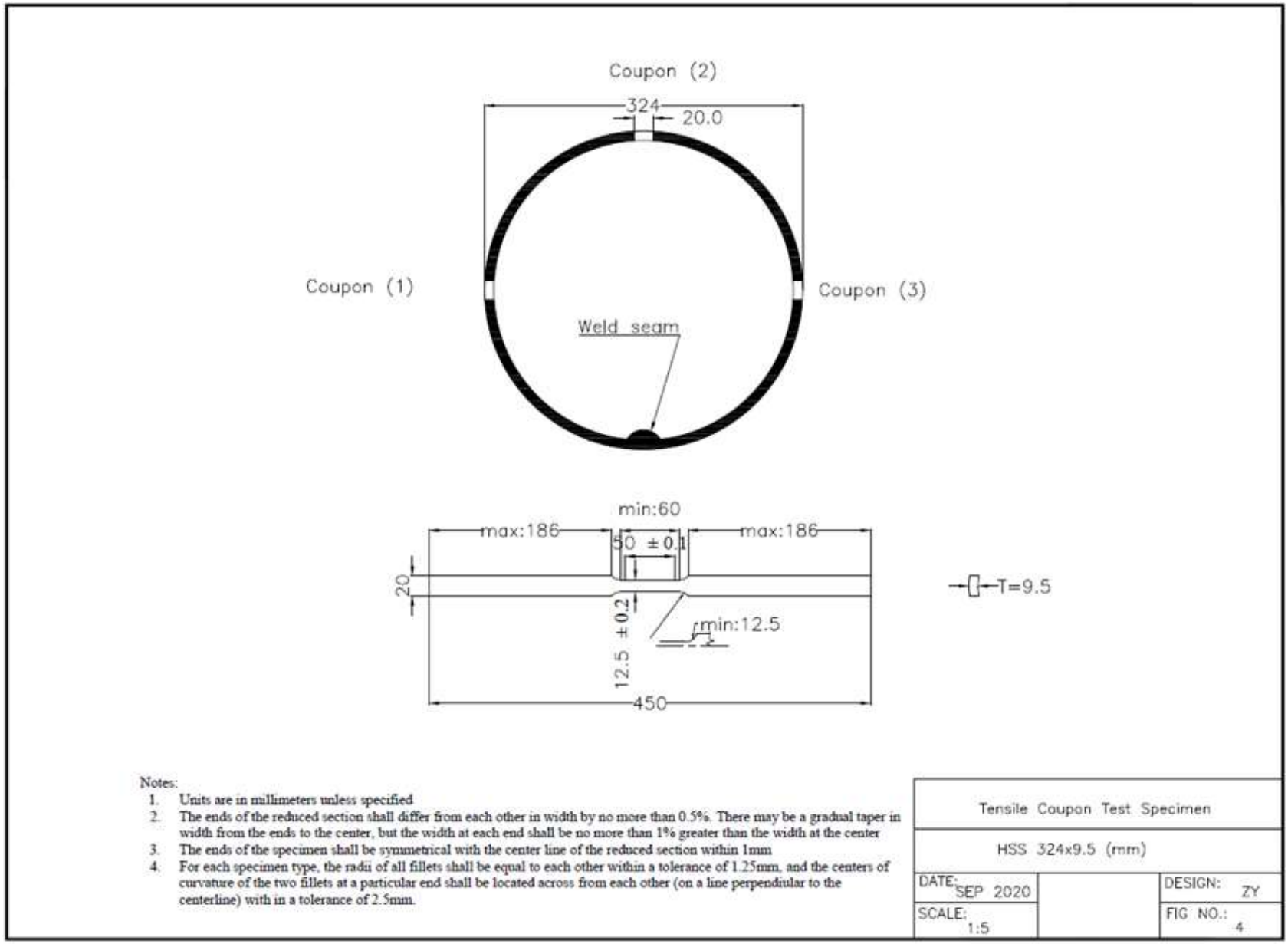

Figure B-19 HSS 406×9.5 tensile coupon drawing

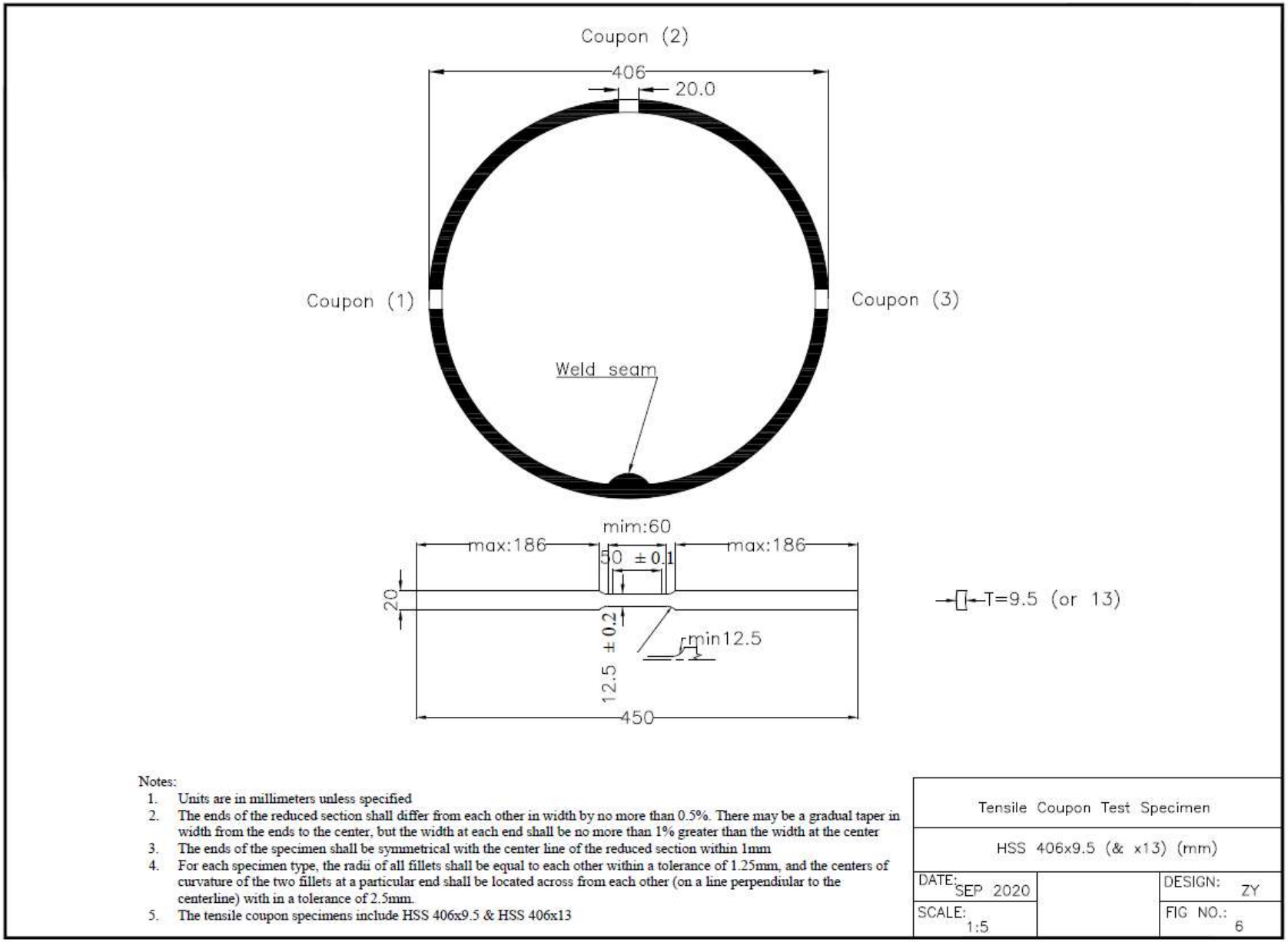

Figure B-20 HSS 406×13 tensile coupon drawing

Appendix C: TEST SETUP AND INSTRUMENTATION

Appendix C provides the supplementary drawing for the test setup.

C.1. TEST SETUP AND STRAIN GAUGES DISTRIBUTION

The sample test setup drawing is shown here as well as the strain gauge distribution where the bending direction is shown in the drawing.

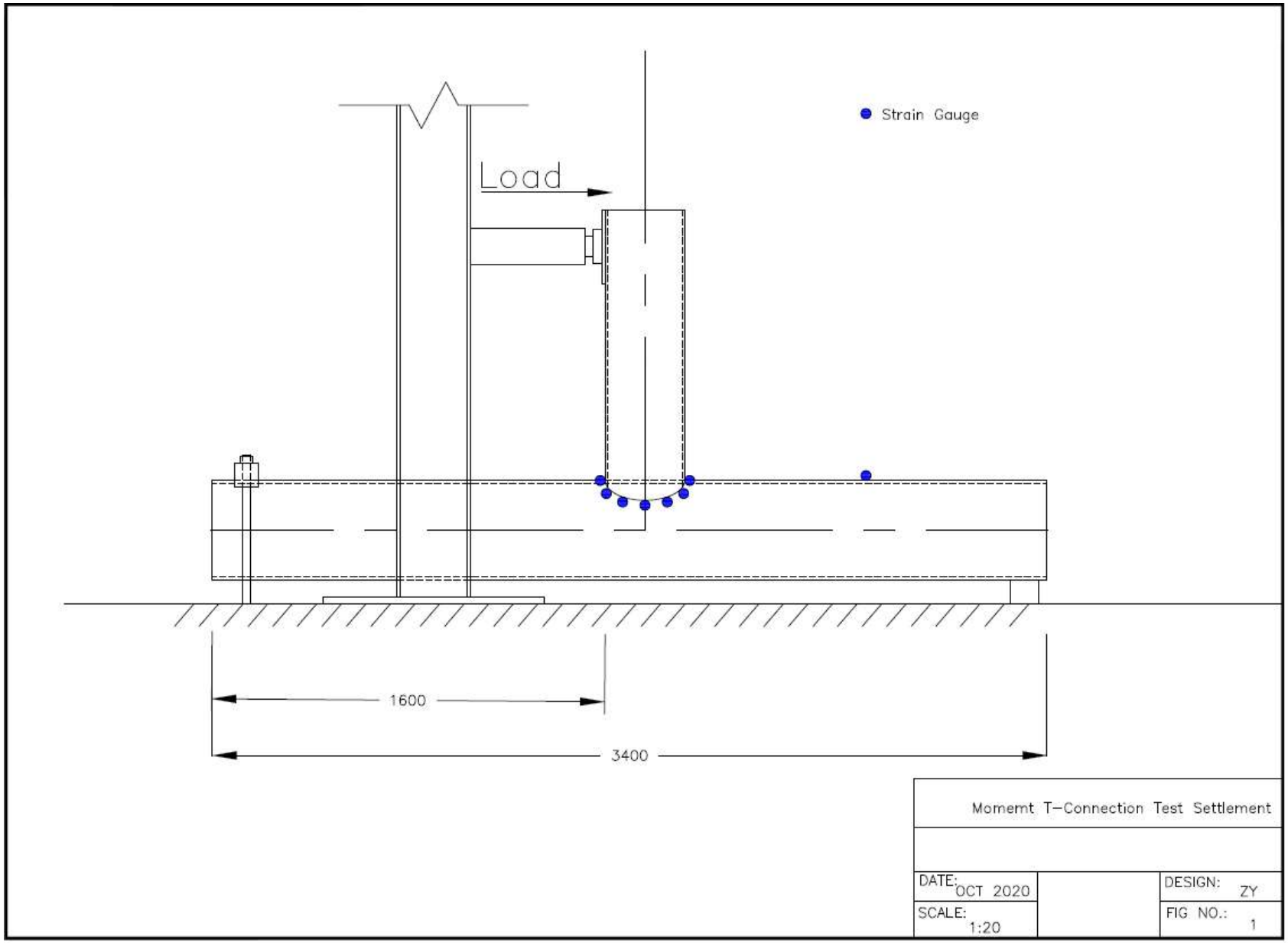

Figure C-1 Test settlement drawing (overview)

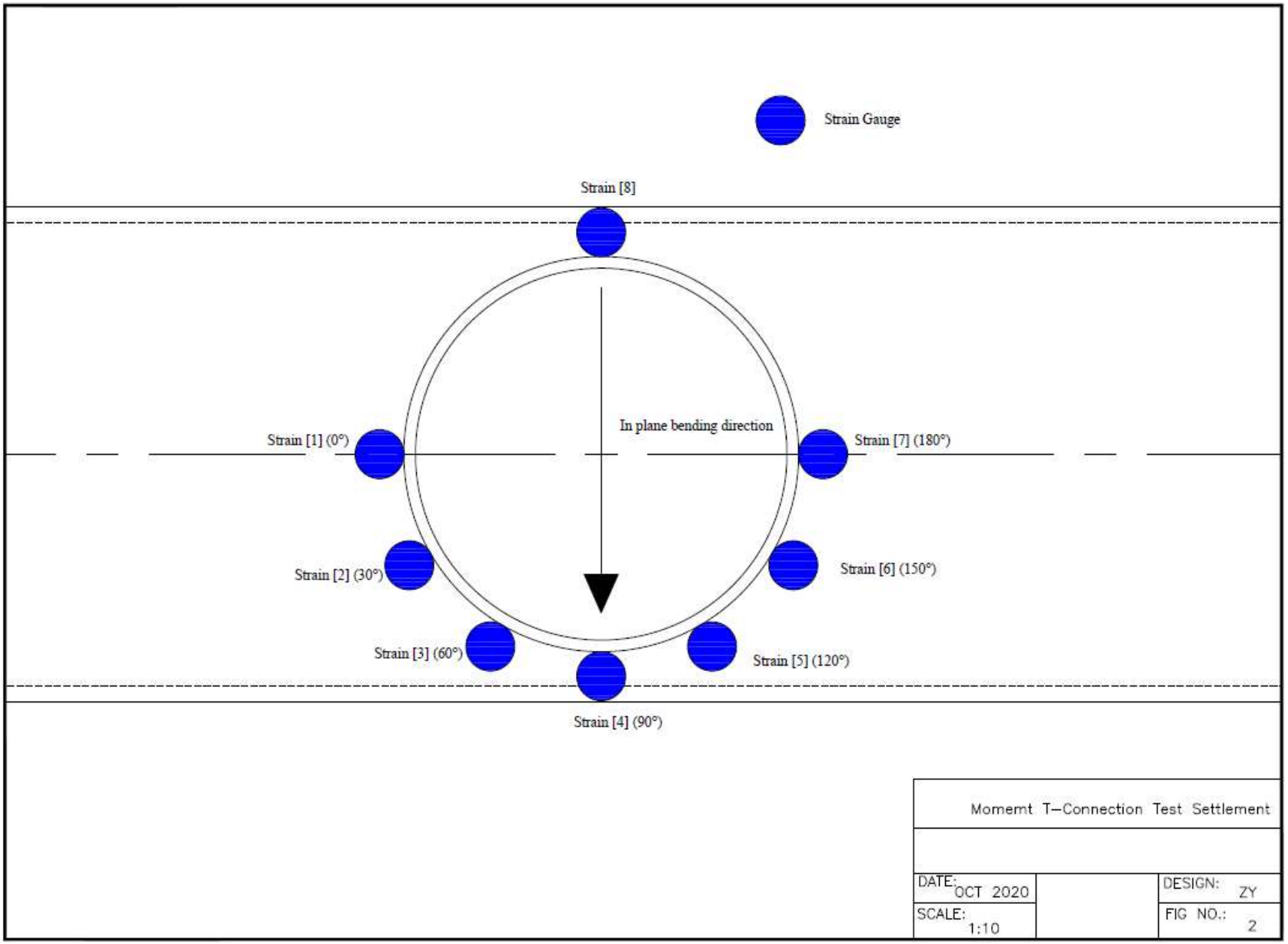

Figure C-2 Strain gauges settlement drawing

Appendix D: CHS MATERIAL PROPERTY TEST RESULT

Appendix D provides the supplementary data for the strength of HSS base metal:

D.1. TENSILE COUPON TEST RESULTS

Appendix D.1 provides general supplementary figures.

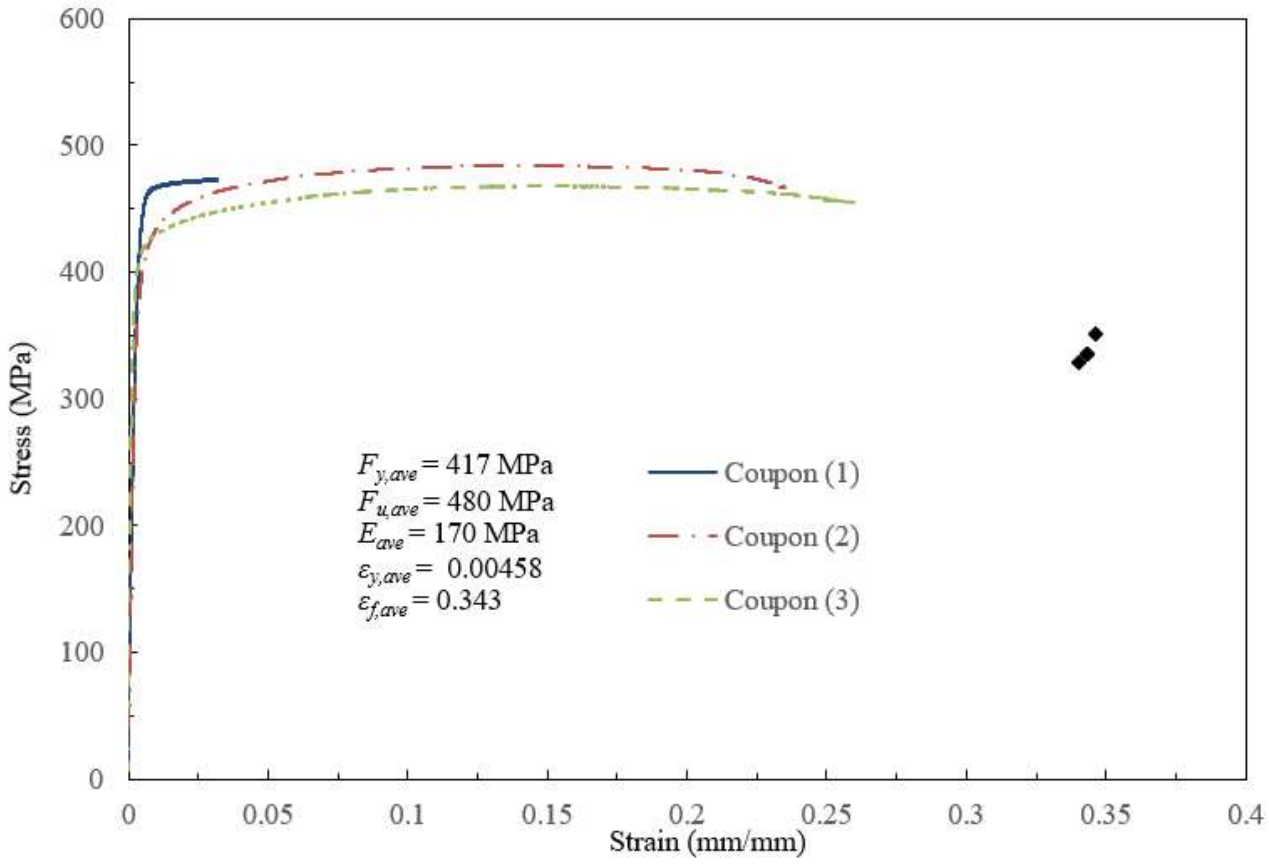

Figure D-1 Tensile coupon test result for HSS 127×9.5

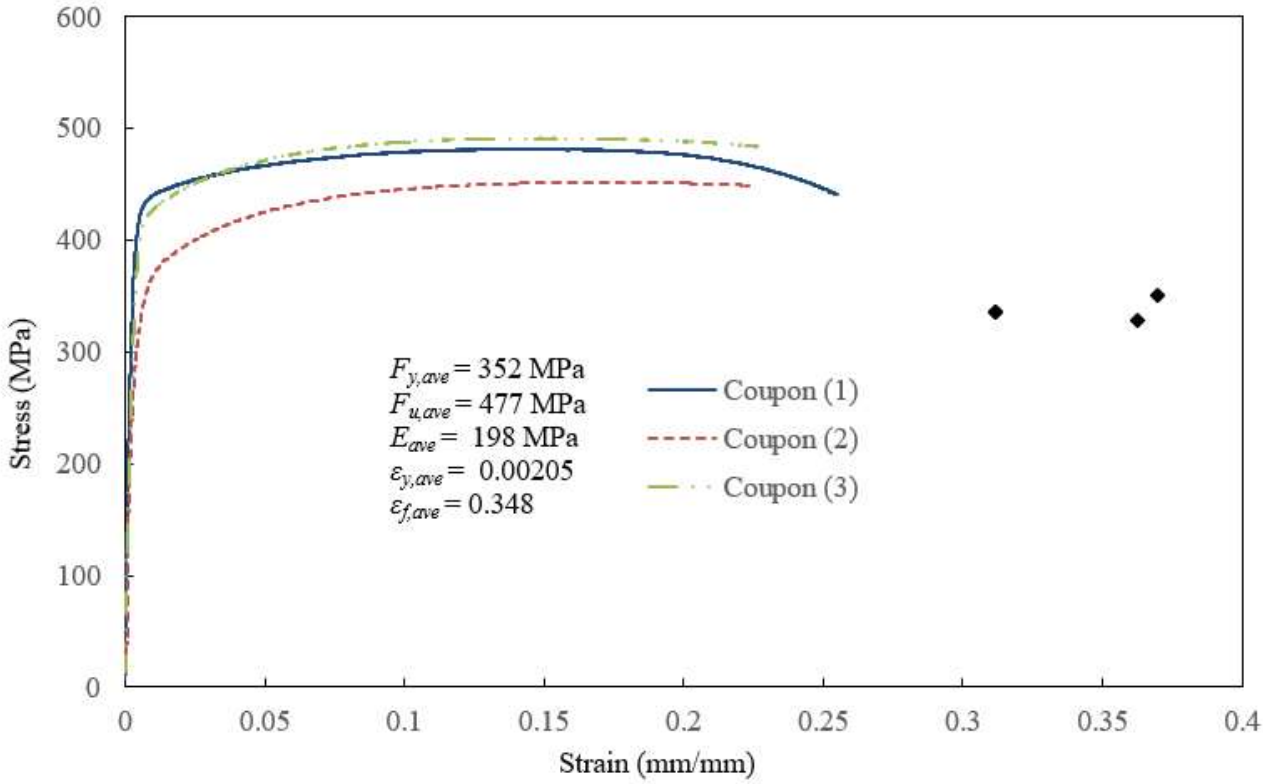

Figure D-2 Tensile coupon test result for HSS 273×9.5

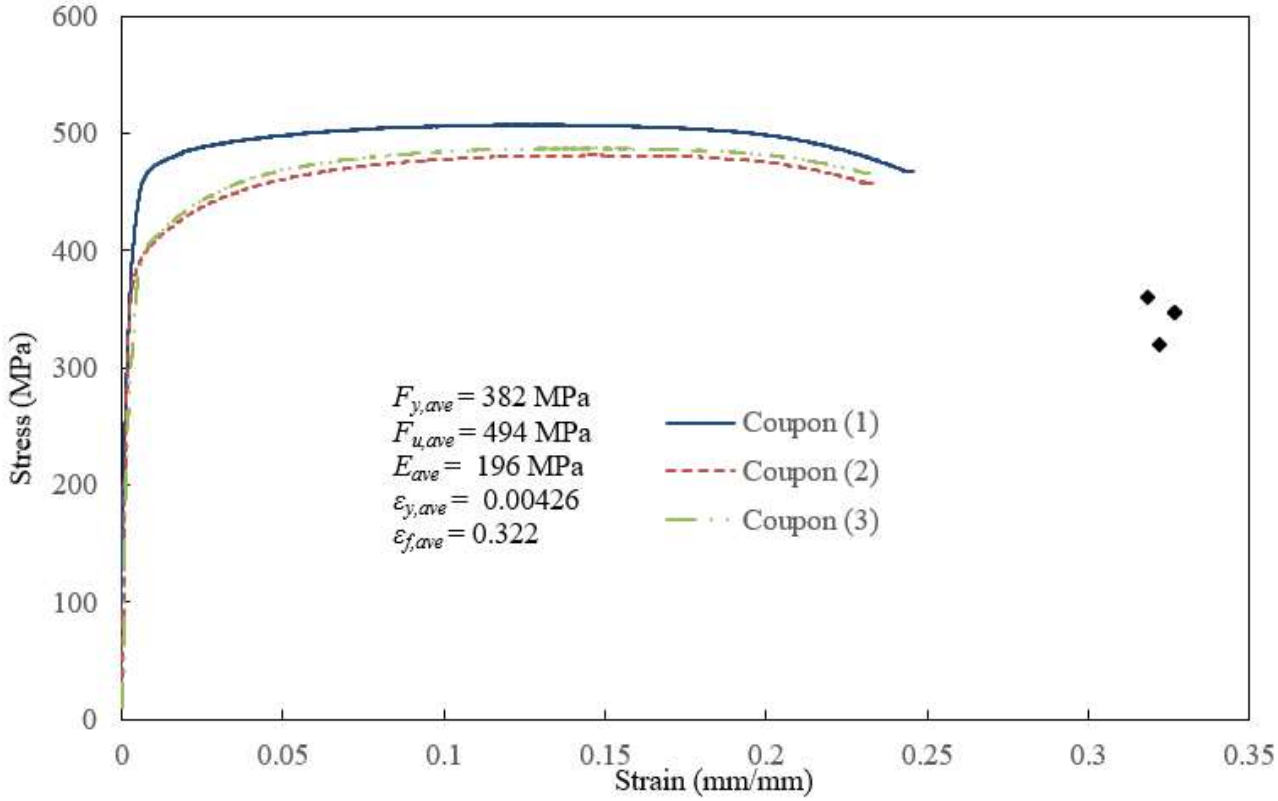

Figure D-3 Tensile coupon test result for HSS 324×9.5

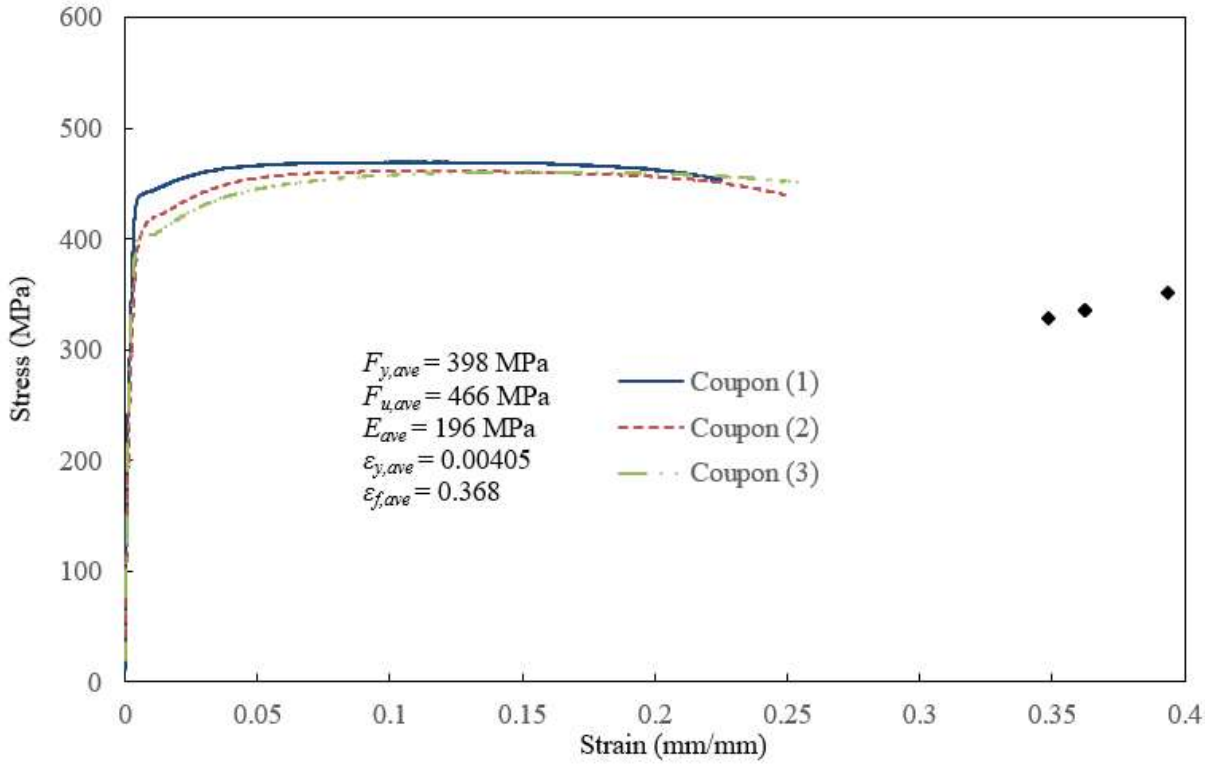

Figure D-4 Tensile coupon test result for HSS 356×9.5

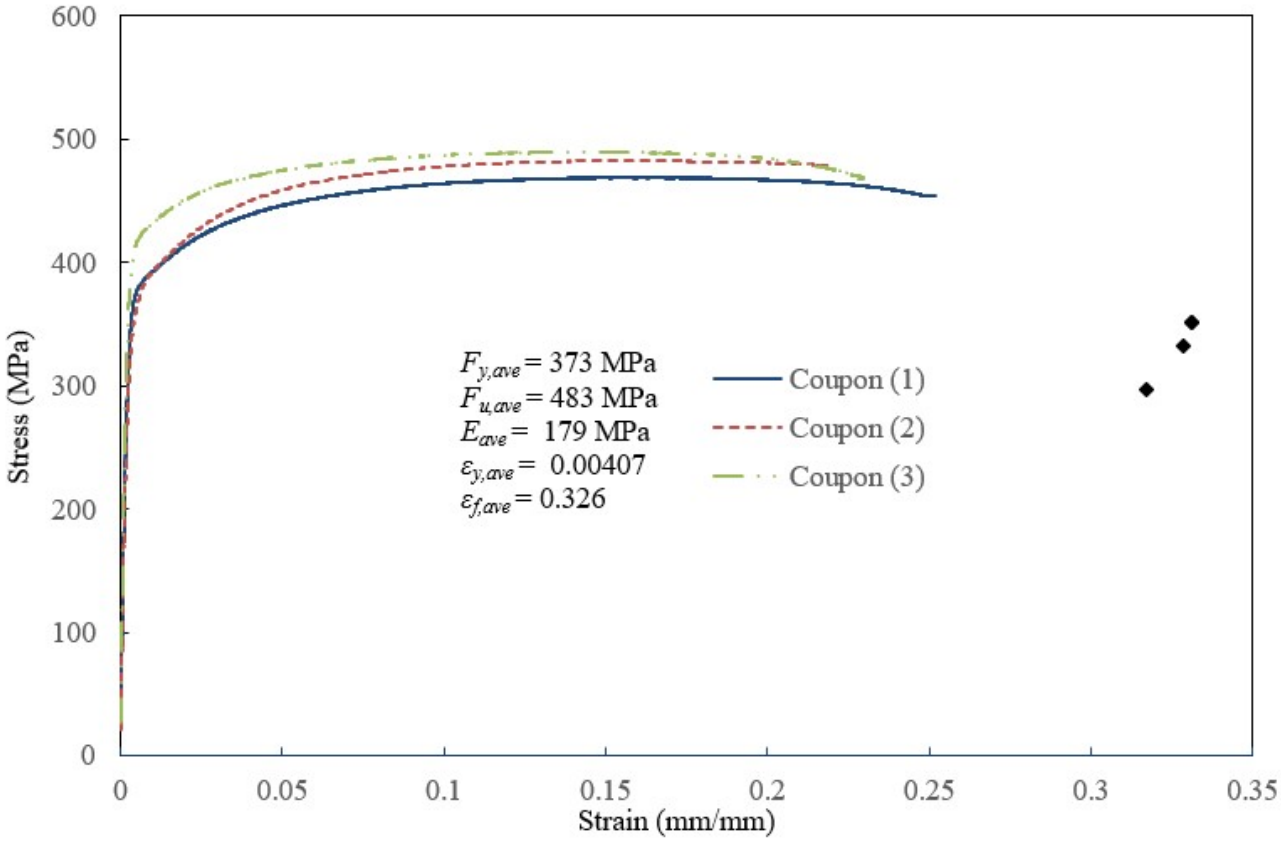

Figure D-5 Tensile coupon test result for HSS 406×9.5

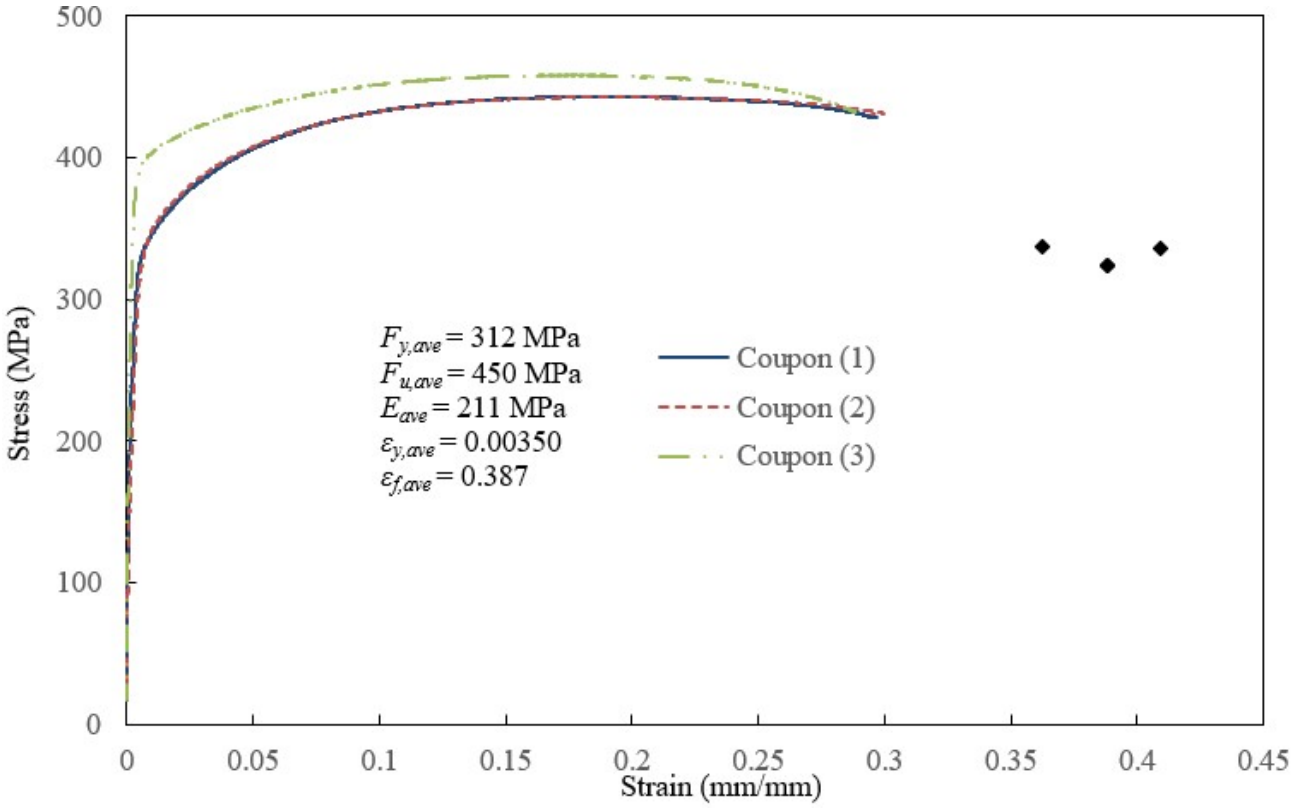

Figure D-6 Tensile coupon test result for HSS 406×13

Appendix E: WELDS GEOMETRIC AND MATERIAL PROPERTIES

Appendix E provides the supplementary strength and geometric property for weld metal:

E.1. WELD METAL TENSILE COUPON TEST RESULT

Appendix E.1 provides a general supplementary figure for all-weld metal tensile coupon test result.

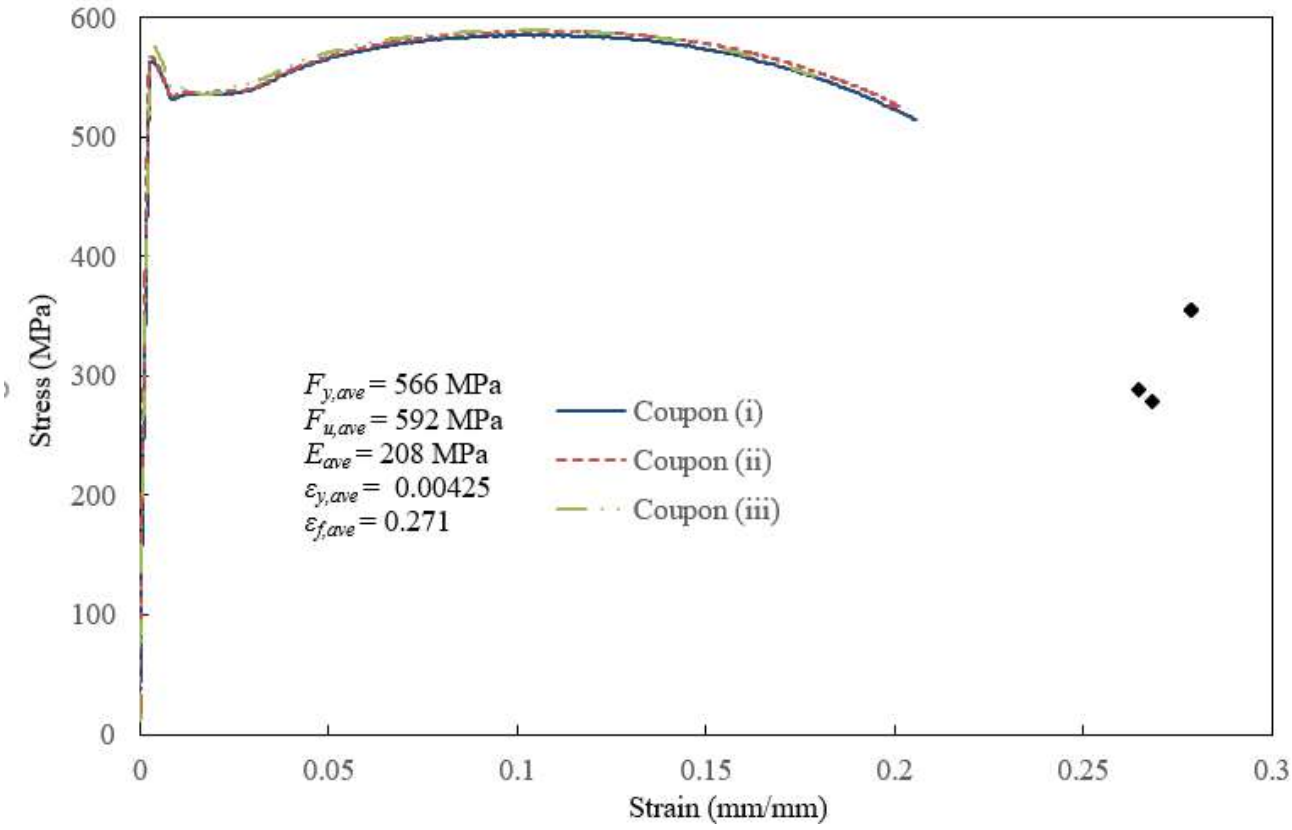

Figure E-1 Tensile coupon test result for all-weld metal

E.2. WELD METAL GEOMETRIC MEASUREMENT

Appendix E.2 provide pictures for weld macroetch examinations for each specimen. One picture per cut face is shown in Figure E-2 to E-13. The size of measured weld throat also summarized in the table after picture.

The color of lines represents the same as described in Chapter 4.2.2:

1. The yellow line shows the boundary between the weld and base metal and the fractural patten.
2. The blue line shows the weld size from leg measurement.
3. The dashed blue line shows the weld size from external leg measurement.
4. The red line shows the minimum distance from the root to weld surface (might be covered by blue lines).

Table E-1 Weld throat measurement of T273-127-1P

Location	Measurement type		
	Minimum distance	Fractural distance	Leg size calculation
0°	3.55	3.55	
	4.00	4.00	
90°	6.10	6.10	
	6.59	6.59	
180°	2.91	3.07	NA
	2.43	2.97	
270°	5.79	5.79	
	5.26	5.26	
Average	4.58	4.67	

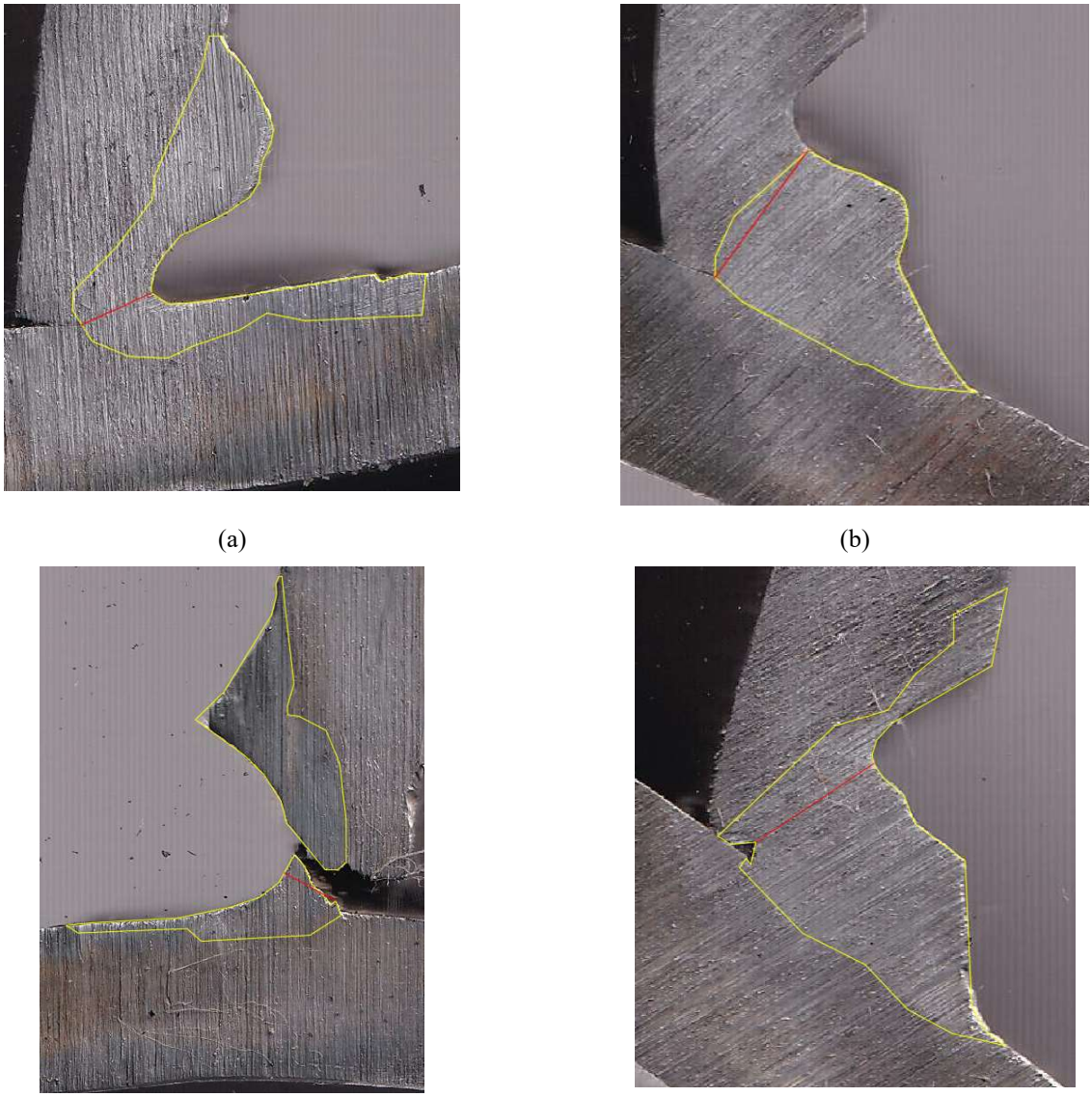

(a) (b)

(c) (d)

Figure E-2 Macroetch examination for T273-127-1P (a) 0° (compression side), (b) 90° (saddle side), (c) 180° (tension side) and (d) 270° (saddle side)

Table E-2 Weld throat measurement of T273-127-1

Location	Measurement type		
	Minimum distance	Fractural distance	Leg size calculation
0°	2.47	2.47	3.14
	2.85	2.85	3.37
90°	2.16	2.73	2.27
	2.53	2.81	2.18
180°	2.71	3.10	2.22
	2.41	2.70	2.10
270°	3.11	3.13	2.59
	2.61	2.74	1.50
Average	2.61	2.81	2.42

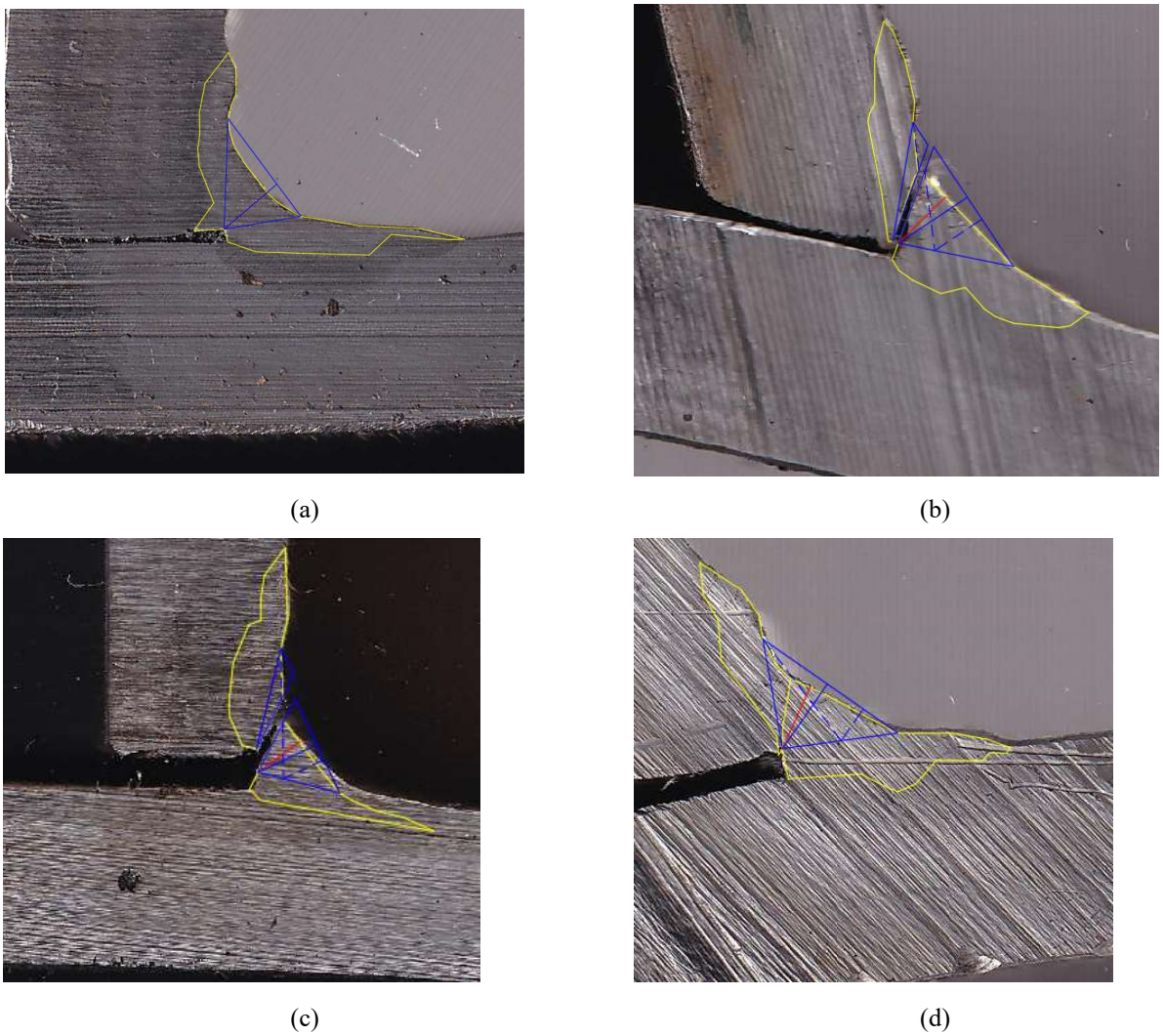

(a) (b)

(c) (d)

Figure E-3 Macroetch examination for T273-127-1 (a) 0° (compression side), (b) 90° (saddle side), (c) 180° (tension side) and (d) 270° (saddle side)

Table E-3 Weld throat measurement of T324-127-1

Location	Measurement type		
	Minimum distance	Fractural distance	Leg size calculation
0°	3.19	3.19	3.57
	3.57	3.57	2.83
90°	2.80	2.80	2.39
	2.94	2.94	1.99
180°	2.70	2.77	3.27
	2.70	2.77	3.27
270°	2.86	2.86	2.93
	2.88	2.88	2.22
Average	2.96	2.97	2.81

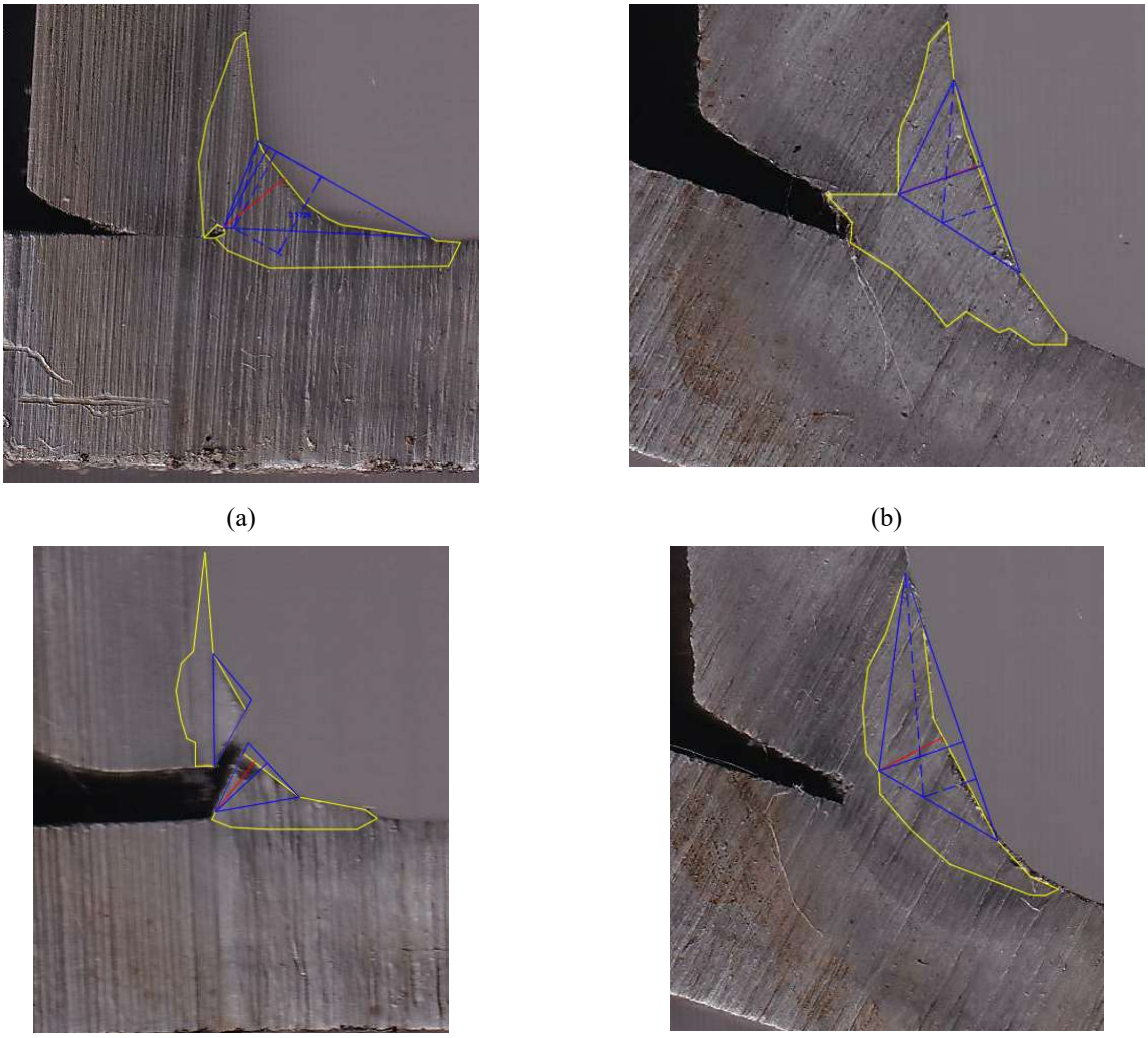

(a) (b) (c) (d)

Figure E-4 Macroetch examination for T324-127-1 (a) 0° (compression side), (b) 90° (saddle side), (c) 180° (tension side) and (d) 270° (saddle side)

Table E-4 Weld throat measurement of T356-127-1

Location	Measurement type		
	Minimum distance	Fractural distance	Leg size calculation
0°	2.81	2.81	2.49
	2.90	2.90	3.32
90°	2.64	2.64	3.21
	2.57	2.57	3.69
180°	1.78	2.06	3.45
	1.57	1.68	3.19
270°	1.93	2.01	2.61
	2.39	2.01	3.25
Average	2.32	2.33	3.15

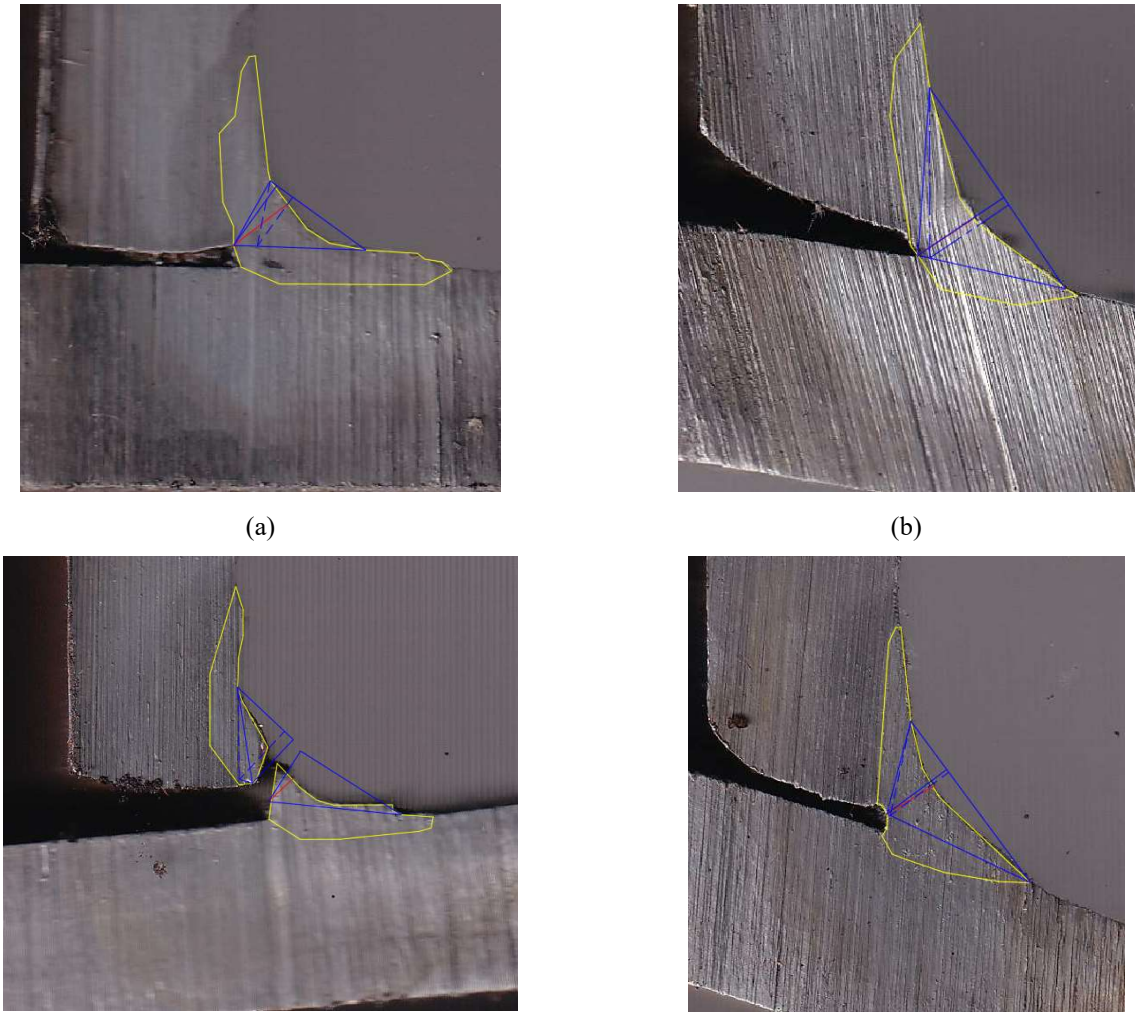

(a) (b) (c) (d)

Figure E-5 Macroetch examination for T356-127-1 (a) 0° (compression side), (b) 90° (saddle side), (c) 180° (tension side) and (d) 270° (saddle side)

Table E-5 Weld throat measurement of T356-273-1P

Location	Measurement type		
	Minimum distance	Fractural distance	Leg size calculation
0°	6.31		
	6.38		
90°	6.00		
	6.00		
180°	4.95	NA	NA
	4.35		
270°	5.32		
	5.27		
Average	5.57		

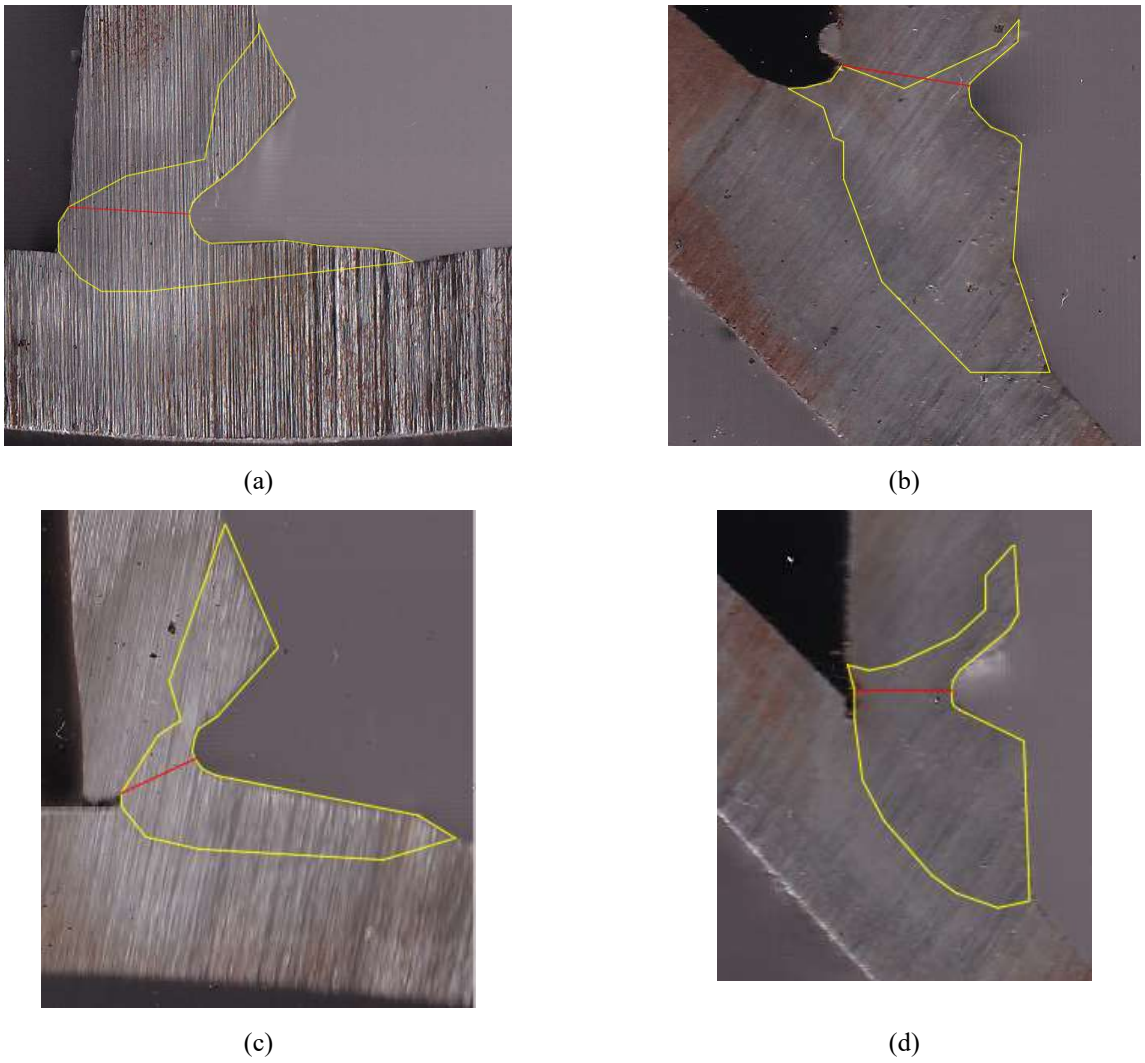

(a) (b) (c) (d)

Figure E-6 Macroetch examination for T356-273-1P (a) 0° (compression side), (b) 90° (saddle side), (c) 180° (tension side) and (d) 270° (saddle side)

Table E-6 Weld throat measurement of T356-324-1P

Location	Measurement type		
	Minimum distance	Fractural distance	Leg size calculation
0°	3.07	3.07	NA
	3.33	3.33	
90°	6.03	6.03	
	6.04	6.04	
180°	3.75	3.98	
	3.75	3.98	
270°	7.23	7.23	
	7.26	7.26	
Average	5.06	5.12	

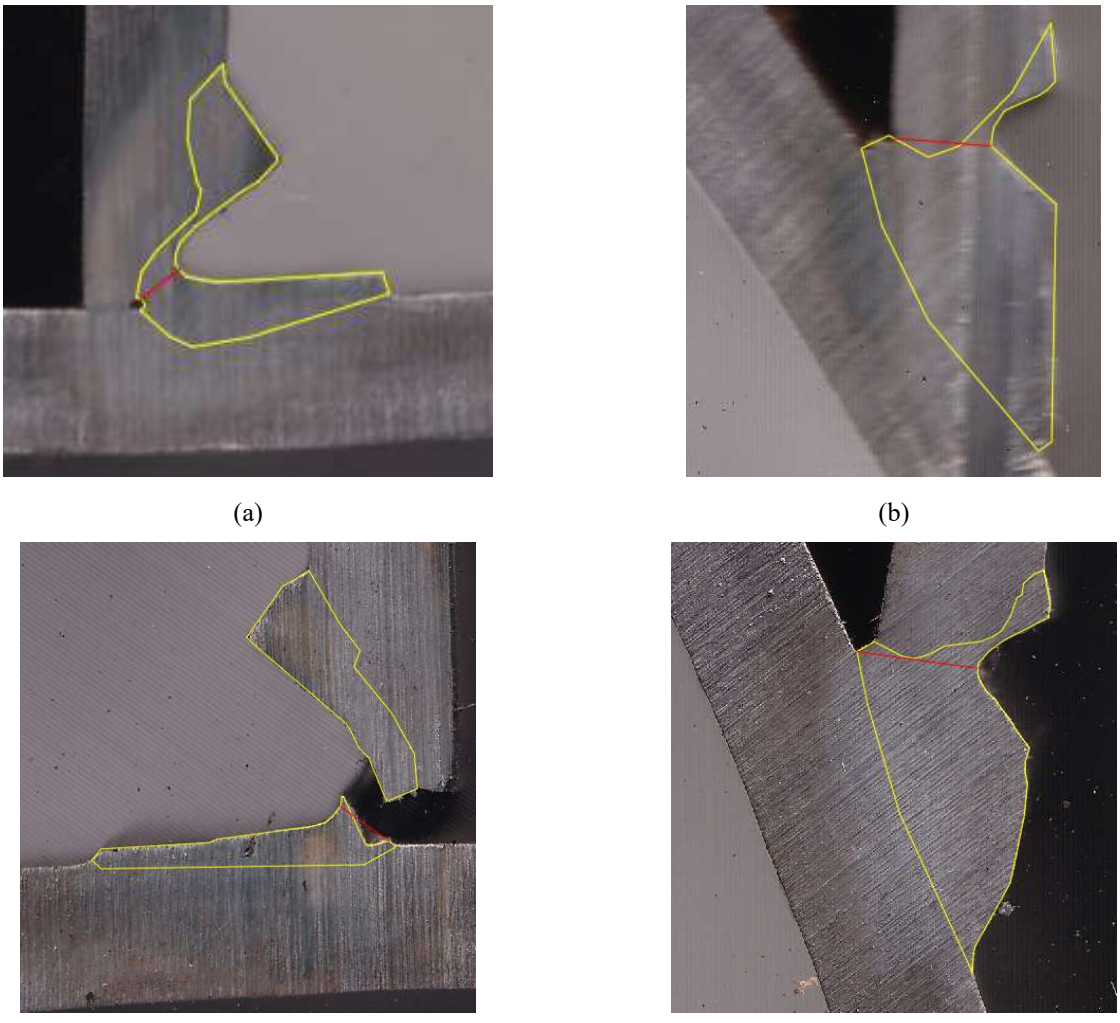

(a) (b)

(c) (d)

Figure E-7 Macroetch examination for T356-324-1P (a) 0° (compression side), (b) 90° (saddle side), (c) 180° (tension side) and (d) 270° (saddle side)

Table E-7 Weld throat measurement of T406-127-1

Location	Measurement type		
	Minimum distance	Fractural distance	Leg size calculation
0°	3.51	3.51	3.84
	3.31	3.31	3.40
90°	2.33	2.42	2.83
	2.28	2.42	2.77
180°	2.89	3.22	2.57
	2.41	2.61	2.31
270°	2.78	2.78	2.49
	2.98	2.98	2.61
Average	2.81	2.90	2.85

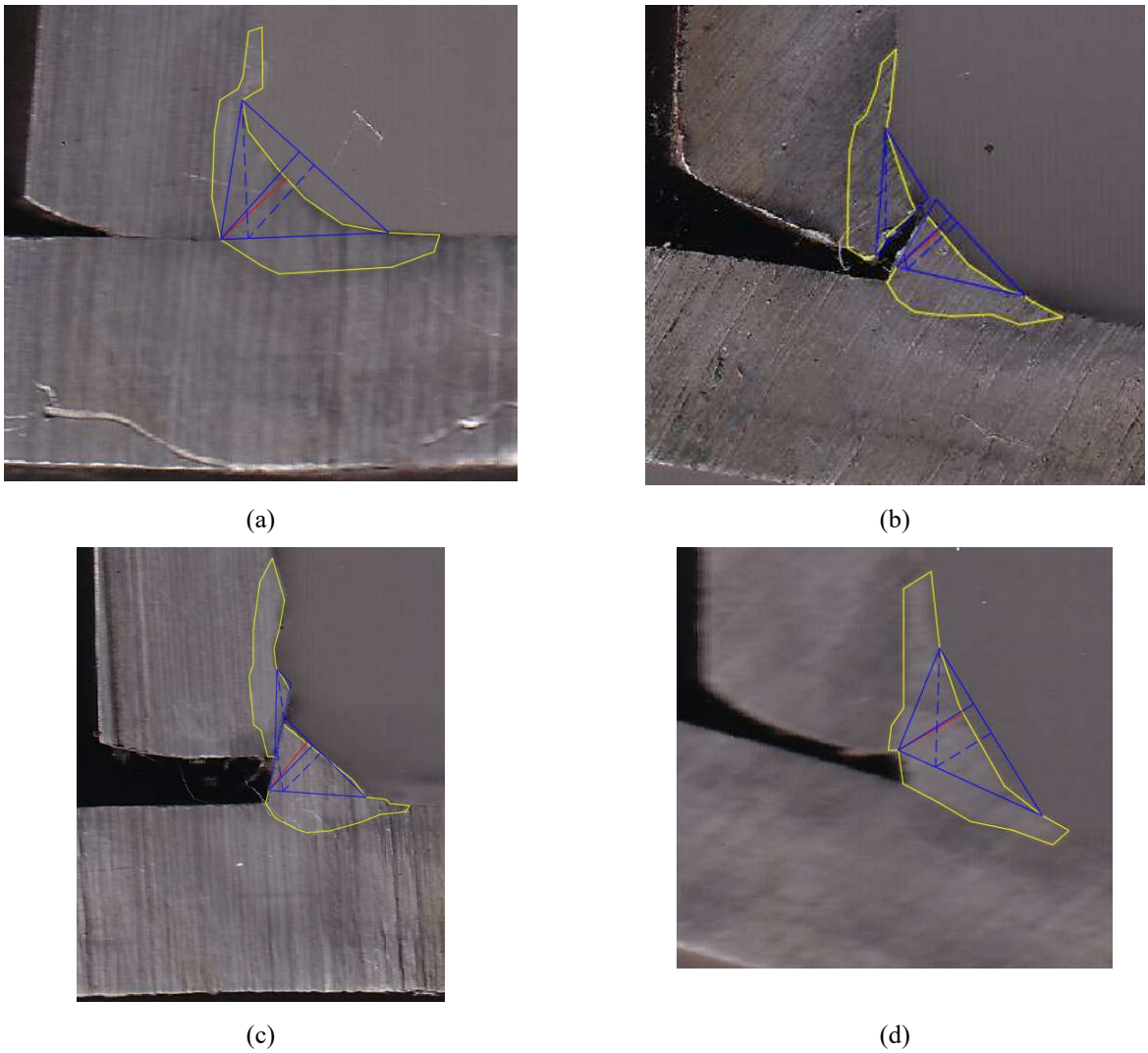

(a) (b) (c) (d)

Figure E-8 Macroetch examination for T406-127-1 (a) 0° (compression side), (b) 90° (saddle side), (c) 180° (tension side) and (d) 270° (saddle side)

Table E-8 Weld throat measurement of T406-273-1P

Location	Measurement type		
	Minimum distance	Fractural distance	Leg size calculation
0°	3.37	3.37	NA
	3.32	3.32	
90°	5.21	5.21	
	5.34	5.34	
180°	2.50	2.50	
	3.76	3.75	
270°	5.87	5.87	
	5.99	5.99	
Average	4.42	4.42	

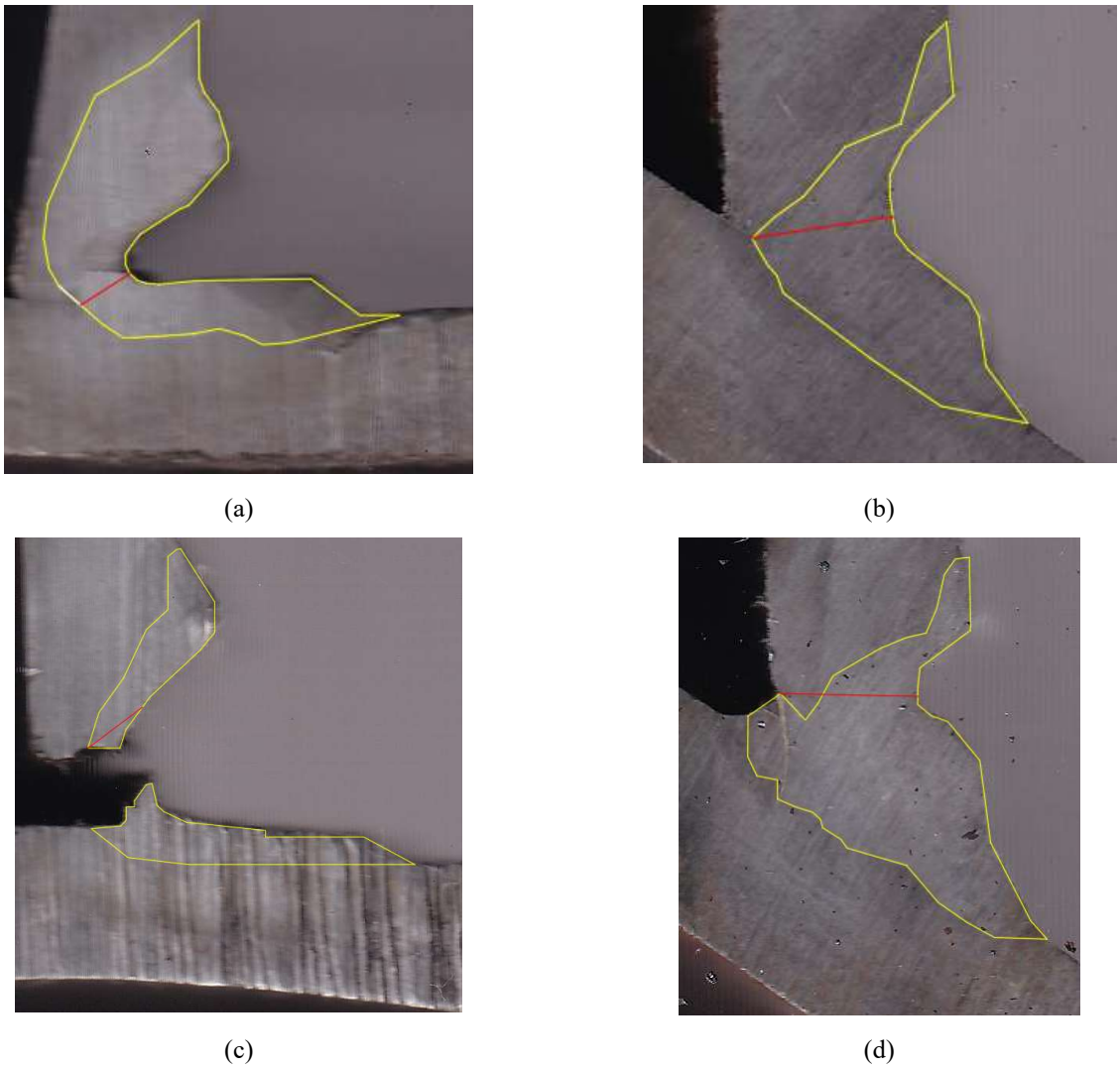

(a) (b)

(c) (d)

Figure E-9 Macroetch examination for T406-273-1P (a) 0° (compression side), (b) 90° (saddle side), (c) 180° (tension side) and (d) 270° (saddle side)

Table E-9 Weld throat measurement of T406-324-1P

Location	Measurement type		
	Minimum distance	Fractural distance	Leg size calculation
0°	3.93	3.93	NA
	4.24	4.24	
90°	5.00	5.00	
	5.50	5.50	
180°	2.52	2.52	
	3.07	3.36	
270°	4.33	4.33	
	4.31	4.31	
Average	4.11	4.15	

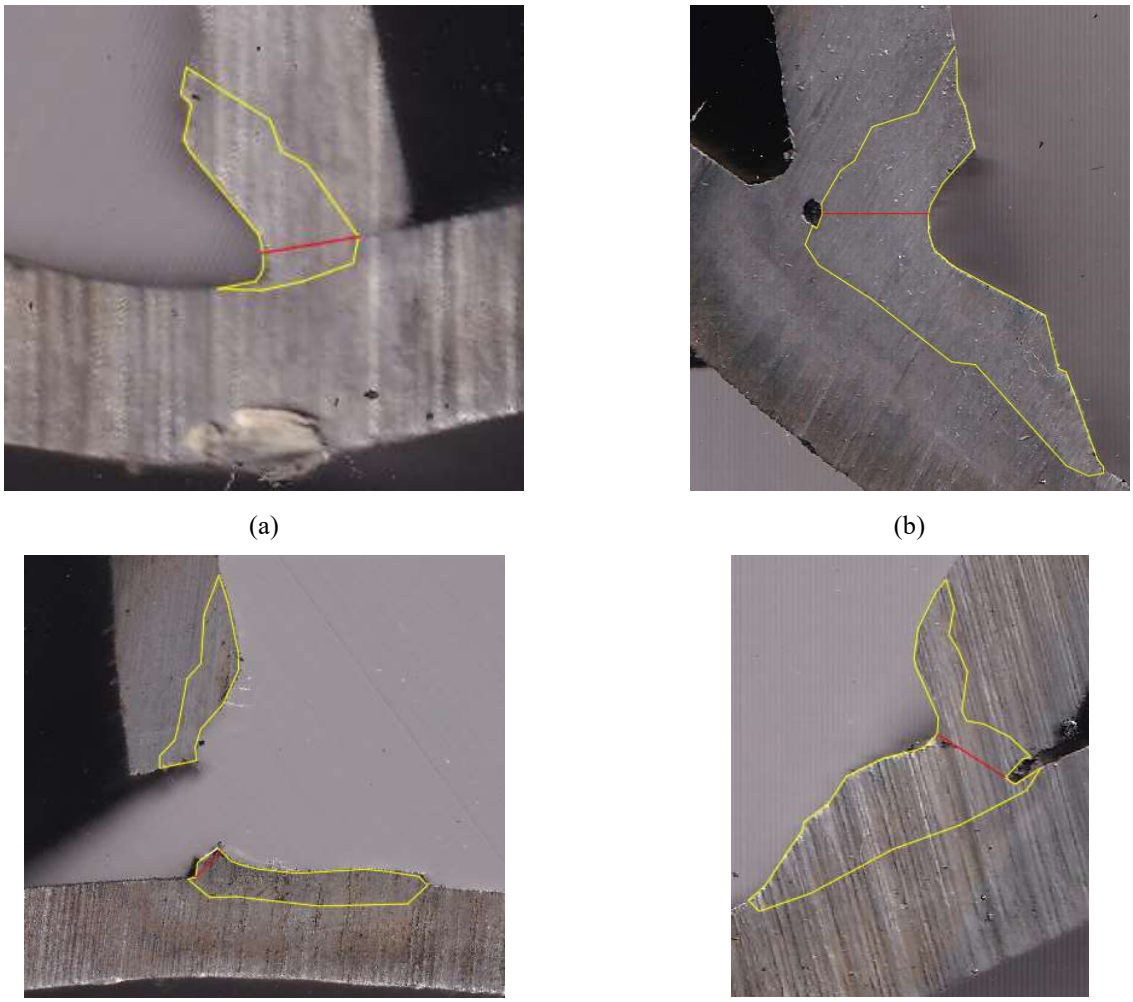

(a) (b)

(c) (d)

Figure E-10 Macroetch examination for T406-324-1P (a) 0° (compression side), (b) 90° (saddle side), (c) 180° (tension side) and (d) 270° (saddle side)

Table E-10 Weld throat measurement of T406-127-0.7

Location	Measurement type		
	Minimum distance	Fractural distance	Leg size calculation
0°	3.42	3.42	3.94
	3.04	3.04	3.53
90°	2.26	3.24	2.10
	2.68	3.24	2.22
180°	1.92	1.97	3.58
	1.92	1.97	3.58
270°	1.29	1.68	1.64
	1.37	1.55	1.71
Average	2.24	2.51	2.79

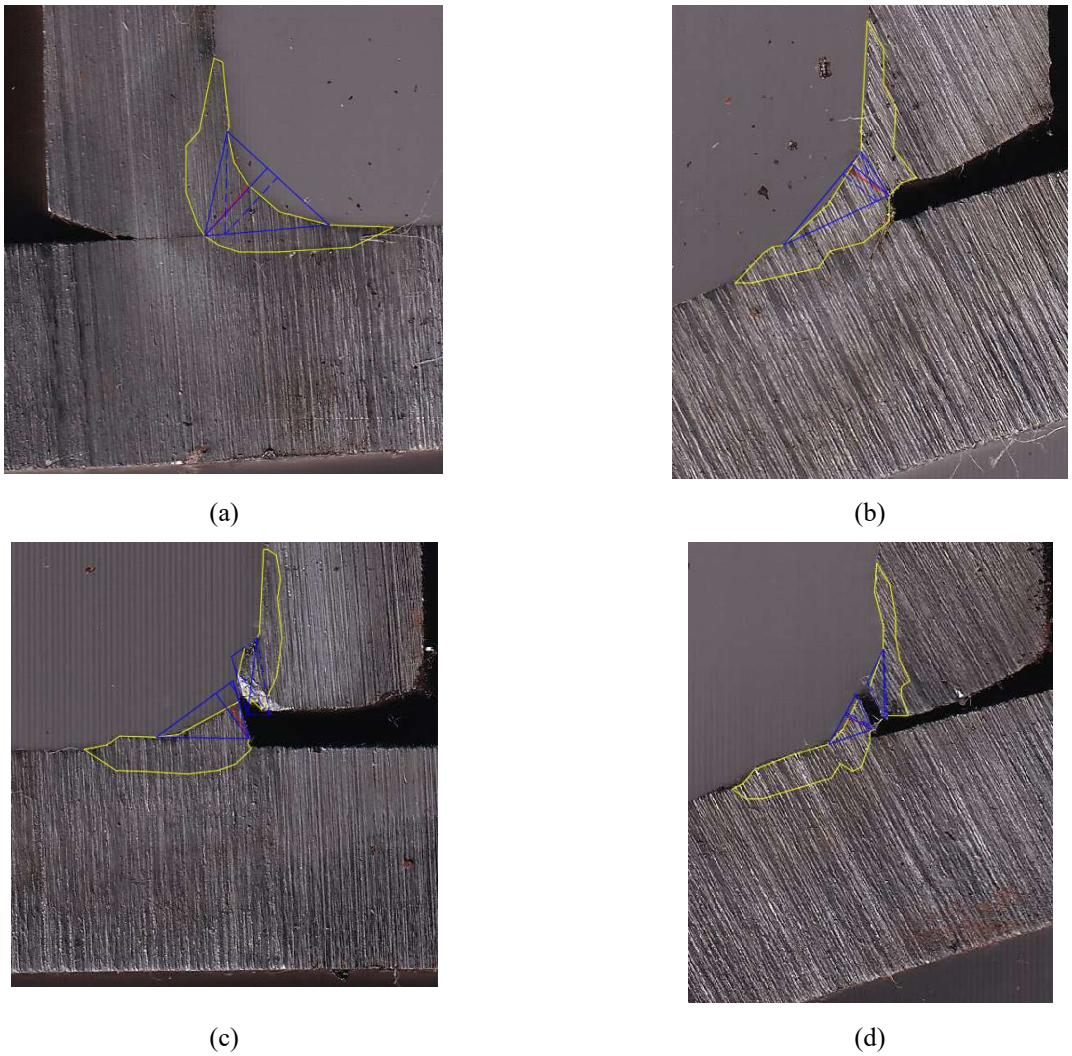

(a) (b) (c) (d)

Figure E-11 Macroetch examination for T406-127-0.7 (a) 0° (compression side), (b) 90° (saddle side), (c) 180° (tension side) and (d) 270° (saddle side)

Table E-11 Weld throat measurement of T406-273-0.7P

Location	Measurement type		
	Minimum distance	Fractural distance	Leg size calculation
0°	5.22	5.22	
	5.24	5.24	
90°	5.84	5.84	
	5.75	5.75	
180°	2.57	2.57	NA
	2.57	2.57	
270°	6.20	6.20	
	6.22	6.22	
Average	4.95	4.95	

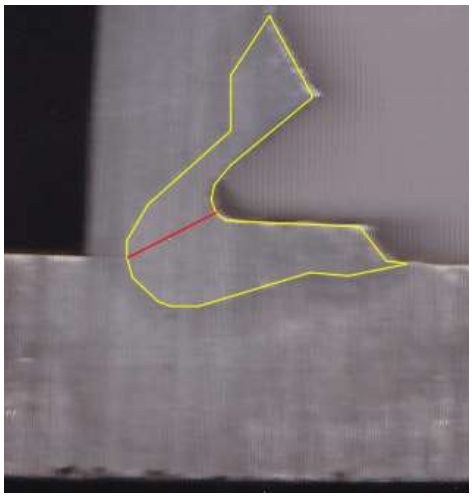

(a)

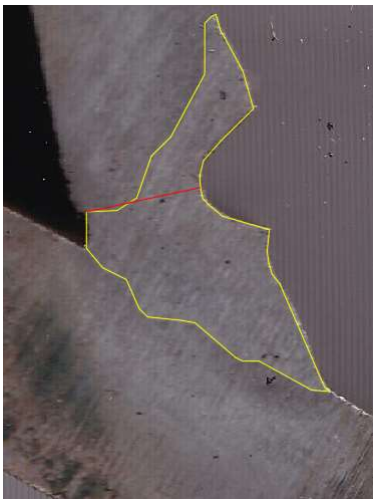

(b)

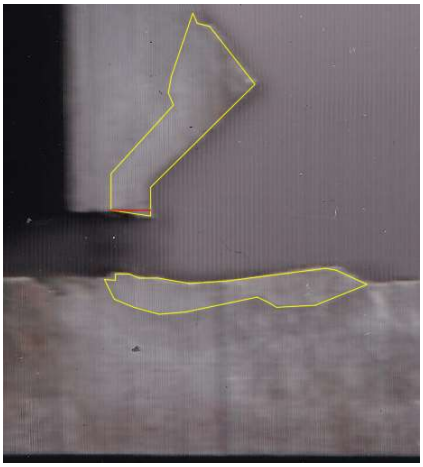

(c)

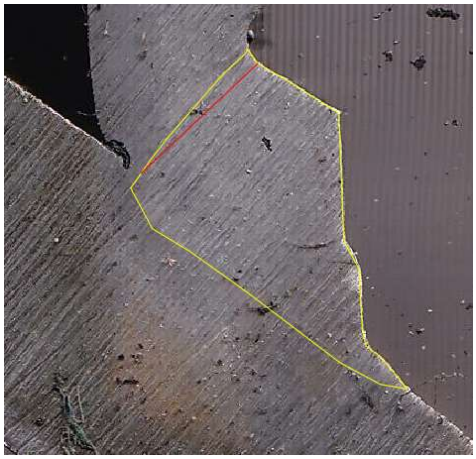

(d)

Figure E-12 Macroetch examination for T406-273-0.7P (a) 0° (compression side), (b) 90° (saddle side), (c) 180° (tension side) and (d) 270° (saddle side)

Table E-12 Weld throat measurement of T406-324-0.7P

Location	Measurement type		
	Minimum distance	Fractural distance	Leg size calculation
0°	3.67	3.67	NA
	4.25	4.25	
90°	8.84	8.84	
	8.81	8.81	
180°	3.19	3.19	
	3.15	3.10	
270°	5.65	5.65	
	5.31	5.31	
Average	5.36	5.35	

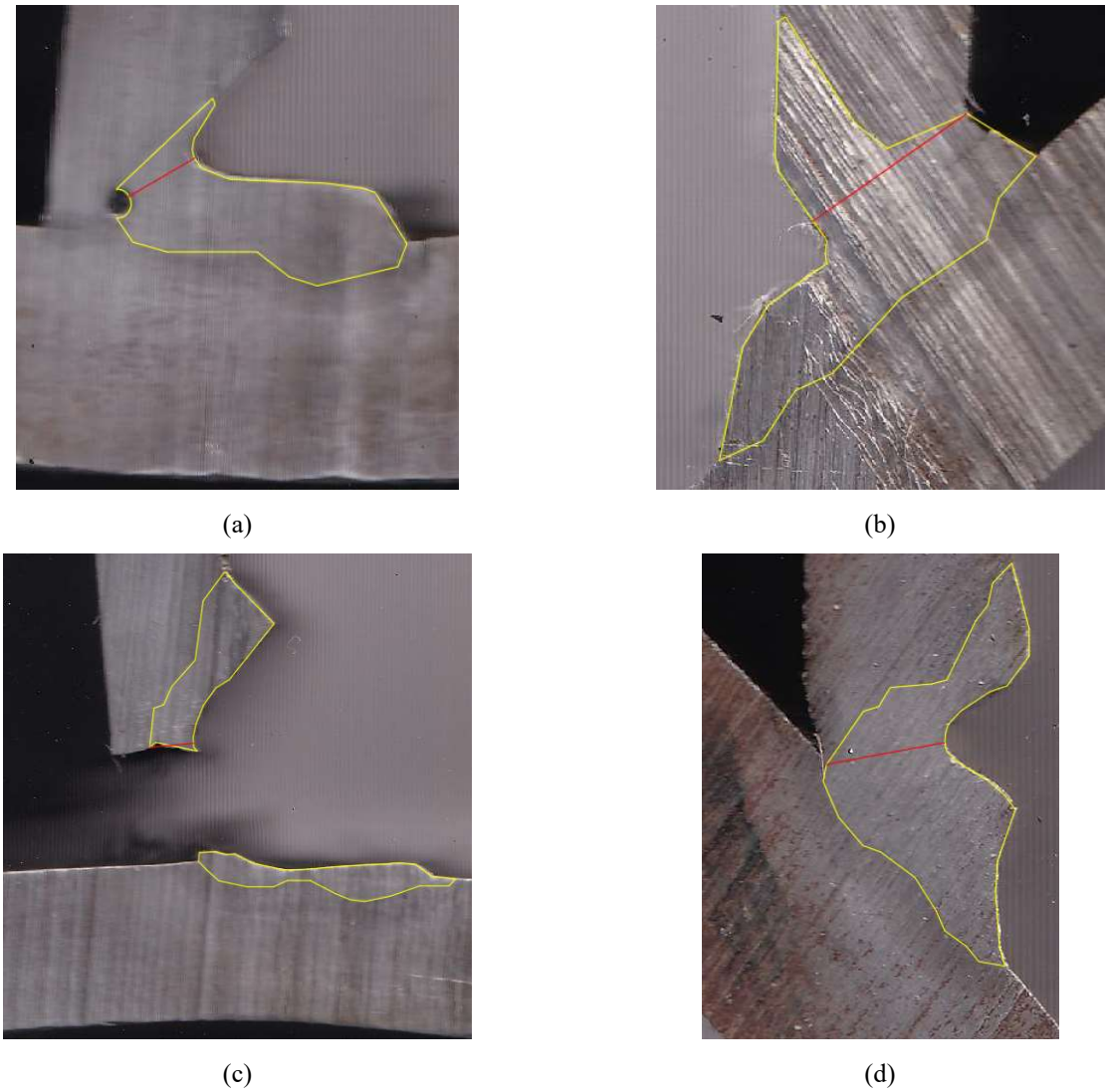

(a) (b) (c) (d)

Figure E-13 Macroetch examination for T406-324-0.7P (a) 0° (compression side), (b) 90° (saddle side), (c) 180° (tension side) and (d) 270° (saddle side)

Appendix F: MOMENT-STRAIN PLOTS

Appendix F provides the supplementary figures for moment-strain relationship for each test specimen

F.1. PJP WELD RHS T-CONNECTION FABRICATION DRAWINGS

Figure F-1 to F-12 shows the relationship between moment and strain where the number of strain is shown in Appendix C, Figure C-2.

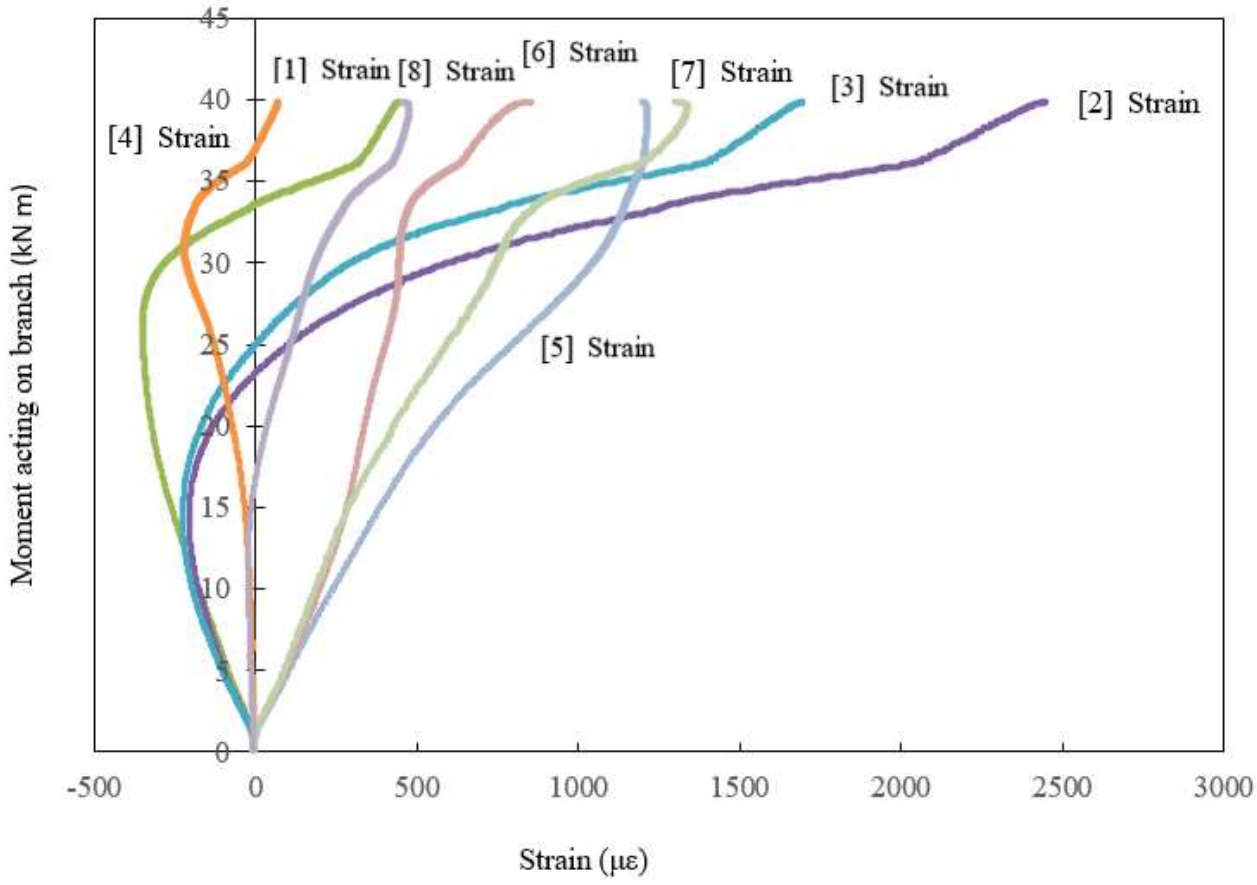

Figure F-1 Moment-Strain plot of T273-127-1P

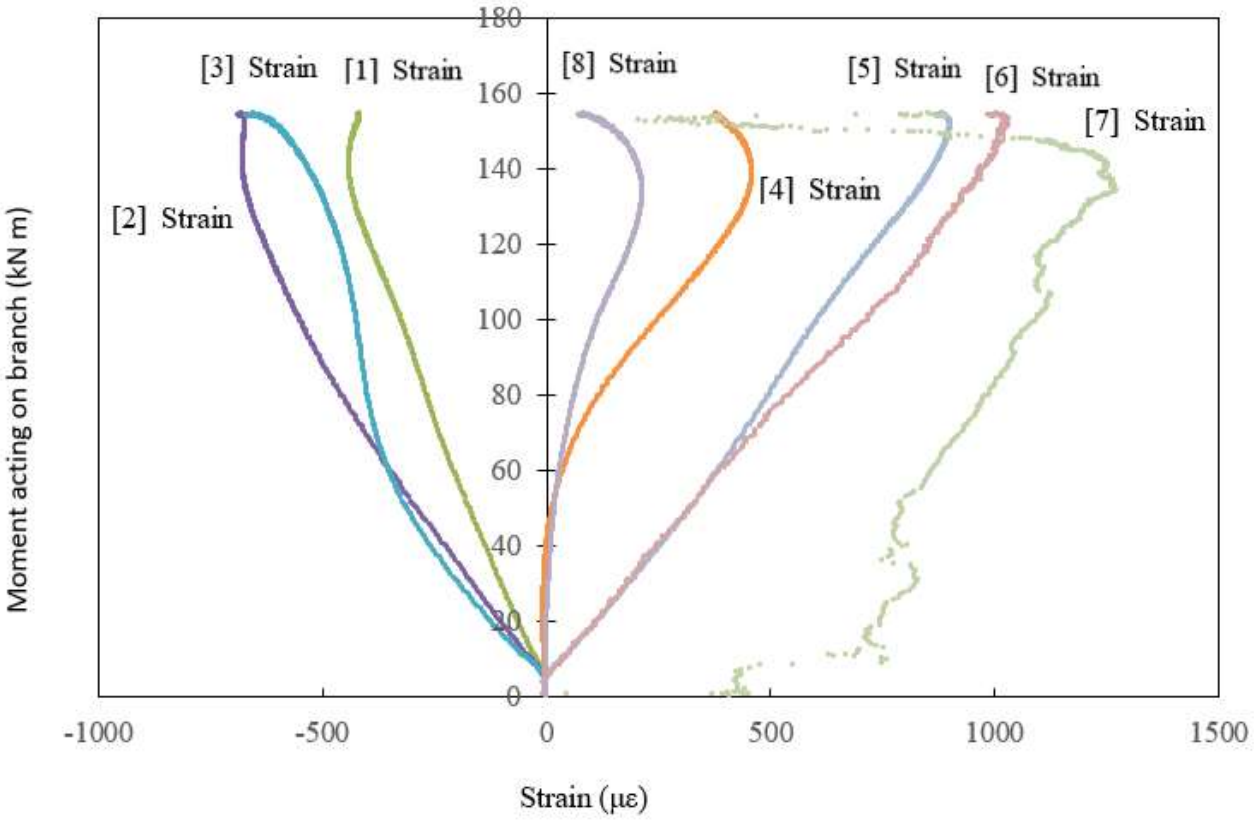

Figure F-2 Moment-Strain plot of T273-127-1

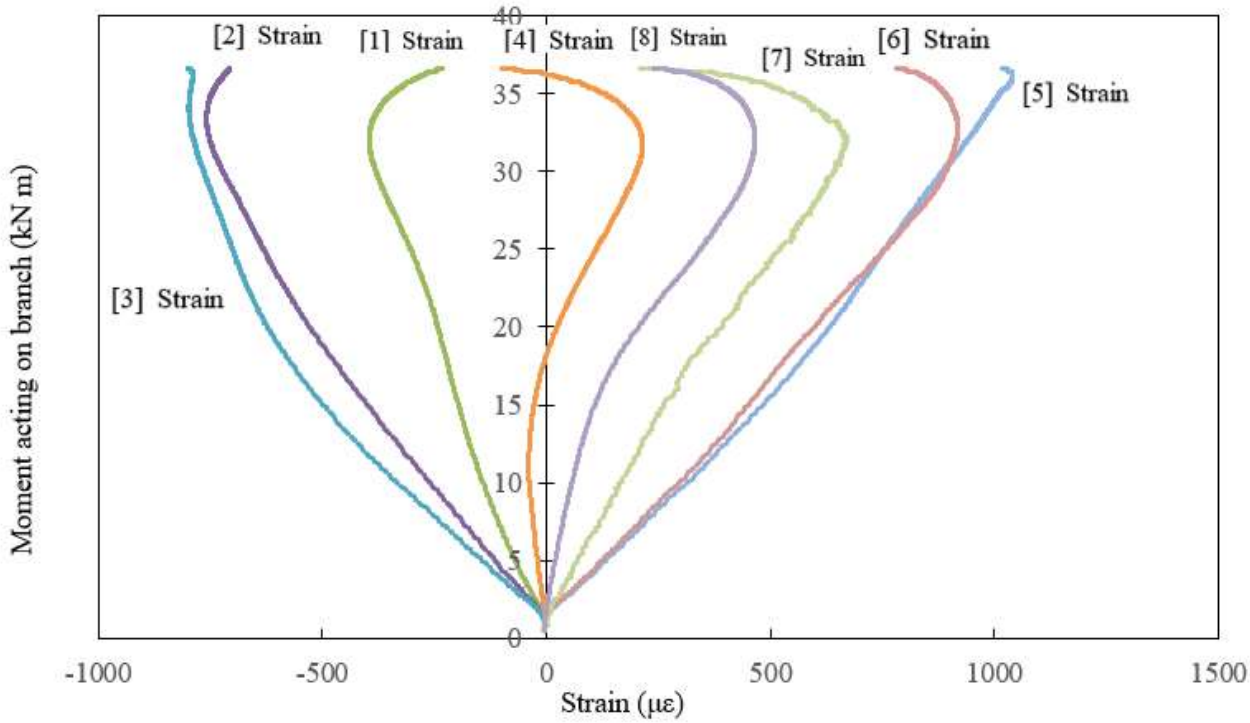

Figure F-3 Moment-Strain plot of T324-127-1

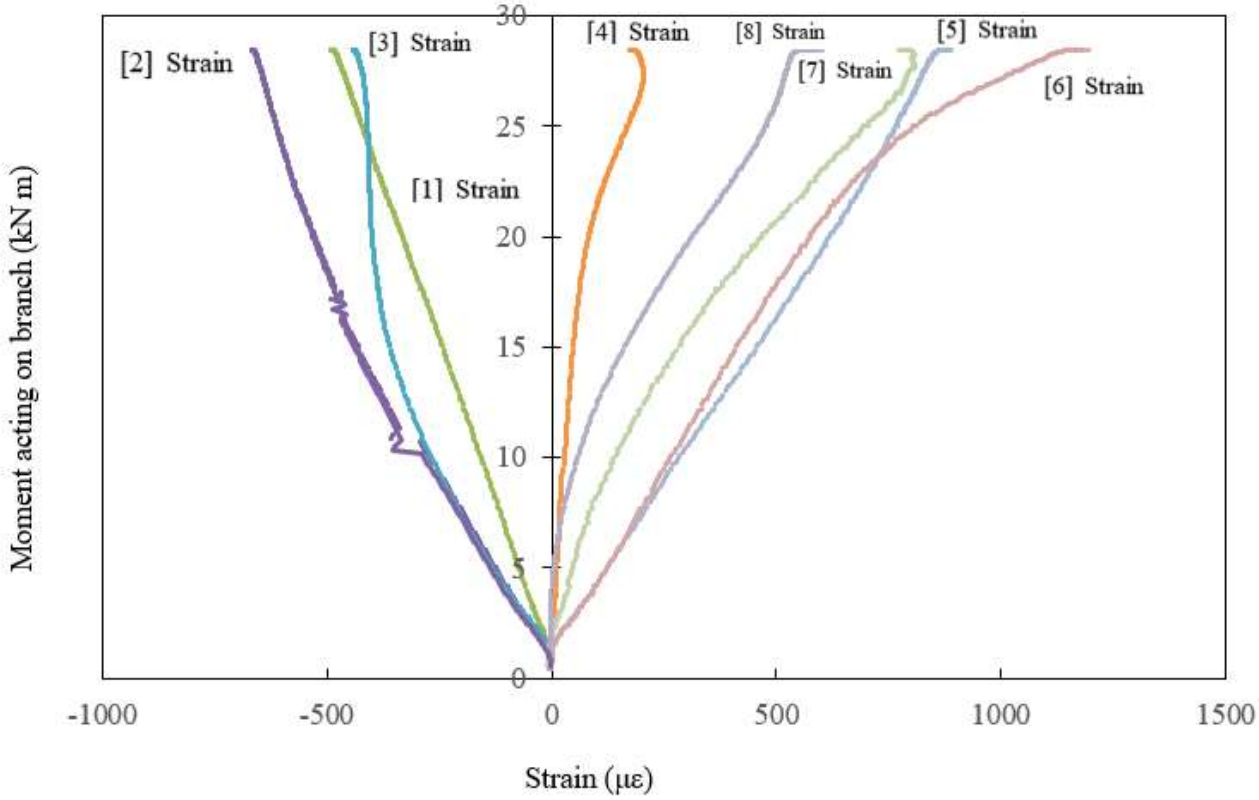

Figure F-4 Moment-Strain plot of T356-127-1

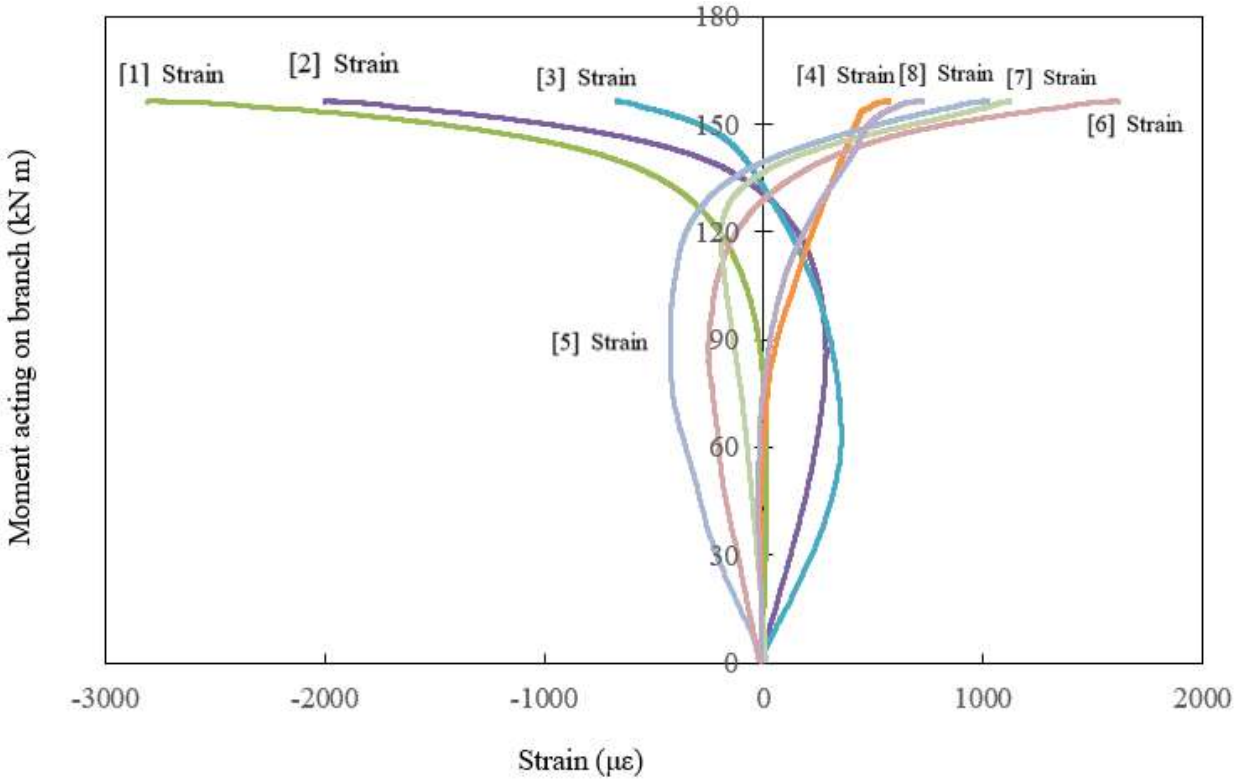

Figure F-5 Moment-Strain plot of T356-273-1P

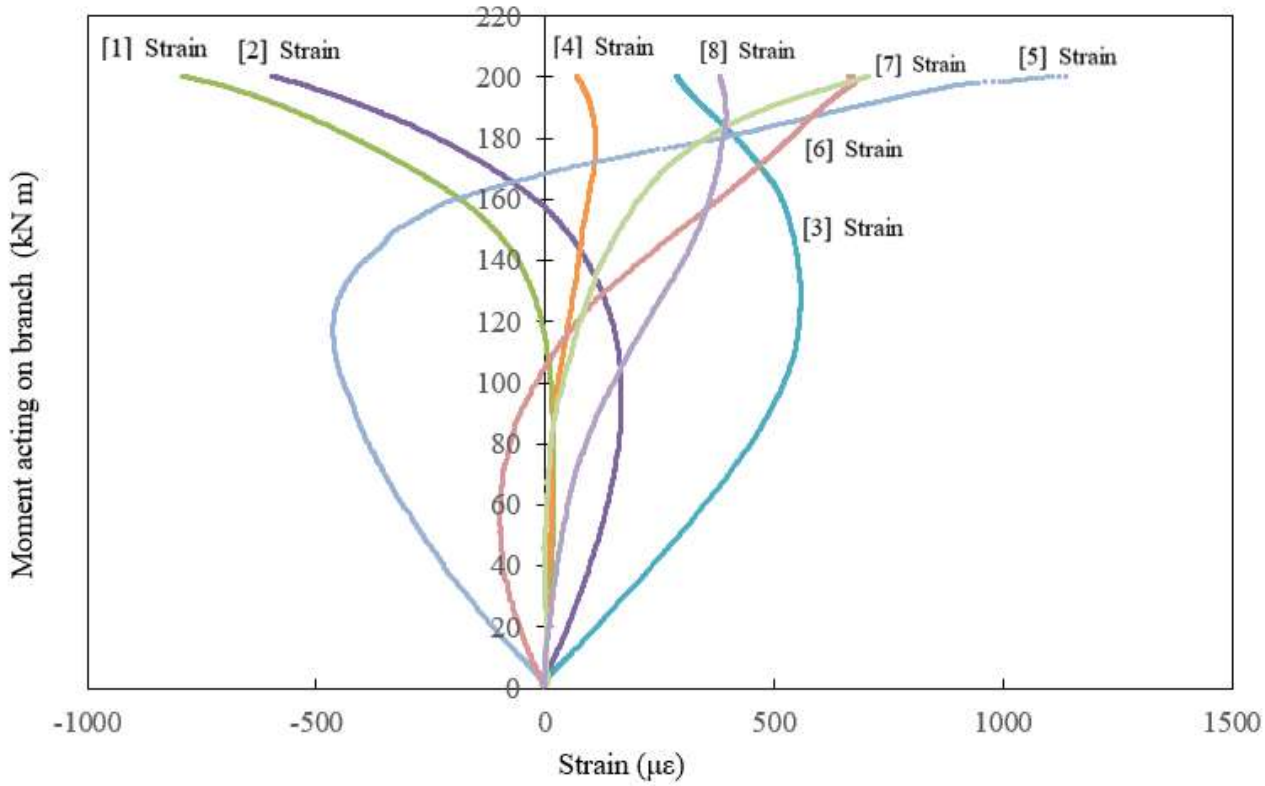

Figure F-6 Moment-Strain plot of T356-324-1P

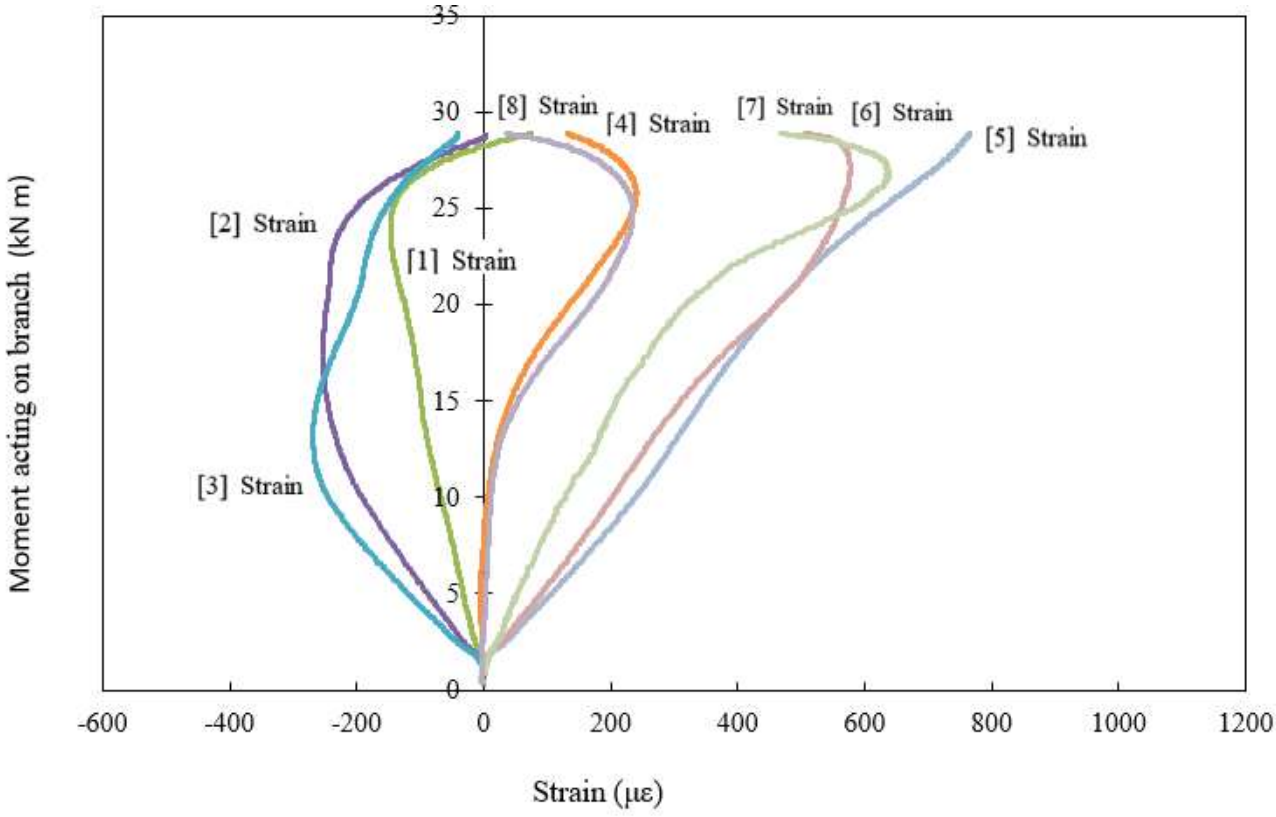

Figure F-7 Moment-Strain plot of T406-127-1

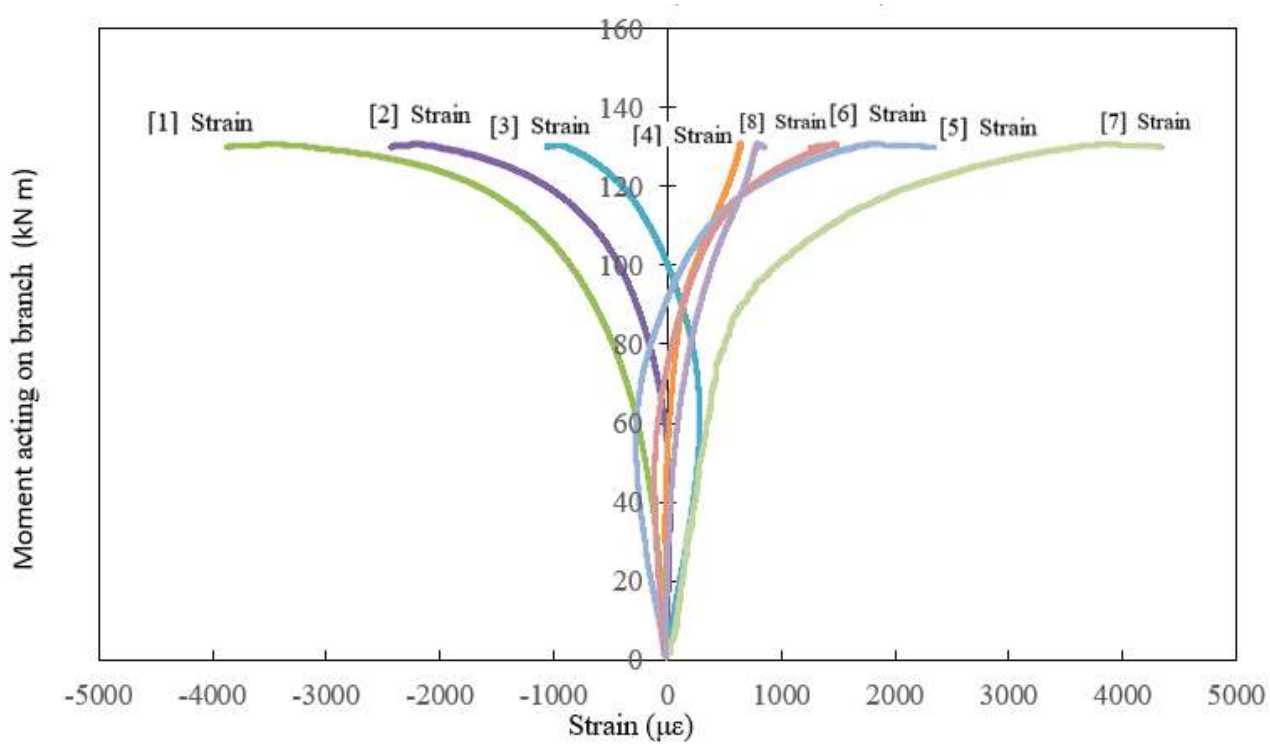

Figure F-8 Moment-Strain plot of T406-273-1P

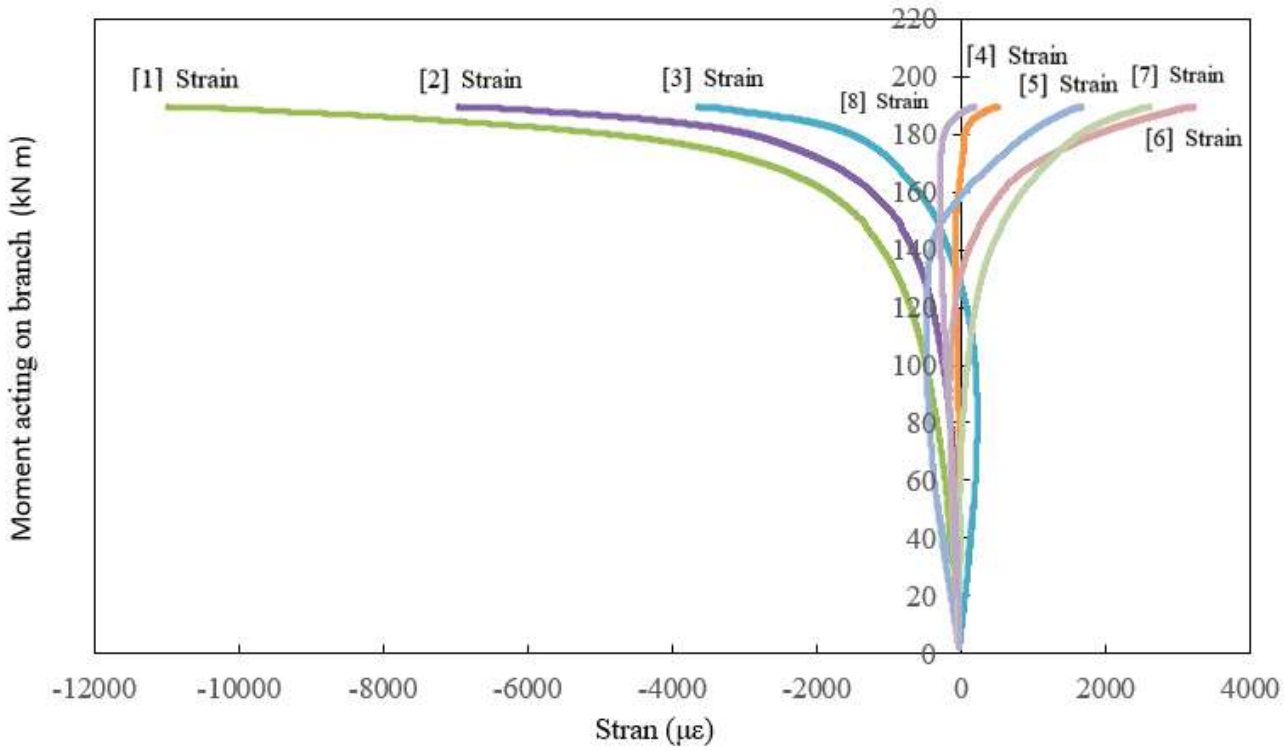

Figure F-9 Moment-Strain plot of T406-324-1P

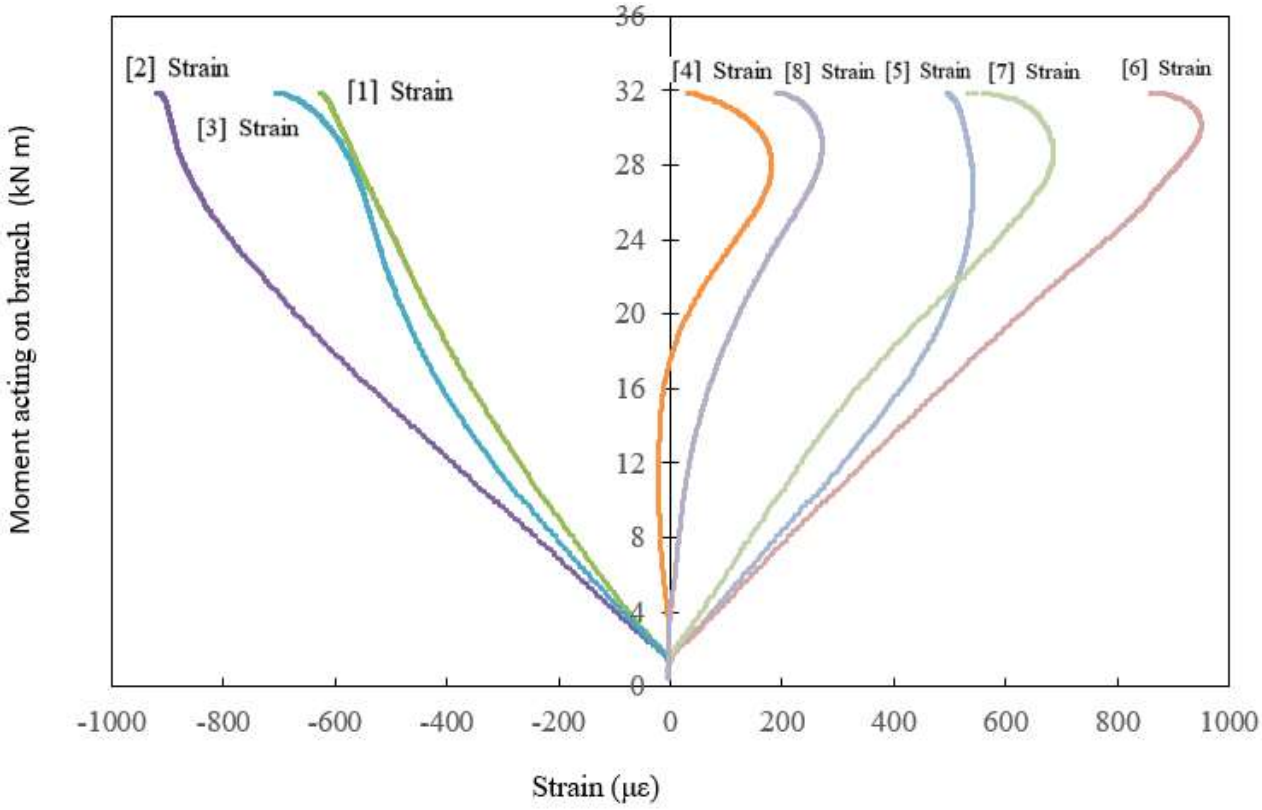

Figure F-10 Moment-Strain plot of T406-127-0.7

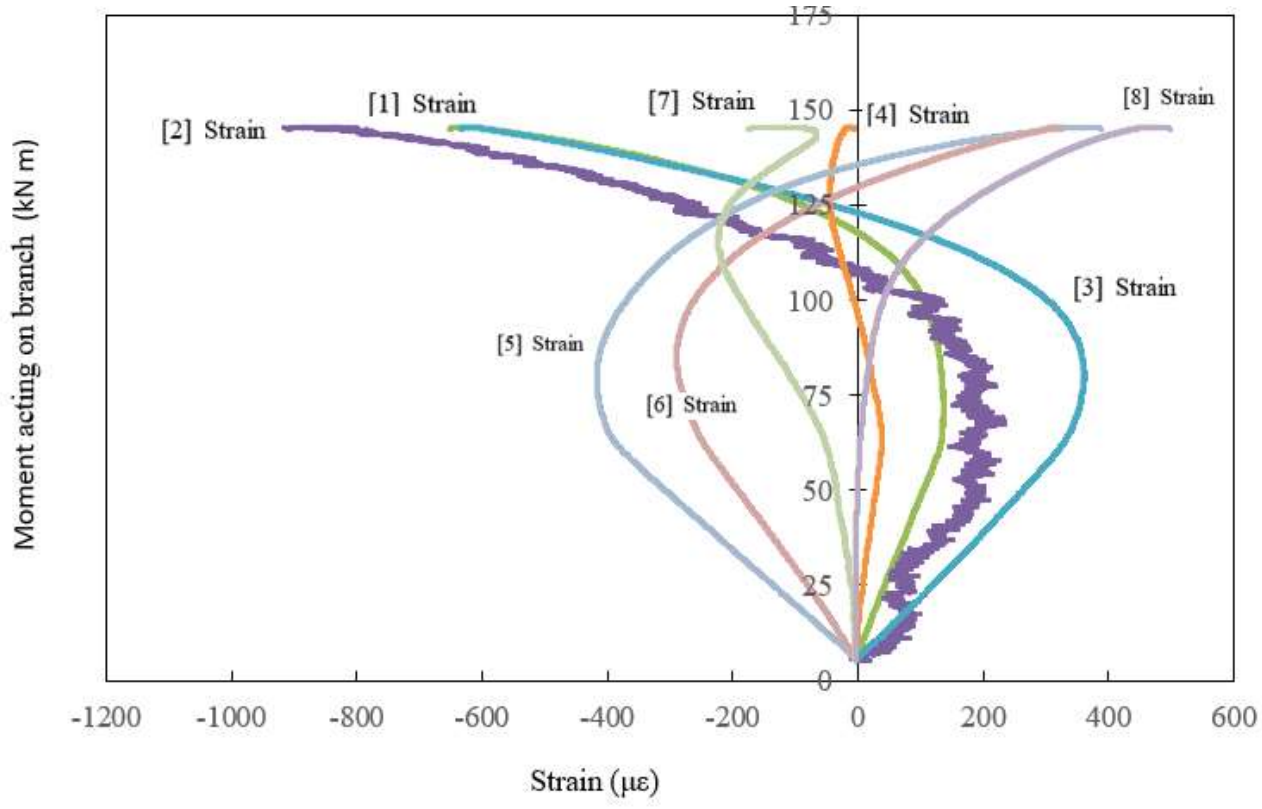

Figure F-11 Moment-Strain plot of T406-273-0.7P

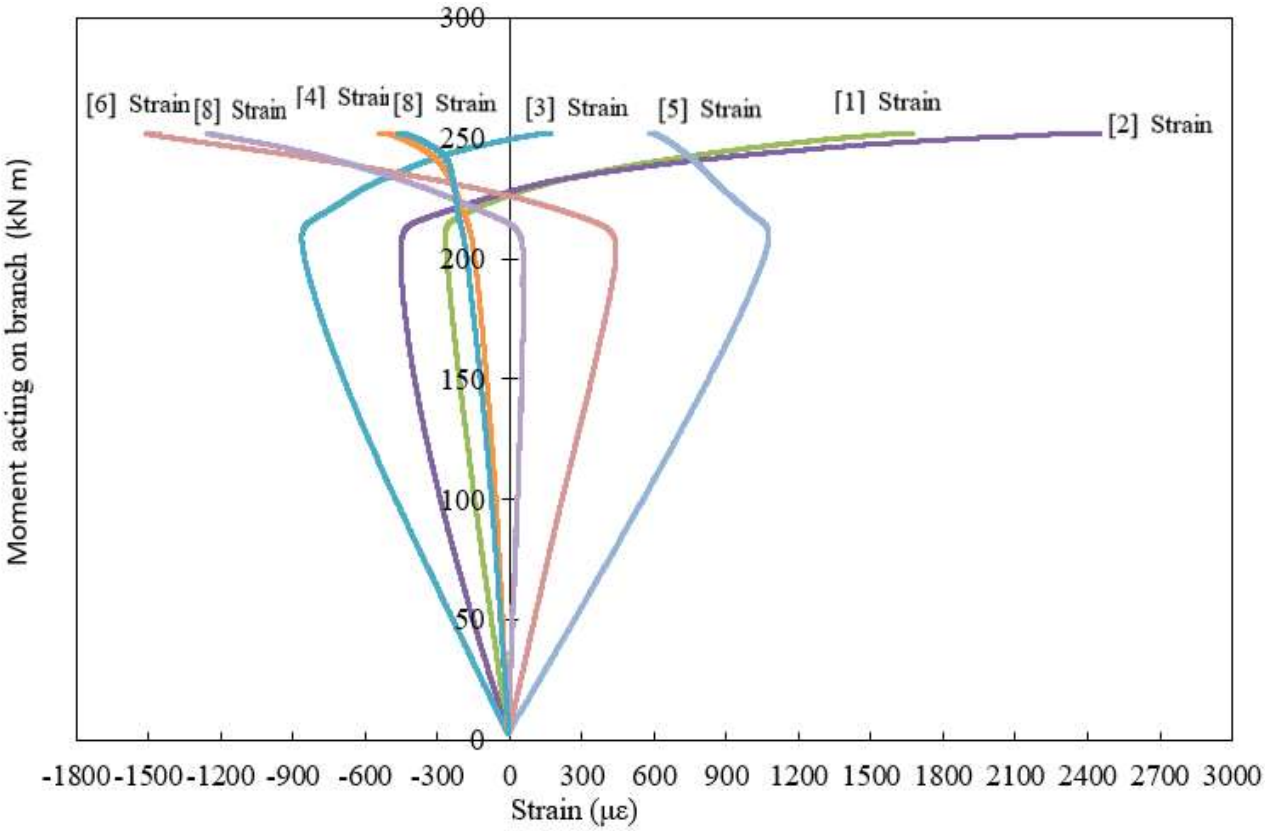

Figure F-12 Moment-Strain plot of T406-324-0.7P

Appendix G: MOMENT-DEFLECTION RELATIONSHIP

Appendix G provides the supplementary data for the branch chord face deformation:

G.1. BRANCH AND CHORD FACE DEFORMATION

Appendix G.1 provides the summary of branch deformation and the chord face deformation in term of percentage diameter deformation:

Test T273-127-1 have an extreme large moment where the calculated deformation is considered as a wasted data.

Table G-1 Deformation table

Test	Moment	String pot	Branch deformation	Deformation by chord	Chord face deformation
	kNm	mm	mm	mm	%
T273-127-1P	39.77	168.99	18.04	150.94	3.08
T273-127-1	154.12	76.15	69.79	6.36	0.13
T324-127-1	36.47	76.04	14.57	61.47	1.13
T356-127-1	28.33	42.14	10.67	31.47	0.54
T356-273-1P	155.88	91.76	4.64	87.13	3.19
T356-324-1P	199.83	38.69	3.47	35.23	1.55
T406-127-1	28.75	74.18	10.34	63.84	0.98
T406-273-1P	129.97	81.61	3.65	77.97	2.57
T406-324-1P	188.97	84.47	3.09	81.37	3.21
T406-127-0.7	31.59	43.33	11.47	31.86	0.49
T406-273-0.7P	144.97	33.61	3.99	29.62	0.99
T406-324-0.7P	251.60	71.08	4.12	66.97	2.64

Appendix H: RELIABILITY ANALYSIS

Appendix H provides the supplementary data for the branch chord face deformation:

H.1. PREDICTION BASED ON DIFFERENT MEASUREMENT TYPE

Following table shows the predicted and actual strength for each specimen based on different calculation method and measurement type.

Table H-1 Predicted strength associate with EESM and actual strength (according to AISC standard)

Test Designation	Actual Strength	Predictions Associate with (kNm)		
	(kNm)	MDM	FLM	LSM
T273-127-1P	39.77	9.07	9.22	NA
T273-127-1	154.12	10.54	11.43	9.74
T324-127-1	36.47	12.65	12.73	11.98
T356-127-1	28.33	9.81	9.85	13.55
T356-273-1P	155.88	28.78	NA	NA
T356-324-1P	199.83	37.38	37.79	NA
T406-127-1	28.74	11.47	11.88	11.66
T406-273-1P	129.97	23.57	23.56	NA
T406-324-1P	188.97	27.79	28.02	NA
T406-127-0.7	31.59	15.13	13.44	14.99
T406-273-0.7P	144.97	34.65	34.65	NA
T406-324-0.7P	251.60	47.26	47.21	NA

Note: NA means there are no available data, or the measurement type does not apply for the connection.

Table H-2 Predicted strength associate with EPSM and actual strength (according to AISC standard)

Test Designation	Actual Strength	Predictions Associate with (kNm)		
	(kNm)	MDM	FLM	LSM
T273-127-1P	39.77	17.21	17.53	NA
T273-127-1	154.12	14.55	15.71	13.51
T324-127-1	36.47	17.29	17.39	16.44
T356-127-1	28.33	13.60	13.66	18.44
T356-273-1P	155.88	48.74	NA	NA
T356-324-1P	199.83	62.68	63.40	NA
T406-127-1	28.74	15.76	16.28	16.00
T406-273-1P	129.97	39.36	39.35	NA
T406-324-1P	188.97	45.53	45.92	NA
T406-127-0.7	31.59	20.52	18.35	20.34
T406-273-0.7P	144.97	58.02	58.02	NA
T406-324-0.7P	251.60	78.08	78.01	NA

Note: NA means there are no available data, or the measurement type does not apply for the connection.

Table H-3 Predicted strength associate with FEESM and actual strength (according to AISC standard)

Test Designation	Actual Strength	Predictions Associate with (kNm)		
	(kNm)	MDM	FLM	LSM
T273-127-1P	39.77	25.44	25.86	NA
T273-127-1	154.12	18.14	19.61	16.82
T324-127-1	36.47	20.62	20.74	19.58
T356-127-1	28.33	16.14	16.20	22.02
T356-273-1P	155.88	158.12	NA	NA
T356-324-1P	199.83	204.19	206.42	NA
T406-127-1	28.74	19.59	20.25	19.89
T406-273-1P	129.97	127.08	127.04	NA
T406-324-1P	188.97	169.27	170.68	NA
T406-127-0.7	31.59	19.59	17.47	19.41
T406-273-0.7P	144.97	141.51	141.51	NA
T406-324-0.7P	251.60	217.88	217.67	NA

Note: NA means there are no available data, or the measurement type does not apply for the connection.4

Table H-4 Predicted strength associate with FEPSM and actual strength (according to AISC standard)

Test Designation	Actual Strength (kNm)	Predictions Associate with (kNm)		
		MDM	FLM	LSM
T273-127-1P	39.77	33.63	34.21	NA
T273-127-1	154.12	23.55	25.51	21.80
T324-127-1	36.47	26.84	27.00	25.46
T356-127-1	28.33	20.91	20.99	28.70
T356-273-1P	155.88	205.54	NA	NA
T356-324-1P	199.83	264.15	267.08	NA
T406-127-1	28.74	25.47	26.35	25.88
T406-273-1P	129.97	164.49	164.43	NA
T406-324-1P	188.97	218.31	220.15	NA
T406-127-0.7	31.59	25.47	22.67	25.23
T406-273-0.7P	144.97	183.52	183.52	NA
T406-324-0.7P	251.60	282.10	281.83	NA

Note: NA means there are no available data, or the measurement type does not apply for the connection.

Table H-5 Predicted strength associate with EPSM and actual strength (according to CSA standard)

Test Designation	Actual Strength (kNm)	Predictions Associate with (kNm)		
		MDM	FLM	LSM
T273-127-1P	39.77	10.08	10.25	NA
T273-127-1	154.12	11.77	12.77	10.88
T324-127-1	36.47	14.13	14.21	13.38
T356-127-1	28.33	10.95	11.00	15.13
T356-273-1P	155.88	31.97	NA	NA
T356-324-1P	199.83	41.53	41.99	NA
T406-127-1	28.74	12.81	13.26	13.02
T406-273-1P	129.97	26.19	26.18	NA
T406-324-1P	188.97	30.88	31.13	NA
T406-127-0.7	31.59	16.90	15.01	16.74
T406-273-0.7P	144.97	38.50	35.50	NA
T406-324-0.7P	251.60	52.51	52.46	NA

Note: NA means there are no available data, or the measurement type does not apply for the connection.

Table H-6 Predicted strength associate with EPSM and actual strength (according to CSA standard)

Test Designation	Actual Strength	Predictions Associate with (kNm)		
	(kNm)	MDM	FLM	LSM
T273-127-1P	39.77	19.12	19.48	NA
T273-127-1	154.12	16.25	17.54	15.08
T324-127-1	36.47	19.31	19.42	18.35
T356-127-1	28.33	15.19	15.25	20.59
T356-273-1P	155.88	54.15	NA	NA
T356-324-1P	199.83	69.65	70.45	NA
T406-127-1	28.74	17.60	18.18	17.86
T406-273-1P	129.97	43.73	43.72	NA
T406-324-1P	188.97	50.59	51.02	NA
T406-127-0.7	31.59	22.92	20.49	22.71
T406-273-0.7P	144.97	64.46	64.46	NA
T406-324-0.7P	251.60	86.76	86.67	NA

Note: NA means there are no available data, or the measurement type does not apply for the connection.

Table H-7 Predicted strength associate with FEESM and actual strength (according to CSA standard)

Test Designation	Actual Strength	Predictions Associate with (kNm)		
	(kNm)	MDM	FLM	LSM
T273-127-1P	39.77	18.85	19.16	NA
T273-127-1	154.12	20.26	21.90	18.78
T324-127-1	36.47	23.03	23.16	21.86
T356-127-1	28.33	18.02	18.09	24.59
T356-273-1P	155.88	117.13	NA	NA
T356-324-1P	199.83	151.25	152.90	NA
T406-127-1	28.74	21.88	22.62	22.21
T406-273-1P	129.97	94.13	94.10	NA
T406-324-1P	188.97	125.38	126.43	NA
T406-127-0.7	31.59	21.88	19.51	21.67
T406-273-0.7P	144.97	104.82	104.82	NA
T406-324-0.7P	251.60	161.40	161.24	NA

Note: NA means there are no available data, or the measurement type does not apply for the connection.

Table H-8 Predicted strength associate with FEPSM and actual strength (according to CSA standard)

Test Designation	Actual Strength (kNm)	Predictions Associate with (kNm)		
		MDM	FLM	LSM
T273-127-1P	39.77	24.91	38.01	NA
T273-127-1	154.12	26.30	28.48	24.35
T324-127-1	36.47	29.98	30.15	28.43
T356-127-1	28.33	23.35	23.44	32.05
T356-273-1P	155.88	152.25	NA	NA
T356-324-1P	199.83	195.66	296.75	NA
T406-127-1	28.74	28.44	29.43	28.89
T406-273-1P	129.97	121.84	182.70	NA
T406-324-1P	188.97	161.71	244.61	NA
T406-127-0.7	31.59	28.44	25.32	28.18
T406-273-0.7P	144.97	135.94	203.91	NA
T406-324-0.7P	251.60	208.96	208.76	NA

Note: NA means there are no available data, or the measurement type does not apply for the connection.

Following table shows the predicted and actual strength for each specimen based on different calculation method and measurement type associate with rational analysis:

Table H-9 Predicted strength associate with EESM and actual strength of each test specimen based on rational analysis (AISC)

Test Designation	Actual Strength (kNm)	Predictions Associate with (kNm)		
		MDM	FLM	LSM
T273-127-1P	39.77	19.46	19.78	NA
T273-127-1	154.12	10.80	11.65	9.79
T324-127-1	36.47	12.83	12.90	11.99
T356-127-1	28.33	10.13	10.17	13.60
T356-273-1P	155.88	61.74	NA	NA
T356-324-1P	199.83	80.19	81.06	NA
T406-127-1	28.74	11.68	12.07	11.70
T406-273-1P	129.97	50.56	50.53	NA
T406-324-1P	188.97	59.61	60.11	NA
T406-127-0.7	31.59	15.42	13.80	15.23
T406-273-0.7P	144.97	74.33	74.33	NA
T406-324-0.7P	251.60	101.38	101.28	NA

Note: NA means there are no available data, or the measurement type does not apply for the connection.

Table H-10 Predicted strength associate with EPSM and actual strength of each test specimen based on rational analysis (AISC)

Test Designation	Actual Strength	Predictions Associate with (kNm)		
	(kNm)	MDM	FLM	LSM
T273-127-1P	39.77	36.92	37.61	NA
T273-127-1	154.12	14.91	16.00	13.57
T324-127-1	36.47	17.54	17.63	16.45
T356-127-1	28.33	14.05	14.10	18.51
T356-273-1P	155.88	104.54	NA	NA
T356-324-1P	199.83	134.46	136.00	NA
T406-127-1	28.74	16.05	16.54	16.05
T406-273-1P	129.97	84.43	84.40	NA
T406-324-1P	188.97	97.66	98.51	NA
T406-127-0.7	31.59	20.91	18.85	20.66
T406-273-0.7P	144.97	124.45	124.45	NA
T406-324-0.7P	251.60	167.50	167.33	NA

Note: NA means there are no available data, or the measurement type does not apply for the connection.

Table H-11 Predicted strength associate with EESM and actual strength of each test specimen based on rational analysis (CSA)

Test Designation	Actual Strength	Predictions Associate with (kNm)		
	(kNm)	MDM	FLM	LSM
T273-127-1P	39.77	21.73	22.09	NA
T273-127-1	154.12	10.80	11.65	9.79
T324-127-1	36.47	12.83	12.90	12.00
T356-127-1	28.33	10.13	10.17	13.60
T356-273-1P	155.88	68.94	NA	NA
T356-324-1P	199.83	89.54	90.52	NA
T406-127-1	28.74	11.68	12.07	11.70
T406-273-1P	129.97	56.45	56.43	NA
T406-324-1P	188.97	66.56	67.12	NA
T406-127-0.7	31.59	15.42	13.80	15.23
T406-273-0.7P	144.97	83.00	83.00	NA
T406-324-0.7P	251.60	113.21	113.10	NA

Note: NA means there are no available data, or the measurement type does not apply for the connection.

Table H-12 Predicted strength associate with EPSM and actual strength of each test specimen based on rational analysis (CSA)

Test Designation	Actual Strength	Predictions Associate with (kNm)		
	(kNm)	MDM	FLM	LSM
T273-127-1P	39.77	41.23	42.00	NA
T273-127-1	154.12	14.91	16.00	13.57
T324-127-1	36.47	17.54	17.63	16.44
T356-127-1	28.33	14.05	14.10	18.51
T356-273-1P	155.88	116.74	NA	NA
T356-324-1P	199.83	150.15	151.87	NA
T406-127-1	28.74	16.05	16.54	16.05
T406-273-1P	129.97	94.28	94.25	NA
T406-324-1P	188.97	109.05	110.00	NA
T406-127-0.7	31.59	20.91	18.85	20.66
T406-273-0.7P	144.97	138.97	138.97	NA
T406-324-0.7P	251.60	187.04	186.85	NA

Note: NA means there are no available data, or the measurement type does not apply for the connection.

Following table shows the mean and COV for each specimen based on different calculation method and measurement type:

Table H-13 Mean and COV calculate based on effective section modulus and AISC standard

Measurement type	EESM		EPSM	
	Mean	COV	Mean	COV
Minimum distance	4.22	0.375	2.63	0.312
Fracture length	4.08	0.385	2.56	0.317
Leg size	2.43	0.184	1.78	0.179

Table H-14 Mean and COV calculate based on effective section modulus and CSA standard

Measurement type	EESM		EPSM	
	Mean	COV	Mean	COV
Minimum distance	3.78	0.375	2.35	0.312
Fracture length	3.65	0.385	2.30	0.317
Leg size	2.17	0.184	1.59	0.179

Table H-15 Mean and COV calculate based on fully effective section modulus and CSA standard

Measurement type	FEESM		FEPSM	
	Mean	COV	Mean	COV
Minimum distance	1.49	0.159	1.15	0.152
Fracture length	1.52	0.1.60	1.17	0.152
Leg size	1.39	0.159	1.07	0.160

Following table shows the mean and COV for each specimen based on different calculation method and measurement type associate with the rational analysis:

Table H-16 Mean and COV calculate based on effective section modulus and AISC standard associate with rational method

Measurement type	EESM		EPSM	
	Mean	COV	Mean	COV
Minimum distance	2.49	0.157	1.61	0.212
Fracture length	2.49	0.156	1.63	0.219
Leg size	2.41	0.188	1.77	0.184

Table H-17 Mean and COV calculate based on effective section modulus and CSA standard associate with rational method

Measurement type	EESM		EPSM	
	Mean	COV	Mean	COV
Minimum distance	2.34	0.171	1.52	0.251
Fracture length	2.35	0.173	1.54	0.257
Leg size	2.41	0.188	1.77	0.184

H.2. BRANCH AND CHORD FACE DEFORMATION

Appendix G.1 provides the summary of branch deformation and the chord face deformation in term of percentage diameter deformation:

Test T273-127-1 have an extreme large moment where the calculated deformation is considered as a wasted data.

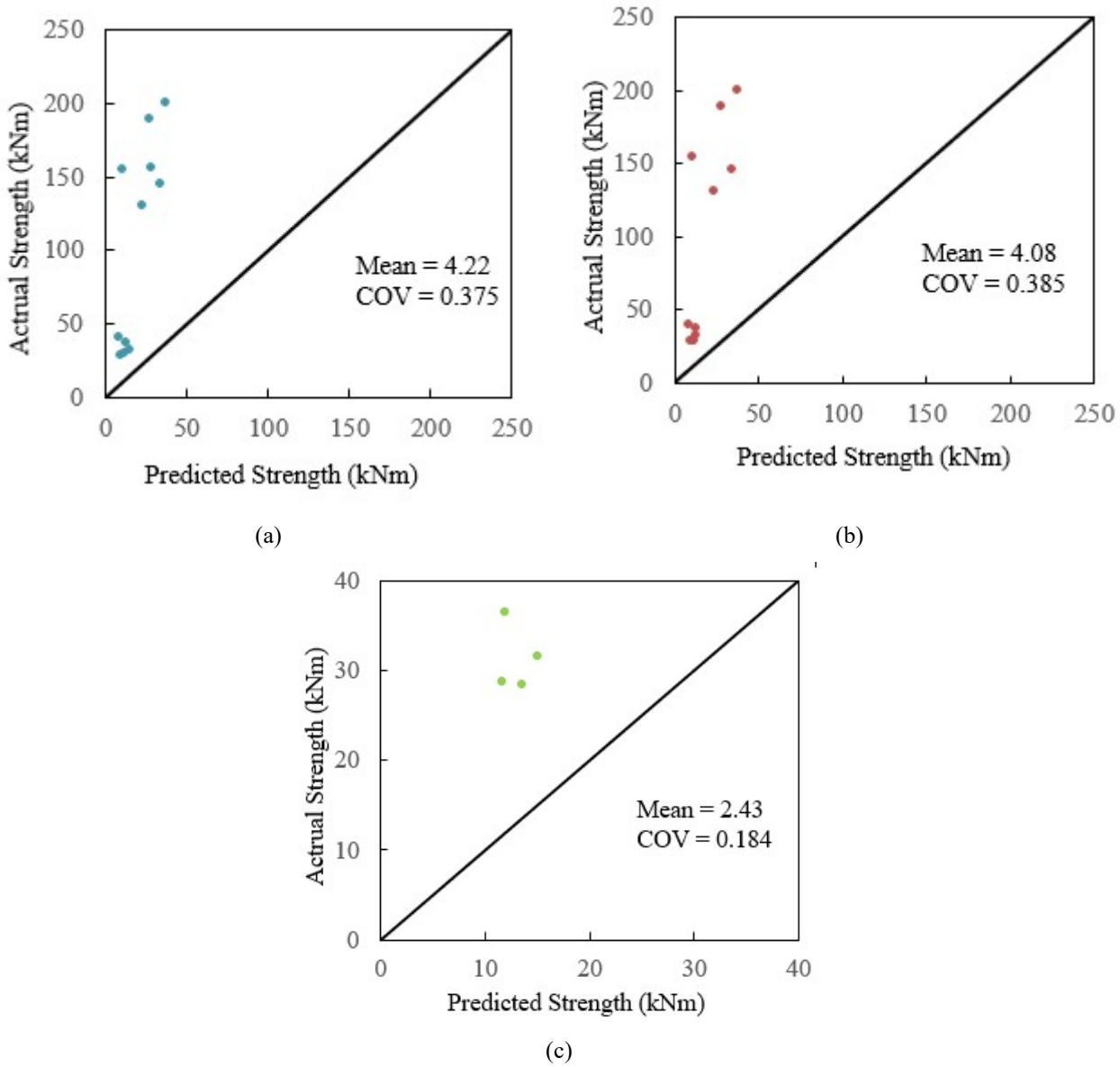

Figure H-1 Correlation plot of actual strength and prediction using EESM with (a) minimum distance (b) fractural length and (c) leg size measurement according to AISC standard

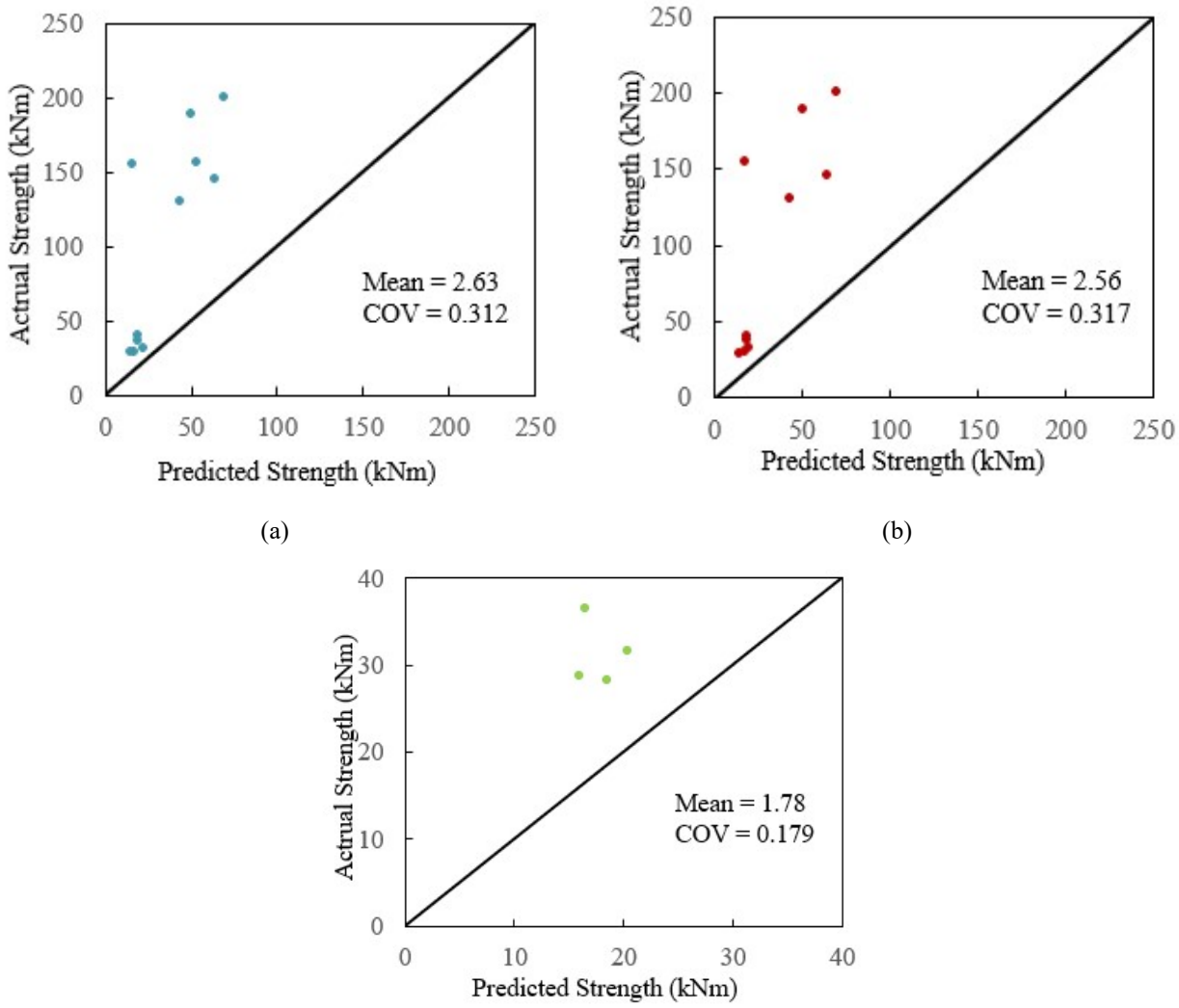

Figure H-2 Correlation plot of actual strength and prediction using EPSM with (a) minimum distance (b) fractural length and (c) leg size measurement according to AISC standard

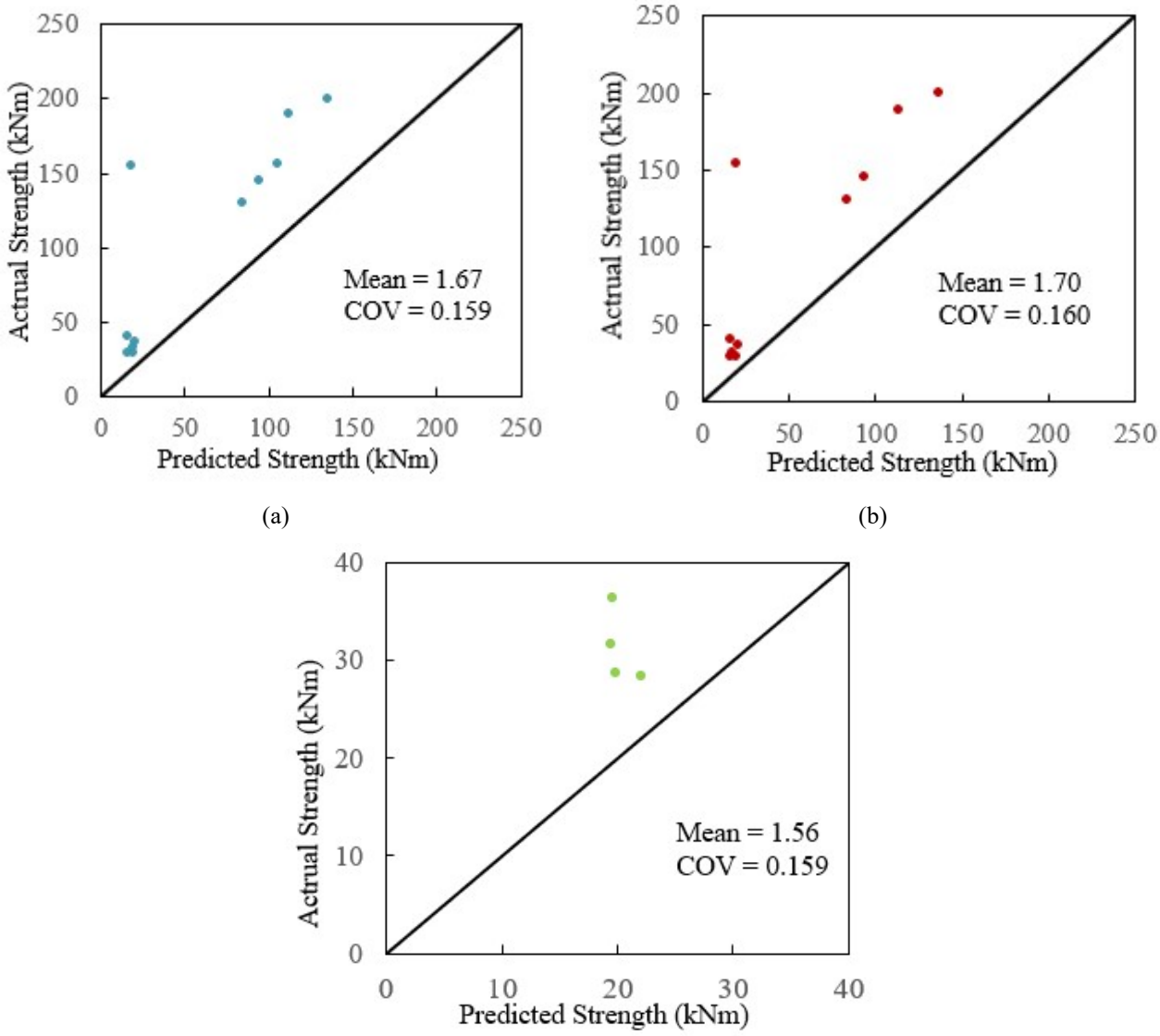

Figure H-3 Correlation plot of actual strength and prediction using FESM with (a) minimum distance (b) fractural length and (c) leg size measurement according to AISC standard

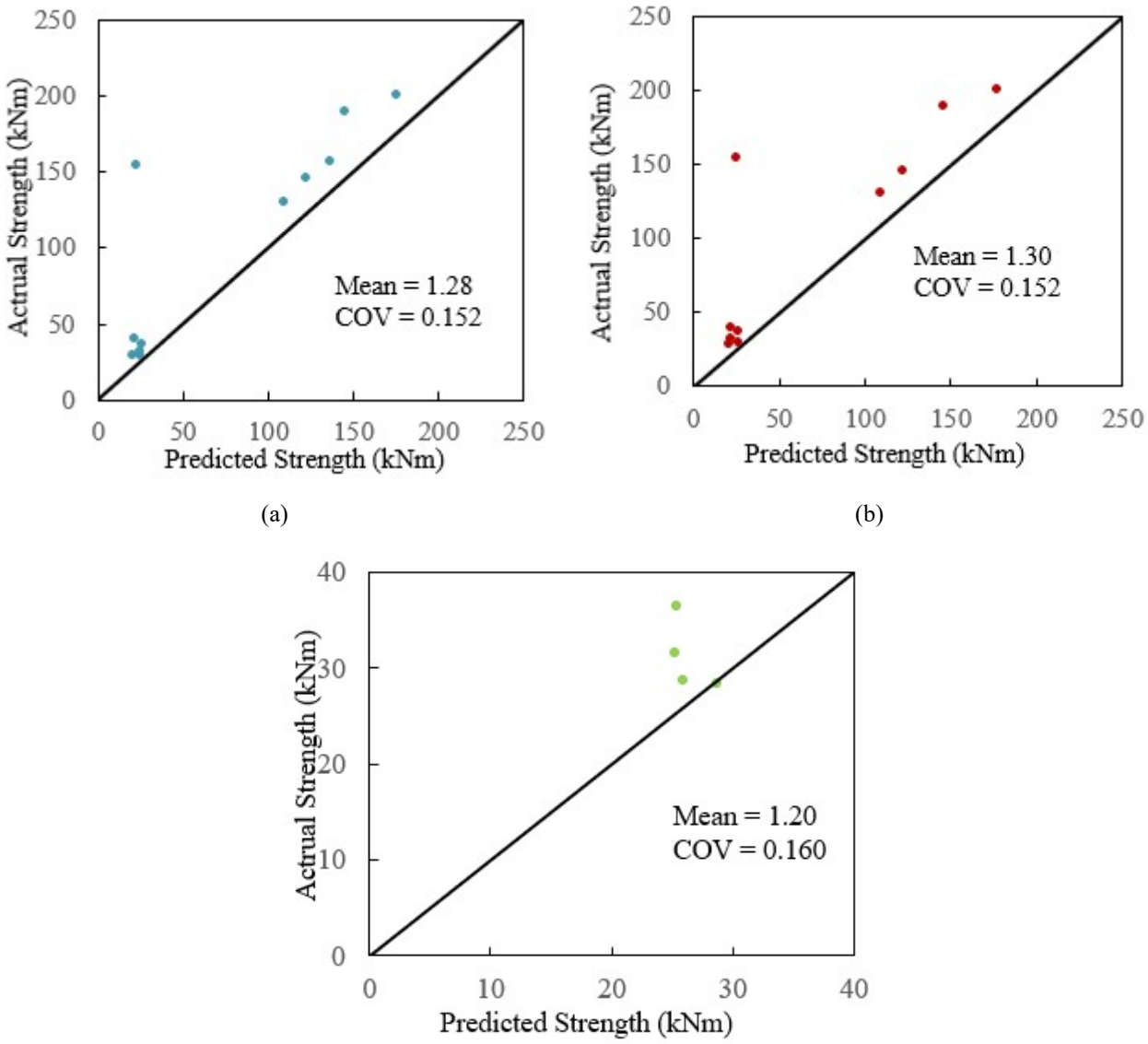

Figure H-4 Correlation plot of actual strength and prediction using FEPSM with (a) minimum distance (b) fractural length and (c) leg size measurement according to AISC standard

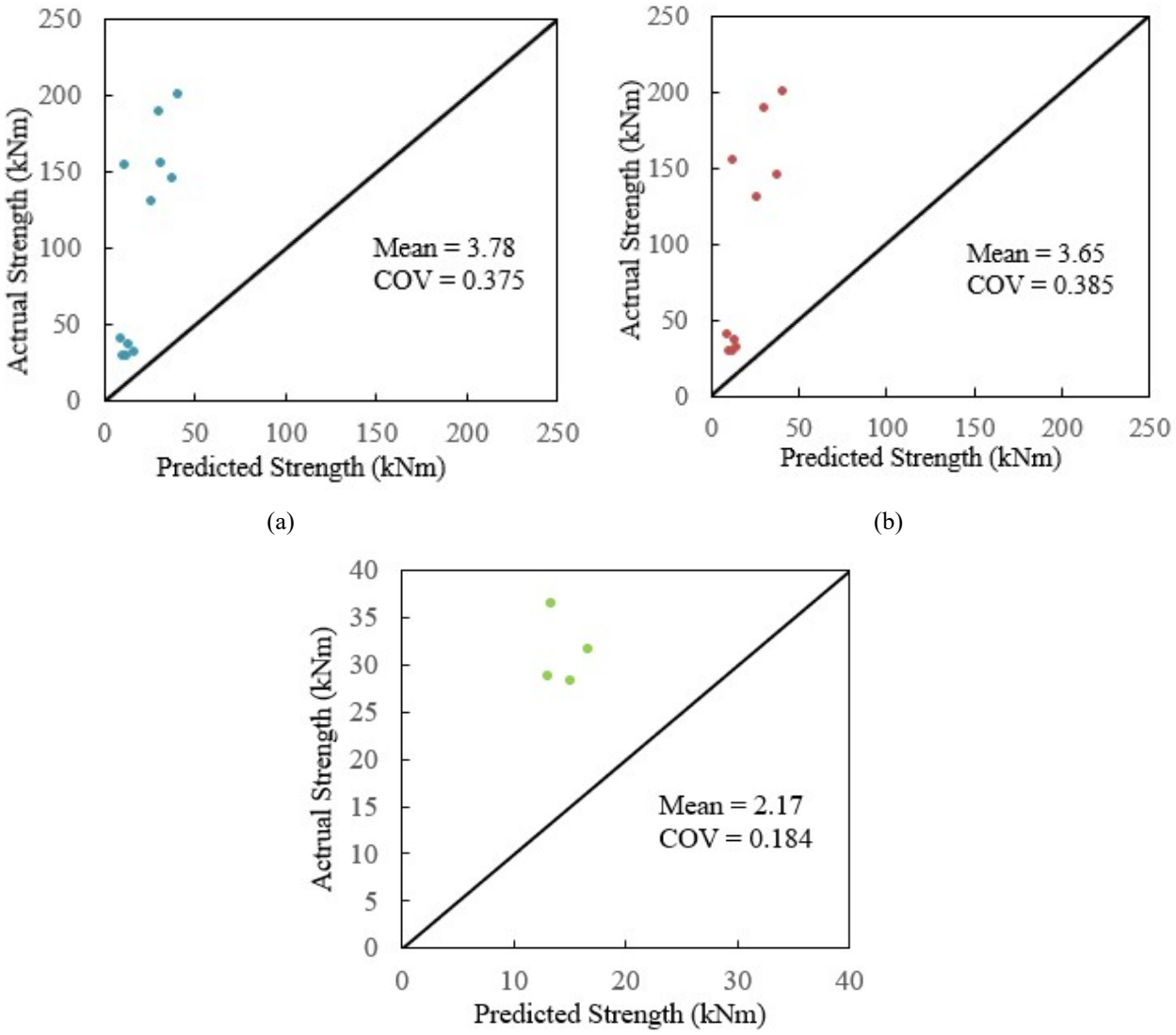

Figure H-5 Correlation plot of actual strength and prediction using EESM with (a) minimum distance (b) fractural length and (c) leg size measurement according to CSA standard

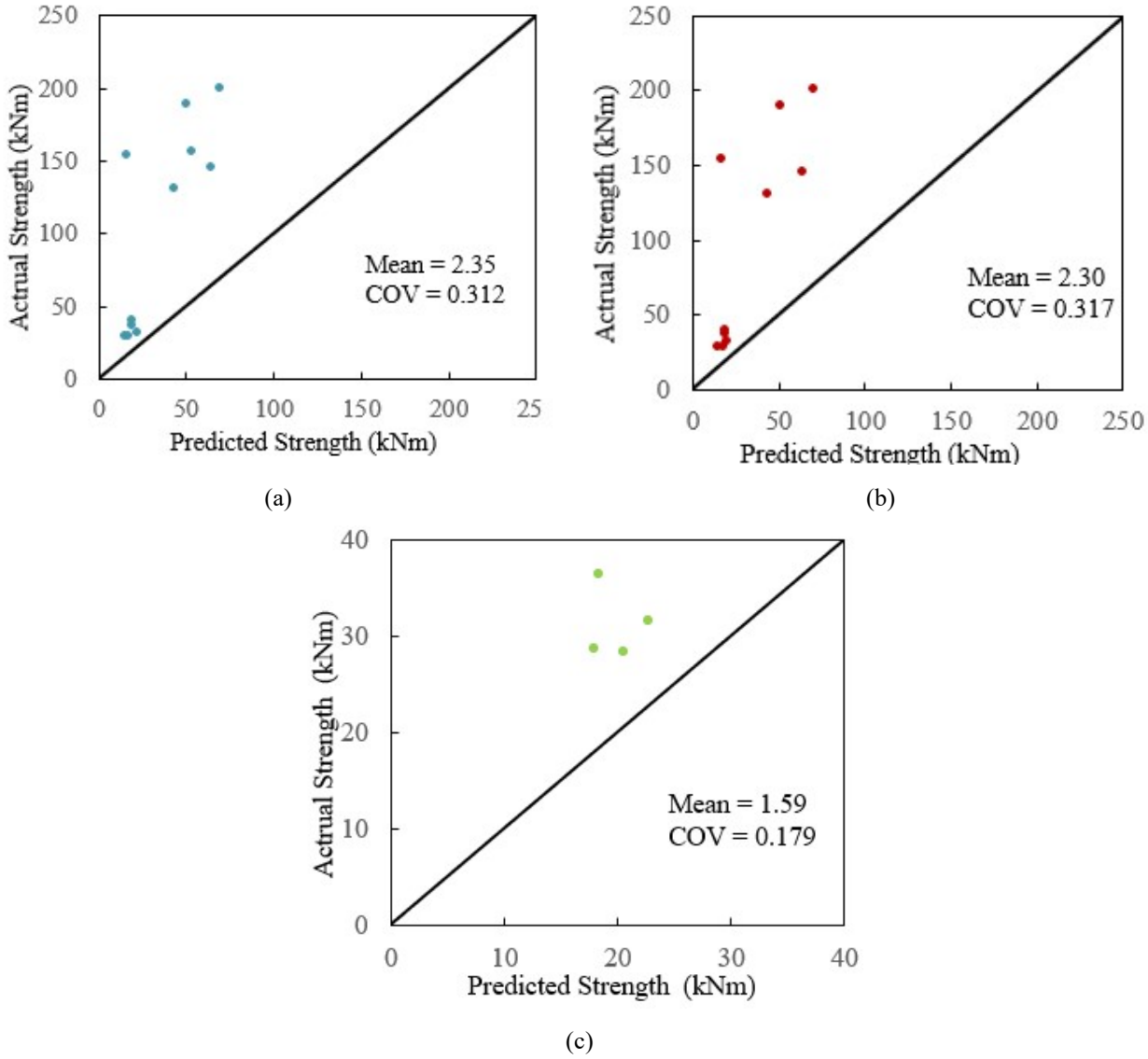

Figure H-6 Correlation plot of actual strength and prediction using EPSM with (a) minimum distance (b) fractural length and (c) leg size measurement according to CSA standard

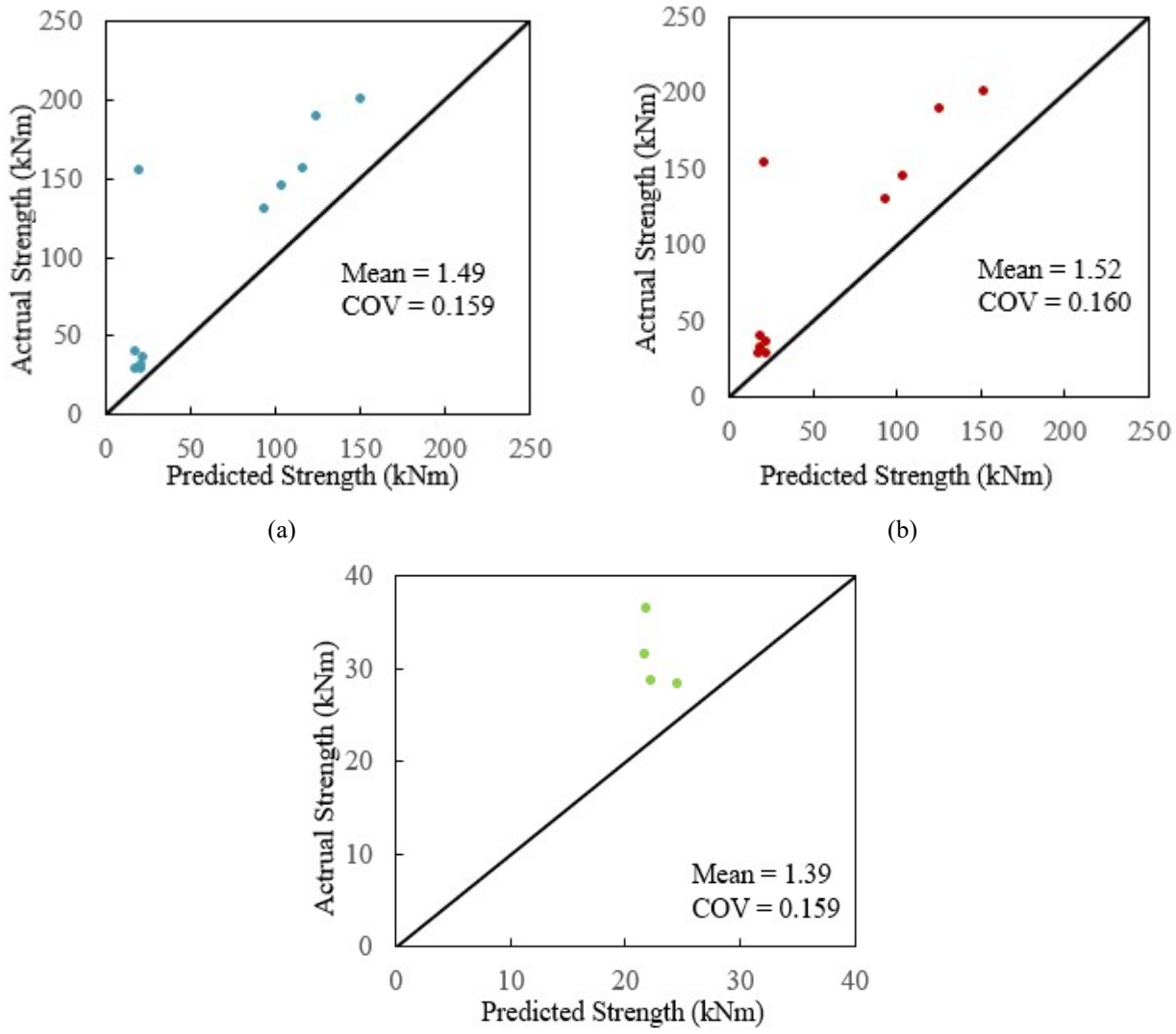

Figure H-7 Correlation plot of actual strength and prediction using FEESM with (a) minimum distance (b) fractural length and (c) leg size measurement according to CSA standard

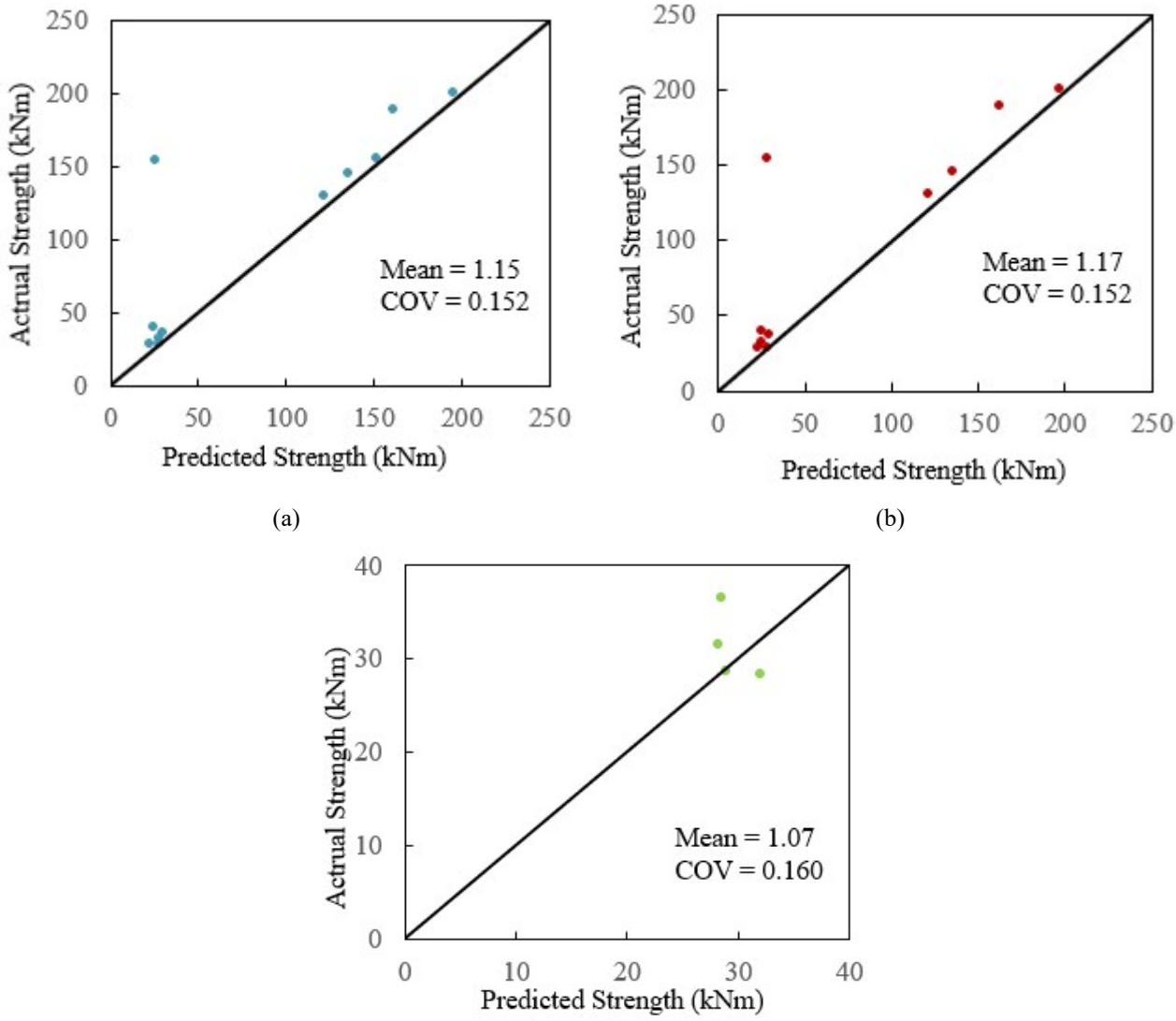

Figure H-8 Correlation plot of actual strength and prediction using FEPSM with (a) minimum distance (b) fractural length and (c) leg size measurement according to CSA standard

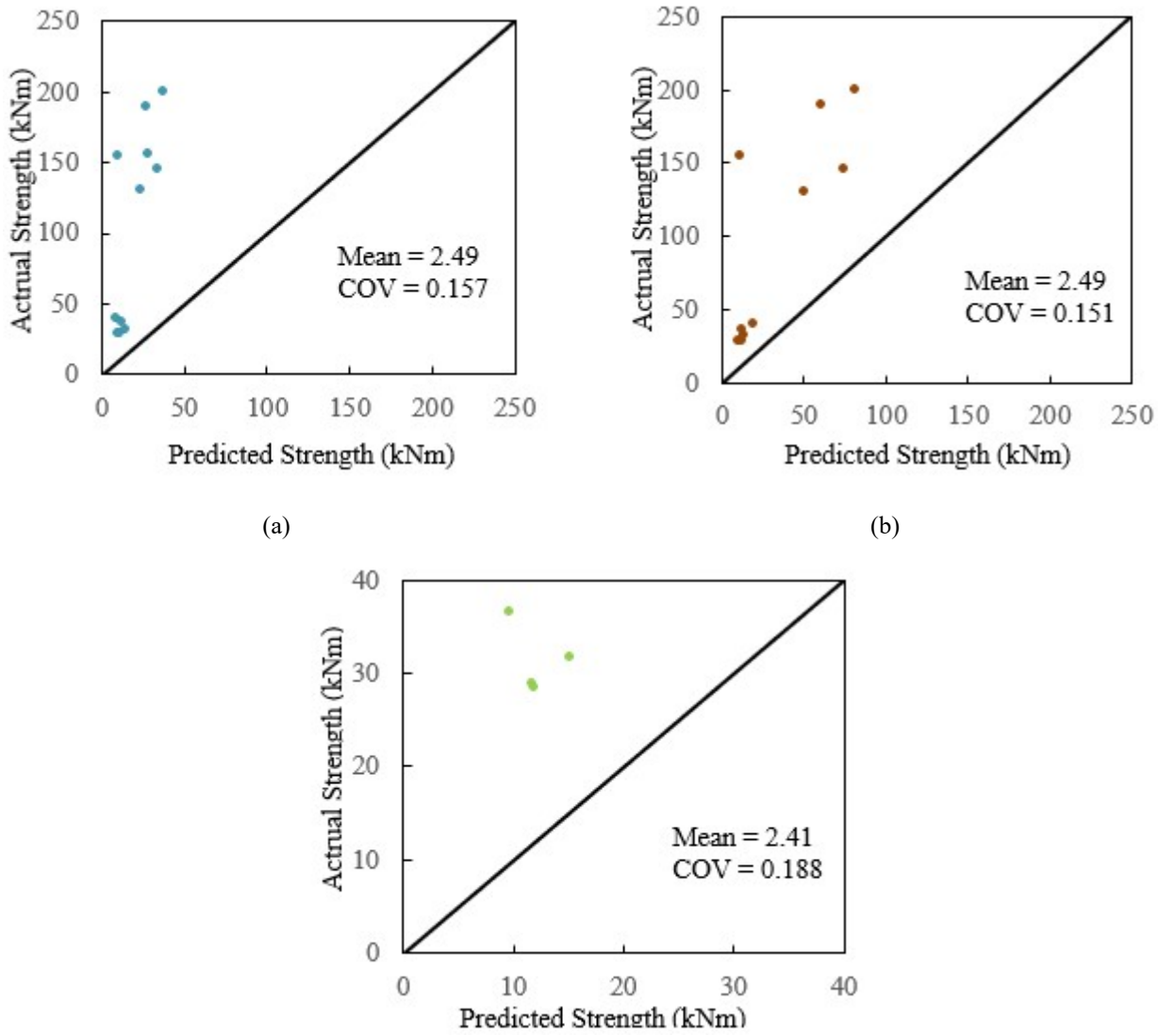

Figure H-9 Correlation plot of actual strength and prediction using EESM (AISC) and rational method with (a) minimum distance (b) fractural length and (c) leg size measurement according to AISC standard

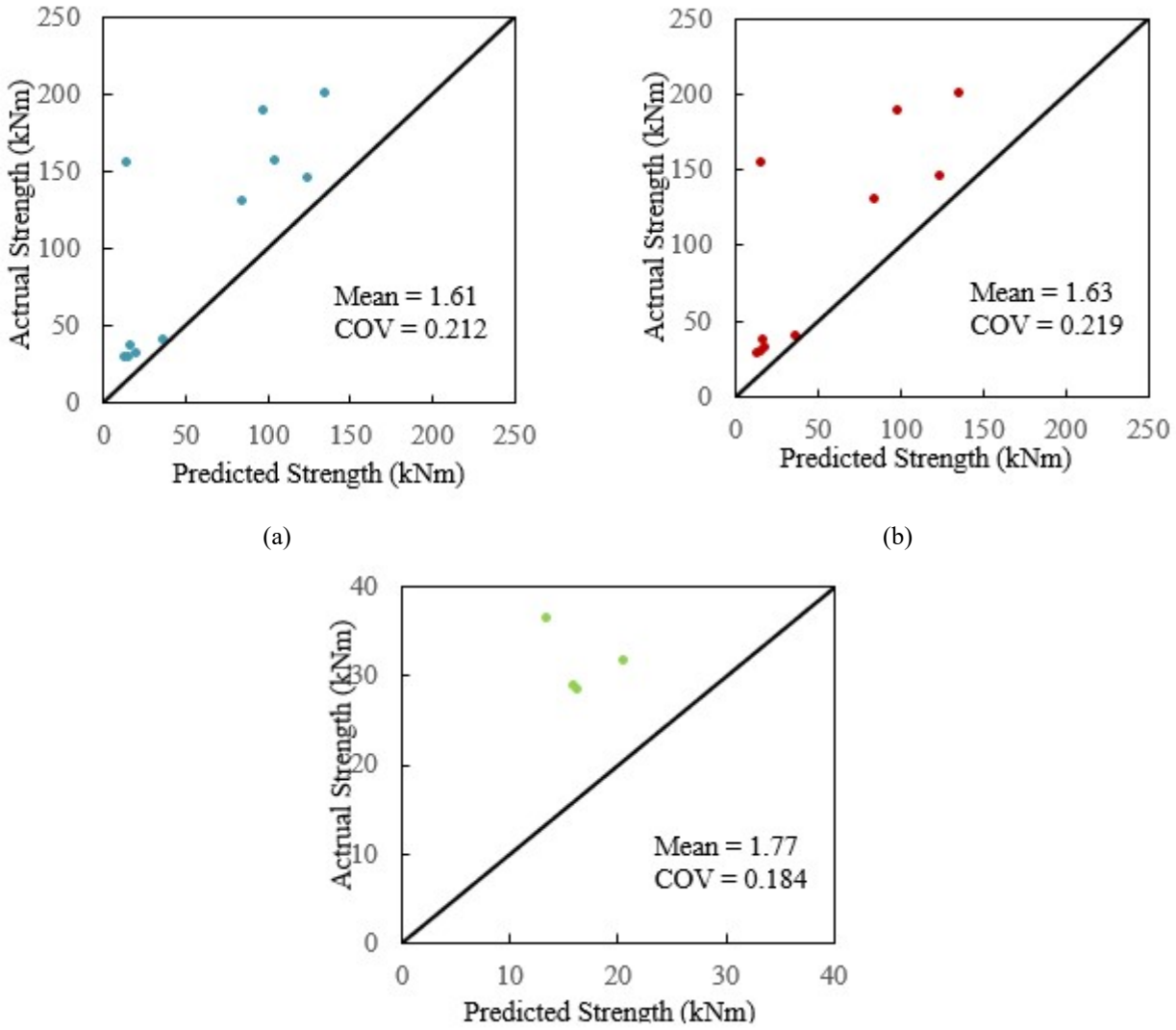

Figure H-10 Correlation plot of actual strength and prediction using EPSM (AISC) and rational method with (a) minimum distance (b) fractural length and (c) leg size measurement according to AISC standard

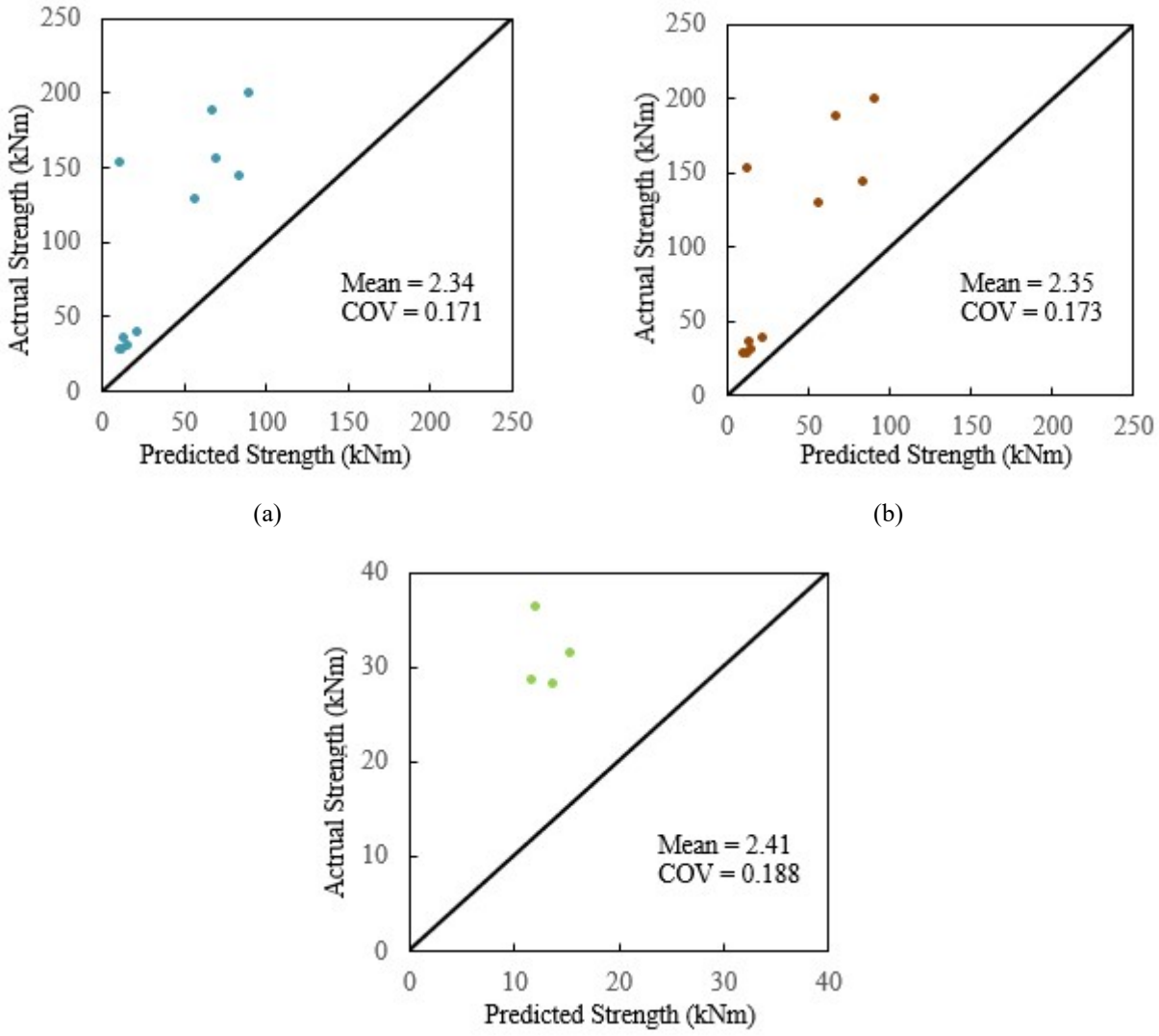

Figure H-11 Correlation plot of actual strength and prediction using EESM (CSA) and DIF with (a) minimum distance (b) fractural length and (c) leg size measurement according to CSA standard

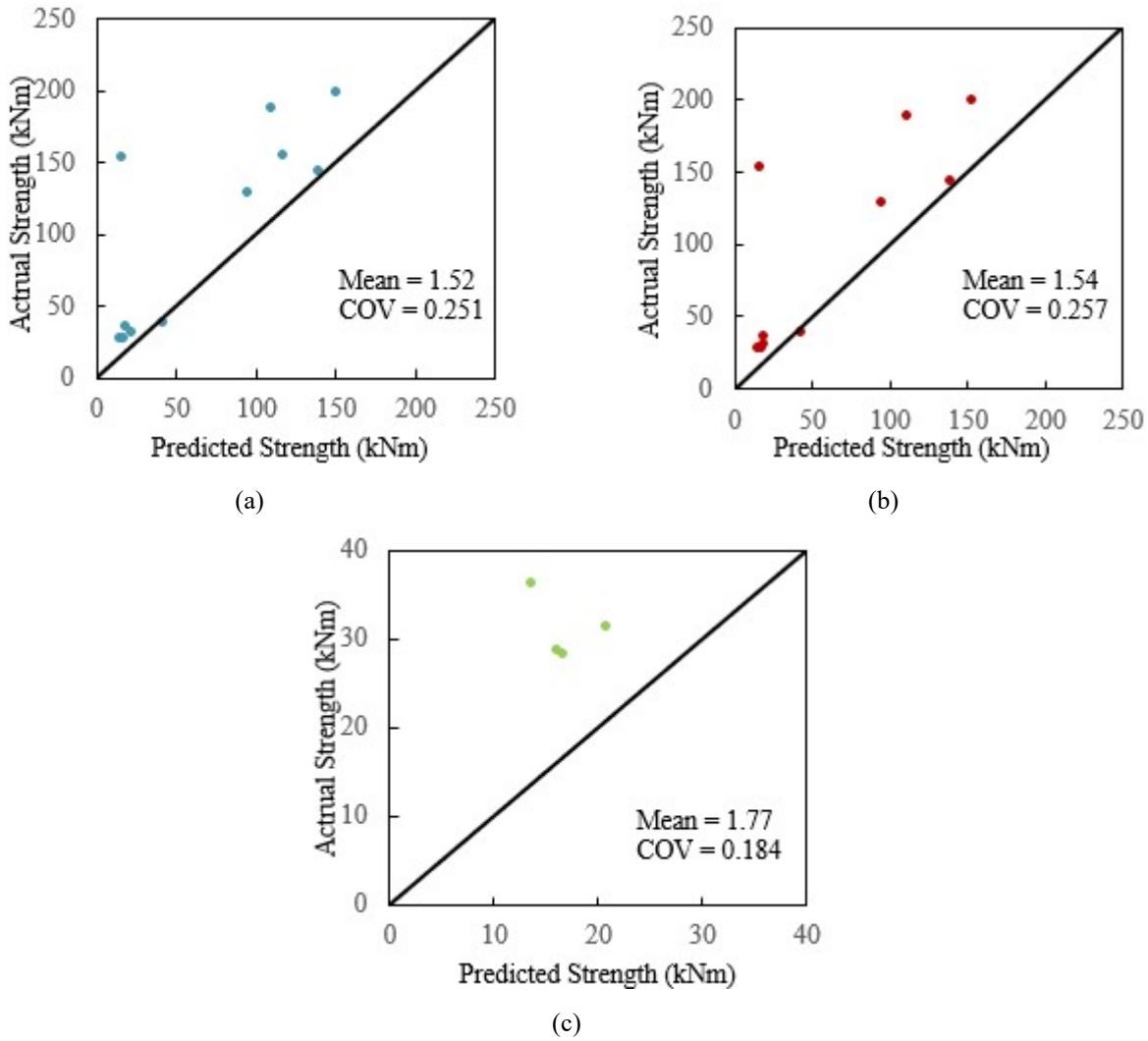

Figure H-12 Correlation plot of actual strength and prediction using EPSM (CSA) and DIF with (a) minimum distance (b) fractural length and (c) leg size measurement according to CSA standard

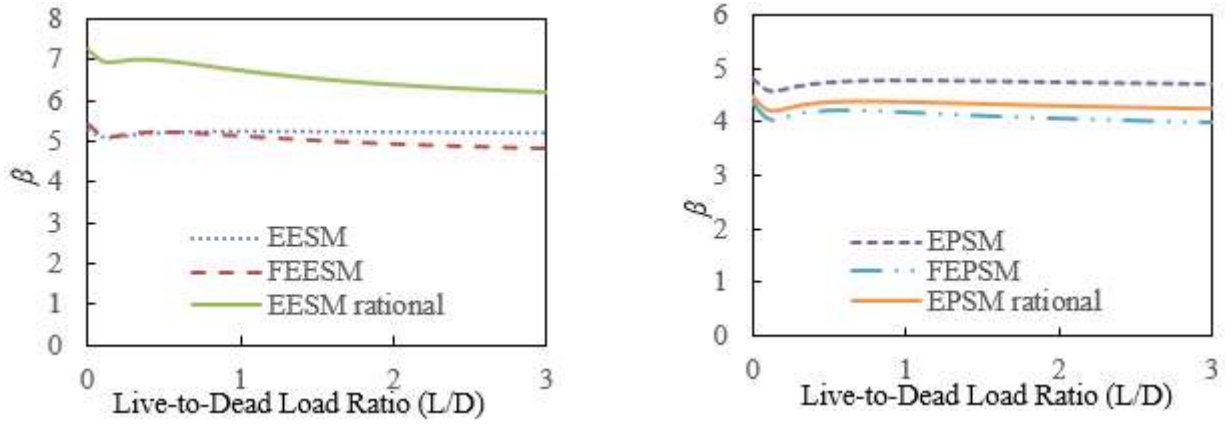

(a) (b)

Figure H-13 Reliability index of minimum distance for AISC on section modulus of: (a) elastic and (b) plastic $\phi = 0.75$

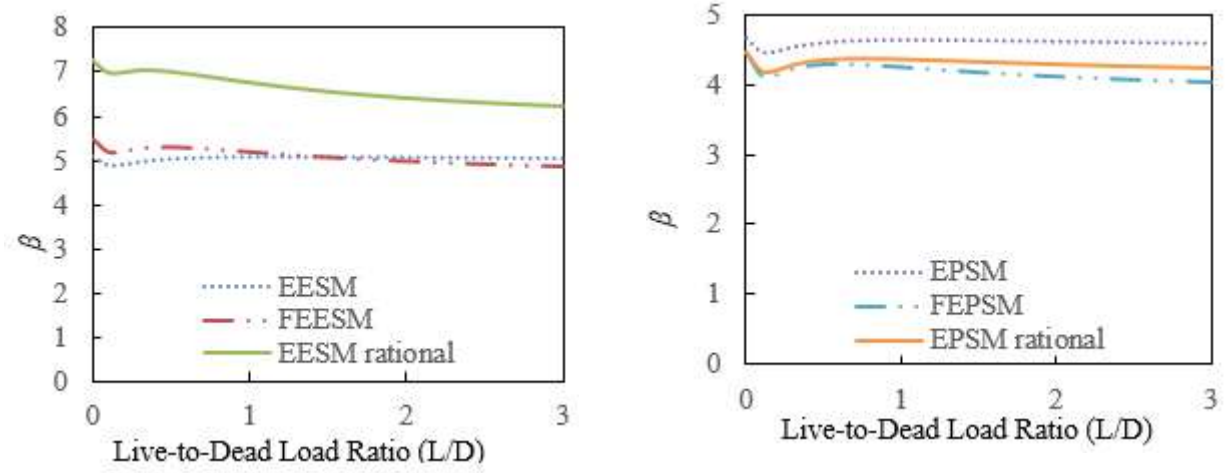

(a) (b)

Figure H-14 Reliability index of fractural length for AISC on section modulus of: (a) elastic and (b) plastic $\phi = 0.75$

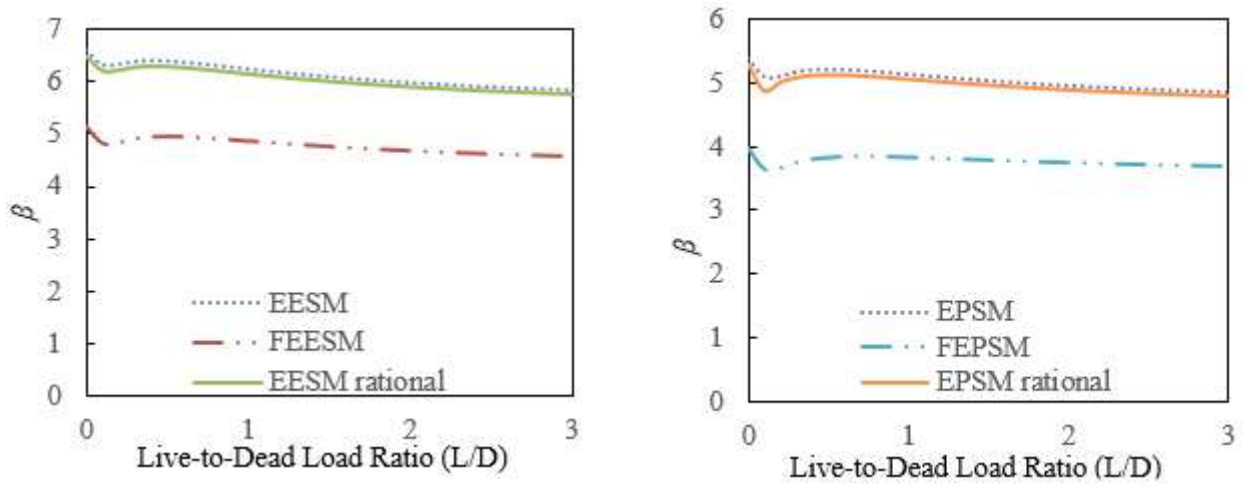

(a) (b)

Figure H-15 Reliability index of leg size calculation for AISC on section modulus of: (a) elastic and (b) plastic $\phi = 0.75$

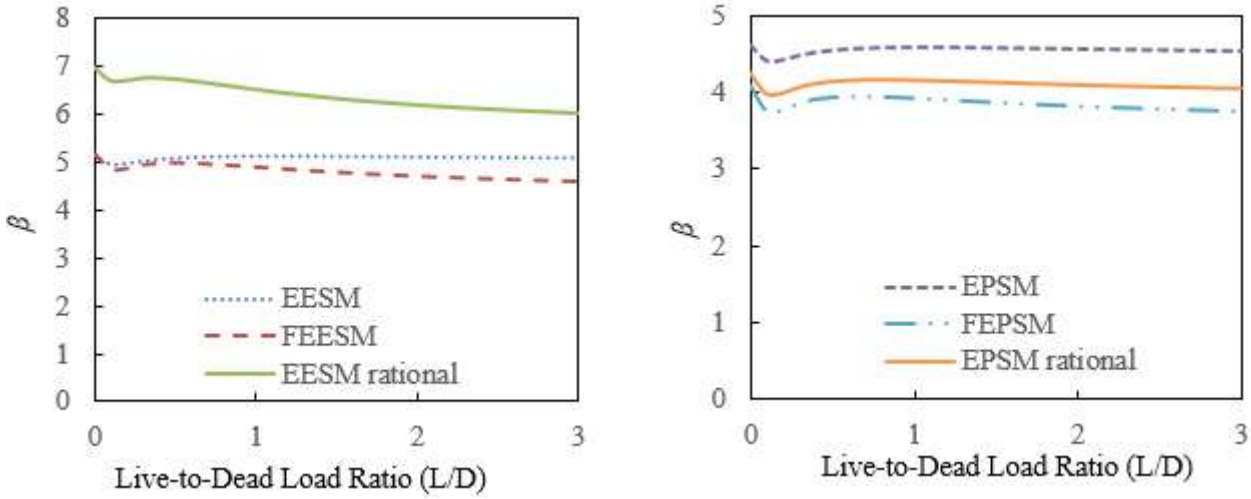

(a) (b)

Figure H-16 Reliability index of minimum distance for AISC on section modulus of: (a) elastic and (b) plastic $\phi = 0.80$

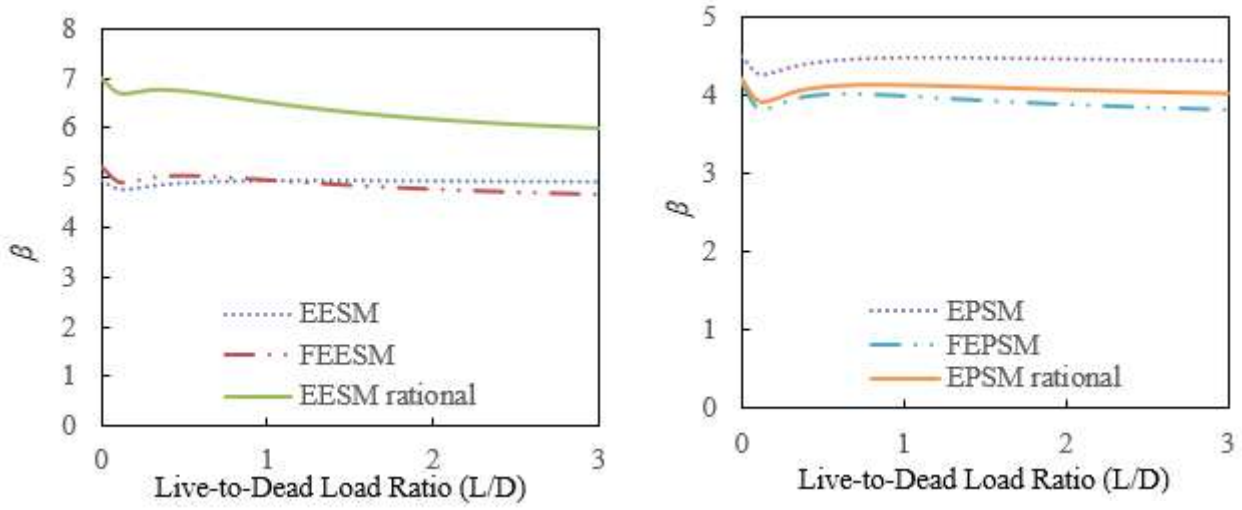

(a) (b)

Figure H-17 Reliability index of fractural length for AISC on section modulus of: (a) elastic and (b) plastic $\phi = 0.80$

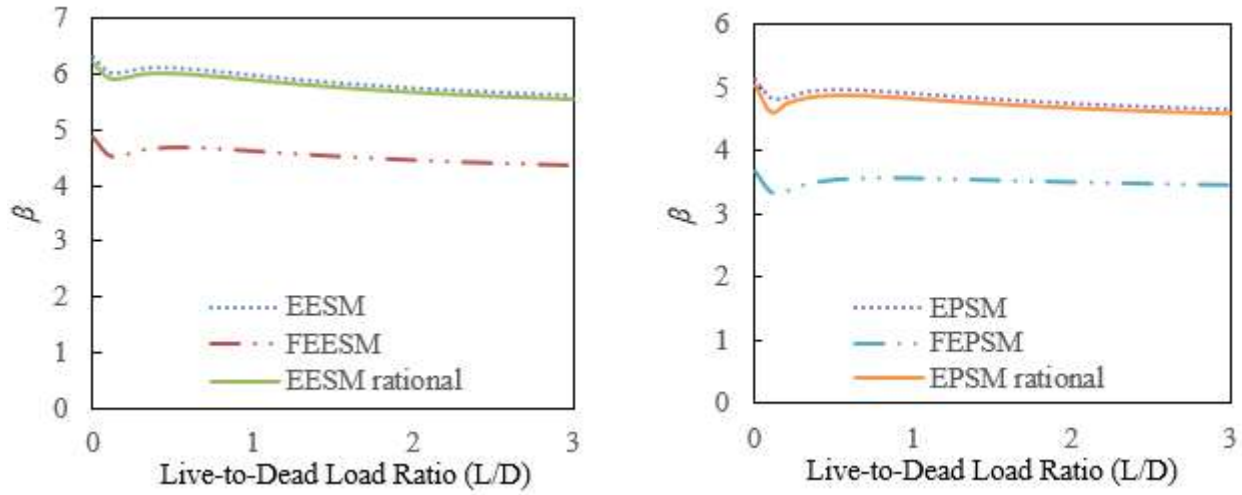

(a) (b)

Figure H-18 Reliability index of leg size calculation for AISC on section modulus of: (a) elastic and (b) plastic $\phi = 0.80$

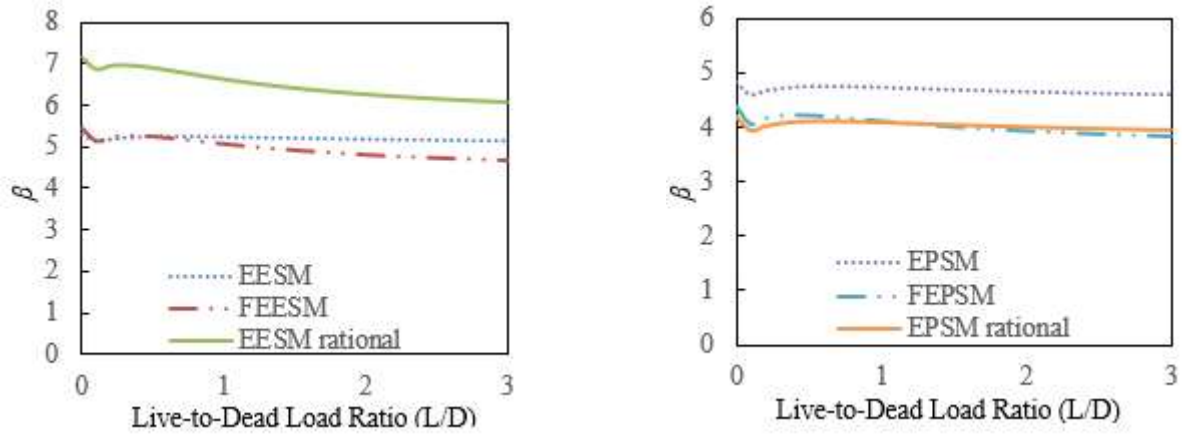

(a) (b)

Figure H-19 Reliability index of minimum distance for CSA on section modulus of: (a) elastic and (b) plastic

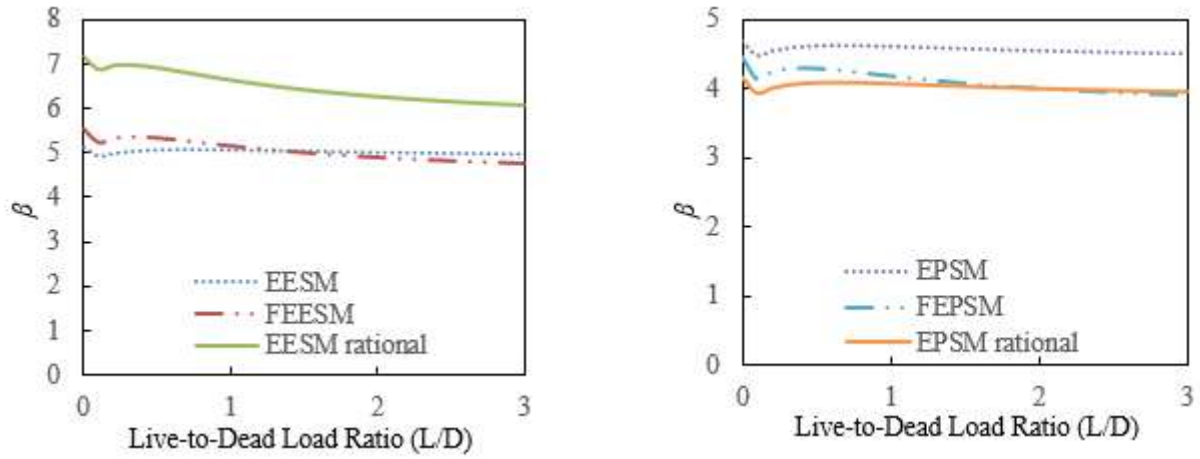

(a) (b)

Figure H-20 Reliability index of fractural length for CSA on section modulus of: (a) elastic and (b) plastic

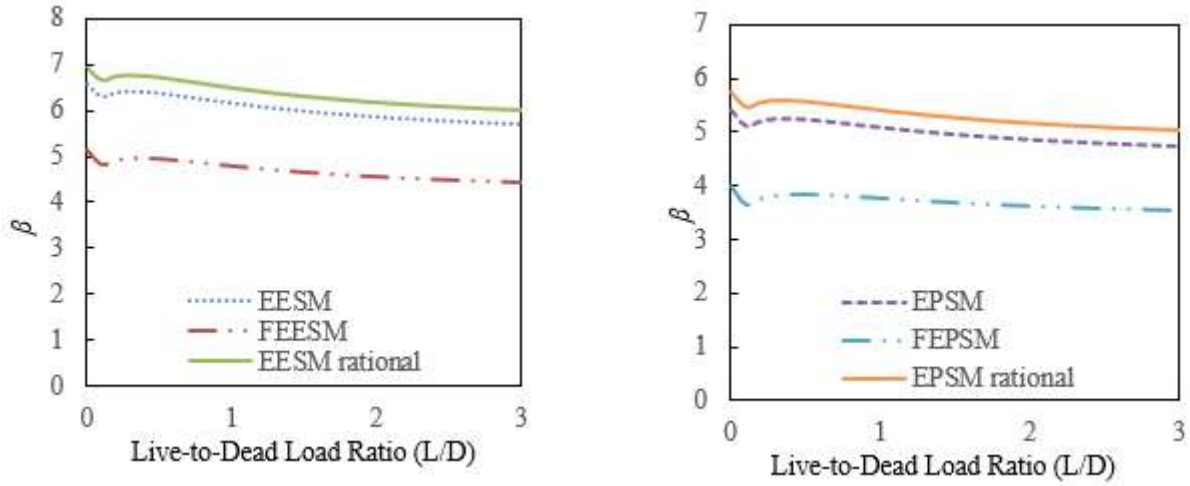

(a) (b)

Figure H-21 Reliability index of leg size calculation for CSA on section modulus of: (a) elastic and (b) plastic

Table H-18 Reliability index for AISC standard with ϕ = 0.75

Measurement type	Data type	Calculation method					
		EESM	FEESM	EESM (rational)	EPSM	FEPSM	EPSM (rational)
Minimum distance	Max	5.29	5.44	7.26	4.81	4.38	4.49
	Min	5.11	4.83	6.22	4.60	3.98	4.22
Fracture distance	Max	5.10	5.51	7.29	4.67	4.45	4.45
	Min	4.92	4.88	6.23	4.46	4.04	4.18
Leg size calculation	Max	6.58	5.14	6.47	5.38	3.96	5.28
	Min	5.83	4.59	5.76	4.86	3.64	4.80

Table H-19 Reliability index for AISC standard with ϕ = 0.80

Measurement type	Data type	Calculation method					
		EESM	FEESM	EESM (rational)	EPSM	FEPSM	EPSM (rational)
Minimum distance	Max	5.14	5.16	6.98	4.63	4.09	4.25
	Min	4.95	4.92	6.00	4.42	3.76	3.97
Fracture distance	Max	4.94	5.22	7.00	4.49	4.16	4.21
	Min	4.76	4.66	6.01	4.28	3.82	3.94
Leg size calculation	Max	6.32	4.85	6.21	5.11	3.68	5.02
	Min	5.62	4.37	5.55	4.65	3.36	4.59

Table H-20 Reliability index for CSA standard

Measurement type	Data type	Reliability index from calculation method:					
		EESM	FEESM	EESM (rational)	EPSM	FEPSM	EPSM (rational)
Minimum distance	Max	5.30	5.45	7.16	4.82	4.39	4.20
	Min	5.12	4.69	6.08	4.61	3.85	3.95
Fracture distance	Max	5.10	5.52	7.14	4.68	4.46	4.18
	Min	4.92	4.75	6.08	4.47	3.90	3.93
Leg size calculation	Max	6.59	5.15	6.92	5.39	3.97	5.75
	Min	5.70	4.45	5.99	4.73	3.55	5.03